

10/1/70
P. 331

Taurus Lightweight Manned Spacecraft

Earth Orbiting Vehicle

ENAE 412 Design Project

University of Maryland

Aerospace Engineering

(NACA-CR-130000) TAURUS LIGHTWEIGHT MANNED
SPACECRAFT EARTH ORBITING VEHICLE (Maryland
Univ.) 331 p CSCL 220

NP2-21244

Unclass
05/18 0073220

INTRODUCTION

The Taurus Lightweight Manned Spacecraft (LMS) was developed by students of the University of Maryland's Aerospace Engineering course in Space Vehicle Design. That course required students to design an Alternative Manned Spacecraft (AMS) to augment or replace the Space Transportation System and meet the following design requirements:

- Launch on the Taurus Booster being developed by Orbital Sciences Corporation.
- 99.9% assured crew survival rate.
- Technology cutoff date of January 1, 1991.
- Compatibility with current space administration infrastructure.
- First flight by May 1995.

The Taurus LMS design meets the above requirements and represents an initial step towards larger and more complex spacecraft. The Taurus LMS has a very limited application when compared to the Space Shuttle, but it demonstrates that the United States can have a safe, reliable and low-cost space system. The Taurus LMS is a short mission duration spacecraft designed to place one man into Low Earth Orbit (LEO). The driving factor for this design was the low payload carrying capabilities of the Taurus Booster--1300 kilograms to a 300 kilometer orbit.

The Taurus LMS design is divided into six major design sections. The Human Factors system deals with the problems of life support and spacecraft cooling. The Propulsion section contains the Abort system, the Orbital Maneuvering System (OMS), the Reaction Control System (RCS), and Power Generation. The thermal protection systems and spacecraft structure are contained in the Structures section. The Avionics section includes Navigation, Attitude Determination, Data Processing, Communication systems, and Sensors. The Mission Analysis section was responsible for ground processing and spacecraft astrodynamics. The Systems Integration Section pulled the above sections together into one spacecraft, and addressed costing and reliability.

TAURUS SYSTEMS OVERVIEW

The Taurus Lightweight Manned Spacecraft (LMS) is a single crew, short mission spacecraft. The spacecraft is configured with a re-entry capsule and a service module that is disposed of before re-entry. The capsule will carry the pilot, main and secondary life support systems, avionics, back-up power supply, and parachute recovery system. The service module will carry the Orbital Maneuvering System,

the main Reaction Control System as well as the Primary Power Generation System (see Figure 1).

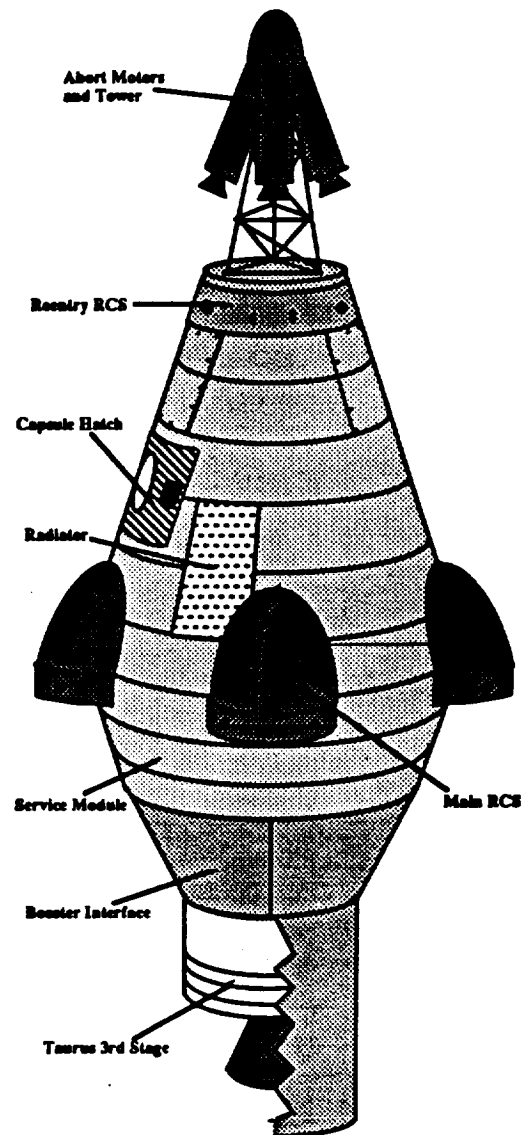


Figure 1. Taurus LMS Atop the Booster

The configuration of the service module/capsule design was chosen for two reasons. First, the spacecraft needed minimal mass on re-entry to meet the required control characteristics. This is accomplished by disposing of all unnecessary mass such as the propulsion system. Second, a stepdown from 2.0 meters to 0.9 meters was needed to place a capsule onto the booster.

The size of the Taurus LMS was predominantly chosen by the constraints imposed by the human factors group to place one man into a space capsule. The base of the capsule (above the heat shield) is 2.1 meters in diameter, which is the smallest possible dimension to put one man into the capsule. The top of the capsule is 0.74 meters, which is the minimal

Taurus LMS Students

Kevin A. Chase, Project Manager
Eric J. Vandersall, Systems Group Leader
Jennifer Plotkin
Jeffrey J. Travisano, Avionics Group Leader
Dennis Loveless
Michael Kaczmarek
Anthony G. White
Andy Est, Human Factors Group Leader
Gregory Bulla
Chris Henry
J. Alan Sandusky, Mission Analysis Group Leader
Sean Connelly
Bernie Kelm
Deborah Sewell
James Clegern, Propulsion/Power Group Leader
Michelle Bosset
Edison Villacis
Khanh Le
Curtis Neidhart, Structures Group Leader
TzuHeng (Kenny) Peng
James Paterson

Faculty Advisors

Dr. David Akin
Dr. Mark Lewis
Mr. Charles Lind

Editors

Michelle Bosset
Kevin A. Chase
James Clegern

Table of Contents

Introduction/Executive Summary.....	II
Chapter 1 Systems Integration.....	1
Section 1.1 The Taurus Spacecraft by K. Chase	
Section 1.2 Re-entry/Crew Capsule by K. Chase	
Section 1.3 The Service Modual by K. Chase	
Section 1.4 Capsule Aerodynamics E. Vandersall	
Section 1.5 Aerodynamic Heating by C. Neidhart	
Section 1.6 Costing by A. Sandusky	
Section 1.7 Reliably by C. Henry	
Chapter 2 Mission Analysis.....	24
Section 2.1 Mission Definitions by B. Kelm and A. Sandusky.	
Section 2.2 Launch Preparations by D. Sewell	
Section 2.3 Orbital Maneuverability by S. Connelly	
Section 2.4 Re-entry Trajectory by B. Kelm	
Section 2.5 The TLMS Recovery System by G. Bulla	
Section 2.6 The Recovery System by G. Bulla	
Chapter 3 Human Factors.....	46
Section 3.1 Life support systems by A. Est	
Section 3.2 Affects on Humans by C. Henry	
Section 3.3 Crew Compartment by C. Henry	
Chapter 4 Propulsion and Power.....	60
Section 4.1 Abort System Hardware by J. Clegern	
Section 4.2 Orbital Maneuvering System by M. Bosset	
Section 4.3 Reaction Control Systems by K. Le	
Section 4.4 Power Generation System by E Villacis	
Chapter 5 Avionics.....	101
Section 5.1 Navigation and Control by A. White	
Section 5.2 Attitude Determination and Control by J. Travisano	
Section 5.3 Data Processing by J. Travisano	
Section 5.4 Sensors by M. Kaczmarek	
Section 5.5 Communication by D. Loveless	

Chapter 6 Structures	131
Section 6.1 Selection of Materials by J Paterson	
Section 6.2 Abort Escape Tower by J. Paterson	
Section 6.3 Capsule Structure by J. Paterson	
Section 6.4 Service Module by K. Peng	
Section 6.5 Structural Interface by J. Plotkin	
Section 6.6 Thermal Protection System by C. Neidhart	
Section 6.7 Tank Design by J. Paterson	

Bibliography	158
--------------------	-----

Appendix A by K.Chase	
Appendix B by E. Vandersall	
Appendix C by C. Henry	
Appendix D by C. Neidhart	
Appendix E by S. Connelly	
Appendix F by B. Kelm	
Appendix G by G. Bulla	
Appendix H by C. Henry	
Appendix I by J. Clegern	
Appendix J by M. Bosset	
Appendix K by S. Connelly	
Appendix L by E. Villacis	
Appendix M by B. Kelm	
Appendix N by J. Paterson	
Appendix O by J. Paterson and M. Bosset	
Appendix P by G. Bulla	
Appendix Q by J. Plotkin	
Appendix R by E. Vandersall	
Appendix S by E. Vandersall	
Appendix T by G. Bulla	
Appendix U by K. Peng	

dimension required by the propulsion group to attach the abort system. The height is fixed at 2.1 meters to allow the sides of the capsule to be straight.

The top dimension of the service module is fixed by the bottom dimension of the capsule at 2.1 meters in diameter. The height is 0.75 meters. This dimension is selected because of the need to have the propulsion system in the service module. The bottom dimension is fixed at 1.6 meters in diameter for attaching the Taurus booster structural interface (see Figure 2).

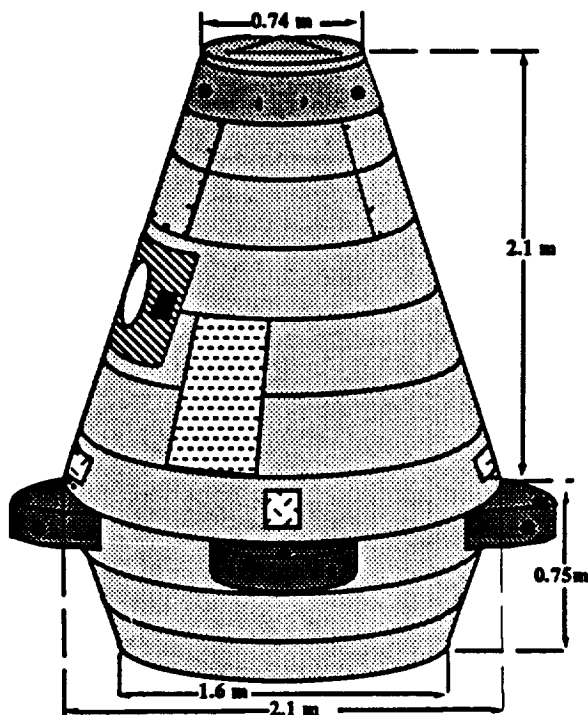


Figure 2. Taurus LMS Dimensions

The major constraint on the design of the Taurus LMS is the mass of the spacecraft. The maximum payload mass of the Taurus Booster is 1300 kg to a 300 km LEO. The systems masses are kept to a minimum, and are presented in Table 1. The total mass for the Taurus LMS is 1168.21 kg. This figure includes a budget margin of 50 kg for miscellaneous hardware. This launch mass is under the maximum payload allowable for the booster, thereby making the Taurus LMS a viable program.

The mass budget listed in Table 1 is corrected to show the mass gains from ejecting the abort system and the booster interface before the low earth orbit is achieved.

The crew capsule will be the primary component of the Taurus LMS. It contains the pilot, the dual life support systems, the avionics systems, and the emergency / re-entry power systems. Mounted to the exterior of the capsule will be the Re-entry Reaction Control System, the Abort System (during launch),

the Guidance and Navigation Sensors, and the Communications Antennas. The major components of the capsule are shown in Figures 3 & 4.

Table 1. Systems Mass Budget

System	Mass (kg.)
Capsule Structure	133.88
Life Support system	120.00
Crew Cabin	112.50
Abort system (effective)	40.00
RCS capsule	9.00
RCS Fuel and Tank	0.54
RCS Oxidizer and tank	0.86
RCS Helium and tank	1.29
Batteries	21.05
Thermal control	40.00
Communications	11.50
Sensors	40.00
Data Processing	45.00
Guidance and Control	15.20
Parachute system	60.00
Service Module Structure	150.00
Interface to capsule	20.00
RCS Main	20.00
OMS engine	20.00
Fuel and Tank	85.64
Oxidizer and tank	106.52
Helium and tank	4.73
Power Generator	25.20
Booster Interface (effective)	31.30
Misc. Hardware	50.00
TOTAL	1168.21

The Service Module carries the Orbital Maneuvering Engine, the Power Generation System, and the main Reaction Control System. All three of these systems feed off a central fuel and oxidizer system. The size of the Propulsion system determined the height of the Service module. The placement of the propulsion system is shown in Figures 5 & 6.

MISSION ANALYSIS

The limited mass capability of the Taurus booster restricts the orbital maneuvering abilities of the Taurus LMS. With a total ΔV of approximately 270 m/sec available for the OMS, the Taurus LMS is not capable of performing a rendezvous mission, which would require a ΔV of at least 400 m/sec. Consequently, the baseline mission for the Taurus LMS is a single-manned launch and return. The spacecraft is designed to be launched due east from Cape Canaveral at an inclination of 28.5° and with an orbital altitude of 300 km.

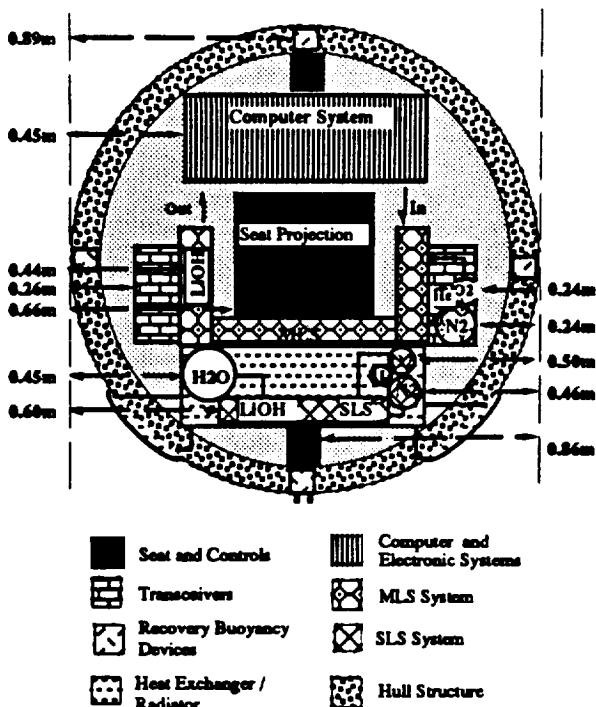


Figure 3. Capsule Internal Cross-Section 10% from Bottom

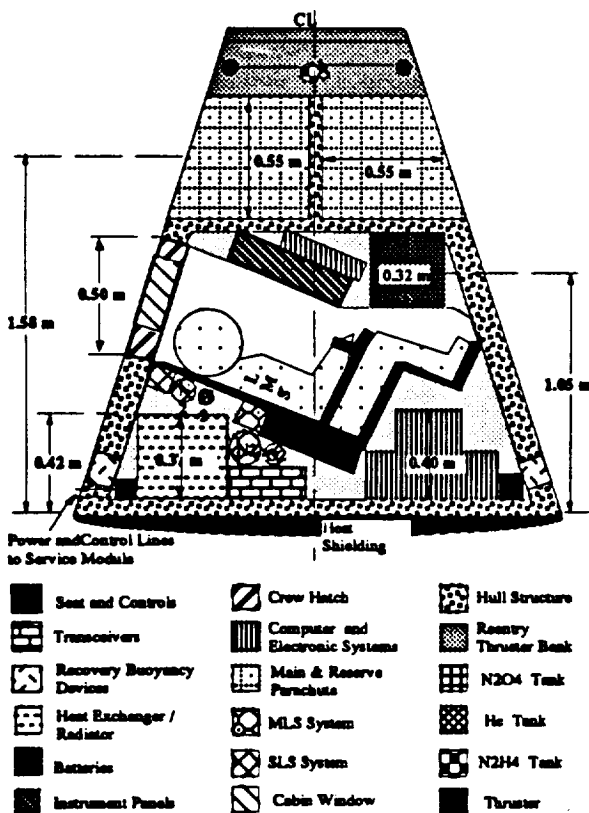


Figure 4. Capsule Internal Side View

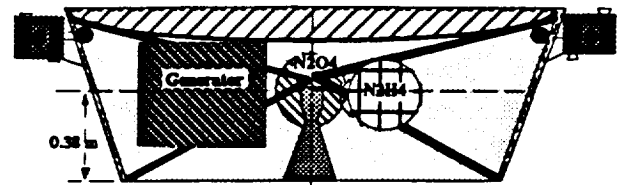


Figure 5. Service Module Internal Side View

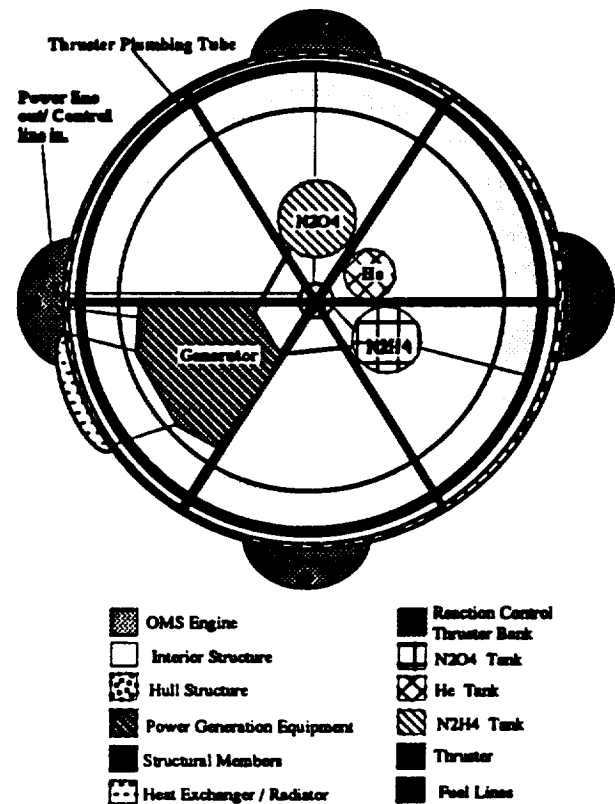


Figure 6. Service Module Internal Top View

HUMAN FACTORS

The life support system of the Taurus LMS has been designed around a single astronaut on a twenty-four hour mission to LEO. The main life support system (MLS), as outlined in Figure 7, consists of a pressurized crew compartment held at 21° C and 50% humidity (Ref 1). Continual recirculation of the cabin atmosphere (80% of which is nitrogen and 20% of which is oxygen at a total pressure of 101.3 kPa) is achieved through a single duct that will contain scrubbers to remove excess water vapor, carbon dioxide, and trace contaminants. The MLS air supply is stored cryogenically in two tanks: one for oxygen

and one for nitrogen. Enough air is stored on liftoff to allow for repressurizing the cabin during orbit in the event of contamination or loss of cabin air, while allowing for an average astronaut metabolic consumption value of oxygen of 0.91 kg per a period of twenty-four hours. A cabin volume of 4.08 m³ is estimated in the calculations of the required mass of gas to repressurize the cabin.

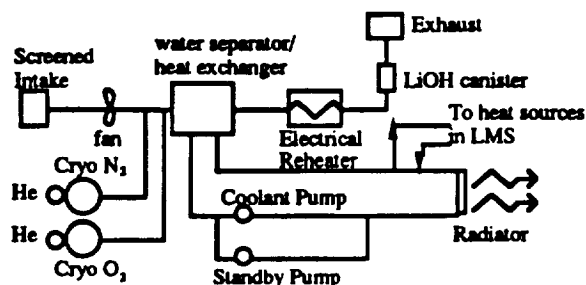


Figure 7. Main Life Support System

One cryogenic tank contains 4.055 kg of liquid nitrogen, the other contains 2.066 kg of liquid oxygen. Electrical reheaters supply the energy to vaporize and heat the cryogenic fluids to a cabin temperature of 21° C. The computer regulates the pumping of the gas on a need basis, determined by its sensors.

A water separator serves as a heat exchanger. The separator is composed of a bank of four hundred aluminum tubes with an overall mass of 16.12 kg. Ethylene glycol will flow through these tubes, entering the bank at 0° C and leaving it at 5° C. Air will enter the heat exchanger at 21° C and will be cooled down to 10° C by the ethylene glycole, which in turn will flow to two radiators located on the exterior skin of the spacecraft (Ref 2). These radiators will be oriented towards deep space during the mission and will radiate to space a total of 383 W of heat. The radiator is a tube-and-fin type, in which the coolant tubes have fins attached to them to increase the radiating area. Each radiator is constructed of aluminum and weighs 3 kg.

Once the air is reheated, it will pass through a lithium hydroxide (LiOH) canister that will chemically remove excess carbon dioxide. Each LiOH canister is cylindrical, with a diameter of 12 cm and a length of 0.26 m. One canister contains enough LiOH for 12 hours of carbon dioxide removal. Three (rather than two) canisters are used in the 24 hour mission for safety reasons.

The secondary life support system (SLS), as shown in Figure 8, consists of a 10 kg pressure suit. This suit is worn by the astronaut throughout the mission, but is not pressurized unless there is an MLS malfunction. The SLS provides a self-contained environment for the astronaut until successful de-orbit and landing is achieved. The pressure suit is

composed of the helmet and the body. A special seal separates the two parts, allowing for a one-time pressurization of the body by pure nitrogen gas, while continually circulating 50% oxygen and 50% nitrogen at a total pressure of 55.16 kPa inside the independent helmet. The SLS gasses are carried in a pair of separate cryogenic tanks that contain 1 kg of oxygen and nitrogen, respectively. The gasses are heated electrically before being injected into the SLS loop. A water-cooled undergarment, with tiny tubes woven into the fabric through which cooling water flows, provides thermal control for the astronaut. There are three attachment points on the pressure suit for hookups into the communications system, the atmospheric filtering system, and both the liquid-cooled undergarment and the pressurizing line from the cryogenic nitrogen storage tank.

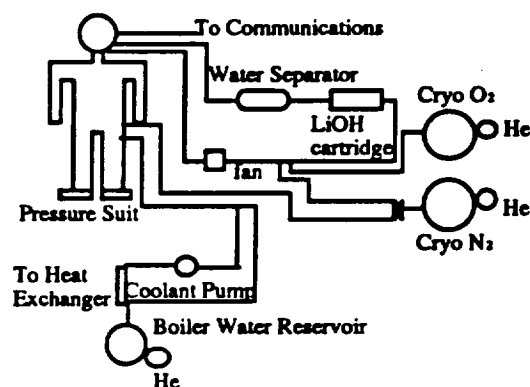


Figure 8. Secondary Life Support System

The mission duration is short enough that only 5kg of weight is used to supply the necessary rations. A large plastic squeeze bottle will be filled with drinking water and placed aboard the capsule for the astronaut, along with several freeze-dried food bars. Additional life support equipment include a 4.5 kg carbon dioxide fire extinguisher, a first-aid kit, and a 17.7 kg survival pack similar to the ones carried by the U.S. military pilots.

There is no waste removal from the spacecraft. The astronaut will use catheters and plastic bags for liquid waste, and will wear a diaper-like undergarment for solid waste collection.

Two major requirements influenced the design of the pilot seat: it had to be conducive to large accelerations and it had to occupy a minimal cross-sectional area and volume inside the capsule due to the weight restriction. The mass of the seat is 16 kg.

PROPULSION AND POWER

The abort system will insure crew survival in case of a critical failure of the Taurus booster system, such as an explosive detonation of the booster fuel or a critical malfunction. Assuming a five second

detection time before the fuel in the booster detonates, the abort system would have to place the Taurus LMS crew capsule at a distance of 805 meters from the launch site or moving booster, and place the capsule at a minimum of 500 meters in altitude for recovery parachute deployment. The 805 meters radial distance represents the typical danger radius of a detonating solid rocket booster system.

Thrust termination ports are required hardware additions to the Taurus booster. The thrust termination device, or "blow out" ports, would almost instantaneously vent the pressure and extinguish the flame within the thrust chamber, thereby dropping the acceleration of the Taurus booster to zero and allowing the abort system to function well within the required acceleration limits set by the human factors division for human pilots.

Solid abort rockets will be used in the Taurus spacecraft because of their (1) high thrust-to-weight, (2) simple design, (3) high reliability, (4) lower volume requirements, and (5) ease of storage. A combination of three solid abort motors, placed 120° apart, will reduce the hardware mass, and increase reliability by decreasing the number of failure and heating points on the Taurus capsule during an abort sequence.

A tower structure was designed for the abort rocket placement, providing a mass savings by discarding the entire abort system at a predetermined height to orbit (40 - 50 km) past the point of maximum dynamic pressure. Other advantages of this tower structure are minimal heating of the upper stages of the Taurus booster and capsule by the exhaust plume of the motor, and good directional control characteristics. The motor top is an aerodynamically-designed fairing to reduce drag.

To reduce the mass of the system, a high energy solid double fuel DB/AP - HMX/AL has been selected based on the need for an energetic solid propellant with a high specific impulse of 270 sec (Ref 3). The HTS organic (graphite) composite was selected for the motor casing and nozzle assembly, due to its high tensile strength and low density when compared to current metal alloys and other composite materials. This casing material will be protected from the hot gasses and the solid fuel's chamber temperature of 3707° C by a layer of ablative asbestos phenolic 2.54mm thick. At the motor throat, thermal protection heat transfer consists of an 0.8 mm thick layer of ablative pyrolytic graphite covering a back-up 2.0 cm layer ATJ molded graphite (see Figure 8). The 0.8 mm layer of pyrolytic graphite will extend from the throat to the tip of the nozzle to protect the structural HTS graphite.

The abort initiation can be controlled manually and by ground. The manual abort system is located in the crew cabin. The abort command can be initiated by launch control in the event of a detected malfunction

of the Taurus booster or other critical subsystem. The ignition system for the solid motors consists of a pyrotechnic igniter mounted at the top of the abort motor solid fuel.

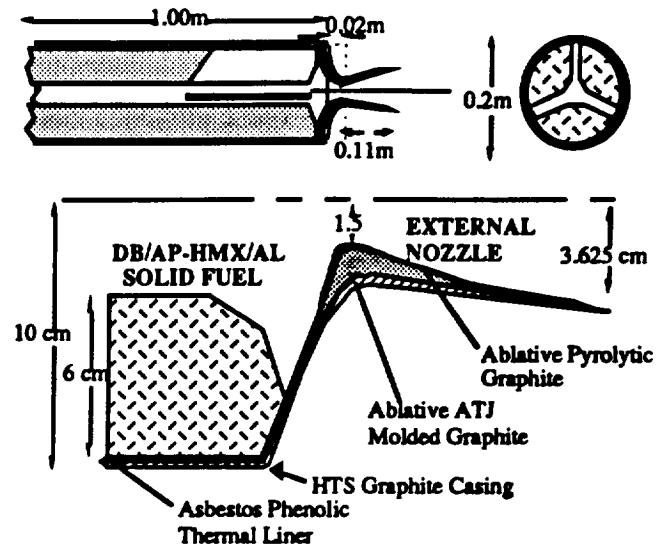


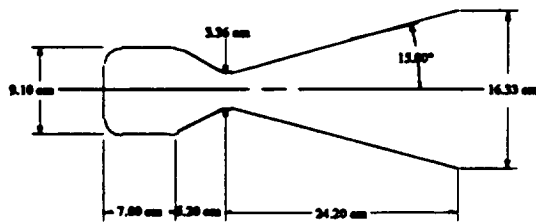
Figure 8. Solid Abort Motor Internal Layout

The orbital maneuvering system (OMS) consists of a non-reusable main liquid propellant rocket engine, two tanks (one for the fuel and one for the oxidizer), an injector, and a pressurized gas system. The OMS must be reliable and have a low mass. It also must be capable of restarting numerous times, and of operating in the vacuum conditions of space with a thrust level of 3158 N. This value was determined by assuming a ΔV of 270 m/sec and an impulsive maneuver of one minute, which is approximately one degree of distance around the Earth's orbit.

The main engine is a liquid propellant type. The advantages of this type of engine over a solid one are: high performance, repeated restarts, and randomly variable duration for each start. Hypergolic propellants are used to allow for a greatly simplified ignition system. Moreover, since hypergolic propellants ignite smoothly upon contact, accumulation of the mixture of fuel and oxidizer in the combustion chamber does not occur in large quantities, and the danger of explosion is minimized. The combination of nitrogen tetroxide and hydrazine is used due to its high specific impulse, ease of storage, and material compatibility for the tank design.

The engine specifications and the properties in the combustion chamber were determined assuming a one-dimensional compressible flow and an isentropic nozzle region. A study of the variation in chamber pressure versus thrust coefficient was undertaken to obtain the optimum chamber pressure. The effects of

increasing the chamber pressure above 2.069 MPa on the thrust coefficient were slight. The optimum chamber pressure, therefore, was determined to be 2.069 MPa. The specific impulse (Isp) of the main engine was found to be 292.3 sec. Using this Isp and a total ΔV of 270 m/sec in the rocket equation, the total propellant mass was found to be 48.08 kg of fuel (hydrazine) and 51.92 kg of oxidizer (nitrogen tetroxide). A summary of the combustion chamber parameters and engine specifications is presented in Figure 9.



	Chamber	Throat	Exit
P (PA):	2.069E6	1.144E6	6894
T (K):	2857	2528	1880
A (cm ²):	65.1	8.9	209.3

Mass = 16 kg
Thrust = 3158 Nt
Isp = 291.3 sec
Propellants = N₂H₄/N₂O₄
Mixture Ratio = 1.08

Specif Heat Ratio = 1.26
Chamber thickness = 1.54 cm
Throat thickness = 1.54 cm
Nozzle Thickness = 0.71 cm

Figure 10. Engine Specifications

Thermal protection using ablative cooling is effective for longer firing durations without significant weight penalties. Although this technique was initially used for solid propellant systems, it has since proved to be quite successful for liquid engines with chamber pressures of 2.069 MPa or less, and pressure-fed systems (Ref 4). The char depth or thickness of the thrust chamber will increase at the combustion chamber and throat, and decrease to a constant thickness along the rest of the nozzle. Using a Refrasil phenolic ablative thrust chamber, the thickness at the combustion chamber and throat is 1.54 cm, and 0.71 cm for the rest of the nozzle.

To introduce and meter the flow into the combustion chamber, an impinging stream-type injector has been selected. The propellants are injected through a number of separate orifices so that the fuel and the oxidizer streams impinge upon each other aiding in the break-down of the liquid.

The OMS is located in the service module of the Taurus LMS, and will use a simple and reliable pressurized gas feed system. The oxidizer and fuel are fed into the combustion chamber by the displacement of helium gas stored at a high pressure of 27.58 MPa. The tanks for the propellants are kept at a constant pressure of 3.45 MPa. They contain all the propellant needed to operate the OMS, Reaction

Control System, and Power System. This design enables any one of the aforementioned systems to draw more propellant from the common tanks in the event of an emergency. The plumbing in the OMS is designed so that active systems are double-stringed to provide redundancies, while passive systems are single stringed. A schematic diagram of the OMS is shown in Figure.

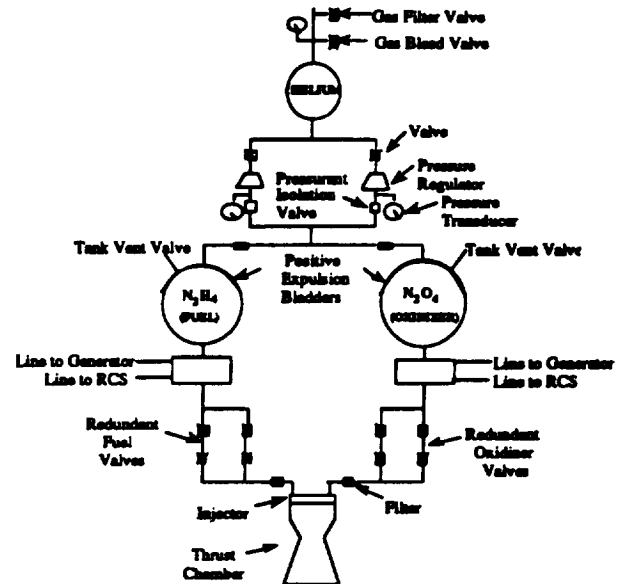


Table Dimensions, Mass and Pressure

	He	N ₂ H ₄	N ₂ O ₄
Radius :	18 cm	27 cm	26 cm
Mass :	4.75 kg	85.64 kg	106.58 kg
Pressure :	27.58 MPa	3.45 MPa	3.45 MPa

Figure 11. Schematic Diagram of the OMS

The RCS measures, corrects, and counteracts adverse motion due to forces and moments which cause the spacecraft to rotate or translate. It also maneuvers the Taurus LMS in attitude control, position keeping, and re-entry. The spacecraft will experience two types of perturbations depending on the inclination of the orbit plane to the equator. These are nodal regression and apsidal shifting. Other principal forces that the spacecraft will experience include aerodynamic drag and internal accelerations produced by propellant shifting and astronaut movements.

The RCS was divided into a re-entry control, located at the top of the Taurus LMS capsule, and a main reaction control, located at the top of the service module. The re-entry system will be used during de-orbit when the service module is detached and the capsule begins to re-enter the earth's atmosphere. Its primary purpose is to allow for cross range maneuvering and re-entry oscillation dampening.

The main reaction control system provides the Taurus LMS with three degrees of freedom control at

all times with two to three redundant thruster directions. The thrusters will be covered by an aerodynamic shroud which is blown off when separation from the Taurus booster occurs.

The primary power supply is a single reciprocating hydrogen - nitrogen tetroxide engine (Ref 5). The mass and size of the engine has been scaled down from an existing engine used in missions similar to the one performed by the Taurus. For the required energy of 19.2 kW-hr, the weight of the engine was scaled down to 25.2 kg. This includes the weight of the compressor, alternator, cooling system, and plumbing. The engine has dimensions of 0.519 m by 0.405 m by 0.463 m which results in a volume of 0.0973 m³.

The secondary power supply is a system of Silver-Zinc rechargeable batteries. They are lightweight and compatible with the other systems. The batteries will be used for re-entry power after the service module containing the primary power system is detached, and whenever the demand for power rises above the primary power supply's output capability. The batteries have a cycle life of 20 to 200 cycles, and can be recharged using the primary system's electrical power output. For a discharge rate of four hours, the total weight of the batteries will be 21.05 kg. The batteries, therefore, can be recharged six times during the entire mission.

The silver-zinc batteries are composed of 45 to 50 cells or plates which are connected together and stored inside two separate sealed boxes to prevent leakage and protect them against the space environment. Selecting two batteries adds redundancy and reduces the risk of a malfunction. When the mission is completed and the spacecraft is ready for re-entry, the batteries will provide the primary power.

AVIONICS

The initial navigation system on board the Taurus LMS is the LCINS (Low Cost Inertial Navigation System). The LCINS is a strapdown configuration with two degrees of freedom gyros. The inertial reference assembly is reduced in size, and a digital microprocessor performs all of the measuring data processing, instrument torquing computation, scaling, attitude, and navigation functions. With dimensions of 152 by 152 by 215 mm, weight of 3.0 kg, and power of 35 W, the LCINS is the ideal system to use in a heavily mass-constrained spacecraft such as the Taurus LMS.

Since the positional error of the LCINS increases every hour, it is updated by another navigation system. The primary satellite navigational system considered for the updates is the Global Positioning System (GPS). GPS is a satellite based navigational system which will give continuous worldwide coverage by the year 1992, when there will be 21

operational satellites in orbit. The satellites orbit every 12 hours and transmit two L band signals: L1 at 1575.42 MHz and L2 at 1227.60 MHz. This system of orbits ensures at least four satellites in view at all times.

An accuracy of better than 0.25 degrees is required for altitude determination and control of the Taurus LMS. Sun, horizon, and laser fiber-optic gyroscopes are used to determine the spacecraft's attitude. Reaction thrusters are used in the Taurus LMS attitude control system (previously discussed in "Propulsion and Power Systems") for their high force ability and accuracy.

The primary function of the data processing system is to monitor all equipment on the Taurus LMS. Through the use of sensors and output devices, this system will keep the astronaut informed about the present condition of all aspects of the spacecraft. Another function of the data processing system is to perform necessary navigation and flight control computations. The goal of this system is to allow for as many on-board processing capabilities as possible, thereby relying less on ground-based computations.

The data processing system will also make the necessary computations for the OMS and the RCS. These computations involve determining the directional vector to the target position, the number and duration of OMS engine burns, and the required thruster firings for attitude control. The data processing system must also interact with other external systems on the spacecraft. For example, the communication system must be linked to the processors to allow for data uplink and downlink. This computer system has been designed to control all systems of the spacecraft in case the astronaut is unable to perform his/her duties, allow for dual control when both the computer and astronaut are functioning, and allow for manual control if the computer malfunctions.

Three major types of architecture were studied for the Taurus LMS design: centralized, federated, and distributed. A centralized system has been selected (see Figure 12). This design consists of two general purpose processors (one as the primary processor, and one as a backup computer) for guidance, navigation and control (Ref 6). These central processors will be linked to the main memory, sensors, display controls, engine interfaces, and other external interfaces.

Each processor will have its own RAM associated with it. The size of the RAM will be 16 Mbyte. This size allows for an estimated 1 Mbyte of software, 8 Mbytes reserved for runtime memory, and 7 Mbyte for temporary data storage and space for uplinked code if needed. In case this memory gets corrupted, the capability to reload the software from the mass memory will exist. The decision to go with individual RAM is made to allow for quicker and

more independent execution. The design of the data bus consists of a two-way linear bus configuration. Six buses are used in the Taurus capsule, two for sensors and mass memory, two for engine and external interfaces, and two for displays and keyboard (all connected to the CPUs). Two liquid crystal displays (LCD) are used in the Taurus capsule (Ref 7). They require little depth space (approx. 2.0 cm) and power, and are digitally compatible. They do, however, require some type of external back light.

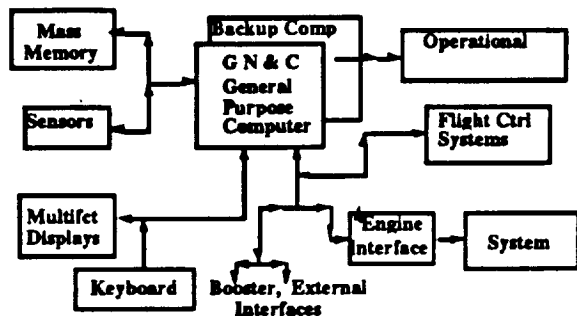


Figure 12. Schematic Diagram of Centralized System

Sensors are required for the Taurus LMS to operate through computer and/or manual control. The sensors return information concerning capsule operational systems to the astronaut for updates and corrections. Consequently, sensors are applied to the propulsion, main life support, secondary life support, reaction control, and abort systems. For the propulsion, it is necessary to measure the conditions of the pressurant, oxidizer, and propellant tank, as well as the conditions of the plumbing and rocket combustion chamber. A total of eight temperature sensors ranging from 20 to 3000 Kelvin are required in the system.

With respect to the main life support system, it is necessary to measure the conditions of the pressurant, nitrogen and oxygen tanks, as well as the heat exchanger and cabin conditions. The total number of pressure sensors needed is eighteen. The sensors for the secondary life support system are similar to those in the main system due to their similar design with the only difference being the addition of a water tank. The total number of sensors required is one hundred and thirty-four. The total number of sensors required in the reaction control system is ninety-eight. Abort control sensors are placed on the system to guarantee that the tower has been armed before launch. Ten solid solid fuel motor sensors are utilized. Eight extra sensors are added to the Taurus system for hatch and ejection determinations. In total, there are four hundred and twenty-eight sensors on the Taurus LMS to check all systems for proper functioning, and to permit necessary changes if malfunctions occur. Because of the weight constraint on the Taurus

system, only those sensors necessary for proper operation are used. The total weight of the sensors is approximately twenty-five kg. Using optical fiber wiring minimizes the amount of heat and radiation shielding. The entire mass of the sensors system on the Taurus service module is fifty kg. All sensors have been made double redundant and are 99.999% reliable.

Two modes of communication have been chosen to ensure reliability. The primary receiving station will be the Telemetry Data Relay Satellite System (TDRSS). It consists of two satellites that enable communications for 80 minutes of the 95 minute orbit. To communicate through TDRSS, frequencies must be chosen for their few atmospheric losses in transmissions to earth. The range of 1 to 10 GHz is the only range that meets this requirement. In the event communications cannot be made with TDRSS, a second choice for a receiving station will be direct transmission to earth. Although the number of earth stations is limited, there could be at least three used per orbit, which would account for about 30 minutes of transmission time per 95 minute orbit. The capsule will also receive transmissions from the Global Positioning System (GPS). These communications are used for navigation purposes, and operate on two frequencies: at 1.575 GHz, and 1.228 GHz. The antenna is placed on the capsule's surface facing outwards to GPS. The frequency assignments are based in the S band and are spaced so that not more than 500 MHz will be assigned for any one transponder. The bandwidth for these frequencies is determined from the amount of data that must be transmitted each second, and the clarity that the data must have in order to be received.

Link budgets are used to determine whether a signal will be receivable. The overall qualifying figure in the link budget determination is the carrier-to-noise ratio. This ratio must be positive, and at least 10 to 12.5 dB, in order for the signal to have good reception. The weakest link is the downlink to TDRSS. In this link the carrier-to-noise ratio has been reduced to the minimum needed for good reception.

To transmit and receive the desired frequencies, different antennas are needed to cover the gaps in the bands used. Each band requires a different type of antenna based on the necessary bandwidth. A dipole antenna will be implemented for the S-band, and housed under a skin blemish to avoid the need for mechanical deployment. There will be two of these antennas, one facing earth, and one facing space. The two antennas supply a mode of redundancy, and make serving earth stations and TDRSS efficient during orbit. The L-band antenna will be mounted on the skin in the same fashion as the S-band antennas, but only on the surface facing GPS satellites.

STRUCTURES

A tower or truss acts as the connection between the abort system and the capsule. It consists of a three-sided structure with a total of twenty-four members made of 6061-T6 aluminum. The abort engines are covered in a graphite/epoxy casing which is bolted directly to the top of the tower. Each longitudinal member of the tower is connected to the capsule by two short members which are fastened to the capsule by explosive bolts. The tower and abort system, therefore, can be jettisoned so that extra mass is not carried into space.

The structural framework of the capsule consists of 14 stringers and a skin thickness of 4.8 mm. I-beams stringers were chosen for two reasons: they are extremely resistant to bending, and flanges on each side make for easy fastening of the skin and pressure vessel. Each stringer will carry an axial loading of 5kN with a cross-sectional area of 0.00012 m². The hatch is designed to hold a small navigation window.

The service module structures are divided into four categories: explosive bolts for the capsule and service module, longitudinal stringers and transverse rings, shear flow, and a capsule supporting truss. These structures are designed to sustain a 10 gee axial acceleration, and a 1 gee sideways acceleration. A safety factor of 1.2 was used throughout the analysis.

Four equally spaced explosive bolt joints connect the capsule and the service module. A riveted-type butt joint was designed so that the bolts are of equal strength in shear, tension, and compression. There are four joints with two 225 mm explosive bolts on each joint.

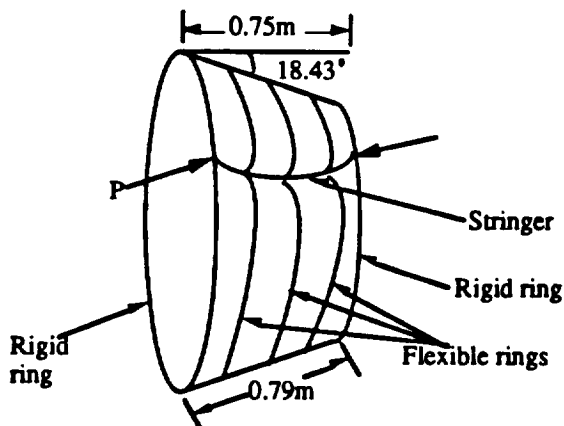


Figure 13. Stringer Under Compressive Load

Eight longitudinal stringers (I-beams with cross-sectional areas of 330 mm²) were chosen to carry the

axial load. Two stiff end rings provide rigid support against lateral displacement, while three relatively flexible intermediate rings give elastic lateral support. The five transverse rings are shown in Figure 13. The stringers and rings are made of 6061-T6 aluminum. The loading acting on each stringer is 11.587 kN.

The shear flow is only carried by the skin and has a maximum value at the bottom of the service module. The skin is also made of 6061-T6 aluminum, and has a thickness of 2 mm. Figure 14 presents the values for the forces and shear flow carried by the stringers and skin.

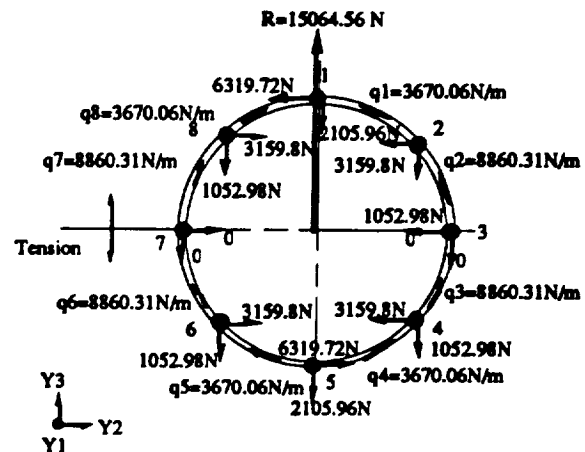


Figure 14. Forces and Shear Flow Carried by the Stringers

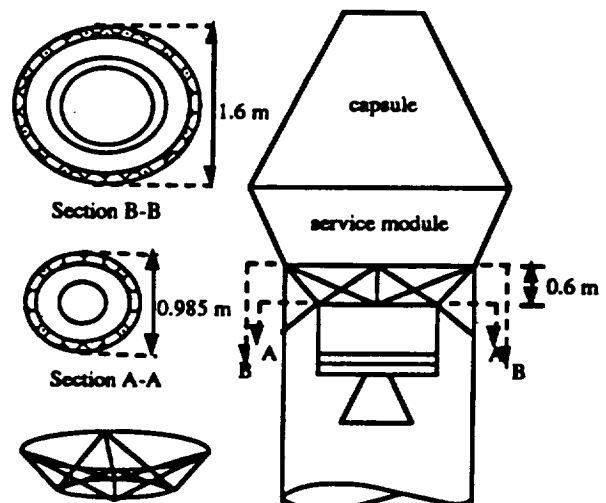


Figure 15. Capsule Configuration and Interface Dimensions

A truss structure will interface the Taurus LMS and the Taurus booster. The design constraints of this structure are prescribed by the dimensions of the service module and the mechanical interface of the Taurus booster. These dimensions are shown in Figure 15. In addition, the structural interface is designed to take a vertical force of 8 gees and a horizontal force of 1.7 gees.

The truss structure will be made of 60601-T6 aluminum and will weigh approximately 31 kg. The axial stresses in each member of the truss are below the yield stress of this material (542 MPa). The design loads with a margin of safety are: 108 kN in the vertical direction, and 23 kN in the horizontal direction. The volume of the material used is 0.0112 m³. The interface will be equipped with explosive bolts around both the upper and lower circular perimeter. The bolts will be equipped with springs to allow for separation from the service module once the orbit is circularized.

RE-ENTRY AND RECOVERY

The first portion of the re-entry trajectory is a free-flight phase which takes the spacecraft from its orbit to the atmosphere (assumed to begin at 120 km). The second portion is the atmospheric flight phase, during which the spacecraft flies through the atmosphere to land. A de-orbit burn is necessary to slow the spacecraft down so that it falls from its orbit to a transfer orbit that brings it down to the atmosphere. Upon reaching the atmosphere, aerodynamic forces will overcome orbital mechanics and control the trajectory. The burn determines the spacecraft's new orbit which sets its flight path angle and velocity at atmospheric interface. The ΔV required to de-orbit is 140 m/sec from an altitude of 300 km. This corresponds to having a re-entry flight path angle of 2.0°. Time of flight and angular distance traveled in the free-flight portion were computed by the method of Eccentric Anomaly (Ref 8). It will take 18 minutes and 52 seconds to fly from the de-orbit burn altitude of 300 km to 120 km. During this time the spacecraft will fly 77.14° around the earth. This will allow the location of the de-orbit burn performance to determine a selected touchdown site.

A computer program was written to predict the atmospheric flight re-entry trajectory. The time of flight between crossing 120 km and earth impact is 775 seconds. The spacecraft gains altitude for 50 sec at an altitude of approximately 59 km before continuing to fall. The velocity does not change significantly until 150 sec into this portion of the flight, at which time the craft has re-entered to 80 km and aerodynamic forces begin to influence the spacecraft's trajectory. The maximum spacecraft

deceleration is 3.07 gees. The craft will have slowed down to 63 m/sec (0.19 Mach) by the time 3 km is reached so that the parachutes can be deployed.

The Taurus LMS will use a phenolic-nylon ablative heat shield with a heat combustion of 12 MJ/kg to protect the capsule from the aerodynamic heating loads upon re-entry. The thermal protection system is composed of a carrier support panel, mounted to the capsule structure via channel beam panel supports, with a layer of insulation between the panel and the skin at the capsule (Ref 9). The capsule will undergo a maximum wall temperature of 1606 K and a maximum heating rate of 563.4 KW. The TPS for the walls of the capsule will be the same as for the heat shield, but bonded directly to the skin of the spacecraft.

The Taurus LMS recovery system consists of two round parachutes deployed simultaneously at a re-entry speed of Mach 0.19. The deployment sequence will begin at 3 km above sea level, at which point a computer command will fire explosive bolts on both parachute hatches, allowing the mortar-deployed pilot chutes to pull the two canopies out into the windstream. Once the parachutes are inflated, the capsule will begin a 10 minute canopy descent to the ocean, inflating its pontoon before splash down. Upon splash down, the canopies will be released and dye markers will be ejected through the parachute hatches. A radio beacon will help guide the recovery aircraft and vessels to the Taurus LMS.

Costing

The costing of the Taurus LMS was done as an expendable vehicle that will become operational with one mission in May 1995. The Taurus LMS will have 3 missions in 1996. The project will be disbanded at the end of the fourth mission to allow the space administration to proceed with the application of the Taurus LMS technologies.

The costing of the Taurus LMS was divided into two parts, Nonrecurring and Recurring. Nonrecurring costs are the costs of Design, Development, Testing and Engineering of the spacecraft, as well as the project management and integration costs. Recurring costs are the costs of the individual spacecrafts as well as the Integration, Assembly and Checkout of the spacecraft, as well as booster and launch/recovery costs. (Ref 10) The Nonrecurring costs of the project will be \$1,148.3 million in 1991 dollars. The total project costs would be \$1491.31 million. This results in cost of \$372.83 million per flight.

GROWTH POTENTIAL

Growth potential for the Taurus LMS takes two forms. The first would involve an increase in the Taurus booster capabilities. The second would entail

launching on a different booster. Assuming the former occurs, the ability to launch with an additional 300 kg of fuel would provide for the necessary ΔV to enable a rendezvous and docking with the Space Station Freedom. Under this scenario, the Taurus LMS could be used for small-scale emergency supply deliveries, space station crew rotation, or as an emergency lifeboat docked at the space station. Moreover, it could perform a visual satellite inspection to determine the cause of failure and evaluate the feasibility of in-orbit repair.

The second option would be to launch the Taurus LMS on a Delta booster. This would permit nearly four times the mass to be launched into orbit, making the aforementioned missions possible.

CONCLUSION

The Taurus Lightweight Manned Spacecraft is a stepping stone for the Alternative Manned Spacecraft program that offers a foundation to build a new space program. The use of the Taurus Booster results in the design of a limited mission vehicle that is capable of putting one man into Low Earth Orbit for a 24 hour mission with minimal life support and minimal crew member comfort. The purpose of the LMS project was to prove that a man can be put into space using a low payload booster.

ACKNOWLEDGMENTS

This work was conducted with the support of the Space Design Program of the University Space Research Association. This support is gratefully acknowledged. Principal author Michelle Bosset was assisted by Kevin A. Chase and James Clegern. This paper summarizes the work of Michelle Bosset, Gregory Bulla, Kevin A. Chase, James Clegern, M. Sean Connelly, Andy Est, Chris Henry, Michael Kaczmarek, Bernie Kelm, Khan Le, Dennis Loveless, Curtis Neidhart, TzuHeng Peng, Jennifer Plotkin, J. Alan Sandusky, Deborah Sewell, Jeff Travisano, Eric Vandersall, Edison Villacis, and Anthony G. White. Faculty advisors were Dr. David Akin, Dr. Mark Lewis and Mr. Charles Lind.

REFERENCES

1. "Manned Spacecraft: Engineering Design and Operation": ed. Paul E. Purser, Maxime A. Faget, and Norman F. Smith, Fairchild Publications, Inc., New York, 1964.
2. Singh, Jasbir: "Heat Transfer Fluids and Systems for Process and Energy Applications," Marcel Dekker, Inc., New York, 1985.
3. Sutton, G. P., "Rocket Propulsion Elements," John Wiley & Sons, Inc., New York, 1986.
4. Huzel K. Dieter and Huang H. David, "Design of

Liquid Propellant Rocket Engine," NASA Scientific and Technical Information Office, Washington DC, 1971.

- 5 Morgan, N. E. and W. D. Morath, "Development of a Hydrogen-Oxygen Internal Combustion Engine Space Power System."
6. Adapted from Rockwell's block diagram for the Shuttle's Data Processing System.
7. Spitzer, C. R., "Digital Avionics Systems," New Jersey: Prentice Hall Inc., 1987.
8. Bate, R. R., D. D. Mueller, and J. E. White: "Fundamentals of Astrodynamics," Dover Publications, New York, 1971.
9. Dow, M. B., and Thompkins, S. S., "Materials and Design for Ablative Heat Shields," NASA TM X-2570, 1972.
10. National Aeronautics and Space Administration, "JSC Cost Model Summary" 1991 (converted by D. Akin)

Chapter 1: Systems Integration

Section 1.1: The Taurus LMS Spacecraft

1.1.1 Introduction

The Taurus Lightweight Manned Spacecraft (LMS) is a single crew, short mission duration spacecraft. The spacecraft is configured with a reentry capsule and a service module that is disposed of before reentry. The capsule will carry the pilot, the main and secondary life support systems, all of the avionics, back up power supply and the parachute recovery system. The service module will carry the Orbital Maneuvering System, the main Reaction Control System as well as the Primary Power Generation System.

The configuration of a service module/capsule design was chosen for two main reasons. First, the mass of the spacecraft needed to be minimum on reentry to meet the required control characteristics. This could be accompanied by disposing of all unnecessary mass like the main propulsion systems. Second the interface to the Taurus Booster is only 0.9 meters in diameter and the minimum size determined to place a man in a capsule is 2.1 meters in diameter. This constraint dictates a step down that is met in two stages. One is achieved by the Service Module and the second is achieved by the Structural Interface.

The configuration of the single crew capsule was derived after a semester long trade study on the benefits and drawbacks of two and one member crews by all the groups. Since the major constraint of the project was the low mass payload of the Taurus booster, the single crew capsule was the best choice for the project since it offered the lowest mass configuration.

1.1.2 LMS Dimensions

The size of the LMS was predominantly chosen by the constraints imposed by the human factors group to place one man into a space capsule. The base of the capsule (above the heat shield) is 2.1 meters in diameter. This dimension was determined to be the smallest possible to put one man into the capsule. The top of the capsule is 0.74 meters, which is the minimum dimension required by the propulsion group to attach the abort system. The height was fixed at 2.1 meters to allow the sides of the capsule to be straight and to give an angle of 18 degrees.

The top dimension of the service module was fixed by the bottom dimension of the capsule at 2.1 meters in diameter. The height was fixed at .75 meters. This dimension was chosen by the constraints of having the propulsion system in the service module. The bottom dimension was fixed at 1.6 meters in diameter for attaching the Taurus booster structural interface. (see Fig. 1.1A)

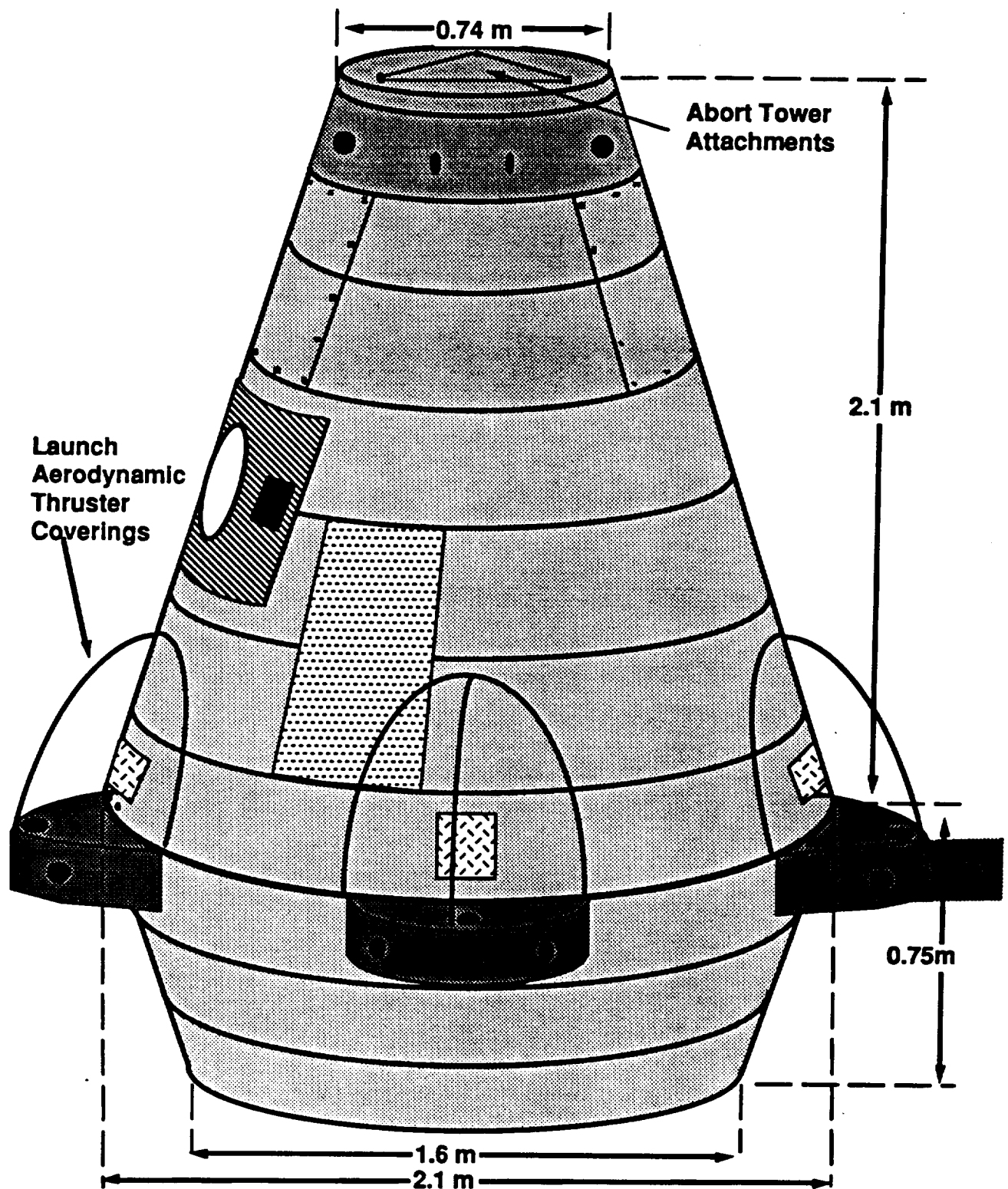


Figure 1.1A: Spacecraft Exterior and Dimensions

1.1.3 The LMS Mass Budget

The major constraint on the design of the LMS was the mass of the spacecraft. The maximum payload mass of the Taurus Booster is 1300 kilograms to a 300 km Low Earth Orbit. Since this was the major constraint a detailed systems mass break down was kept. The final numbers are presented in table 1.1A. The total mass for the Taurus LMS is 1168.21 kg. This figure includes a budget margin of 50 kg. for miscellaneous hardware. This launch mass is under the maximum payload allowable for the booster, therefore the Taurus LMS is a viable program.

The mass budget listed in Table 1.1A is corrected to show the mass gains from ejecting the abort system and the booster interface before the low earth orbit is achieved.

Table 1.1A: Systems Mass Budget

System	Mass (kg.)
Capsule Structure	133.88
Life Support system	120.00
Crew Cabin	112.50
Abort system (effective)	40.00
RCS capsule	9.00
RCS Fuel and Tank	0.54
RCS Oxidizer and tank	0.86
RCS Helium and tank	1.29
Batteries	21.05
Thermal control	40.00
Communications	11.50
Sensors	40.00
Data Processing	45.00
Guidance and Control	15.20
Parachute system	60.00
Service Module	150.00
Structure	
Interface to capsule	20.00
RCS Main	20.00
OMS engine	20.00
Fuel and Tank	85.64
Oxidizer and tank	106.52
Helium and tank	4.73
Power Generator	25.20
Booster Interface	31.30
(effective)	
Misc. Hardware	50.00
-----	-----
TOTAL	1168.21 kg

1.1.4 Mass Moment of Inertia Calculation

A detailed Mass Moment of Inertia calculation was required for the balancing of the capsule, the Attitude and Control Systems, and for the design of the Reaction control systems.

A first approximation was done for a homogeneous body with the same shape and approximate mass of the spacecraft. Using commonly known dynamics formulas the values of the moments of inertia are given below. (in Kg-M²) The c.g. location of the spacecraft was calculated to be along the center line and 1.16 meters from the base of the service module. The c.g. of the capsule alone was calculated to be 1.52 meters from the base of the capsule structure .

<u>MMI</u>	<u>Capsule</u>	<u>Spacecraft</u>
lxx	224.4	627.3
lyy	224.4	627.3
lzz	229.8	398.8

A second approximation was done for the systems components. An Excel spreadsheet was used and it is presented in Appendix A. For these calculations the basic equations of dynamics and the parallel axis theorem to transpose them around a central axis were used. The resulting values are higher but they were expected due to the placement of large components of some main systems near the outer sections of the capsule. The results are given below. (in Kg-M²) The c.g. was calculated to be .63 meters from the base of the capsule as was expected when compared to the homogeneous approximation. The off set of the capsule is .22 meters in the Y direction. (toward back of capsule)

<u>MMI</u>	<u>Capsule</u>	<u>Spacecraft</u>
lxx	813.3	1448.3
lyy	716.6	1346.2
lzz	494.8	689.8

For simplicity approximations had to be made for some of the systems. The structure of both the service module and the capsule were modeled as homogeneous shells of the same mass and same dimension as the space craft. The Human Factors group did the calculations of the seat and the pilot. Many of the avionics components were approximated by modeling them as homogeneous boxes of the sizes that were provided by the Avionics group.

Section 1.2: Reentry/ Crew Capsule.

1.2.1 Introduction

The crew capsule will be the major part of the Taurus L.M.S. and it will contain the Pilot, the dual life support systems, all avionics systems, and the emergency / reentry power systems. Mounted to the exterior of the capsule will be the Reentry Reaction Control System, the Abort System (during launch), Guidance and Navigation Sensors and the Communications Antennas.

1.2.2 Life Support Placement

The layout of the capsule was dictated by the shape of seat for the pilot. The primary and secondary life support systems are placed below the pilot's seat. A requirement of the main life support system was the need for circulation of air around the capsule so the inlet and exit of the system were placed on opposite sides of the capsule. The components of the system were placed to minimize the distance that coolant lines had to run to the external mounted radiator. The exact placement of the components can be best seen in Figures 1.2A-B.

The Human Factors Group had some design constraints pertaining to the placement of the life support equipment. The major constraint was that the pilot of the craft must be able to reach the LiOH and spare LiOH canisters as well as the Fire Extinguisher, the Survival Kit, Food and Water Supply and the First Aid Kit.

1.2.3 Avionics Placement

The placement of the Avionics Equipment had very few constraints. One was that the Computers, Transceivers and the Memory be placed in the capsule for heating concerns while the antennas and Guidance and Control sensors be placed on the outside of the capsule.

The computers and the transceivers were placed below the pilot's seat. The requirements placed on the communications antennas were that one must point to Earth and two must face away from Earth. This constraint dictated the placement of one antenna on the front of the capsule while two were placed on the back. The displays and the keyboard were placed in front of the pilot in the instrument panel.

1.2.4 Placement of the Propulsion and Power Systems

The only propulsion system in the capsule is the reentry Reaction Control System. The only constraint of the system was that it needed to be placed at the top of the capsule. The Auxiliary/Reentry Batteries are the only power system that is in the capsule. These batteries were placed on the back side of the capsule about half way up.

1.2.5 Placement of the Parachute Systems

One of the major problems in the layout of the capsule was the placement of the parachute and the reserve parachute systems. The size of the systems and the constraint that the systems must be at the top of the capsule for stability was a considerable problem.

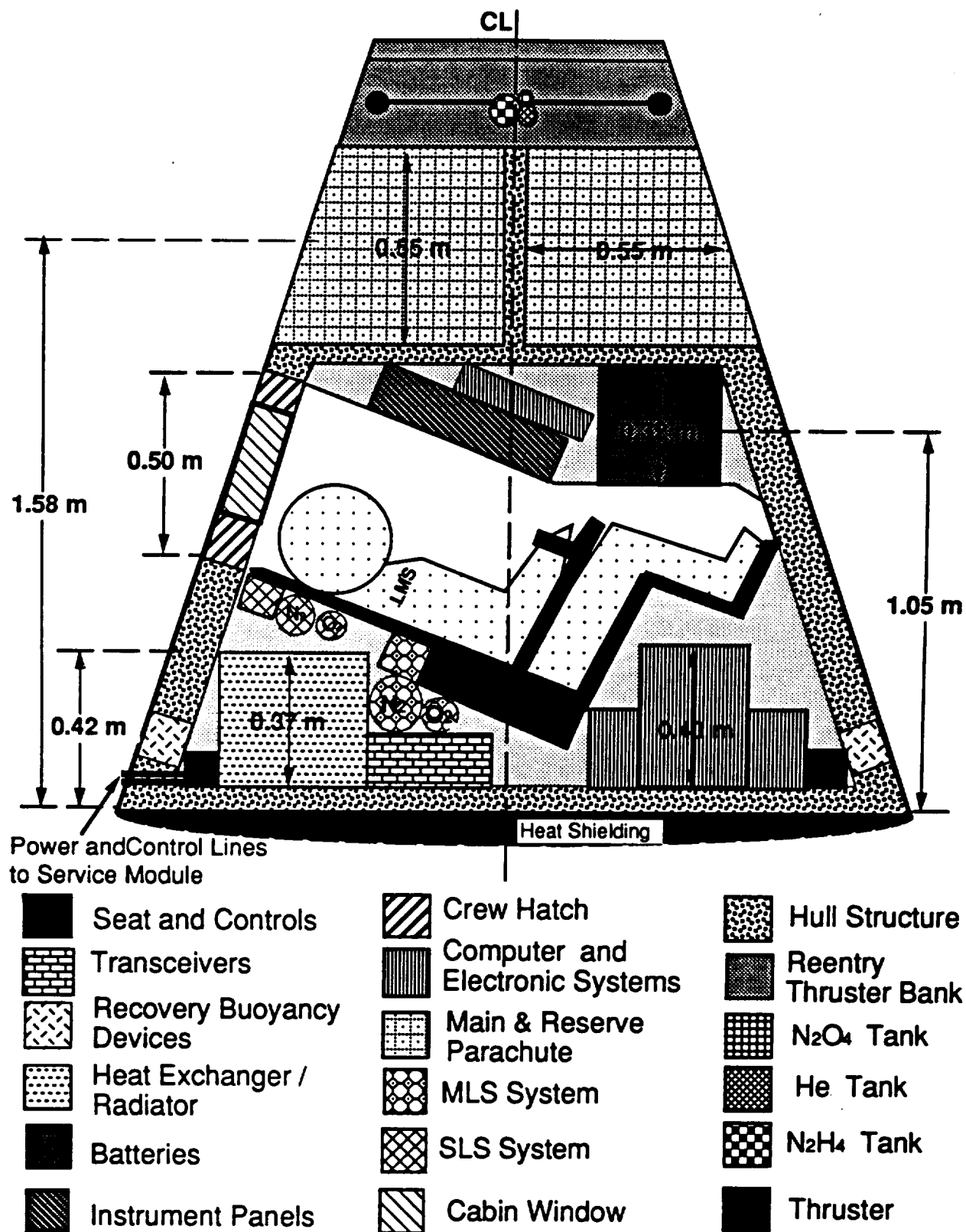


Figure 1.2A: Capsule Side View

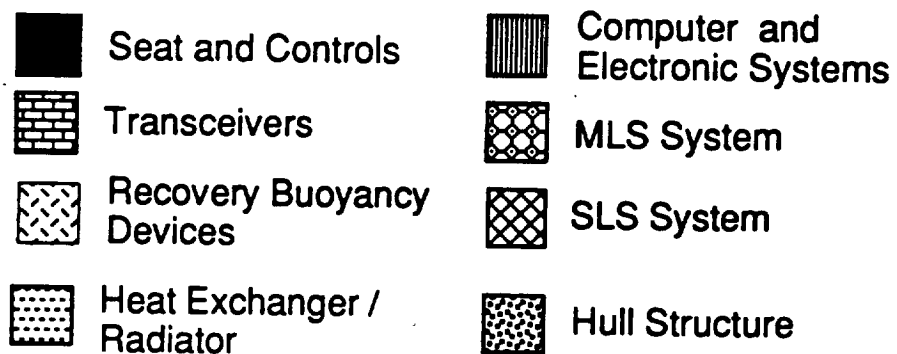
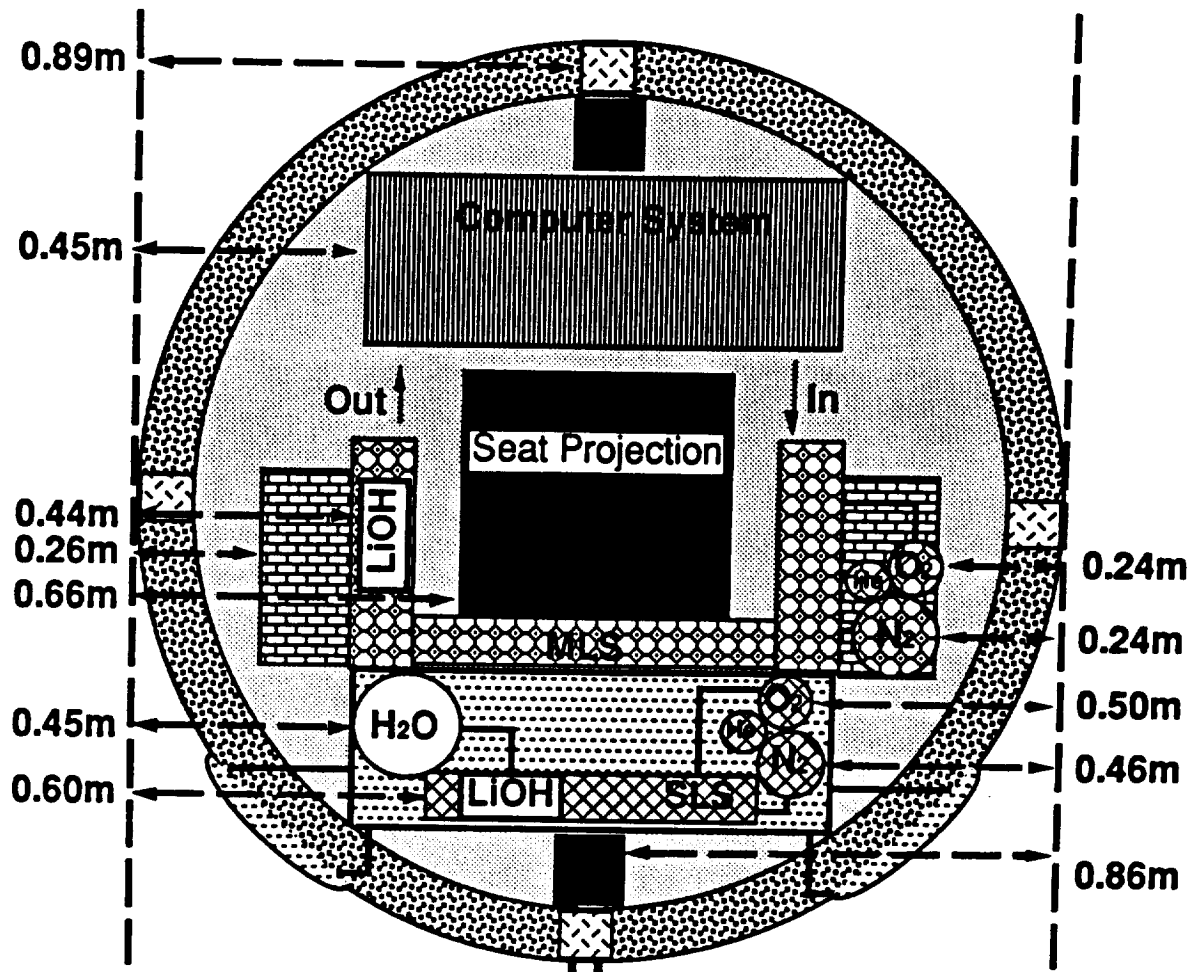


Figure 1.2B: Capsule Bottom View

Section 1.3: Service Module

1.3.1 Introduction to Service Module Systems

The Service Module carries the Orbital Maneuvering Engine, the Power Generation System and the main Reaction Control System. All three of these systems feed off a central fuel and oxidizer system. The Propulsion system sizes determined the height of the Service module.

1.3.2 Layout

The layout was dictated by the constraint that the nozzle of the OMS must be placed in the center of the Service Module. The Main components of the system, Fuel, Oxidizer, Helium tanks and the Power Generator are placed around that nozzle. All four components were placed on an imaginary plane 0.34 meter from the base of the service module and give plenty of clearance from the capsule heat shield. (see figures 1.3A-C)

The OMS, the RCS and the Power Generator all run from the same fuel and oxidizer systems. This creates a very complicated plumbing system for each thruster and is simplified by running all the lines to each thruster by placing them into a plumbing tube that runs on the outside of the service module.

The placement of the thrusters is not complicated because they are designed to bolt on to the outside of the service module and are placed at right angles to each other as prescribed by the propulsion group.

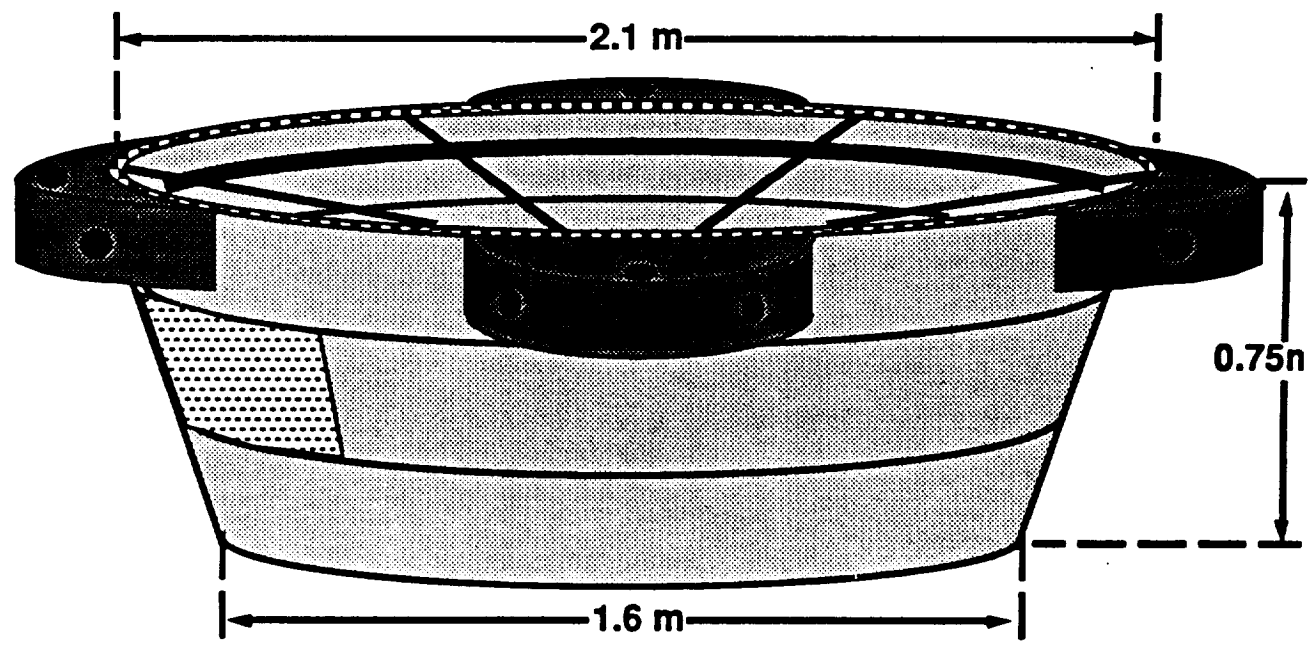


Figure 1.3A: Service Module Exterior View

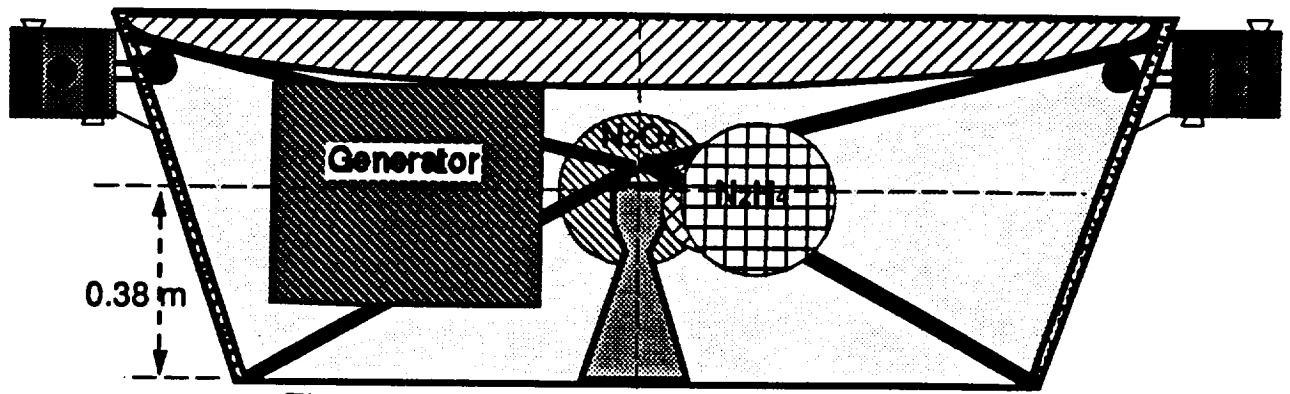


Figure 1.3B: Service Module Side View

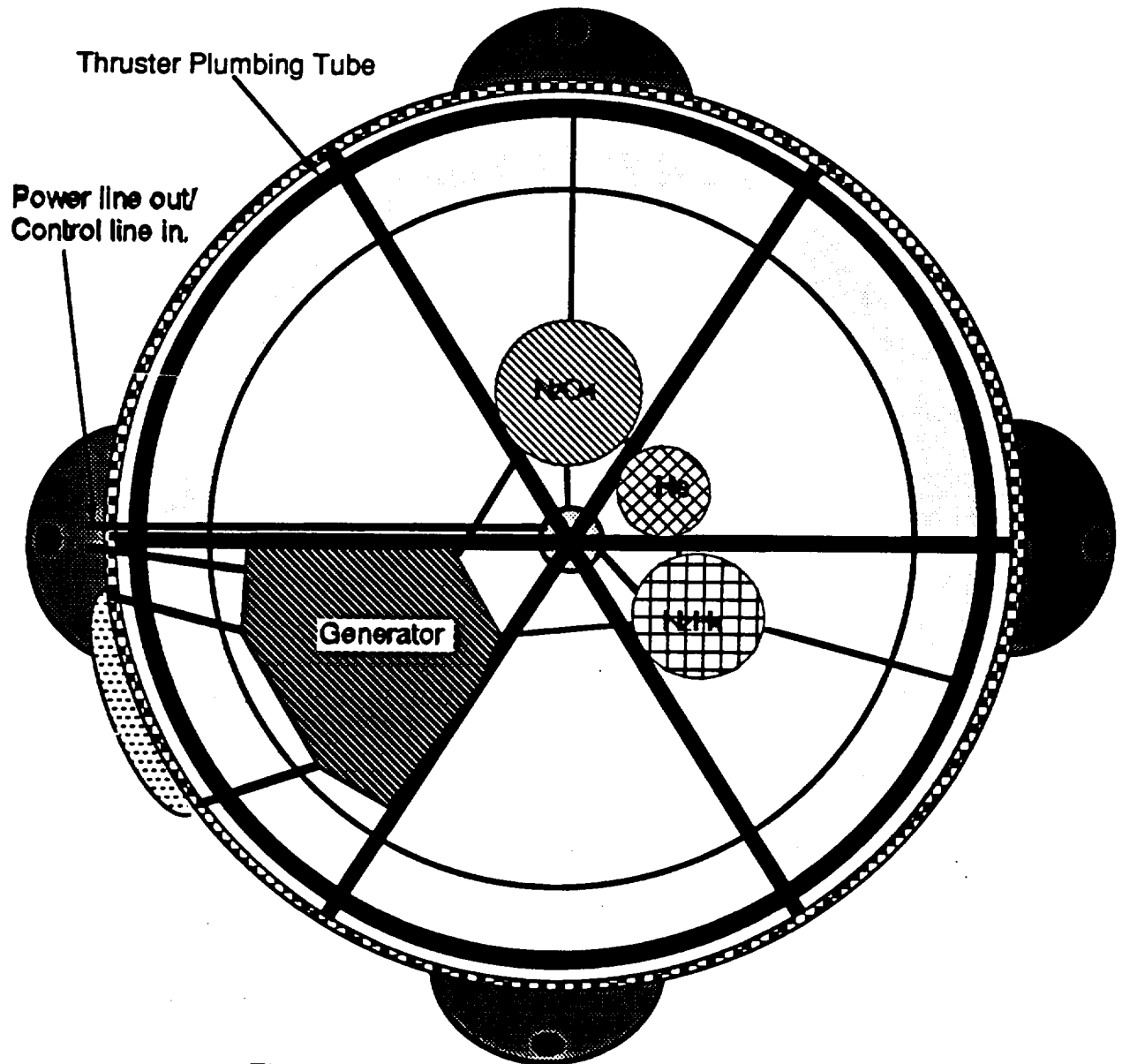


Figure 1.3C: Service Module Top View

1.4 Capsule Aerodynamics

1.4.1 Method

The capsule aerodynamics were modeled using modified Newtonian flow assumptions. The capsule aerodynamic surface during reentry is the heat shield. The heat shield was modeled as a segment of a sphere. Boundary values for the integration were chosen such that the dimensions of the modeled area were the same as those of the heat shield. Integration was carried out arithematically and a spreadsheet program was used to plot the results at a range of angles of attack. The degree of CG offset to achieve the desired L/D was determined by completing a moment balance of the capsule under reentry conditions. The equation obtained was simplified and a spreadsheet program was used to plot the variation of L/D with CG location.

1.4.2 Integration

The Newtonian flow equation states that $C_p = C_{d,max}[\sin^2\theta]$ (Anderson, 1990). Lift and drag components were determined geometrically to be

$$C_l = C_{d,max}[\sin^3\theta]$$

$$C_d = C_{d,max}[\sin^2\theta \cos \theta]$$

$$C_p = C_{d,max}[1/2 \theta - 1/4 \sin 2\theta]$$

$$C_l = C_{d,max}[-1/3 \sin^2\theta \sin \theta + 2/3 \cos \theta]$$

$$C_d = C_{d,max}[2 \sin \theta]$$

The boundary values for the integration were determined by computing the angle normal to the sphere at a radius of 1.05 meters. This angle was determined to be 12.1 degrees (0.212 radians). Because the coordinates were not transformed to body based coordinates, it was nescessary to integrate from $\pi/2-\theta$ to $\pi/2+\theta$ with θ in this case being defined as the boundary value of 12.1 degrees.

1.4.3 Variation of Angle of Attack

The effect of variation in angle of attack was determined by computing the effect of this variation on the boundary values of the integration. The value of the angle of attack, α , was added to the boundary values on either side of the integration. The results of calculations for angles of attack for values ranging from zero to 12.1 degrees are presented in Appendix B. Values are provided for C_p , C_l , C_d , and L/D.

1.4.4 Determination of CG Location Effect on L/D

The effect of an offset CG on the L/D of the vehicle was determined by completing a moment balance for the vehicle under reentry conditions. The moment balance is presented in Appendix B. From the free body diagram, the moment balance equation was determined to be

$$\Delta(Ma + Mg \sin(\psi - \alpha)) = (p - \Delta)C_l q S$$

where Δ is the displacement of the CG in the x (capsule coordinate) direction, ψ is the flight path angle, α is the angle of attack, p is the radius of curvature, M is the capsule mass at reentry, a is the acceleration of the capsule, and the other terms are as standard usage. As the vehicle was initially assumed to have a reentry acceleration of 9-10 gee, it was decided to ignore the body force and the flight path angle term was eliminated. The equation was simplified and solved for CG offset to determine that

$$\Delta = (p - \Delta)C_l q S / Ma$$

The offset was thus determined to be dependant on dynamic pressure if a constant L/D was to be maintained. In order to approximate the L/D dependence on CG offset this equation was solved assuming conditions at maximum deceleration. Charts of these results are presented in Appendix B. From these charts it was determined that a L/D of 0.25 would be a reasonable value to attempt. Charts and graphs showing coefficients, L/D, and CG offset in the region of 0.25 are provided in Appendix B. Physical constraints caused by the limited dimensions of the capsule may limit CG offset.

Section 1.5: Aerodynamic Heating

1.5.1 Equilibrium Equations

One of the primary concerns of reentry is the aerodynamic heating on the Taurus LMS capsule. There are many different advanced methods to calculate the heating rate on the surface of a blunt body, however, their accuracy is not significantly better than simpler, more approximate methods. For the analysis, the spacecraft was assumed to be in thermodynamic equilibrium. There are four basic parts to the equilibrium equation. The primary term is the convective heating term, which is due to the high velocity air impacting the craft. This is equilibrated by three terms: the radiative cooling, due to blackbody radiation of the heat shield; the dissociative cooling, due to the dissociation of the air; and the ablative cooling, caused by the burning, or sublimating of the heat shield. These three terms yield the equation:

$$Q_{\text{convective}} = Q_{\text{radiative}} + Q_{\text{dissociative}} + Q_{\text{ablative}}$$

The convective term is due to the aerodynamic heating at the surface of the craft. For the first cut analysis, the entire heat shield was assumed to have the same heating rate as the stagnation point. Although this will give a slightly higher total heat than a more accurate solution, this difference is insignificant for a first cut estimate. This approximation also has the advantage of allowing the position of the stagnation point to vary without changing the heating load over the heat shield. A good approximation of the stagnation heating rate is given in the following equation as:

$$q_w = \rho_{\infty}^N V_{\infty}^M C$$

For a spherical surface, $N = 1/2$, $M = 3$ and

$$C = 1.83 \times 10^{-8} R^{-1/2} \left(1 - \frac{h_w}{h_o}\right)$$

In the above equations: q_w = heating rate at the wall, ρ_{∞} = freestream density, V_{∞} = freestream velocity, R = radius of curvature, and h_w and h_o = enthalpy at the wall and total enthalpy, respectively (Anderson, 1989). Since enthalpy is proportional to temperature, and the total temperature is a function of mach no., for $\gamma = 1.4$, this term becomes:

$$Q_{\text{convective}} = \rho_{\infty}^{1/2} V_{\infty}^3 \left[1.83 \times 10^{-8} R^{-1/2} \left(1 - \frac{T_w}{T_{\text{atm}}(1 + .2M^2)}\right) \right]$$

The radiative cooling is due to the electromagnetic radiation given off by any hot body. The atmosphere around the capsule is assumed to be transparent to the radiation, thereby allowing the body to radiate off some of its heat. The radiative term is given as:

$$Q_{\text{radiative}} = \epsilon \sigma T^4$$

Where ϵ is the emissivity of the surface, σ is the Stefan-Boltzmann constant, and T is the surface temperature (Ohanian, 1985).

The dissociative cooling is a result of the energy absorbed by the dissociation of the air molecules at high temperature. The energy of air at a given temperature can be determined from standard atmospheric tables. From this energy we can get the heating rate due to dissociation. For the first cut calculations, the energy of the air was approximated by obtaining a linear fit of the energy in the temperature region of interest. For this analysis, the linear fit was determined to be:

$$E = 0.8438T - 67.9$$

(Hansen, 1959). The rate of dissociation is also dependent on the volume of the dissociated air, which depends on the freestream density and velocity. This gives a dissociative heating rate of:

$$Q_{\text{dissociative}} = \rho_{\infty} V_{\infty} (0.8438T - 67.9)$$

The ablative heating rate is dependent on the type of heat shield used. For a radiative heat shield, this term would be zero because this type of shield does not ablate. The rate of ablation for ablative heat shields depends on the type of materials the shield is made of. The Taurus LMS will use a phenolic-nylon ablator with a heat of combustion of 12 MJ/kg. This material also has an ablation rate that varies linearly in the temperature range of interest. The ablative heating rate then becomes:

$$Q_{\text{ablative}} = 101.28T$$

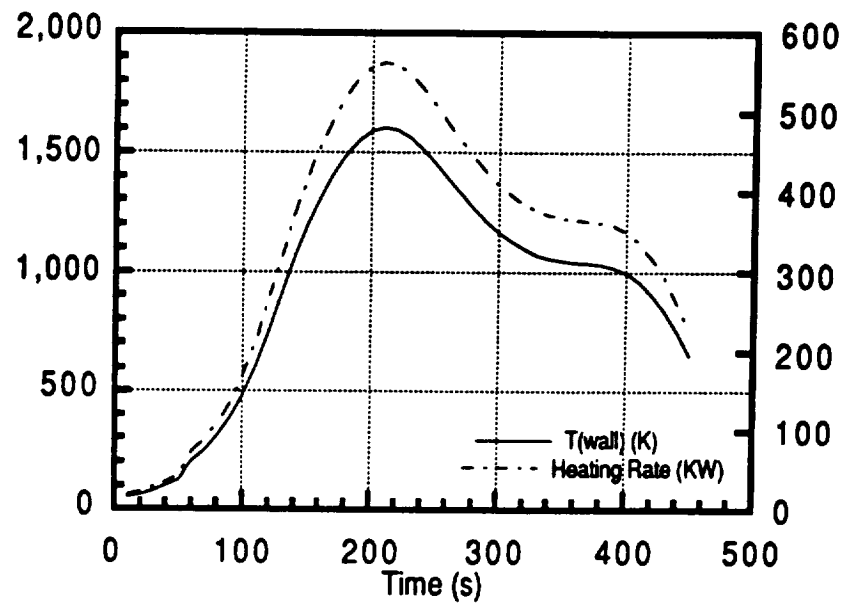
(Clark, 1973). By substituting these terms into the original equilibrium equation above, an equation of thermal equilibrium as a function of temperature is obtained. Using a computer program developed for the Taurus LMS capsule, this equation can be solved for the equilibrium temperature at the wall for a given velocity and density.

1.5.2 Taurus Reentry Heating

Using the reentry profile given by Mission Analysis, the heating rate can easily be determined at any time. A program was developed to determine the equilibrium temperature and from this the heat absorbed by the ablative shield. The velocity and altitude were entered into the program at ten second intervals. From these intervals the above equations were solved for the equilibrium wall temperature. This temperature is then plugged into the ablative heating rate expression to obtain the instantaneous heat absorbed by the heat shield. This heating rate can then be integrated over the surface of the capsule and the time of reentry. The results of this process are shown in Fig. 1.5A. The capsule will undergo a maximum wall temperature of 1606 K and a maximum heating rate of 563.4 kW. These values are very reasonable compared to previous reentry vessels. The total heat to be ablated by the heat shield was found to be 148.6 MJ. A complete description of this procedure and results can be found in Appendix D.

The thermal protection system design and structure will be discussed in section 6 of chapter 6.

Fig. 1.5.A Reentry Heating Profile



Section 1.6 Costing

1.6.1 General Costing

The Taurus LMS shall be costed as an expendable vehicle that will become operational with one flight in 1995. The number of missions would be three in 1996 and then the project would be disbanded after the fourth mission. The cost of making the spacecraft operational, the non recurring cost, is explained first.

Using a detailed mass breakdown of the LMS and grouping these items into the categories listed in the leftmost column of Figures 1.6B and 1.6C (NASA, 1991), the initial Design, Development, Testing and Engineering Cost (DDT&E cost) and the First Unit Cost are calculated. The items that are used in the costing scheme are shown in Figure 1.6A, with notations in parentheses for items that are used more than once in the design. For these items, an effective mass is calculated because only the first item goes through the design phase. Further items are then built exactly as the first one with an assumed 80% learning curve (Akin, 1991). Because the costing scheme yields values based on the masses of each system, it is inaccurate to figure the DDT&E and First Unit costs by calculating the cost of each individual item and then applying the learning curve. Hence, the effective mass principle is used. The effective total masses for each system are then plugged into the equation:

$$\text{System Cost} = A * (\text{System Mass})^B \quad (\text{\$millions 91})$$

This is done with different values of A and B for each system. The values of A and B also vary when doing a DDT&E cost analysis and a First Unit cost analysis. These values are listed with results for the DDT&E costing in Figure 1.6B and for the First Unit costing in Figure 1.6C. Please note that the system masses used for these calculations are dry masses (i.e. fuel, oxidizer, gases etc. are not included). The DDT&E costs come out to \$763.62 million (\$91) and First Unit costs are \$72.38 million (\$91).

The next step is to calculate the total direct cost of the program. This is simply the sum of the DDT&E cost, the Software Development Cost and the Systems Engineering and Integration Cost. The formula for calculating the Software Development Cost is:

$$\text{Software Cost} = 0.001925 * (\# \text{ of compiled words}) \quad (\text{\$millions 91})$$

For the craft, it has been assumed that the software will not change once written and that it will take 100,000 compiled words to perform all needed operations (Akin, 1991). This will cost \$192.5 million (\$91). Systems engineering and integration is calculated by:

$$\text{Systems Engineering \& Integ.} = 0.0084 * (\text{DDT\&E costs}) \quad (\text{\$millions 91})$$

With DDT&E costs of \$763.62 million, this yields a cost of \$6.41 million (\$91) and then a Total Direct Cost of \$962.53 million (\$91). Using the Total Direct Cost, we can now calculate some other important costing parameters. These are the Project

Management Cost, the Subsystems Development Cost and the Ground Support Equipment Cost. The formulae for these costs are listed below:

$$\begin{aligned}\text{Project Management Cost} &= 0.030 * (\text{Total Direct Cost}) \quad (\$ \text{millions } 91) \\ \text{Subsystems Development Cost} &= 0.073 * (\text{Total Direct Cost}) \quad (\$ \text{millions } 91) \\ \text{Ground Support Equipment} &= 0.090 * (\text{Total Direct Cost}) \quad (\$ \text{millions } 91)\end{aligned}$$

The Project Management Cost is \$28.88 million, the Subsystems Development Cost is \$70.265 million and the Ground Support Equipment Cost is \$86.63 million (all \$91). The sum of these three values and the Total Direct Cost is the cost of making the spacecraft operational, the Total Non Recurring Cost (C_{NR}) of the spacecraft. This non recurring cost is \$1.1483 billion (\$91).

The next step is to calculate the recurring costs for the LMS program. These are the costs for each mission. The first step is to calculate the Total First Unit Cost. This is the sum of the First Unit Cost and the cost of Integration, Assembly and Checkout, which is calculated using:

$$\text{Integration, Assembly and Checkout} = 0.596 * (\text{First Unit Costs})^{.832} \quad (\$ \text{millions } 91)$$

This value turns out to be \$21.01 million (\$91). This yields a Total First Unit Cost (C_1) of \$93.39 million (\$91). Other recurring costs include the cost of the booster, the cost of launch operations and crew training and the cost of recovery operations. The booster will cost \$7 million per flight, which will be assumed to be constant throughout the mission lifetime. Launch operations and crew training are also to be provided by Orbital Sciences Corporation (OSC), and the cost of these operations is not known exactly. At this point, it will be assumed that \$3 million will cover this cost per mission during the mission lifetime. The LMS is to land on water and it will be necessary to rent the U.S. Navy for this purpose. A nominal rescue operation would entail renting two destroyers and a range instrumentation ship for five days. The destroyers can be rented for \$150,000 per day and the range instrumentation ship can be rented for \$200,000 per day (ref. Institute for Strategic Defense Studies, 1989-1990). This will cost \$2.5 million per mission which leads to a nominal launch and recovery operations cost of \$5.5 million for the spacecraft. Thus we now have a final formula to calculate the cost of the Taurus program.

$$\text{Total Cost} = C_{NR} + C_1 \sum_{i=1}^N i^p + N * (C_{\text{booster}} + C_{\text{Launch \& Recover}})$$

where: $p = -0.324$ for an 80% learning curve

N = number of missions = 4

C_{NR} = Non Recurring Cost, C_1 = Total First Unit Cost

The total cost for the program adds up to \$1491.31 million (\$91) (Figure 1.6D).

1.6.2 Cost Discounting

The key idea underlying cost discounting is the concept of present value. This concept states simply that a dollar in hand today is more valuable than a dollar in hand in the future. This is so for two reasons. The first is inflation, but this is really not taken into consideration in this simple analysis. The second is opportunity cost, which means that a dollar in hand today can be invested and earn interest (it can also be spent to satisfy some immediate need, but here it will be assumed the dollar is intended for investment). It will be also assumed that the interest rate is 10%, or 0.1, as is generally used in this type of analysis (ref. Akin, 1991). The cost of the program for each year (Constant Year Cost) will first be calculated and then will be multiplied by the discounting rate.

$$\text{Present Value}_i = \text{Constant Year Cost}_i * (1 + \text{interest rate})^{-J}$$

where: i = the year being discounted

J = the number of years between the the Constant Cost year and the present year

The Net Present Value is then just the sum of the present values for each year in the discounting period. Here N is the number of years to be summed.

$$\text{Net Present Value} = \sum_{i=1}^N (\text{Present Value})_i$$

The Net Present Value then becomes the Total Cost of the program and the benefits of this analysis is simply the difference between the Total Cost calculated in Section 1.6.1 and the Net Present Value calculated here. Figure 1.6D presents the costs for each year of the program as calculated using the cost analysis utilized in Section 1.6.1 and the present values associated with each of those years. Note that it is assumed that the non recurring costs to make the spacecraft operational are divided evenly through years 1992-1994 and then discounted. The Net Present Value (or new Total Cost) of the program is \$1171.46 million dollars (Figure 1.6D). With 4 missions, this works out to \$292.87 million dollars per mission (\$91).

Table 1.6A Items to be Costed

ECLSS/CREW ACCOMMODATIONS

<u>Item</u>	<u>Eff. Mass (kg)</u>
MLS Circulation Fan	1.0
MLS Water Separator/Heat Exchanger	16.12
MLS Electrical Reheater	0.5
MLS Coolant Pumps (2 @ 1.0 kg each)	1.80
MLS Radiator	10.0
LiOH Canisters (3 @ 1.211 kg each)	3.236
SLS LiOH Cartridge	2.422
SLS Circulation Fan	0.5
SLS Water Separator	5.0
SLS Coolant Water Pump	0.5
Pressure Suit	10.0
Fire Extinguisher	4.5
First Aid Kit	0.5
Survival Pack	17.7
Crew Cabin (Seat)	<u>16.0</u>
TOTAL	90.22

CRYO TANKS

<u>Item</u>	<u>Eff. Mass (kg)</u>
Nitrogen Tank	1.0
Oxygen Tank	1.0
Helium Tank	<u>1.0</u>
TOTAL	3.0

Table 1.6A Items to be Costed Continued

AVIONICS

<u>Item</u>	<u>Eff. Mass (kg)</u>
Communications	
S-Band Transceiver/Receivers (2 @ 3.0 kg each)	5.40
Switch	0.5
Antenna Dipoles(2 @ 1.0 kg each)	1.80
RF Harness	1.0
Audio Mixer	2.0
Data Processing	
Processors with RAM (2 @ 5.0kg each)	9.00
Displays (2 @ 3.0 kg each)	5.40
Mass Memory	8.0
Keyboard	3.0
Buses (6 @ 2.0 kg each)	8.58
Engine Interfaces (2 @ 3.0 kg each)	5.40
Sensors	<u>40.0</u>
TOTAL	90.08

STABILITY AND CONTROL

<u>Item</u>	<u>Eff. Mass (kg)</u>
GPS Receiver	2.1
Antenna	1.1
Inertial Navigation System (INS)	3.0
Attitude Sensors	
Sun Sensors (2 @ 1.5 kg each)	2.70
Horizon Sensors (2 @ 3.0 kg each)	<u>5.40</u>
TOTAL	14.3

ELECTRICAL POWER

<u>Item</u>	<u>Eff. Mass (kg)</u>
Batteries (2 @ 10.525 kg each)	18.93
Power Generator	<u>25.2</u>
TOTAL	44.13

Table 1.6A Items to be Costed Continued

STRUCTURES

<u>Item</u>	<u>Eff. Mass (kg)</u>
Booster Interface	31.3
Capsule Structure	200.0
Service Module Structure	150.0
Abort Tower	6.0
Thermal Protection System	40.0
Parachute System	
Parachutes (2 @ 19.32 kg each)	34.75
Pilot Chutes (2 @ 2.0 kg each)	3.60
Risers (2 @ 3.0 kg each)	5.40
Bags (2 @ 2.0 kg each)	3.60
Bridles (2 @ 0.5 kg each)	0.90
3 Ring Devices (2 @ 1.0 kg each)	<u>1.80</u>
TOTAL	477.35

RCS/PROPULSION SYSTEM

<u>Item</u>	<u>Eff. Mass (kg)</u>
RCS Engines (20 @ 1.071 kg each--12 in capsule, 8 in SM)	11.23
OMS Engine	20.0
Abort System	
Abort Motors (3 @ 47.96 kg each)	119.87
Igniter	0.19
RCS Tanks (for top RCS engines)	
Fuel Tank	0.2
Oxidizer Tank	0.3
Helium Tank	1.0
OMS Tanks	
Fuel Tank	1.66
Oxidizer Tank	1.46
Helium Tank	<u>3.00</u>
TOTAL	158.91

Table 1.6B DDT&E Costing

<u>System</u>	<u>A</u>	<u>B</u>	<u>Eff. Mass(kg)</u>	<u>Cost(\$M91)</u>
ECLSS/Crew				
Accommodations	32.691	0.414	94.22	214.64
Avionics	24.817	0.579	90.06	336.06
Stabilization and Control	13.834	0.516	14.30	54.59
Structures/TPS	5.226	0.491	477.35	108.01
Electrical Power	1.821	0.584	44.13	16.63
RCS/Propulsion System	0.411	0.876	158.91	34.83
Cryo Tanks	0.120	0.885	3.0	<u>0.32</u>
TOTAL				765.08

Table 1.6C First Unit Costing

<u>System</u>	<u>A</u>	<u>B</u>	<u>Eff. Mass(kg)</u>	<u>Cost(\$M91)</u>
ECLSS/Crew				
Accommodations	2.373	0.502	94.22	23.24
Avionics	0.212	0.917	90.06	13.14
Stabilization and Control	2.544	0.494	14.30	9.47
Structures/TPS	1.204	0.440	477.35	18.17
Electrical Power	0.150	0.784	44.13	2.92
RCS/Propulsion System	0.342	0.550	151.29	5.41
Tanks	0.060	0.625	3.0	<u>0.03</u>
TOTAL				72.38

Table 1.6D Cost Discounting Effects

<u>Year</u>	<u>Cost Per Year</u>	<u>(1+R)^{-t}</u>	<u>Discounted Cost</u>	<u>Benefit</u>
1992	382.77	.909	347.97	34.80
1993	382.77	.826	316.34	66.43
1994	382.77	.751	287.58	95.19
1995	105.89	.683	72.32	33.57
1996	<u>237.12</u>	.621	<u>147.25</u>	<u>89.87</u>
Total Cost 1491.31 Net Present Value 1171.46 Savings 319.86				
All totals are in millions of 1991 dollars				

Section 1.7 Reliability

1.7.1 Background

In determining reliability, there are basically only two equations which are used. The one which is used, depends on whether the two parts are in series or in parallel. Two parts are in series if both parts need to work in order for the whole system to work. Two parts are in parallel if only one needs to work in order for the entire system to work. The two equations which are used are as follows:

$$P(A \text{ and } B) = P(A)P(B), \text{ for parts in series,}$$

$$P(A \text{ or } B) = 1 - Q(A)Q(B), \text{ for parts in parallel.}$$

In the preceding equations, $P(A)$ is the probability of success associated with part A, and $Q(A)$ is the probability of failure associated with part A. In determining the reliability of an entire system, one must first determine which parts are in series and which are in parallel.

1.7.2 Determination of abort reliability

The vehicle was required to have a survivability of 0.999. The Taurus booster only has a reliability of 0.95. Using the formula for parts in parallel, it was determined that the vehicle would need a reliability of at least 0.98. The systems which would be required for a successful abort were then determined. The reliability of many of these systems had been determined by finding what they had to be for a survivability of 0.999 with a successful booster. The main question for the abort system was the reliability needed in the ignition device. This reliability was determined to be 0.983. Figure C.1 in Appendix C shows the breakdown of the abort system.

1.7.3 Mission reliability

Due to the large limitations on the mission of the vehicle, there were very few systems required for mission completion which were not required for crew survivability. The reliability of the Taurus booster was the major factor in the mission reliability. If the astronaut was to perform any kind of experiment, the reliability of the experiment itself would be a large factor. It was determined that the experiment would need to be at least 0.956 reliable. Breakdowns of various systems are presented in Appendix C.

Chapter 1 References

- Anderson, J. D. Jr., *"Modern Compressible Flow,"* McGraw-Hill, New York, 1990
- Anderson, John D., *"Hypersonic and High Temperature Gas Dynamics",* McGraw-Hill, Inc., New York, 1990
- Clark, R.K., *"An Analysis of a Charring Ablator with ThermalNonequilibrium, Chemical Kinetics, and Mass Transfer,"* NASA TN D-7180, 1973
- Hansen, C.F., *"Approximations for the Thermodynamic and Transport Properties of High-Temperature Air,"* NASA TR R-50, 1959
- Institute for Strategic Defense Studies, *"U.S. Defense Issues,"* 1989-1990
- National Aeronautics and Space Administration (NASA), *"JSC Cost Model Summary,"* 1991 (converted by D. Akin)
- Ohanian, H.C.: *"Physics",* W.W. Norton & Co., New York, 1985

Chapter 2 - Mission Analysis

Section 2.1 - Mission Definition

2.1.1 Launch and Return

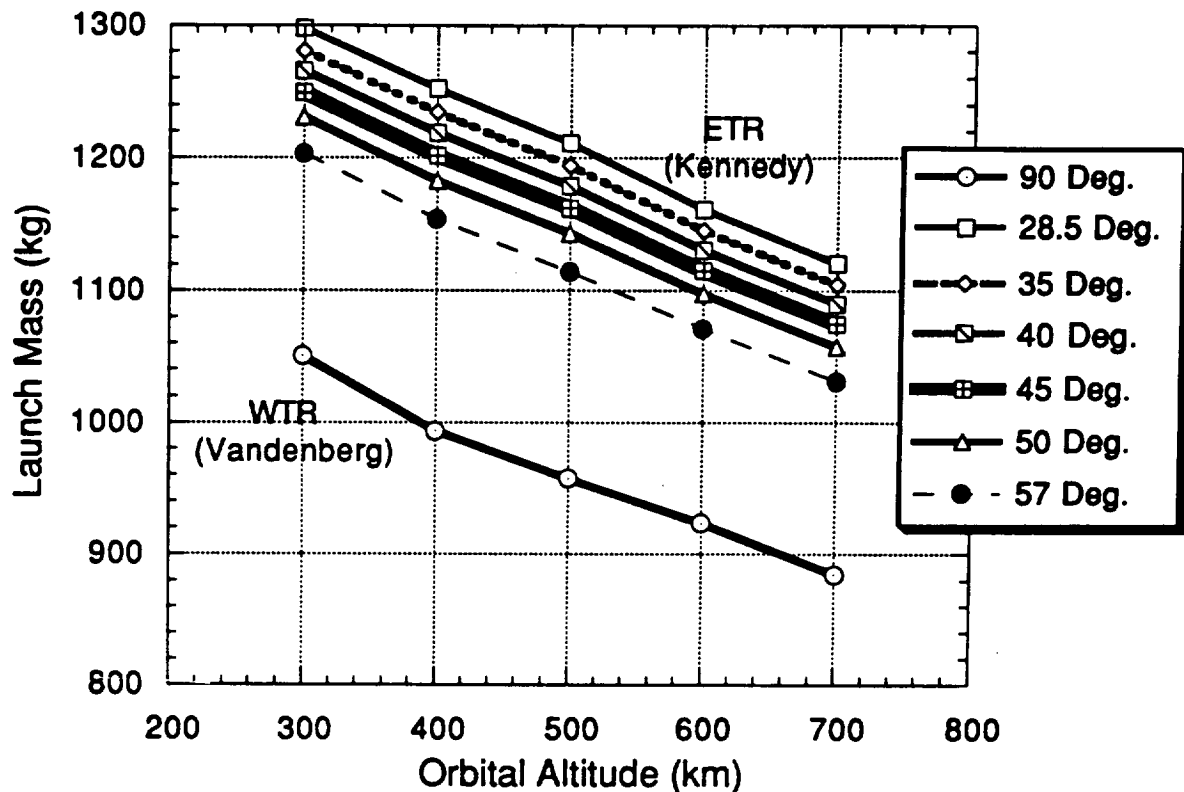
The primary mission for the Taurus Lightweight Manned Spacecraft will be simple launch and return mission. Because of the limited mass capability of the booster, the LMS will not be able to fly with enough mass for performance above the minimum of carrying a human into space.

The preliminary designs for the LMS called for a craft capable of flying two crew members to the space station, docking, re-supplying and spending as much as six days in space. As the design progressed, the mission capability had to be reduced to meet the tight mass constraints. The final design for the LMS will have a single-manned spacecraft with very limited maneuvering ability. The typical mission length will be less than one day.

The LMS will be primarily launched due east from Cape Canaveral resulting in a 28.5° inclination with an orbital altitude of 300 km. It is expected that most launches will be due east as it allows the maximum mass to be carried to orbit. As can be seen on Figure 2.1A, 1300 kg can be flown to a 300 km altitude with an inclination of 28.5° (which results from an easterly launch). If the launch capability of the Taurus booster improves launches to other orbital inclinations would become more feasible. The accompanying Figure 2.1A was created by a cosinusoidal interpolation from information received from Orbital Sciences Corporation (OSC). The information received from OSC only contained altitude vs. mass information for launch azimuths of 0° (due east) and 90° (due north). The relationship was estimated to vary with the cosine of launch azimuth. This was assumed because maximum mass can be carried to orbit with an azimuth of 0° , less with 90° and a minimum mass with an azimuth of 180° . Values were interpolated with azimuths between 0° and 55° (the maximum allowable from Cape Canaveral). These azimuths correspond to the inclinations shown on Figure 2.1A, ranging between 28.5° and 57° . Not enough data on the specifics of the booster was available in order to perform a launch velocity profile to more accurately determine the capability of the booster to other inclinations.

As previously stated, maneuvering ability for the LMS is forced by weight constraints to be very limited. As will be discussed in Section 2.3, with a total ΔV of 270 m/s available for the orbital maneuvering system, the LMS will not be able to perform many significant maneuvers. Appendix E details the amount of fuel that would be needed to perform other missions.

Figure 2.1A Launch Mass vs. Altitude for Different Inclinations



2.1.2 Rendezvous and Inspect

If the capabilities of the Taurus booster improved, this mission would involve performing a visual inspection of a satellite. This could allow its current condition and/or cause of failure to be determined if problems developed. This mission would be expected to save millions of dollars by determining the cause of satellite failures and evaluating whether an in-orbit repair would be practical. Also, experiments could be designed that would require periodic observations which this spacecraft could perform.

The Taurus LMS is currently incapable of performing this mission for several reasons. The first is that the LMS cannot carry the fuel required for rendezvous. As described in Appendix E, a rendezvous mission would require a ΔV of at least 400 m/s, which is significantly more than the craft's current capability. The second requirement would be for an extended mission time. The mission length had to be cut to one day in order to meet the mass requirements, and a rendezvous mission would have to be longer to allow time to catch the target satellite. The mission would most likely need to be three days, depending on the particular target. The third additional requirement would be for an on-board camera to record the observations of the satellite. This would require an additional system to be

designed into the craft. Lastly, launch mass capability would have to be improved to launch the craft to the inclination of the target satellites not in 28.5° inclination orbits.

2.1.3 Space Station Docking

This mission would probably be the most complex mission this craft could accomplish. By having the ability to dock with the space station, the capabilities of the craft are greatly improved. Foreseen reasons for docking include: small scale emergency supply delivery, space station crew rotation, or having Taurus LMS docked at the space station as emergency lifeboats.

This mission cannot currently be accomplished for several reasons. In addition to the first three mentioned above, the craft is not currently designed with a docking ring. This is again because of the tight mass constraints. While a docking ring is expected to have a mass less than 100 kg, all non-essential mass had to be eliminated just to be able to reach orbit. If the capabilities of the Taurus booster improved to allow extra mass to be taken orbit, the craft would have to be re-designed to include a docking ring.

2.1.4 Growth Potential

Growth potential for this craft takes two forms. The first would involve an increase in the Taurus booster capabilities. The second would entail launching on a different booster.

If the capabilities of the Taurus booster improved, the crafts capabilities would also increase. The ability to launch with an additional 100 kg of fuel would allow the additional ΔV to make rendezvous possible. An additional 100 kg would probably be needed to extend the mission time to allow for rendezvous, and roughly an extra 100 kg would be necessary for a docking ring.

The other option for growth potential would be to launch on a Delta booster. This would allow nearly four times the mass to be launched to orbit. This would allow all the needed modifications to be made to the Taurus LMS to achieve all these missions as well as possibly carrying a payload. The service module and booster adapter would need to be completely redesigned to carry the extra fuel and mate to the booster. Launching on a different booster is not recommended as a long term option because the craft is being designed to the very low mass constraints. It is expected that it would be much more efficient to completely re-design the craft to meet a larger launch mass capability.

Section 2.2 Launch Preparations

This section describes the preparations required to launch the Taurus LMS into space. Among these are the transportation of the Taurus LMS, the facilities used and the crew training requirements.

2.2.1 Transportation

The Orbital Sciences Corporation is responsible for shipping, handling, integrating and assembling all of the Taurus booster stages. The transportation of the Taurus LMS will be by air for the following reasons:

- easier to handle and transport
- on-time delivery
- less vibrational problems

There will be two canisters built, one for the capsule and one for the service module. These canisters will be transported on a Boeing Model 747 - 200 F Freighter, capable of delivering 90,720 kg over a range of more than 4,500 nm (8,340 km; 5,180 miles) (Lambert, 1990). The dimensions of these canisters are 3.05 x 2.44 x 2.44 m (10 ft long, 8 ft high, 8 ft wide) (Lambert, 1990). With these specifications the capsule and the service module can be transported with instrumentation to monitor:

- pressure
- humidity
- temperature
- vibration reading

Once the canisters arrive at an airport near Kennedy Space Center, they will be transported by truck to the Taurus LMS Checkout Building. This is where the capsule and the service module will be processed and checked out in a Class 10,000 clean facility.

2.2.2 Facilities

The Taurus launch vehicle should be fully developed, tested, and ready to launch in 1995. Existing facilities at the Kennedy Space Center, such as the Payload Hazardous Service Facility used to store the Taurus solid propellants, will be used to keep with the time table and to keep the cost per flight low. (Class 2: DB/AP - HMX/AP). A list of facilities that need to be built are as follows:

- A) Taurus LMS Checkout Building
- B) Launch Control Center
- C) Mobile Service Structure
- D) Launch Tower

A description of each of these facilities as well as the processing of the Taurus LMS will be discussed.

A) Taurus LMS Checkout Building: To prevent any launch delays, many of the procedures are done here, where corrections can be made quickly and efficiently. This facility will be comprised of a clean room, an equipment room, and a storage room. Furthermore, the checkout building will be large enough so that the mobile service structure can move to and from the launch site on a track.

The clean room will be designed to have a rating of 10,000 as well as temperature and humidity control.

Once the capsule and the service module have been delivered they will be mechanically and electrically interfaced into one unit (LMS). The seals will be checked for any leakage and all the avionics will be integrated and thoroughly checked out by conducting a prelaunch test. Also at this time, the life support equipment and the solid propellants will be loaded.

After the interfacing and testing is completed, the Taurus LMS will be covered by a protective cover and hoisted by a winch from inside the white room (clean room) from the top of the mobile service structure. After this procedure is done, the mobile service structure will move to the launch site.

B) Launch Control Center: This building will consist of office spaces, utilities systems control and two firing rooms. The firing rooms are capable of supplying prelaunch checkouts at the Taurus LMS Checkout Building and at the launch site. A launch processing system will be automated to perform most of the Taurus checkout sequence while the components are being prepared for launch and also to conduct countdown and launch operations (Griffin and French, 1990). The launch processing system is broken down into three major subsystems:

- a) The central data subsystem will consist of large - scale computers that store test procedures, vehicle processing data, a master program library, historical data, pre- and post-test data analyses and other data (ref. NASA, 1988).
- b) The checkout, control and monitor systems will have minicomputers to process and launch the Taurus space vehicle.
- c) The record and playback subsystem's primary function is to record unprocessed Taurus instrumentation data test and launch countdowns. This recording can be used for troubleshooting.

C) Mobile Service Structure: This structure will have a maximum height of 120 ft with a clean room that is capable of moving vertically along the side of the structure. Its primary function is to interface the Taurus LMS to the Taurus booster stages. The mobile service structure will be able to travel on a rail system from the Taurus LMS Checkout Building to the launch site.

The dimensions of the clean room will be 15 ft high x 15 ft long x 15 ft wide, this allows room for the crew to be able to interface the Taurus LMS to its booster stages. A filtering and environmental control system will be placed inside the clean room so it will get a class rating of 10,000. There will be two sets of doors, one will open outward towards the structure and the other set will open downward.

The interfacing processing will consist of the following:

- 1) At the same time as the Taurus LMS was mated, the Taurus booster stages were being assembled horizontally.
- 2) The booster stages will be transported on a trailer to the launch site where they will be erected vertically on the launch pad next to the launch tower. *
- 3) The filtering system in the clean room will be operational at this time.
- 4) The mobile service structure will move to its proper position next to the booster stages with the Taurus LMS.
- 5) Once the mobile service structure is in place, the clean room will move vertically downward so interfacing procedures can be done with the Taurus uppermost

booster stage.

6) The protective covering will be removed from the LMS and the abort system unit will be attached on top of LMS.

7) A final prelaunch test will be conducted to insure that both LMS and its booster stages are properly functioning.

8) On the launch pad, these procedures will be done at the same time:

- launch processing system hardware interface modules will be attached
- system test sets
- propellant - loading equipment
- electrical equipment racks
- supports fluid, gas and electrical requirements
- hydrazine and nitrogen tetroxide aft T-O umbilicals are attached

9) After all the system checks are done, the clean room moves back to its original position with both sets of doors closed.

10) The mobile service structure will move away from the launch pad.

* Note: Orbital Sciences Corporation is responsible for all of the Taurus booster stages.

D) Launch Tower: This structure will have a maximum height of 100 ft. It will have access arm that will be able to rotate an arc of 70° in approximately 30 seconds for lift-off. The dimensions of the arm are 16 ft long x 8 ft high x 5 ft wide (see figure 2.2A). At the end of the access arm, close to the Taurus LMS, there will be an environmental control chamber allowing for two crew personnel to help the astronaut get into the Taurus capsule. There is an emergency egress system set up next to the other end of the access arm.

The emergency egress system or slidewire provides an escape route for the astronaut. The slidewire will extend from the level of the Taurus LMS to the ground on the opposite side of the space vehicle. The basket will have a flat bottom with netting around the sides. There will be a braking mechanism that will slow down the basket before it reaches the ground.

At this time, the Taurus space vehicle is ready for launch and no further systems checks are done.

2.2.3 Crew Training Requirements

The majority of the training for the Taurus personnel team is the responsibility of Orbital Sciences Corporation. The astronaut should be selected and trained by NASA.

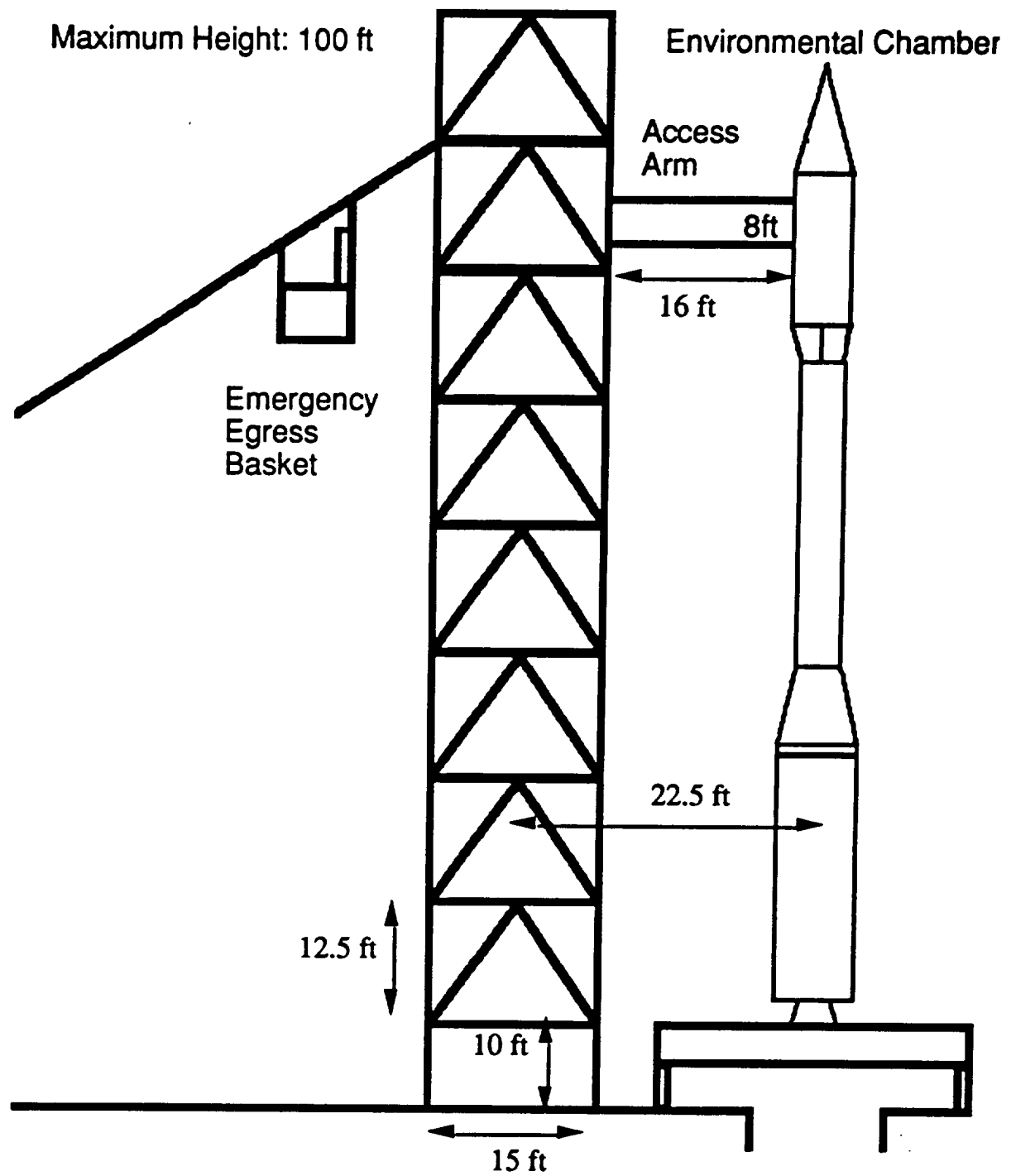


Figure 2.2A Conceptual Launch Tower

Section 2.3 Orbital Maneuverability

The baseline mission for the Taurus LMS is simply to launch and return. Since there is a need to test the capabilities of the maneuvering systems there are three additional mission profiles which deal with the most common low Earth orbital maneuvers. These maneuvers are beyond the simple launch and return mission.

These maneuvers are as follows :

1. Launch and Return
2. Epoch Maneuvers
3. Hohmann Transfer
4. Plane Change

All of these are based on the following assumptions:

1. Launch to 300 km. altitude initially
2. 12-24 hour mission duration
3. Re-entry from a circular orbit
4. A total of 270 m/s ΔV

The necessary ΔV 's for re-entry vary with altitude and are detailed in Section 2.4. For a detailed discription of these maneuver calculations which are possible for the Taurus craft if additional fuel is provided, see Appendix E and K.

2.3.1 Launch and Return

All that is involved in this mission is launching into the initial orbit at 300 km. altitude and re-entering the atmosphere after a set number of orbits. With a 24 hour mission duration this would be approximately 14 orbits.

Section 2.4 Re-entry Trajectory

2.4.1 Introduction

The re-entry trajectory is split into two portions for purposes of analysis. The first is the free-flight phase which takes the craft from its orbit to the atmosphere (taken to begin at 120 km). The second is the atmospheric flight phase, during which the craft flies through the atmosphere to land.

For purposes of demonstration, the calculations will be carried out for a re-entry trajectory from a 300 km circular orbit. The following figure shows the two portions of the trajectory and the results which will be derived. It is assumed that the de-orbit burn and resulting change in velocity (ΔV) are performed instantaneously (Note: this is only for purposes of orbital mechanics calculations.)

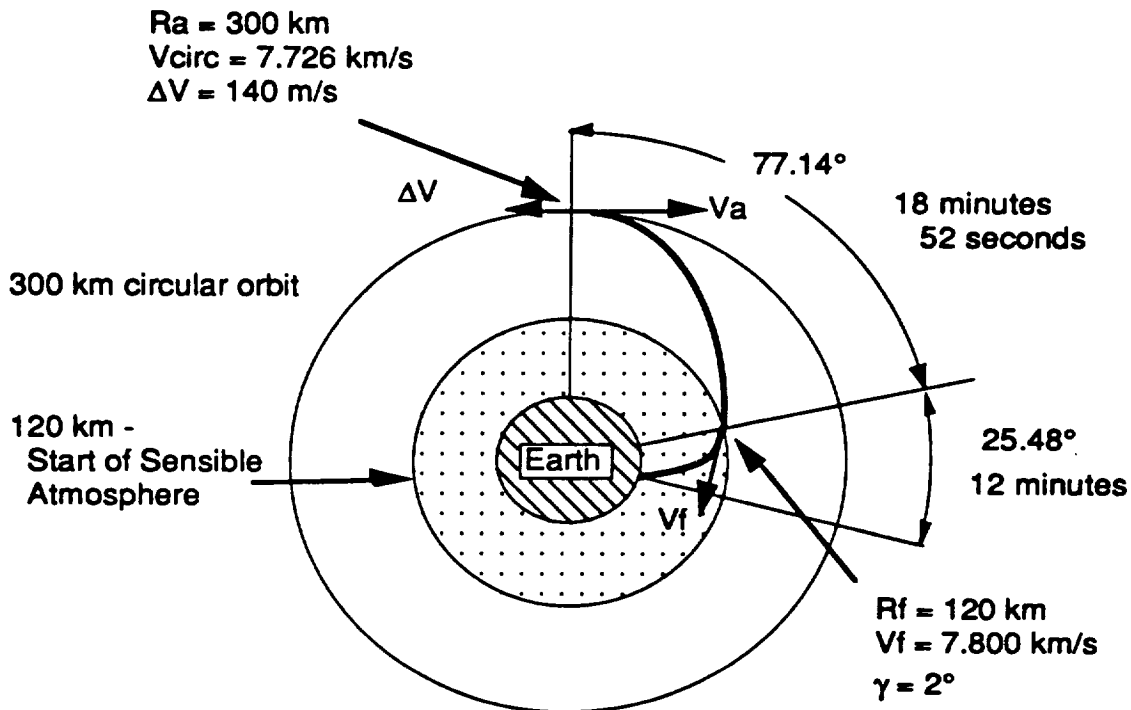


Figure 2.4A: Reentry Trajectory

2.4.2 De-orbit Burn and Free Flight

The de-orbit burn is necessary to slow the craft down so that it falls from its orbit to a transfer orbit that brings it down to the atmosphere. Once the atmosphere is reached aerodynamic forces will dominate orbital mechanics to control the trajectory. The de-orbit burn's size and orientation control the entire re-entry trajectory in the following manner. The burn determines the craft's new orbit which sets its flight path angle and velocity at atmospheric interface, two parameters which are critical for the atmospheric flight region.

The relationship between the burn size (ΔV) and conditions at atmospheric interface (referred to by subscript "f") were derived from the following two

equations, conservation of angular momentum and conservation of energy.

$$h = rV \cos \gamma$$

$$\epsilon = \frac{V^2}{2} - \frac{\mu}{r}$$

In the above equations:

h = angular momentum

r = orbital radius, measured from the center of the Earth

V = magnitude of velocity

γ = flight path angle, the angle between the local horizontal and the velocity vector

ϵ = specific mechanical energy

μ = gravitational parameter

The conditions at the burn location (subscript "a") were equated to the conditions at 120 km. The known values are:

$$V_a = V_{\text{circ}} - \Delta V = \sqrt{\frac{\mu}{r}} - \Delta V$$

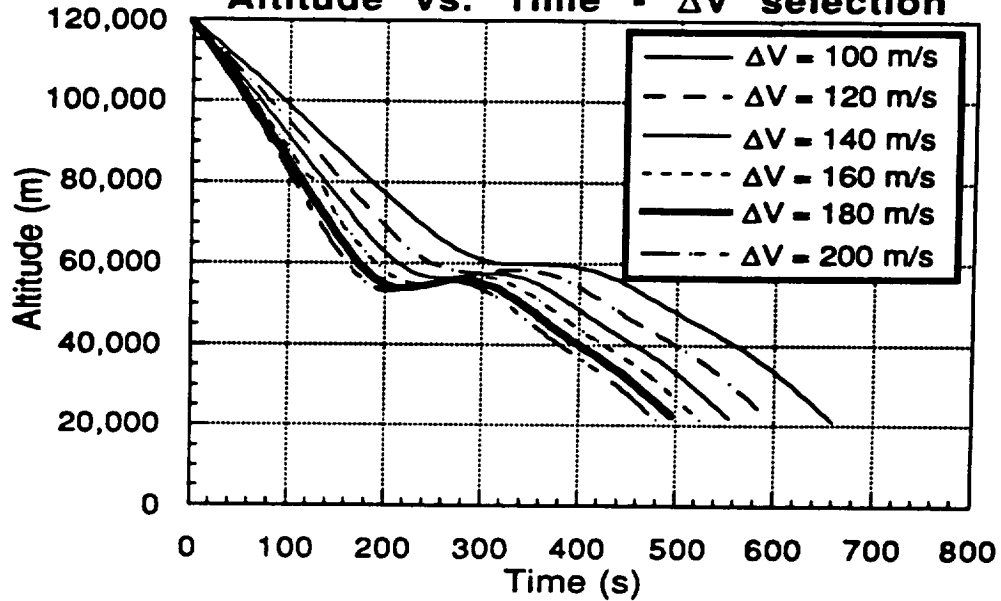
$$r_a = 6378 \text{ km} + 300 \text{ km} = 6678 \text{ km}$$

$$r_f = 6378 \text{ km} + 120 \text{ km} = 6498 \text{ km}$$

The first known, V_a , was based on the simplifying assumption that the burn is performed directly opposing the motion of the craft, so that $\gamma_a = 0^\circ$. The second two are the orbital radii, the radius of the Earth plus the altitude of the orbit. This leaves V_f and γ_f as unknowns. After setting $h_a = h_f$ and $\epsilon_f = \epsilon_a$ algebraic manipulation allows velocity and flight path angle (γ) at 120 km to be found.

Figure 2.4B shows trajectory plots of altitude vs. time with varying ΔV . (Note: Data below 20 km is deleted on these trajectories to avoid clutter. Also the derivation of the atmospheric flight trajectory is explained in section 2.4.3.) Qualitative analysis shows that for de-orbit burn sizes above 140 m/s, the trajectory begins experiencing diminishing marginal returns; that is, for increasing ΔV the change in the trajectory becomes smaller. For this reason the ΔV required to de-orbit was selected as 140 m/s from 300 km. This corresponds to having a re-entry flight path angle of 2.0° . For this reason the initial flight path angle will be 2.0° for all altitudes for which this is feasible. Manipulation of the conservation of energy and momentum equations in Figure 2.4C shows the ΔV required to achieve $\gamma_f = 2^\circ$ from altitudes between 160 km altitude and 900 km. It can be seen that below 250 km altitude, the ΔV required increases greatly. For this reason, shallower re-entries will be permitted below 250 km; the de-orbit burn will simply be held at 140 m/s. These trajectories were analyzed and found to be acceptable as they produced maximum deceleration of about 3 gees and an atmospheric time of flight equivalent to that which will be experienced re-entering from higher altitudes. Also, at high altitudes the ΔV required to achieve 2° increases steadily. This does not present a problem as the current L.M.S. mission scenarios will not fly to very high orbits.

Figure 2.4.B - Varying ΔV
Altitude vs. Time - ΔV selection



Time of flight and angular distance traveled in the free flight section were computed by the method of Eccentric Anomaly (ref. Bate, 1971). The results from 300 km (as shown on the main figure) are that it will take 18 minutes and 52 seconds to fly from the de-orbit burn altitude of 300 km to 120 km, and during this time the craft will fly 77.14° around the Earth. This is important because it (along with the distance traversed in the atmosphere) will allow the location of the de-orbit burn performance to be determined to reach a selected touchdown site.

2.4.3 Atmospheric Flight

Atmospheric re-entry is one of the most crucial portions of any manned space flight. The main design challenge is to minimize the maximum deceleration as well as the time of high decelerations. A computer model has been developed (see appendix F for listing and complete explanation) to predict the re-entry trajectory. The model was created to integrate the following dynamic equations of motion (Loh, 1968):

$$\begin{aligned} \sqrt{\frac{R}{g}} \frac{d\left(\frac{V}{\sqrt{gR}}\right)}{dt} &= -\frac{1}{2} \left(\frac{C_D A}{m} \right) R \rho_0 e^{-\beta y} \left(\frac{V^2}{gR} \right) + \sin \theta \\ \sqrt{\frac{R}{g}} \frac{d(\theta)}{dt} &= \left[\frac{\sqrt{gR}}{V} - \frac{V}{\sqrt{gR}} \right] \cos \theta - \frac{R}{2} \left(\frac{L}{D} \right) \left(\frac{C_D A}{m} \right) \rho_0 e^{-\beta y} \left(\frac{V}{\sqrt{gR}} \right) \\ \sqrt{\frac{R}{g}} \frac{d(\beta y)}{dt} &= -\beta R \left(\frac{V}{\sqrt{gR}} \right) \sin \theta \end{aligned}$$

These equations control, velocity, flight path angle and altitude as functions of time, respectively. The model integrated these equations and Figures 2.4D, 2.4E and 2.4F. were obtained. (Note: 0 seconds on the time axis is the time crossing the 120 km altitude mark.)

Figure 2.4.D - Altitude vs. Time

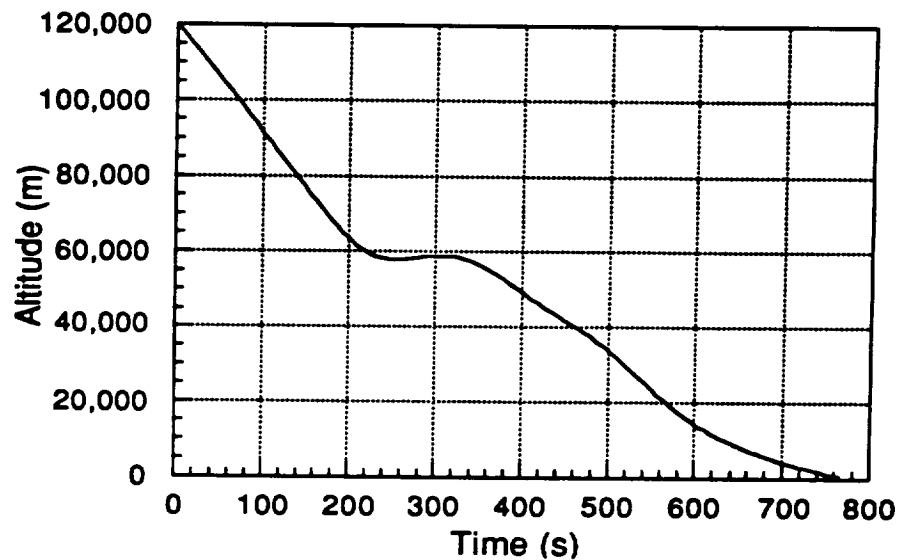


Figure 2. Π- Velocity vs. Time

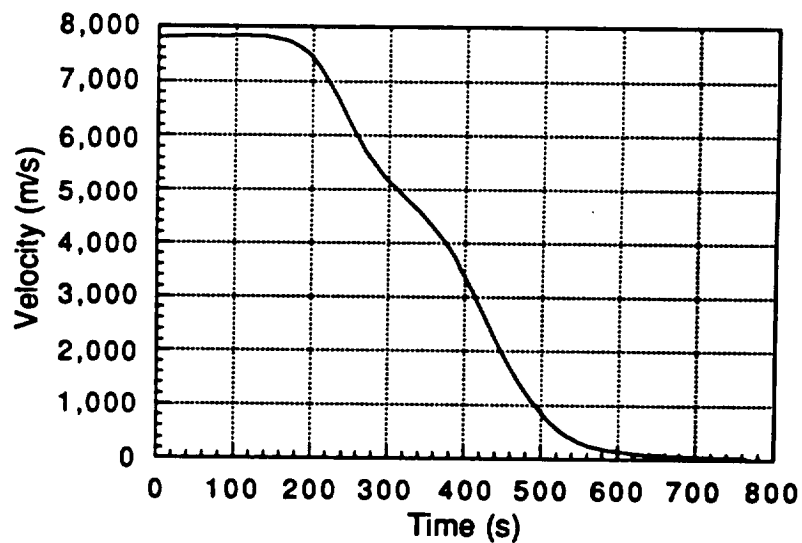
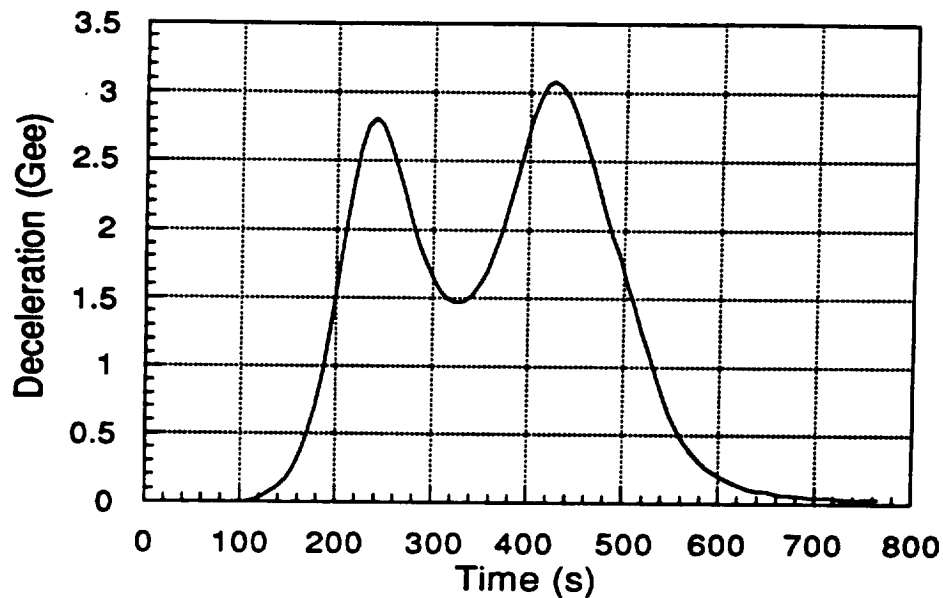


Figure 2.4.F - Deceleration vs. Time



From these plots it can be seen that:

- 1) Time of flight between crossing 120 km and Earth impact is 775 seconds.
- 2) At an altitude of roughly 59 km the craft gains altitude for 50 seconds before continuing to fall.
- 3) The velocity does not change significantly until 150 seconds into this portion of the flight at which time the craft has re-entered to 80 km and aerodynamic forces begin to influence the craft's trajectory.
- 4) The maximum deceleration is 3.07 gees and the deceleration decreases while the craft gains altitude. The craft will have slowed to 63 meters per second (0.19 Mach) by the time 3 km is reached so that the parachute can be deployed.

Section 2.5 The Taurus LMS Recovery System

2.5.1 Introduction

The Taurus LMS recovery system will consist of two round parachutes deployed simultaneously at a reentry speed of approximately Mach 0.19. The deployment sequence will begin at 3 km above sea level when a computer command will fire explosive bolts on both parachute hatches, allowing the mortar-deployed pilot chutes to pull the two canopies out into the windstream. Once the parachutes are inflated, the capsule will begin a ten minute canopy descent to the ocean, inflating its pontoon before splash down. Upon splash down, the canopies will be released and dye markers will be ejected through the parachute hatches. A radio beacon will help guide the recovery aircraft and vessels to the Taurus LMS.

2.5.2 The Parachutes

When considering the type of recovery system to be used on the Taurus LMS, three types of systems were considered; a round parachute, a ram-air parachute, and a para-sail (hang-glider) type device. Ram-airs have high maneuverability, good forward glide (25-30 m.p.h.) and flarable landings (Poynter, 1989). Their disadvantages are a somewhat high malfunction rate (approximately one in a thousand) and no past record of spacecraft recovery operations. Para-sails have very high maneuverability, outstanding forward glide and flarable landing. However, they are difficult to deploy at high speeds, have stability problems, require a smoother landing zone than a parachute, and have no past history with manned spacecraft recovery. Round parachutes have reliable openings and a proven track record of space recovery, but they have negligible forward glide, sluggish maneuverability, and cannot be flared on landings, resulting in harder impact speeds. The round canopy was picked for both its reliability and for the fact that maneuverability is not needed since the Taurus LMS is expected to land in water. Its proven record as a spacecraft recovery system will also allow the Taurus LMS to be built and tested at a lower cost.

For safety purposes, the Taurus LMS will carry and deploy two parachutes instead of one, each being large enough to descend the capsule at an acceptable rate of descent in case the other parachute malfunctions. Therefore, if both chutes deploy successfully, the rate of descent will be especially slow, allowing for a softer touch down, which will be more important if the launch is aborted on the launch pad.

In determining the size and volumes of the parachutes, an estimate was obtained by using information from a sport parachute sales catalog on the Phantom 22 and 28 round canopies (Poynter, 1989).

Given the following specifications:

	22	28
Diameter	22 ft.	28 ft.
Shape	conical	conical
Area	304 ft. ²	492 ft. ²
Pack Volume	263 in. ³	421 in. ³
Pack Weight	4.1 lbs.	6.8 lbs.
Line Strength	400 lbs.	400 lbs.
Max. Suspended Weight	140 lbs.	240 lbs.

and taking the following ratios:

Area Ratio	(492/304) = 1.618
Pack Volume Ratio	(421/263) = 1.601
Pack Weight Ratio	(6.8/4.1) = 1.659
Max. Suspended Weight	(240/140) = 1.714

it can be estimated with reasonable accuracy that the parachute pack weight and volume increase linearly with increasing suspended weight. This of course does not include the fact that the suspension lines and risers will have to be strengthened to take the extra weight and gee forces of opening.

With the current Taurus LMS reentry mass of approximately 600 kg without the parachutes, and with a factor of safety of 10%, the total suspended weight for one chute to descend is 660 kg. Using the specifications of the Phantom 28, in metric equivalence:

Diameter	8.5344 m
Area	28.243 m ²
Pack Volume	6.899 x 10 ⁻³ m ³
Pack Weight	1.8597 kg
Line strength	181.44 kg
Max. Suspended Weight	63.5 kg

and using the following ratios:

Max. Suspended Weight Ratio	(660/63.5) = 10.39
Pack Volume Ratio	(V /6.899 x 10 ⁻³) = 10.39
Pack Weight Ratio	(W /1.8597) = 10.39

the pack weight and volume for each Taurus LMS parachute are:

$V=71.71 \times 10^{-3} \text{ m}^3$	$W=19.32 \text{ kg}$
--------------------------------------	----------------------

In calculating the diameters of the inflated parachutes, taking an area ratio of (A /28.243) = 10.39, the area of one Taurus LMS parachute will be 293.4 m², with a diameter of 19.33m across.

2.5.3 Peripherals

There are six parts to a round parachute (Figure 2.5D); the pilot chute, deployment bag, bridle, main canopy, suspension lines, and risers. The pilot chute is essentially a mini-parachute with a connecting line or bridle to the deployment bag with main canopy. The pilot chute will be deployed into the windstream by a mortar which will fire an explosive charge beneath it and eject it outward at 90 degrees from the capsule's direction of descent. The bridle must be relatively short so that the pilot chutes do not entangle with either parachute.

Each parachute must be able to be released from the vehicle once it splashes down to prevent it from reinflating and dragging the capsule across the water. Two types of cutaway devices were considered; a 3-ring mechanical device (Poynter, 1979) (Figure 2.5A), and an explosive bolt assembly that shears off the riser retainer via an electrical command from the computer (Figure 2.5B).

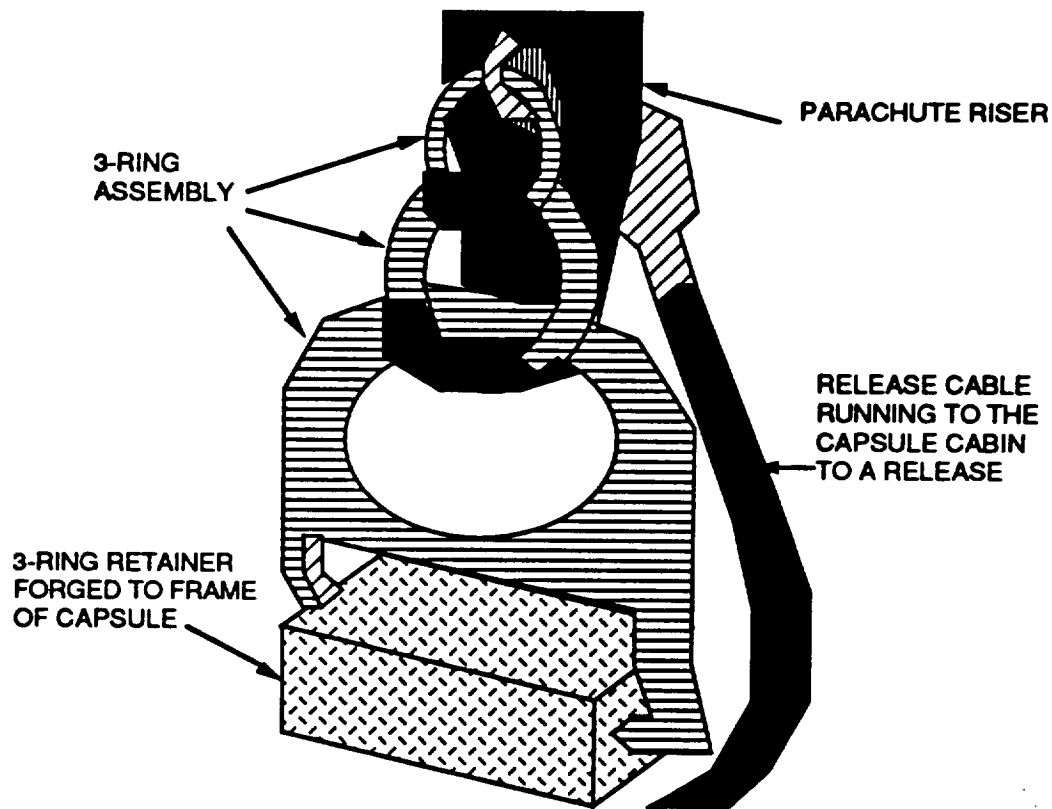


Figure. 2.5A 3-Ring Release

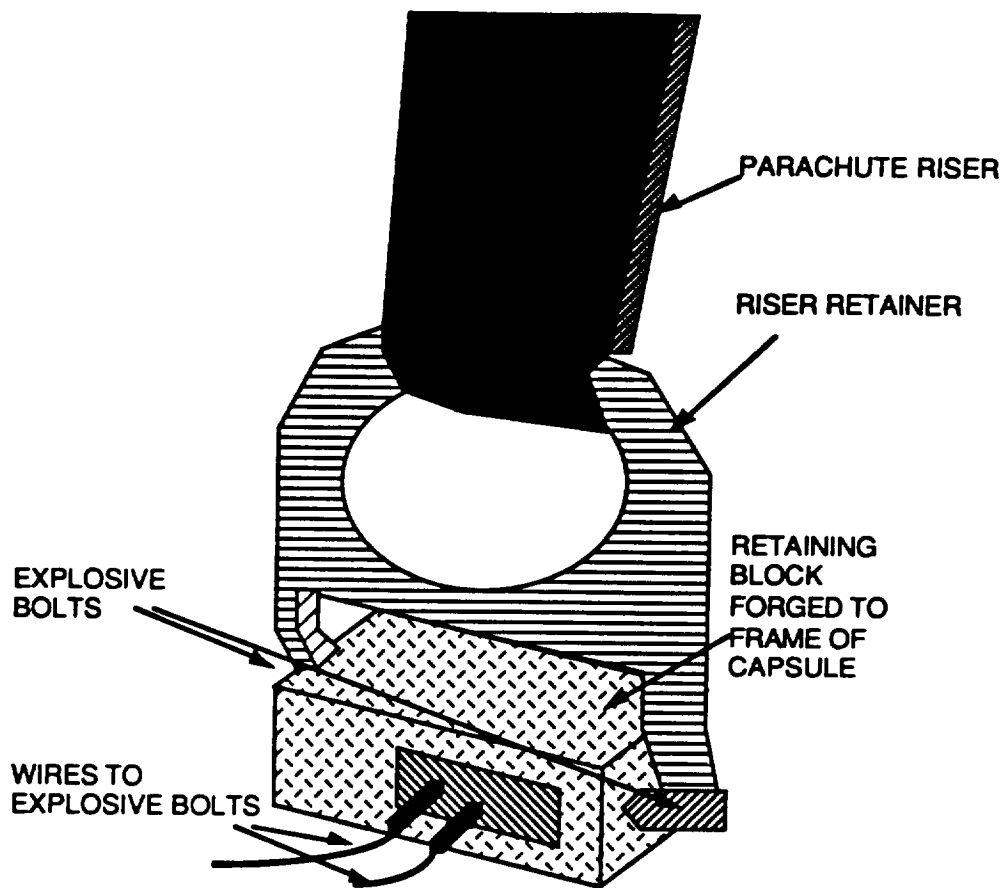


Figure 2.5B: Explosive Bolt Release

The mechanical device is virtually foolproof, requiring only about 5 pounds of force from the pilot activate via a ripcord device. But since a cable must be run through the pressure vessel to each of the parachute compartments, this could cause sealing problems. A mechanical device would also require a conscious pilot to activate it, whereas an electrical device could be fired by a computer command. Therefore, the explosive bolt release will be used, firing after sensing that the rate of descent of the capsule is zero for a time span of four seconds. This should be quick enough so that the capsule does not get dragged in the water or land.

Estimating the above peripherals' weight by comparing known parachute weights and scaling them to size (Paragear, 1986):

Pilot Chute	2 kg
Risers (2)	3 kg
Bag	2 kg
Bridle	0.5 kg
Explosive bolts (2)	1 kg

The total weight of the peripherals per chute is approximately 8.5 kg. The total weight is therefore 55.64 kg.

2.5.4 Placement and Deployment

The parachutes will be located up towards the nose of the capsule, below the reentry thruster bank, which ends 0.3 m below the nose (see figure 2.5C).

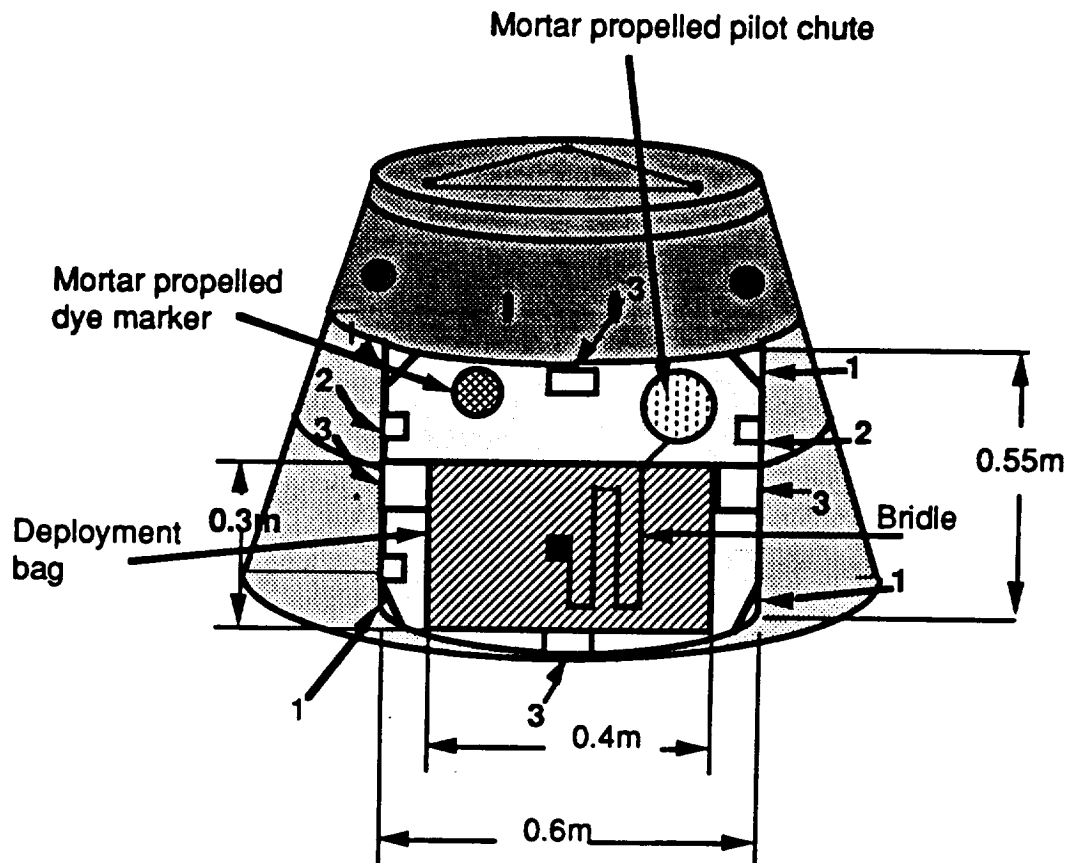


Figure 2.5C Placement of Parachute and Peripherals

The above diagram shows that one parachute compartment houses a pilot chute, dye marker, and deployment bag, with the lines and risers stowed beneath the bag. The bag's dimensions are 0.4 m wide, 0.3 m high and 0.067 m deep (allowing the volume of the parachute to increase to 0.08 m³ for the deployment bag's added volume) with the actual cover and well being 0.6 m wide by 0.55 m high. The shapes with numbers represent:

- 1 - explosive bolt devices
- 2 - sensors to detect when cover has left
- 3 - spring devices to propel the cover off once the bolts fire.

The second parachute has the same layout and is placed on the opposite side.

At deployment altitude, the Taurus LMS computer will automatically fire the parachutes' covers off by explosive bolt detonation, allowing spring devices built into the parachute hatches to fling the covers away from the capsule into the windstream (the springs will connect to the covers so that they leave the deployment area and do not entangle with the parachute lines). Since the skin is 4.763 mm thick, the cover has $1.572 \times 10^{-3} \text{ m}^3$, or 95.9 in³ volume. The skin will be

made of aluminum alloy AA 2024, which has a density of 0.100 lb/in³. Therefore, the cover will weigh 9.59 lbs, or 4.35 kg. Estimating a re-entry deceleration of 0.02 gees at opening altitude, the spring stiffness k can be calculated using $F = ma = -kx$, but since the deceleration will be at a 72 degree angle from the spring force direction, $F = (4.35)(0.02)(9.81)\cos 72 = 0.264$ N total force against all four springs combined. Therefore, the k constant could simply be calculated by $0.264 / 4 = -kx$, selecting a reasonable value of 0.333 m for x . The force on each spring should be sufficient to jettison the hatches. Therefore, 0.264 N = $-k(-0.333$ m), and $k = 0.8$ for each spring. Since this constant is very low, it will be given another safety factor of ten and $k = 8.0$. The sensors will detect the hatch leaving and send a signal to a 1 second timer that fires the pilot chute mortar. The separate pilot chutes will shoot in opposite directions to ensure that the two parachutes do not entangle with each other on opening, causing one or both to malfunction. The pilot chutes will shoot out perpendicular to the capsule's direction of reentry.

The opening shock for the Taurus LMS will be limited to 3-5 gees so that the parachutes are not damaged by the deceleration. Higher gees could blow out the canopy panels, thereby increasing the rate of descent of the capsule. The opening shock can be estimated by using the equation:

$$F = \rho \frac{V^2 C_D S_o X K}{2}$$

with K a variable depending on the type of parachute and X a variable depending on the inflation time, drag area, deployment speed, density and recovered weight (Kiker, 1964). This equation does not hold for every deployment condition, so should only be used for insight as to how these conditions affect opening. For a flat circular chute, $X \approx 1.7$ and $C_D = 1.193$ for the Taurus LMS parachutes (see calculations below).

The opening shock can only be reduced at the expense of inflation time and distance, which is not a concern. This is because at 3 km above sea level and 63 m/s, the capsule will still have more than 45 seconds pre-impact time. Therefore, the opening shock should be reduced as much as possible, opening just enough so that a safe launch abort from the launch pad can be achieved, which is a full canopy inflation from a minimum altitude of 1500 ft, 458m high.

Rate of descent of the TLMS will be especially slow for a reentry vehicle. Previous reentry capsules accepted a rate of descent of 6.1 to 9.1 m/s, and required an impact-attenuation system, which is typically 3% of the vehicle's landing weight (Kiker, 1964). Therefore, increasing the size and weight of the parachutes is a trade-off to eliminate the impact-attenuation system. Since the parachute chosen has a rate of descent of 5.5 m/s, using the equation:

$W = mg = q C_D A$ we can find the coefficient of drag to be:

$$C_D = \frac{2mg}{\rho A V^2} = \frac{2(660\text{kg})(9.81\frac{\text{m}}{\text{s}^2})}{1.225\frac{\text{kg}}{\text{m}^3}(293.4\text{m}^2)(5.5\frac{\text{m}}{\text{s}})^2} = 1.193$$

assuming a standard density and gravity. The rate of descent of the two parachutes inflated simultaneously can be found by doubling the area and allowing for some spillage of air due to the chutes interfering with each other, with a loss of 5-10% of their combined drag area to be expected (Kiker, 1964) (Figure

2.5D). Assuming the worst case of a 10% loss, the rate of descent is found by the equation:

$$V^2 = \frac{2gm}{\rho C_D A}, \quad V = \sqrt{\frac{2(9.81)(660)}{1.225(1.193)(293.5)(2)(.9)}}$$

The rate of descent of the TLMS under both canopies is 4.1 m/s.

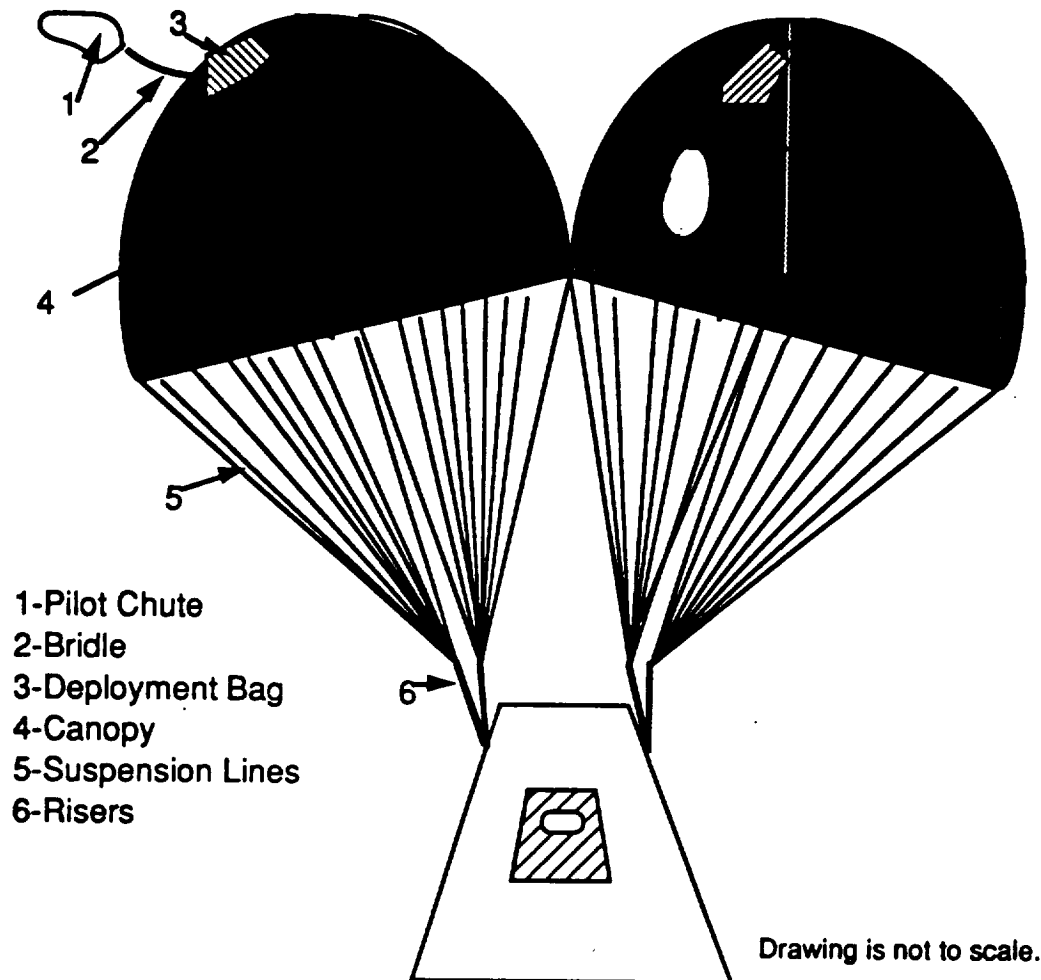


Figure 2.5D: Capsule Under Canopies with Parachute Peripherals Labeled.

Section 2.6 Recovery Operations

2.6.1 Dye Markers

Once the Taurus LMS splashes down, the canopies will be released as stated in Section 2.5.3. Immediately afterwards dye marker packets in each of the parachute compartments will be ejected by a mortar system similar to the pilot chutes (see figure 2.5C). Dyes are yellow-green in color and should be large enough to be spotted at an altitude of 10,000 ft. (3048 m) from a distance of 10 miles (16.1 km) under favorable visibility conditions (Kiker, 1964). Shark repellent may also be included with the dye as a safety precaution for the astronaut.

2.6.2 Strobe Light

If the Taurus LMS splashes down at night, a strobe light will be needed to help both aircraft and ships to determine its location. The ideal spot for the strobe would be at the very top of the capsule. However, this may cause problems with the interface of the shroud. Therefore, the strobe light will be located beneath the skin of the center of the RCS, popping up once the Taurus LMS is under canopy via an electrical motor. Requirements are that the strobe be intense enough so that in normal darkness it can be spotted at an altitude of 12,000 ft. or 3657.6 m and a distance of 40 nautical miles (Kiker, 1964).

2.6.3 Beacon

The Taurus LMS will not employ any special type of transmitter as a beacon but will use its normal radio transmitter to emit a beacon. Naval ships and aircraft will pick up this HF signal and will find the TLMS using directional finders.

2.6.4 Flotation

Inflatable buoyancy balloons must be employed on the TaurusLMS to prevent the capsule from capsizing, since waves from 2 to 4 feet high can be expected in the open ocean. Inflated pontoons will extend out of the lower diameter of the capsule and inflate immediately after the dye markers are ejected. They will be inflated by small compressed air canisters, initiated by computer command.

2.6.5 Recovery Aircraft / Ships

Due to the low mass of the Taurus capsule, which is approximately 660 kg, virtually any size helicopter except possibly a UH-1 Huey could be used to lift the capsule and astronaut out of the water and to a recovery vessel (there will be a lifting attachment ring on the top of the capsule). For example, CH-53's have a lifting capability of 30,000 lbs., or 13,608 kg and can land on carriers or battleships. UH-60's can lift 8,000 lbs or 3,629 kg, and could be used if the splash down point is close to a land base.

Chapter 2 References

- Bate, R.R., D.D. Mueller, and J.E. White: *"Fundamentals of Astrodynamics,"* Dover Publications, New York, 1971.
- Griffin, Michael D. and James R. French, *"Space Vehicle Design,"* American Institute of Aeronautics and Astronautics, Inc., Washington, D.C., 1990
- Kiker, John W. and Campbell, Carlisle C. Jr., "Spacecraft Landing Systems-Design Criteria and Components", *Manned SpaceCraft*, 1964.
- Lambert , Mark, *"Jane's All the World's Aircraft 1990-91,"* New York, 1990
- Loh, W.H.: *"Re-entry and Planetary Entry Physics and Technology,"* Springer-Verlag, New York, 1968.
- National Space Transportation System Reference, *"Volume 1: Systems and Facilities,"* NASA, June 1988
- Paragear Equipment Co., catalog #51, 1986.
- Poynter, Dan , "Parachuting Equipment", *Parachuting, The Skydiver's Handbook*, 1989.

Chapter 3: Human Factors

Section 3.1 Life Support Systems

3.1.1 General

The life support system of the Taurus LMS has been designed around a single astronaut on a twenty-four hour mission into low-earth orbit. This life support system is based on a pressurized crew compartment with continual recirculation of the cabin atmosphere through a series of scrubbers that remove excess water vapor, carbon dioxide, and trace contaminants. Should the main system fail, a backup system exists which relies on a pressure suit and separate atmospheric and temperature control to support the astronaut. The limited mission of the Taurus LMS has enabled a "bare bones" design of the life support system. Operating only in low-earth orbits of moderate inclinations within a time frame of twenty-four hours, no radiation shielding was required besides the skin of the spacecraft due to lack of significant exposure to Van Allen belts or solar cosmic radiation.

The Taurus LMS will only carry a twenty-four hour air supply. This is justified because the mission length was determined as the sufficient time to get a man into space and then back down to a desirable landing site. As a back-up, a second twenty-four hour air supply will be carried for use by the pressure suit. This satisfies the worst-case scenario of the astronaut losing his main supply as soon as orbit is reached because it will still give the astronaut enough time to deorbit and land at one of the proposed sites.

There will be no waste removal for the astronaut on the Taurus LMS. Astronauts will use catheters and plastic bags for liquid waste and will wear diaper-like undergarments for solid-waste collection. Several days prior to launching, the astronaut's diet will be regulated to minimize waste production during the mission.

Bare minimum food and water will be carried aboard the Taurus LMS. The mission duration is short enough that only a few kilograms of weight will be used up to supply the necessary rations. A large plastic squeeze bottle will be filled with drinking water and placed aboard the capsule for the astronaut along with several freeze-dried food bars that will be rehydrated by the astronaut's own saliva (Purser 1964). These rations will be placed in the same location as the astronaut's survival pack so any unused portions can be used if there is a significant waiting time for pickup upon landing, as in an emergency deorbit.

The cabin will be held at twenty-one degrees Centigrade and the astronaut will be allowed to vary this value up or down by three degrees, depending on individual preference. This temperature range is designed to promote comfort and a good working environment for the astronaut. It is also an acceptable range for the electronics associated with the Taurus LMS (Purser 1964).

The relative humidity in the capsule will be held at 50%, with the astronaut able to increase or decrease that level by 10%. Again, this range is designed for astronaut comfort, productivity, and the tolerances of electronics (Purser 1964).

The cabin atmosphere will be a mixture of 80% nitrogen and 20% oxygen at a total pressure of 101.3 kPa. Early in the design, consideration was given to either a depressurized capsule or an atmosphere of 100% oxygen at low pressure. The depressurized capsule was deemed a safety concern because the astronaut would be relying solely on his pressure suit for life support. The only conceivable backup would be another pressure suit, but there was neither room nor weight for this and there probably would not be time in an emergency to change into the second suit even if one was available. The low-pressure pure oxygen mix was tragically shown to be a fire hazard in the Apollo program, and the Taurus LMS had neither the room nor the allowable weight to install a complex fire extinguishing system. Thus, the standard atmospheric mix and pressure was chosen.

The backup pressure suit will be operated at a pressure of slightly more than half that of the cabin, or 55.16 kPa. The breathing mixture for the astronaut will be 50% oxygen, 50% nitrogen while in the pressure suit. Problems with pressure suit mobility occur at a pressure differential exceeding 55.16 kPa between the interior suit pressure and the ambient outside pressure. The pressure suit in the Taurus LMS will be required to function in one of two different worst case scenarios. In the first, there is a degradation in the quality of the cabin atmosphere, but not its pressure. There are many possible causes, including a fire or other contamination or a main life support component failure, such as the circulation fan. In either case, the cabin atmosphere still exists at 101.3 kPa. Rather than vent the cabin, the astronaut may be either able to filter it through the life support scrubbers if the problem was contamination or be able to repair the failed component if the problem was a main life support system breakdown. In any event, the astronaut must have mobility, so his pressure suit can operate at a pressure of 46.14 kPa or higher to stay within the required differential of 55.16 kPa with the cabin pressure. In the second worst case scenario, the cabin loses pressure either through a leak or intentionally by the astronaut. In any event, the astronaut now will require suit mobility with an outside ambient pressure of zero. This means the interior suit pressure can be as high as 55.16 kPa to keep in the requisite differential. The design pressure suit pressure is set at 55.16 kPa, a value which allows mobility within all of the scenarios just described.

A second concern of the pressure suit design was the proportions of the atmospheric constituents. Since the astronaut, when falling back on his pressure suit, will be going immediately from a high pressure gas mixture containing nitrogen to a gas mixture at much less pressure, there is a significant danger of the bends. A 50% oxygen, 50% nitrogen mixture at the specified 55.16 kPa will not be enough of a drop from the cabin pressure to cause the bends in the astronaut.

The entirety of the life support system will be computer monitored and controlled. The computer will be linked to sensors in the various tanks and flow regulators. According to the astronaut's inputs with respect to temperature and humidity, the computer will vary the flow rates of the various pumps and fans.

Both the main life support system and the pressure suit backup will be able to run either on the primary or secondary power sources. This prevents problems such as the astronaut having to switch over to his pressure suit if the main power supply goes down.

3.1.2 Main Life Support System

The main life support system is composed of a single duct containing equipment to scrub air that is circulated into it of waste water, carbon dioxide, and trace contaminants. A schematic diagram is shown in figure 3.1A.

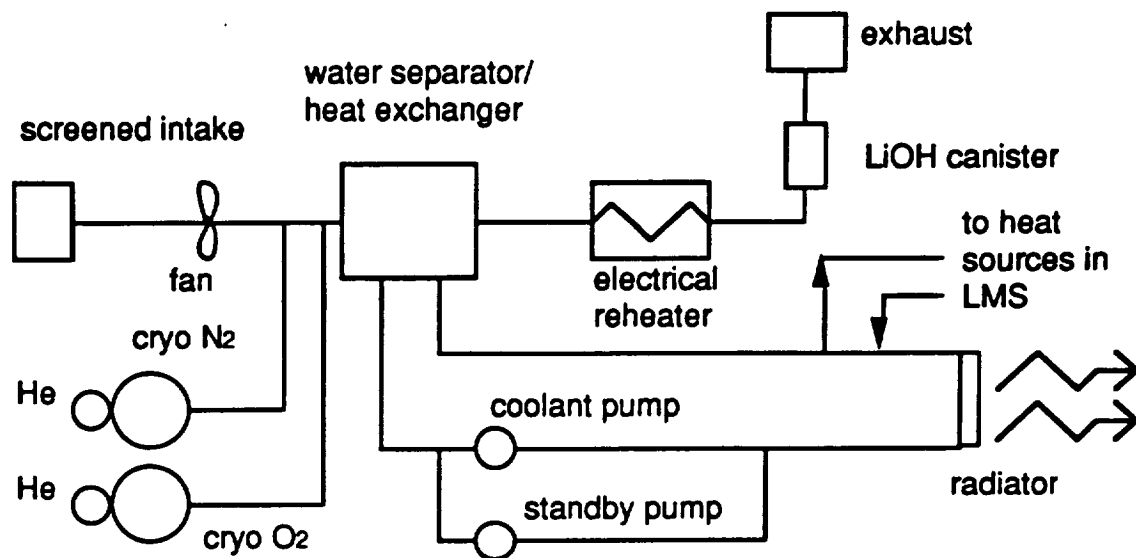


Figure 3.1A Main Life Support System

The intake of the main life support, or MLS, duct is located on the astronaut's left side. This duct has a screen over it to prevent the ingestion of foreign debris. The diameter of this intake and the entire duct is 12 cm.

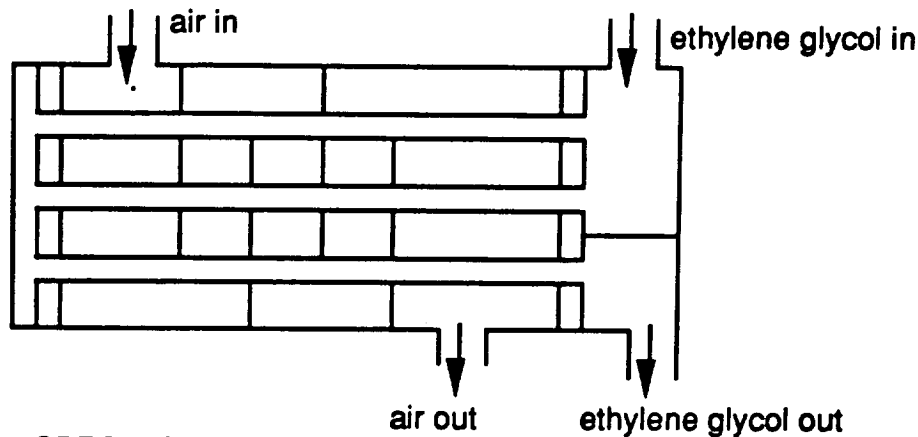
Located just inside the duct is the MLS circulation fan. This fan provides a volumetric flow rate of 0.1131 cubic meters per second by blowing air through the duct at a velocity of 10 m/s. The fan weighs 1 kg and utilizes 20 watts of power.

Downwind from the fan are the oxygen and nitrogen gas injectors. The MLS air supply is stored cryogenically in two tanks, one for oxygen, one for nitrogen. Enough air is stored on liftoff to allow for repressurizing the cabin once in orbit in the event the cabin air is contaminated or lost in orbit, and allowing for the astronaut's metabolic consumption of oxygen over a twenty-four hour period, with leakage from the spacecraft. A cabin volume of 4.08 cubic meters was estimated in the calculation of the mass of gas to repressurize the cabin. The metabolic rate for a human being was taken at the average value of .9071 kg/day of oxygen (Koelle 1961). A leakage rate of 200 cubic centimeters per hour was assumed for both nitrogen and oxygen. This last assumption is based on leakage rates measured on spacesuits in the Mercury program and has proved so insignificant a value (0.2674 kg for nitrogen leaked to space over a 24 hour period) do not warrant a better calculation until actual tests can be conducted on the Taurus LMS.

One cryogenic tank will hold 4.055 kg of liquid nitrogen, the other 2.066 kg of liquid oxygen. These tanks will be pumped by positive expulsion bladders utilizing high-pressure helium from co-located tanks. The cryogenic fluids will be heated by electrical reheaters which will supply the energy to vaporize them and heat them to the cabin temperature of 21 degrees Centigrade. The computer will pump in gas on a need basis as determined by its sensors. These gases are

injected just downwind from the fan so that they will pass through the entire scrubbing system before entering the cabin, as a safety concern.

The water separator, shown in figure 3.1B, is the next component in the MLS system.



SPECIFICATIONS

1. 30 kg of ethylene glycol in system
2. cross-flow heat exchanger
3. volumetric flow rate of 0.01083 cubic meters per second of glycol
4. exchanger is constructed of 16.12 kg of aluminum
5. air enters at 21 and leaves at 10 degrees Centigrade
6. glycol enters at 0 and leaves at 5 degrees
7. overall dimensions are 0.39 m X 0.39 m X 1 m

Figure 3.1B MLS Water Separator

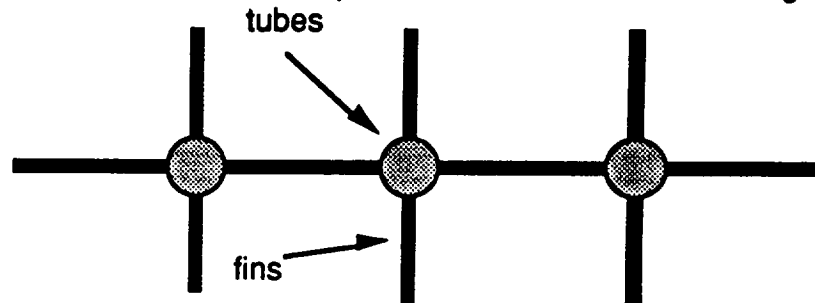
This component is a heat exchanger composed of a bank of four hundred aluminum tubes. The bank has 20 tubes to a side and has an overall mass of 16.12 kg. Each tube is 0.5 mm thick, 1 m long, and has an outer diameter of 0.005m. Ethylene glycol will flow through these tubes, entering the bank at 0 degrees and leaving it at 5 degrees Centigrade. Air will enter the heat exchanger at 21 degrees and will be cooled to 10 degrees by the ethylene glycol, well below the dew point (Singh 1985). The cooling of the air will cause the condensation of water vapor onto a network of wicks located between the heat exchanger tubes. These wicks will transport the excess water vapor away through capillary action (Purser 1964). To accomplish its task of cooling the air, the heat exchanger will transfer 9.3 watts of heat to the ethylene glycol.

The ethylene glycol in the heat exchanger will flow to a radiator located on the exterior skin of the spacecraft. Other pipes will carry ethylene glycol to the radiator from various locations inside the spacecraft where the fluid has absorbed waste heat. The exact geometry of this second coolant system will be determined by the location of various heat-producing electronic components within the capsule. It will be a separate branch of the water separator/radiator loop shown in figure 3.1A, but will utilize the same pumps and working fluid.

Heat will be introduced to the capsule from a number of agencies, including the sun, solar albedo flux reflected from the earth, the earth's own thermal radiations, aerodynamic heating, the astronaut's metabolism, and the Taurus LMS

electronics. These heat inputs to the spacecraft exceed the heat radiated to earth and deep space by the spacecraft, even assuming the aluminum skin has a coating of white paint, which offers extremely good absorptivity and emissivity characteristics (Agrawal 1986). The extra 374 watts of heat will be radiated to space by the radiator, for a total of 383 watts including the heat taken from the water separator in cooling the cabin air below the dew point.

The radiator must be oriented towards deep space during the mission, not earth. It will have an area of 1.49 square meters and is shown in Figure 3.1C.



SPECIFICATIONS

1. Fin-and-tube type radiator
2. 9 tubes and 28 fins
3. tube inner diameter is 0.01 meter
4. tube thickness is 0.002 meter
5. fin thickness is 0.002 meter
6. fin width is 0.03 meter
7. overall dimensions are 0.44m X 0.78 m
8. radiator dumps 200 watts of heat
9. constructed of 10 kg of aluminum
10. radiator radiates at 0 degrees Centigrade

Figure 3.1C MLS Water Separator

It is a tube-and-fin type radiator in which the coolant tubes have fins attached to them to increase the radiating area. Constructed of aluminum, each radiator will weigh 6 kg.

A study was undertaken to determine whether passing through eclipse would cause excessive cooling in the Taurus LMS, requiring electrical heaters to maintain the equilibrium temperature of 21 degrees. The calculations were simplified by neglecting albedo, aerodynamic heating, and the earth's thermal radiation. The period of eclipse for a typical orbit of the Taurus LMS is approximately 30 minutes, and the study showed that the temperature of the capsule would only drop 2 degrees during that time due to radiative cooling. In other words, the capsule will experience no significant cooling when orbiting in the earth's shadow (Agrawal 1986).

After the air has passed through the water-separating heat exchanger, it will be at a temperature of 10 degrees. Electrical reheaters are located in the duct immediately following the heat exchanger to heat the air back up to 21 degrees. These heaters will require approximately 10 watts of power.

Once reheated, the air will pass through a lithium hydroxide (LiOH) canister

that will remove excess carbon dioxide chemically. Each LiOH canister will be cylindrical, with a diameter of 12 cm, the same as the air duct, and a length of 0.26 m. It will contain enough LiOH for 12 hours of carbon dioxide removal, so 3 will be included in the 24 hour mission with the third added for safety. When in use, the canister will be located on the astronaut's righthand side, in an easily accessible location. When the 12 hours is up, the astronaut will simply reach over and pull the canister out by its built-in handle, replacing it with the spare. The computer will monitor the life of the canister and remind the astronaut when to replace it. This system allows adaptability to missions of longer duration by simply adding more spare canisters to the cargo manifest.

The LiOH canisters have the second function of trace contaminant removal. Attached to one end of the canister will be a small cartridge of activated charcoal. This charcoal will filter out any minor impurities or odors from the cabin air (Purser 1964). Air leaving the LiOH canister, having been filtered of excess water vapor, carbon dioxide, and trace contaminants, will then be vented back into the cabin.

3.1.3 Secondary life support system

The secondary life support system (or SLS), as shown in Figure 3.1D, will revolve around the 10 kg pressure suit.

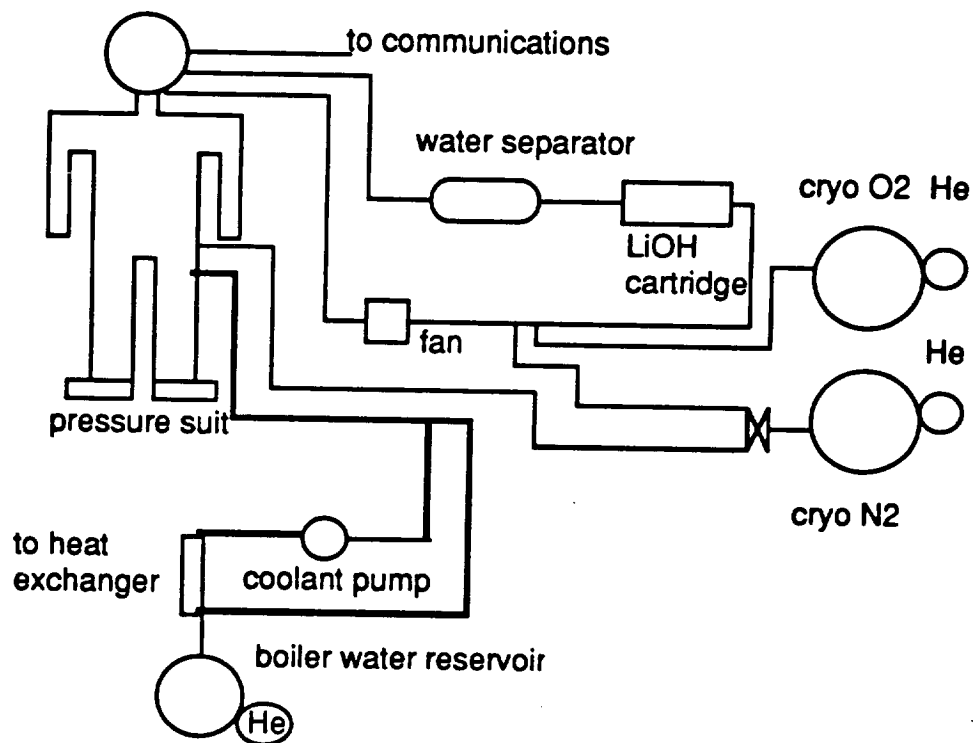


Figure 3.1D Secondary Life Support System (SLS)

This pressure suit will be worn by the astronaut throughout the mission, but will not be pressurized unless there is an MLS failure. The SLS will provide a self-contained environment for the astronaut, until successful deorbit and landing. Its lightweight nature indicates that this pressure suit is not EVA-rated.

The pressure suit is a composite of two separate entities, the helmet and the body. A special seal separates the two, allowing a one-time pressurization of the suit body by pure nitrogen gas while the independent helmet will be circulated continually with 50% oxygen, 50% nitrogen at 55.16 kPa total pressure. The SLS life support gases will be carried in a pair of separate cryogenic tanks. These tanks will carry ~1 kg of oxygen and nitrogen, respectively, which will be electrically heated before being injected into the SLS loop.

A LiOH cartridge immediately follows in the SLS loop. This cartridge is not removable. It will contain appropriate amounts of LiOH and activated charcoal for carbon dioxide and trace contaminant removal over twenty-four hours.

Downwind of the LiOH cartridge, a turbine-operated centrifugal water separator will remove water vapor from the astronaut's exhalations. This type of water separator was used on the lunar excursion module of the Apollo program, another vehicle under tight weight constraints. Given the two-decade technological gap between that program and the Taurus LMS, it is felt that the design goal of 5 kg for the separator's mass can be met. (Purser 1964).

Underneath the pressure suit, the astronaut will be wearing a water-cooled undergarment. This garment will have tiny tubes woven into the fabric through which cooling water will flow and will provide for thermal control inside the suit. Once the water has passed through the undergarment, it will be pumped to the MLS heat exchanger. Design requirements for this system are 5 kg of coolant water, and a 0.5 kg pump for the coolant water.

The pressure suit, as stated, will not be pressurized until an MLS failure. Warning will come from either the computer while monitoring its sensors or from the astronaut's own perceptions. Once warned, the astronaut will lower his helmet's visor, sealing the suit and activating the SLS system. Immediately, the computer will pressurize both the suit and the helmet and activate the atmospheric scrubbing and thermal control systems of the SLS.

There will be three attachment points on the pressure suit for hookups into essential systems, two on the helmet and one on the pressure suit body. The first helmet attachment point will be a plug-in for the capsule communications system. The second helmet attachment point will be a hose connection for the SLS atmospheric filtering system. The body attachment will be for both the liquid-cooled undergarment and the pressurizing line from the cryogenic nitrogen storage tank. Note that all three attachment points will be quick-releasing so that the astronaut may decouple from the spacecraft and egress in a minimum amount of time should there be an emergency on the launch pad or upon landing.

3.1.4 Contingency equipment

Additional life support equipment will be carried in the Taurus LMS for various contingencies. In the event of a fire, a 4.5 kg carbon dioxide fire extinguisher will be easily accessible to the astronaut. A first aid kit will also be included, containing drugs to alleviate the various debilitating conditions that the astronaut might reasonably expect to encounter during the mission. Finally, a 17.7 kg survival pack will be carried in the craft (Koelle 1961). This pack, similar to ones carried by U.S. military pilots, will carry a life raft and other survival equipment the astronaut may need upon landing at an unplanned landing site or any other instance where pickup time may be substantially longer than a few hours

Table 3.1A Mass / Power Breakdowns for Life Support

COMPONENT	MASS (KG)	POWER(WATTS)
1. MLS NITROGEN	4.055	0
2. MLS OXYGEN	2.066	0
3. MLS CIRCULATION FAN	1	20
4. MLS WATER SEPARATOR	16.12	0
5. MLS ELECTRICAL REHEATER	0.5	10
6. MLS COOLANT PUMP (EACH)	1	30
7. ETHYLENE GLYCOL	30	0
8. MLS RADIATOR	10	0
9. LIOH CANISTER (EACH)	1.211	0
10. SLS NITROGEN	1	0
11. SLS OXYGEN	0.9835	0
12. SLS LIOH CARTRIDGE	2.422	0
13. SLS CIRCULATION FAN	0.5	5
14. SLS WATER SEPARATOR	5	0
15. SLS COOLANT WATER PUMP	0.5	5
16. SLS COOLANT WATER	5	0
17. PRESSURE SUIT	10	0
18. FOOD/WATER	4	0
19. FIRE EXTINGUISHER	4.5	0
20. FIRST AID KIT	0.5	0
21. SURVIVAL PACK	17.7	0
<u>TOTALS</u>	<u>120</u>	<u>60 (MLS) / 15(SLS)</u>

Section 3.2 Affects on Humans

3.2.1 Acceleration

The affects of large accelerations on human beings is of concern on the Taurus booster due to the fact that achieves a relatively high acceleration. For a short period of time, the acceleration will reach 10 gees. Large accelerations will also be encountered in the case where the use of the abort system is necessary. Large accelerations have many affects on humans; including loss of peripheral vision, difficulty breathing, chest pain, and can go as far as blackout and death (Stapp, 1960). Colonel John Paul Stapp did an indepth study limitations of acceleration which the humans can withstand in varying positions. He found that when the human is positioned with his/her back at a 65-70 degree angle to the direction of the acceleration and their thighs in the direction of the acceleration, they could withstand the largest amounts of acceleration for the longest periods of time. Figure 3.2A shows the plotted data which Colonel Stapp found.

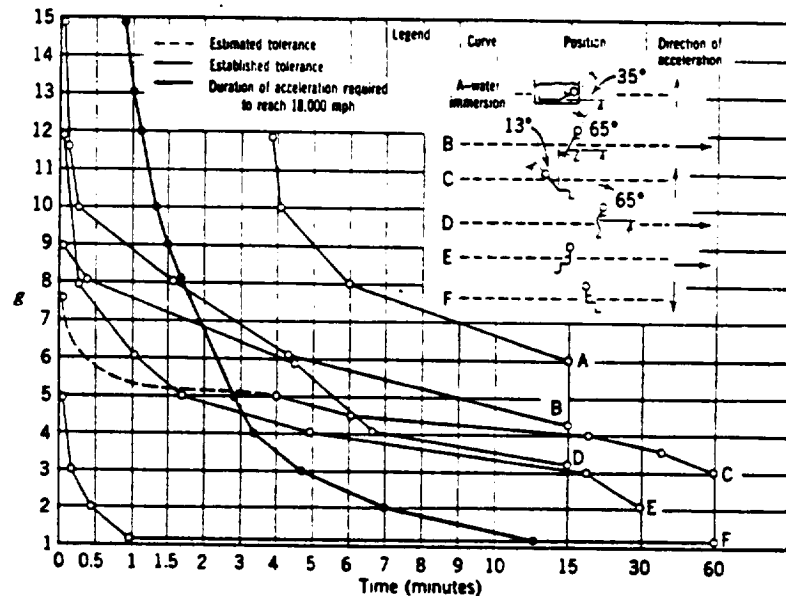


Figure. 3.2A : Accelerations tolerable to human beings(Stapp,1960)

These time limits were determined such that the humans would still be able to see, think, and retained at least finger control (Stapp,1960). This position will be used in the capsule in order to reduce discomfort during take-off and reduce the chances of the astronaut becoming incapacitated.

Section 3.3 Crew Compartment

3.3.1 Ingress/Egress

Ingress and egress will both be through a single hatch located on the side of the capsule behind and slightly above the position of the astronaut's head when positioned in the seat. The hatch will be approximately 0.75 m wide and 0.50 m high. The astronaut will enter the capsule feet first. When the astronaut is in the seat, the feet will be placed into pressure sensitive slots which securely hold the feet and are released when the harness is unbuckled or manual switches are thrown. Then the waist and shoulder harness lock together over the astronaut's stomach. Figure 3.3A shows how they come together into a single buckle.

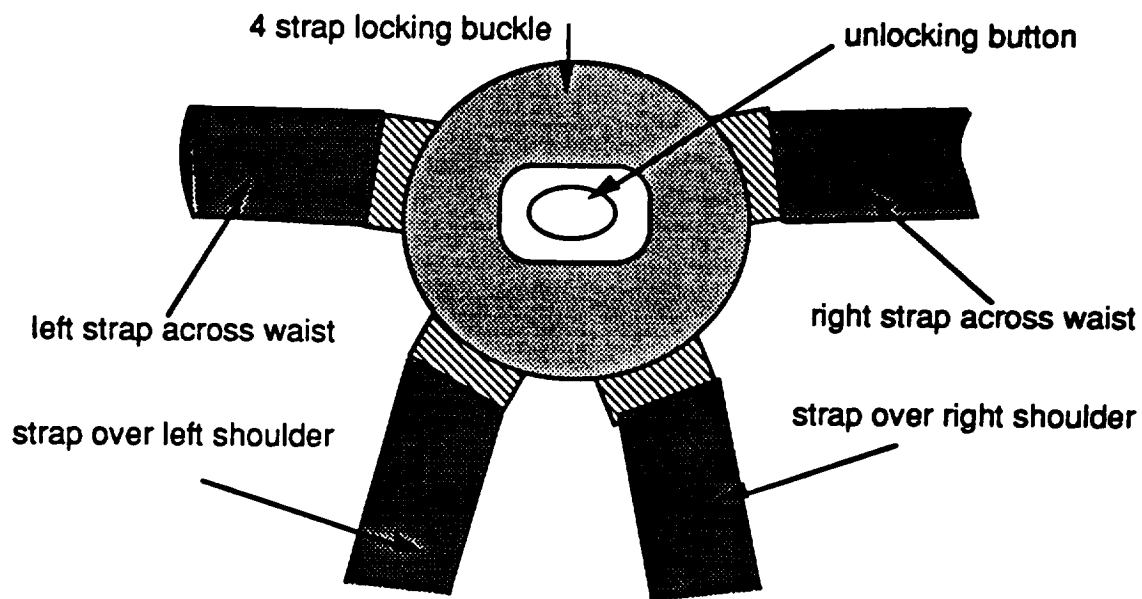


Figure 3.3A Central Buckle for Seat Belt System

The hatch will then be shut and locked into place.

For egress, the astronaut will first release the upper body by pressing the button on the buckle. This will release all straps over the upper body and the holders on the feet. Next, the explosive bolts on the hatch will be blown. The hatch will open outward and the pilot will pull himself/herself out of the capsule. The estimated time of egress is about 20-30 seconds.

3.3.2 Pilot Seat

There were two major requirements in designing the seat. One was that the seat be conducive to the accelerations which would be encountered. The other was that the seat require the least amount of cross-sectional area and volume inside the capsule. This is mainly due to the major weight restriction which have on the Taurus booster. Because the mission is intended to be one of short duration, at

most 24 hours, the pilot's comfort has been forfeited somewhat. Figure 3.3B shows the basic position of the astronaut. B, T, and L represent the lines which the pilot's back, thigh, and lower leg will make, respectively, when positioned in the seat. This figure also shows that the thigh will be approximately in line with the acceleration. The values for B, L, and T which were used are 1.02 m, 0.56 m, and 0.48 m, respectively (Webb Associates, 1978). These values refer to the values under which 95% of the population fall under. Figures 3.3C and 3.3D show the side view and the top view of the seat with measurements. These measurements were all determined as the minimum measurements required for the maximum size astronaut. The mass of the seat was determined to be 16 kg, this includes the stick control on each arm rest. The location of the center of gravity and the moment of inertia about this center of gravity were determined for the 16 kg seat and an average human with a mass of 81.5 kg (Webb Associates, 1978). The location is referenced to the central point where the thigh portion of the seat and the back portion meet. The values are as follows: $X_{cg}=0.18$ m, $Y_{cg}=0$ m, and $Z_{cg}=0.30$ m. The values of the moments of inertia were determined to be: $I_{x,cg}=6.48$ kg-m², $I_{y,cg}=10.37$ kg-m², and $I_{z,cg}=8.47$ kg-m².

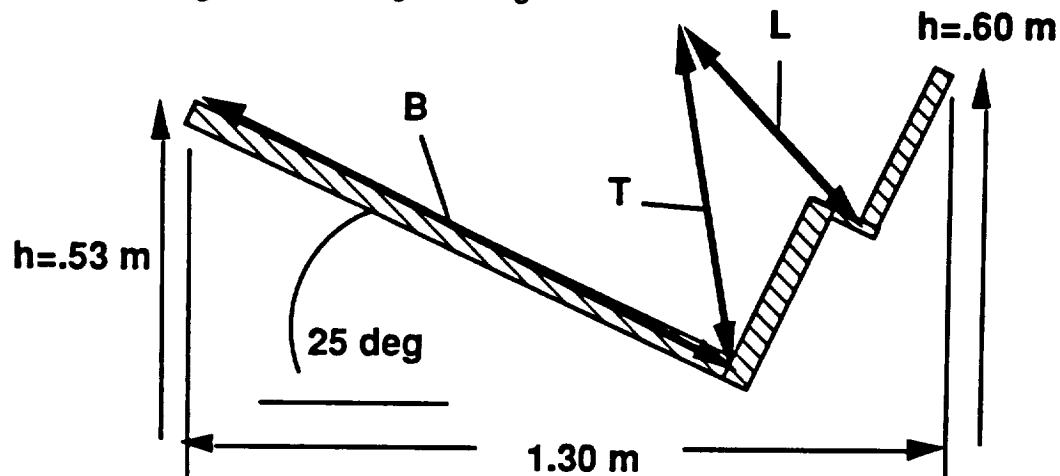


Figure 3.3B: Basic Astronaut Position

The seat was then used to determine the minimal amount of volume and cross-sectional area required in the vehicle. This was done graphically. Figure 3.3E shows the minimal volume and cross-sectional areas. These values were then used in determining the actual vehicle size and shape. Assuming the walls to slope at approximately 20 degrees, it was determined that the seat itself, requires a base diameter of at least 1.66 meters. At a height of 0.66 meters above the base of the seat, an internal diameter of 1.18 meters was necessary. These values were then used by systems analysis to determine the shape and size of the vehicle.

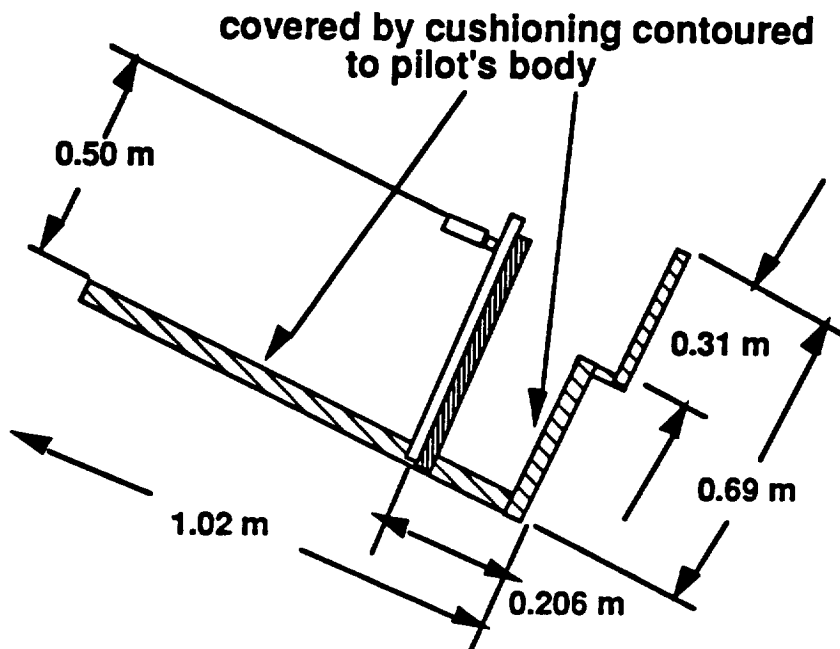


Figure 3.3C: Side View of Seat

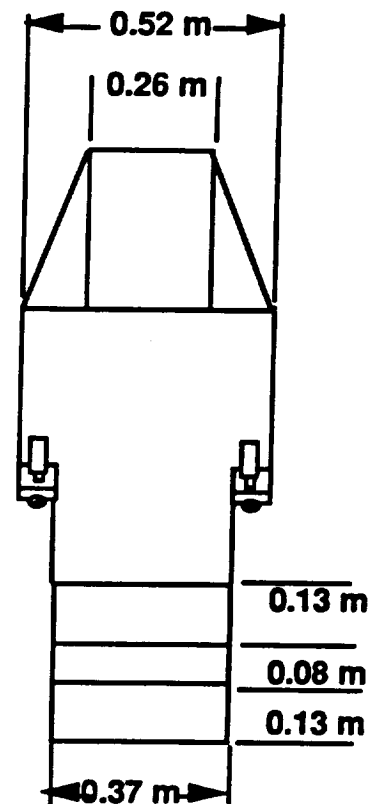


Figure 3.3D: Top View of Seat

The vehicle will be more conducive to smaller astronauts. They will have more room to move around. The larger astronauts will be cramped. They may be able to move their legs into the space available along the wall of the capsule, but the space will be limited and in general these astronauts will have to bear the discomfort. The discomfort will be tolerable for the length of the mission. One obvious requirement in the choosing of an astronaut will be that they are not claustrophobic.

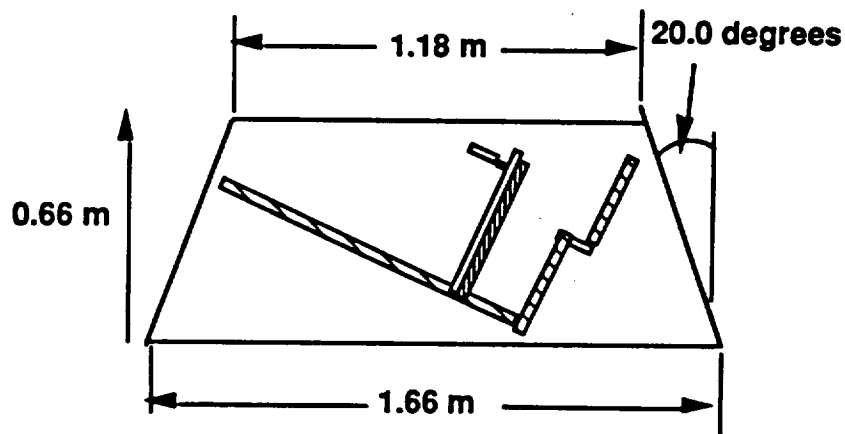


Figure 3.3E: Minimal Volume Required for Seat

3.3.3 Display Panel

The display panel has been designed to be as simple as possible in order to save weight. It will have two six inch displays with various modes which will show all the information necessary to the pilot. The information will be divided among the two screen when both are operational. On the left screen, information which is used for the actual flight of the vehicle will be displayed (Koelle, 1961). The displays included among the modes on the left side will be pitch, roll, yaw, heading, velocity, altitude, thrust, orbital velocity, orbital altitude, longitudinal acceleration, and latitudinal acceleration. The right screen will have the quantitative information such as environmental information, time, power plant and fuel information, and communications. This is information which the pilot does not need to be continually observing (Koelle, 1961). Displays among the various modes of the right side include temperature, pressure, humidity, radiation, O₂/N₂ partial pressure, O₂/N₂ flow rate, O₂/N₂ remaining, LiOH time remaining, power remaining, fuel/oxidizer flow, fuel/oxidizer remaining, fuel / oxidizer pressures, present time, elapsed time, and communications. In the case of a failure of one of the screens, all the information can be displayed in a different set of modes on a single screen. This is the redundancy provided for the display. Figure 3.3F shows what the display should look like. The buttons around the screens will be used to call up the various modes. The buttons will be 2.54 cm by 2.54 cm. They will be big enough so that the astronauts will be able to use them while wearing the gloves of their pressure suits. The overall size of the display panel should be about 0.46 meters by 0.23 meters. There will also be a second keyboard to provide redundancy on the keyboards. There will also be at least one button on each of the joysticks, one for initiating abort and one for firing the reentry rocket. Although the abort will most likely be initiated automatically due to the lack of time associated with a solid booster, it is felt that there should still be possible to manually abort for redundancy.

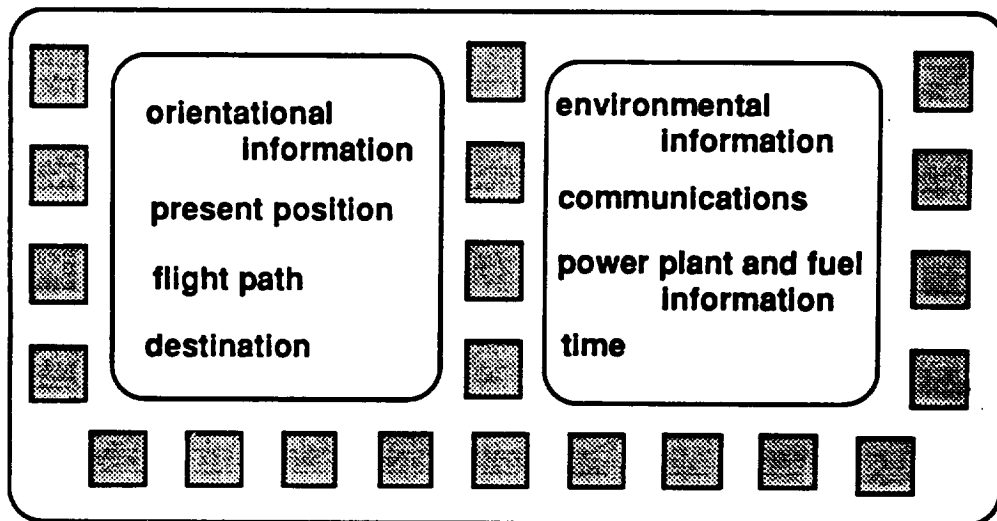


Figure 3.3F: Display Panel

Chapter 3 References

Agrawal, Brij N.: *"Design of Geosynchronous Spacecraft,"* Prentice-Hall, Inc., Englewood Cliffs, New Jersey, 1986.

"Anthropometry for Designers." ed. Staff of Anthropology Research, Webb Associated, NTIS, Springfield, VA, 1978.

"Handbook of Astronautical Engineering": ed. Heinz Hermann Koelle, McGraw-Hill Book Company, New York, 1961.

"Manned Spacecraft: Engineering Design and Operation": ed. Paul E. Purser, Maxime A. Faget, and Norman F. Smith, Fairchild Publications, Inc., New York, 1964.

Singh, Jasbir: *"Heat Transfer Fluids and Systems for Process and Energy Applications,"* Marcel Dekker, Inc., New York, 1985.

Stapp, Colonel John Paul. "Human Tolerance to Accelerations of Space Flight." *Physics and Medicine of the Atmosphere and Space.* Wiley, NY, 1960.

Chapter 4: Propulsion and Power

4.1 Taurus L.M.S. Abort System Hardware

This chapter section starts with the driving requirements for the abort system hardware, then describes the initial trade studies for the optimization of the system placement, finally describes the step-by-step rocket motor engine development and description. Specific equations and data for the abort system design will be provided in each appropriate section and in Appendix I as noted.

4.1.1 Specific Requirements

The abort system is required to insure crew survival in case of a critical failure of the Taurus booster system. A critical failure denotes an explosive detonation of the booster fuel and/or a critical malfunction which would make the Taurus booster system uncontrollable. Each would result in the destruction of the Taurus booster system, and there would be a minimal chance of crew survival without an adequate abort system attached.

Starting with the assumption of a five second detection time before the fuel in the booster detonates, the abort system would have to place the Taurus LMS crew capsule at a distance of one half mile or 805 meters from the launch site or moving booster, and place the capsule at a minimum of 500 meters in altitude for recovery parachute deployment. References for these abort criteria were established by space systems specialist Dr. David Akin, at the University of Maryland, and the Air Force space launch facility at Vandenberg AFB, California. Five seconds corresponds to the average detection time of a critical failure by electronic sensing devices. The 805m radial distance represents the typical danger radius of a detonating solid rocket booster system.

Consider the constant thrust from an activated abort system, with a few assumptions. These assumptions are, the effects of atmospheric drag on the system was negated, and the "coasting" of the aborted capsule after the abort system burns out was not accounted for in the distance. The constant acceleration equation states that:

$$\bullet \text{ Distance} = \text{initial velocity} \cdot \text{time} + (.5) \cdot \text{acceleration} \cdot \text{time}^2$$

rearranging the above equation yielded the calculation required for determining the minimal acceleration of the aborting Taurus capsule :

$$\bullet \text{ Acceleration} = 2 \cdot (\text{Distance} - \text{initial velocity} \cdot \text{time}) / \text{time}^2$$

With time and distance known, and the worst case occurring during the booster ignition with an initial velocity equal to zero, the constant acceleration required from the abort system was calculated to be 64.4 m/sec^2 . Looking at the worst case of accelerating in the pure vertical direction fighting gravity, the final required acceleration came to be 74.21 m/sec^2 or 7.56 gees.

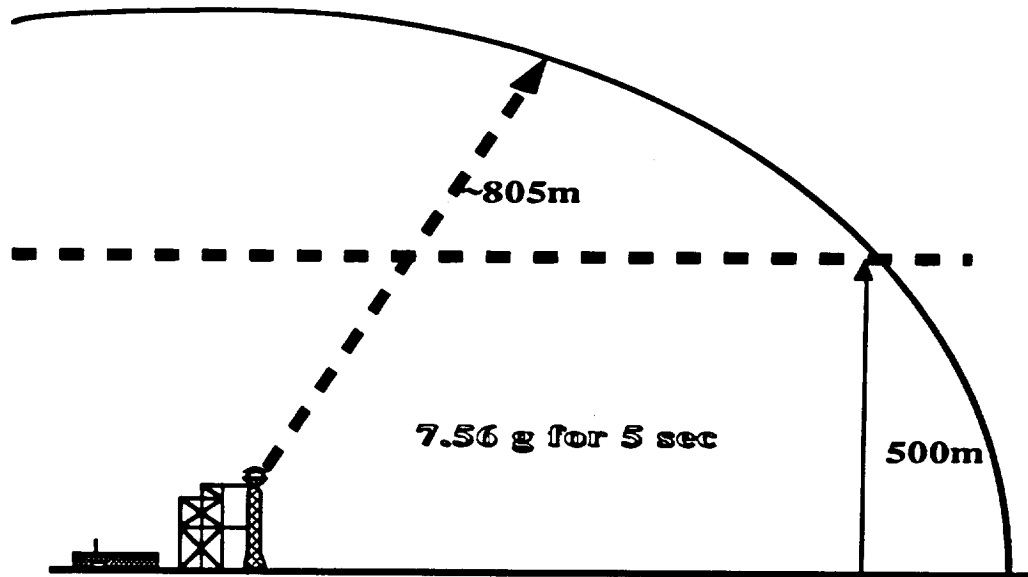


Figure 4.1A: Requirements for the Taurus LMS Abort System.

After examining the specifics of the Taurus booster system, it was noted that the booster produces a peak acceleration of ~ 9 gees. If the critical failure was to occur at this time, the required abort would have to overcome the Taurus booster's acceleration as well as accelerating away from the booster. The combination of these accelerations would be over the eleven gees sustained forces limit which was deemed hazardous to the capsule crew by the human factors division.

Three options were available for the Taurus abort system. First was to accept the danger of not being able to abort from the accelerating Taurus booster while it was in the high thrust/acceleration region. Second was to increase the thrust of the abort rocket motors to provide the required acceleration to separate the two vehicles and complete the abort scenario. The third solution was to modify the Taurus booster with thrust termination ports.

The first solution was unacceptable for the 99.9% crew survival rate. Since the Taurus booster has a reliability of 95% and with no capability for abort during the high thrust range, the danger to crew safety was too high.

The second solution was also unacceptable since an increased acceleration would black out and possibly injure the crew. A sample "quicker" abort of three seconds would require an acceleration of over 20 gees. The crew would be unconscious or unable to work controls, so the deployment of the parachute and landing of the aborted capsule would have to be completed by a computer-controlled auto-pilot.

The third solution was picked for incorporation into the abort system since thrust termination ports have been widely used on solid rocket systems, like the Minuteman ICBM, and the technology is well developed. (Hill & Peterson, 1970) The thrust termination device or "blow out " ports would ~instantaneously vent the pressure and extinguish the flame within the thrust chamber, thereby dropping the acceleration of the solid Taurus booster to zero. With the trust termination ports activated, the acceleration of the Taurus booster would be negated, and the abort system could function well within the required thrust limits.

4.1.2 Abort Motor / Engine Selection

A trade study of solid motors verses liquid engines was conducted to compare the advantages and disadvantages of each propulsion type. Table 4.1A illustrates the result, including examples of the relative engine sizes, shown in figure 4.1B.

	SOLID	LIQUID
PROS	<ul style="list-style-type: none"> - High thrust to weight - Simple in design - Very reliable - Few, if any moving parts - Lower volume requirements - Easy to store 	<ul style="list-style-type: none"> - Controllable thrust duration - Multiple starts - Higher specific impulse - Longer thrust duration times - Requires less fuel mass per unit thrust
CONS	<ul style="list-style-type: none"> - One shot operation - Thrust not controllable after motor ignition - Lower specific impulse - Toxic exhausts (HCl gas) - Fuels can be highly explosive 	<ul style="list-style-type: none"> - Lower thrust to weight - Complex system with multiple parts - Less reliable, requires redundancies - Separate oxidizer and fuel with pressurant (He) or pumps - Liquid propellants require higher volumes - Requires special storage facilities - Fuels & Oxidizer often highly toxic - Fuel/Oxidizer mixtures explosive

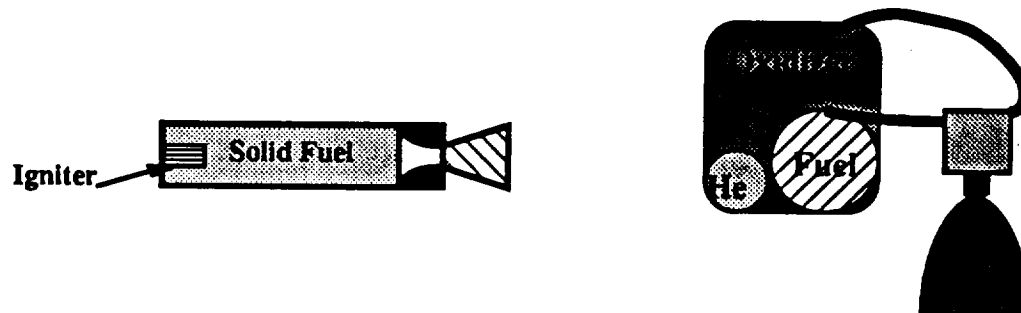


Table 4.1A & Figure 4.1B: Motor / Engine Selection

The selection of solid abort motors can come without any big surprises. Solid rockets meet the criteria of the abort system with the largest thrust per mass, simple design, one time operation, high reliability, and having a complete rocket motor in a storable, movable container. Solid abort motors were also used in the earlier Apollo and Gemini space programs. This shows a historical trend of solid motor application to similar abort operations.

4.1.3 Motor Number Selection

The Taurus Spacecraft will use a combination of three (3) solid abort motors, placed 120° apart. The motor number selection was based on the facts that fewer motors reduce the hardware mass associated with the motor, increase the reliability by decreasing the number of failure points, and fewer motors reduce the heating points on the Taurus capsule during an abort sequence. The initial placement of each motor at 120° results from the analysis of the thrust vectors from each engine which generate moments from their firing position. At 120° , each motor is horizontal thrust occurring from the angled attachment would be canceled by the other two operating engines. Figure 4.1C. illustrates the thrust vector cancellation of the three motors set at the same attachment angle θ .

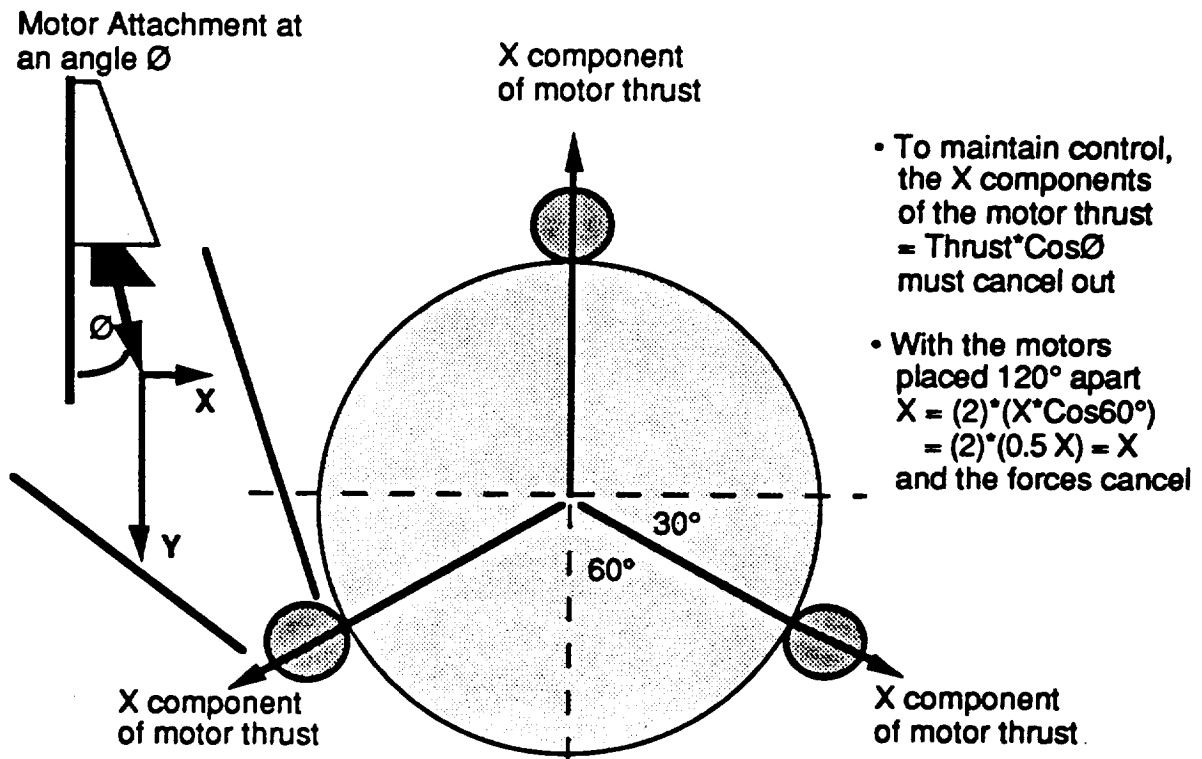


Figure 4.1.C.: Thrust Vector Cancellation on Engine Placement.

4.1.4 Motor Attachment Selection

Attachment of the abort motor system was the next main area of concern. Again three basic designs were analyzed in a trade study. The first system was a tower attachment similar to the systems used on the Gemini and Apollo programs with abort motors attached to the top. The second system consisted of abort motors bolted to the lower diameter of the crew capsule. The third system involved placing the abort motors underneath the crew capsule. Examples of each of the designs and trade studies are illustrated in figure 4.1D. and table 4.1B.

	Bolt-on Attachment	Tower Attachment	Internal Attachment
PROS	<ul style="list-style-type: none"> - Exhaust plume does not effect crew capsule or booster - Can carry the system to orbit for reentry burn - Little attachment hardware 	<ul style="list-style-type: none"> - Exhaust plume does not effect booster - System is "dumped" at altitude to save payload mass - Best directional control characteristics 	<ul style="list-style-type: none"> - Exhaust plume does not effect the crew capsule - System is carried into orbit and used for reentry burn - Min. attachment hardware - Motors fire straight down, yields minimal motor mass
CONS	<ul style="list-style-type: none"> - A delayed or misfired engine creates a large, uncontrollable moment - High powered control system required - Payload mass penalty from carrying system to orbit 	<ul style="list-style-type: none"> - Exhaust plume may heat the capsule beyond tolerance levels - Angled motors will require increased motor mass - The additional mass of the tower and attachments added 	<ul style="list-style-type: none"> - Exhaust plume will ignite the stored fuel in the service module - Directional control system will be required - Payload mass penalty for carrying the abort system to orbit

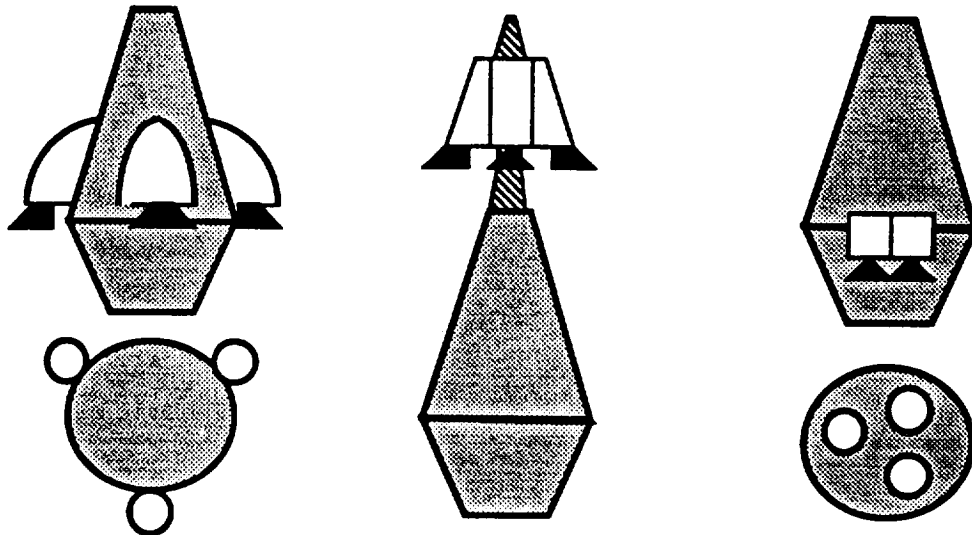


Table 4.1B and Figure 4.1D : Abort Motor System Attachment Options

The tower structure for the abort rocket placement was chosen due to many factors. These factors include mass savings from "dumping" the entire abort system at a predetermined height to orbit (~40-50 km) past maximum dynamic pressure (maxQ), thrust of the motors along the centerline of the craft to reduce the moments generated from a misfired engine, and minimal heating of the upper stages of the Taurus booster and the capsule itself by the exhaust plume of the motor.

4.1.5 Preliminary Performance Calculations and Fuel Selection

Entering into the design stage of the abort motor system, the total mass of the aborting capsule was estimated to be 900 kg. This value includes the crew capsule and the mass of the attached abort system. To reach 805 meters in 5 seconds, the solid motors must be able to produce 7.56 gees of acceleration on the 800 kg Taurus capsule. The average thrusting force required is calculated by:

$$\bullet \text{Force (thrust)} = \text{Mass} * \text{Acceleration} = 66,789 \text{ Newtons.}$$

The total impulse of the system is:

$$\bullet \text{Force} * \text{time} = \text{Total Impulse (N-sec)} = 333,945 \text{ N-sec}$$

The mass of the solid fuel required for the abort motor operation is:

$$\bullet \text{Fuel Mass} = \text{Total impulse} / (\text{Specific Impulse} * \text{acceleration of gravity, } g_0)$$

To reduce the mass of the system, a high energy, solid double base fuel was selected based on the need for a solid propellant with the highest specific impulse possible. The DB/AP-HMX/AL double base fuel was chosen with an Isp of 270 sec. (Sutton, 1986) With this selected Isp, and $g_0 = 9.8065 \text{ m/sec}$, the base amount of solid fuel mass needed, neglecting losses was 126 kg.

4.1.6 Motor Casing Material Selection

Motor casing was based on the selection of materials which offered the lowest density, the best resistance to high tensile stress loadings, and compatibility with the solid fuel being used. Based on a sampling of current data, as displayed in Table 4.1C, there are a wide variety of metals alloys, glass composites, and graphite composites which can be used as casing materials. Due to the high operating temperature of the double base fuel, a thermal liner will be required to protect the selected material since all the metals and composites have melting points well below 3707°C solid fuel flame temperature. Thermal protection methods will be described in section 4.1.8. The HTS organic (graphite) composite was found to have the best characteristics of high tensile strength and low density when compared to current metal alloys and other composite materials. The HTS composite will be used for the motor casing and nozzle assembly.

	D6aC Steel	Maraging Steel	Titanium (6% Al - 4%V)	S-Glass Filament Composite	Organic Filament Composite HTS
Tensile Strength (MPa)	1585.8	1379 to 2068.4	965.3	4500	1723.7
Density (kg/m^3)	7833.4	7999.5	4622.5	2490	1384
Modulus (GPa)	200	190	110	31.7	75.8
Melting Point (°C)	~1400	~1500	~1700	~2000	~2500

Table 4.1C Possible Casing Materials for the Abort Motors (Sutton,1986)

4.1.7 Abort Motor Specific Impulse Analysis

Specific impulse was analyzed to increase the performance of the abort motor while decreasing the required mass for an operational system. Specific impulse was found to be directly tied to the characteristics of the double base fuel as a function of flame temperature, chamber pressure, and exit pressure. A trade study, looking at the effects of varying the temperature and pressures (Appendix I), yielded important information based on the equation for specific impulse:

$$I_{sp} = \frac{1}{g_0} \left(\frac{2 \gamma R}{\gamma - 1} \right) T_0 \left(1 - P_e / P_0 \right)^{(\gamma - 1) / \gamma} \quad ^{0.5}$$

where γ equals the specific heat ratio of the solid fuel. When chamber pressure (P_0) and exit pressure ($P_e = P_a$ ideally expanded) were varied, the I_{sp} changed approximately 0.2%. The benefit of raising the chamber pressure for that 0.2% I_{sp} increase would be outweighed by the increase in the casing mass required to enclose the higher pressure abort motor.

The variable which had the largest effect on specific impulse resulted from increasing the flame temperature (T_0) of the burning propellant within the abort motor. An increase of 100°C yielded an average 3.5 sec increase in I_{sp} . Since the temperature of the burning double base fuel was 3707°C, very little could be done to increase the overall specific impulse of the fuel and decrease the fuel mass through increasing the I_{sp} .

4.1.8 Heat Transfer System

Current and future fuels which burn hotter will generally have the higher specific impulses, but the limiting factor comes with the material encasing the burning fuel and expanding the exhaust. Current casing materials like aluminum alloy 24S-T, alloy steel SAE X4130 (melting points $\sim 2700^{\circ}\text{C}$), and graphite epoxy (melting point $\sim 2300^{\circ}\text{C}$) have melting points well below the flame temperature of 3707°C for the double base solid fuel selected. Therefore the casing material must be protected from the hot gasses and solid fuel by selecting a heat transfer system such as an ablative liner, a heat sink, or an active liquid cooling system.

Due to mass constraints, the heat sink was ruled out as being too heavy and not needed for the short abort burn of five seconds. The active cooling system was not selected due to the complexity required and the lack of liquid fuel, usually used as a coolant, in a solid motor system. The ablative liner was chosen for the mass savings, and simplicity. The thickness and material type of the ablative material will vary depending on the location of the heating load. Figure 4.1E illustrates the operation of a typical ablative material.

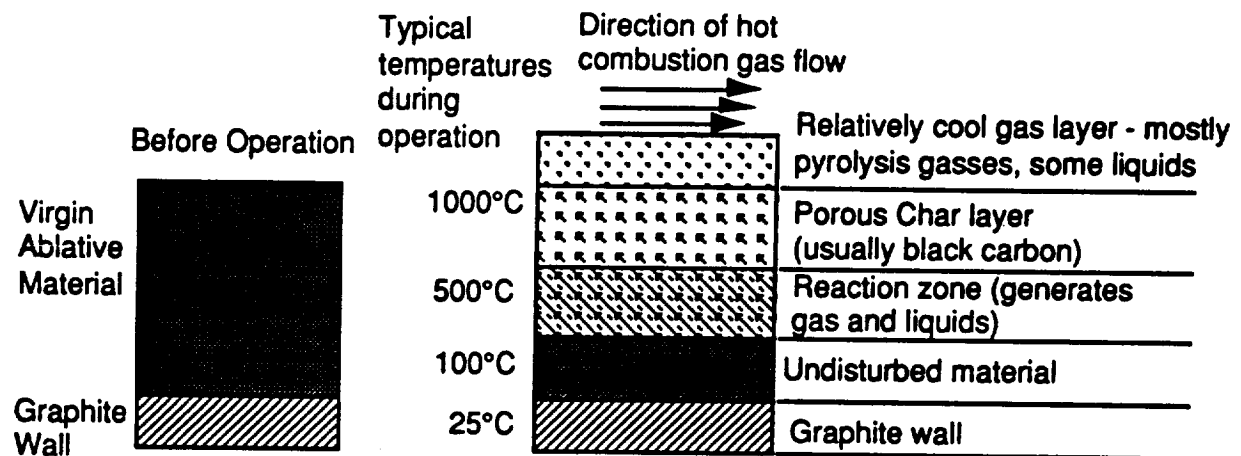


Figure 4.1E : Ablative Material During the Abort Motor Operation (Sutton 1986)

For the casing ablative liner, the heating load will depend on the last few seconds in which the burning solid fuel approaches the casing wall. Assuming the possibility that certain sections of the fuel will burn faster and reach the wall in three seconds, the ablative surface will have to resist the chamber temperature of 3707°C for two seconds to protect the integrity of the casing wall to complete the abort. Due to the high chamber temperature, an asbestos phenolic was selected as the insulation lining for the casing wall. (Sutton, 1986) With two second of exposure to the 3707°C temperature, and a safety factor of three, the ablative asbestos phenolic will be ~ 2.54 mm thick.

Due to the high thermal loads, the throat and nozzle will see a high heating load for the full five seconds of the abort, as well as reactive gasses and solid particulates. With these considerations at the throat and a factor of safety of three, a throat insert will consist of an ~ 0.8 mm thick layer of the ablative pyrolytic graphite covering a back-up ~ 2.0 cm layer ATJ molded graphite. The ~ 0.8 mm thick layer of the pyrolytic graphite will extend from the throat down to the tip of the nozzle to

protect the structural HTS graphite. (Sutton, 1986) The low erosion rate of the pyrolytic graphite makes it an excellent protective material for the throat and nozzle. Since the performance of the motor is dependent on the expansion ratio from the throat to the nozzle exit, throat diameter should not change more than 5% so to maintain the required thrust characteristics. (Hill & Peterson, 1970) For an estimated three centimeter diameter nozzle, the expected ablative material loss for the five second motor operation would be ~0.3 mm. The effective change in the throat diameter would be 1.0% which is well within acceptable limits.

4.1.9 Ignition System and Igniter Design

The ignition system for the solid abort motors will consist of a pyrotechnic igniter mounted at the top of the abort motor solid fuel. The ignition system will use energetic chemical formulations which heat the solid fuel to the ignition point. The pyrotechnic ignition system was chosen for its reliability, simplicity and small hardware mass. To prevent accidental engine firings occurring from static electricity build up or environmental conditions, a safe and arm device will be installed on each igniter system. Figure 4.1F shows a simplified typical pyrotechnic-type igniter in a pellet-basket configuration. (Sutton, 1986)

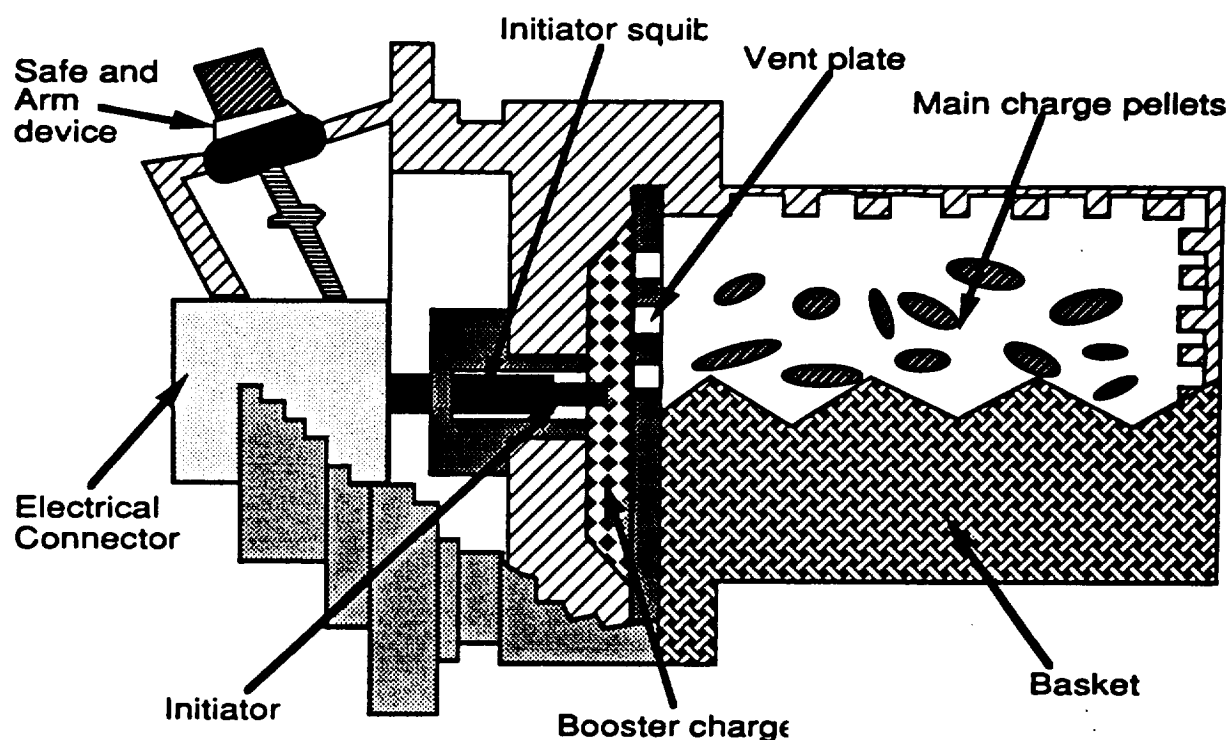


Figure 4.1F : Pyrotechnic-type Igniter Configuration.

4.1.10 Performance Trade Studies

To finish the motor design, a spreadsheet was developed to calculate the aspects of the abort solid motors, and to do trade study optimizations on chamber pressure, cylindrical motor diameter, cone nozzle angle, and tower attachment angle to reduce the overall motor mass. The data on the trade studies is available in Appendix I.

First, the chamber pressure and the burn rate were varied to find the best combination which gave the lowest abort motor mass. As denoted on figure 4.1G, the solid fuel burn rate and chamber pressure are linked exponentially for this type of solid double base fuel. (Sutton, 1986)

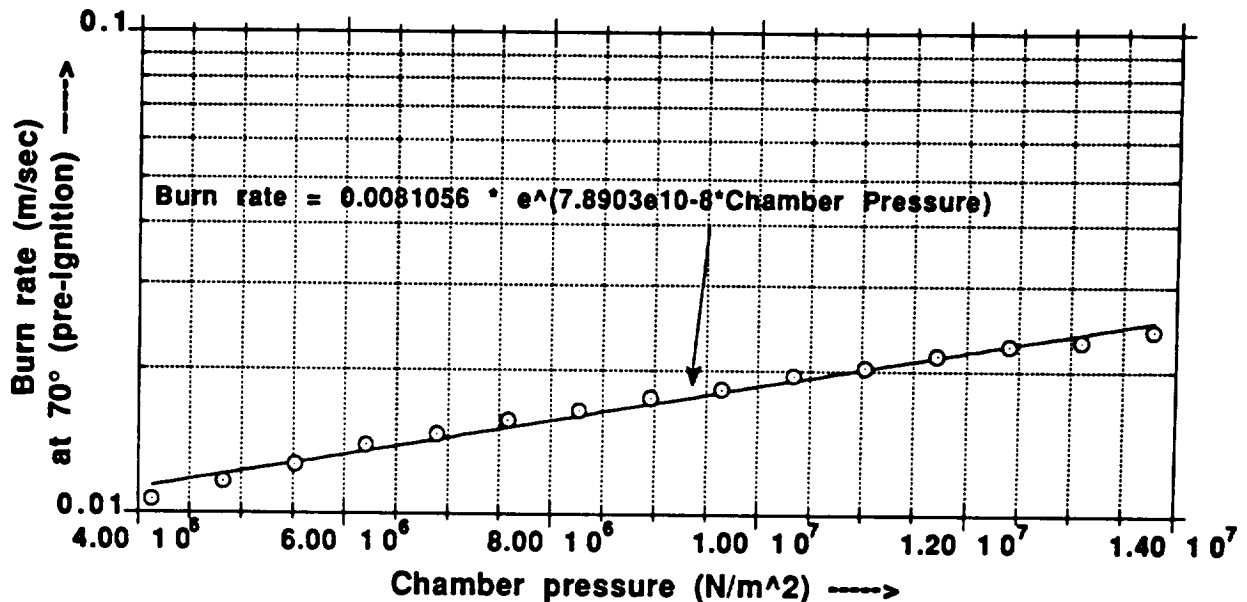


Figure 4.1G: Graph of Burn Rate vs. Chamber Pressure

Using Sutton's 1986 Rocket Propulsion Elements as a guide to the motor design, the selection of the chamber pressure was highly dependent on minimizing the mass of the casing, liner, nozzle, and igniter. In general, the spreadsheet calculations completed in Appendix I show that higher chamber pressures required thicker casing walls, a longer expansion nozzle, and an increased igniter mass. The higher pressure also decreases the casing liner mass due to the thicker solid fuel web and shorter motor length.

At lower chamber pressures, the casing liner thickness dominated the mass of the abort system due to a longer motor. The nozzle mass also began to contribute at the lower pressures due to increased thermal protection required to prevent a thermal failure of the nozzle during operation.

The chamber pressure study, illustrated in Figure 4.1H, shows the optimum pressure for the lowest final mass of the abort motors to be 4.9 MPa.

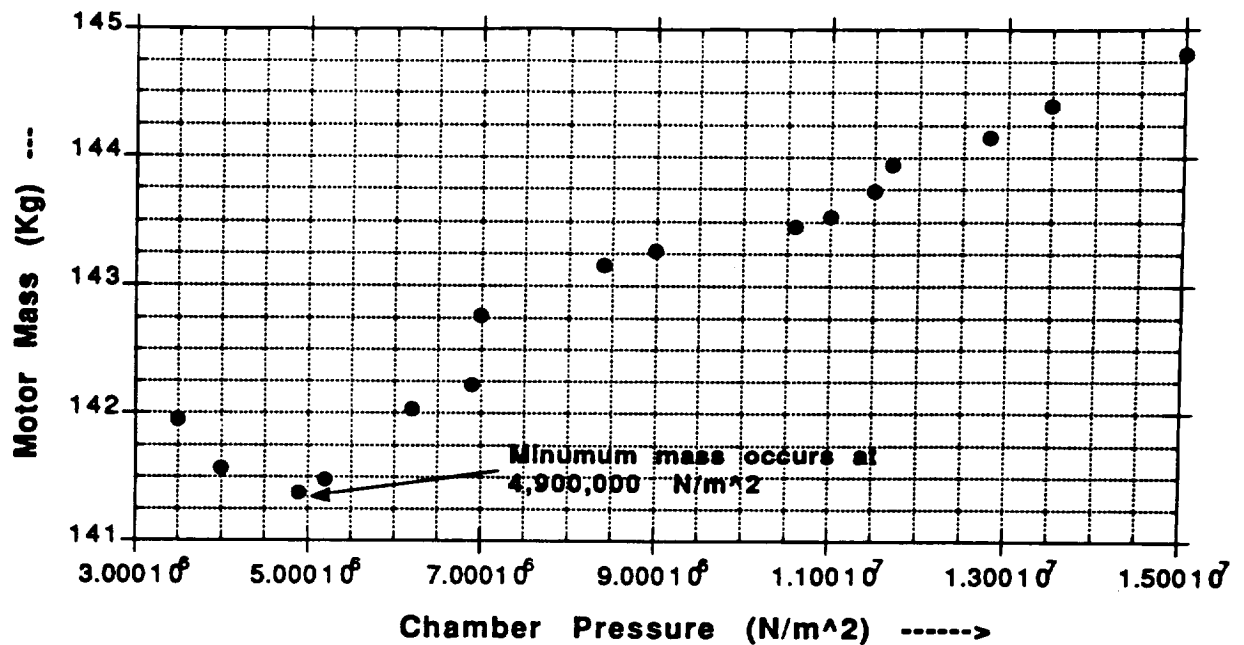


Figure 4.1H: Graph of Chamber Pressure Vs. Abort Motor Mass

Optimization trade studies on the motor diameter and nozzle cone angle were done in a similar manner with the spreadsheet program. The final data is listed in Appendix I, and graphically illustrated in Figures 4.1I and 4.1J.

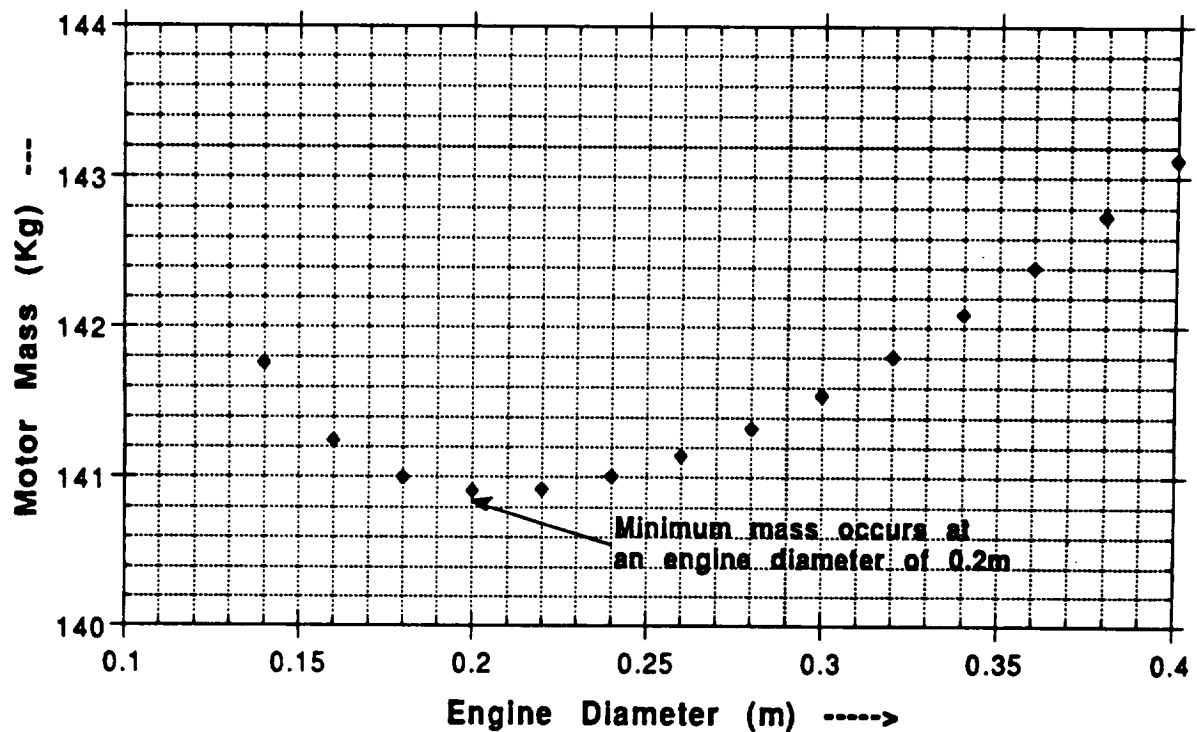


Figure 4.1I: Graph of Motor Diameter vs. Abort Motor Mass

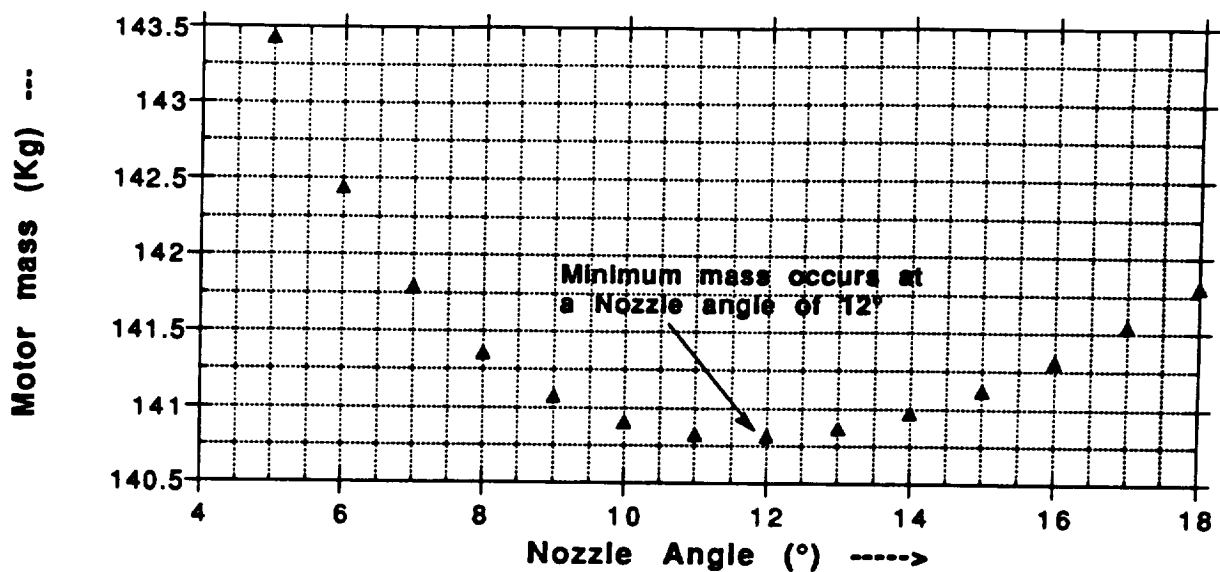
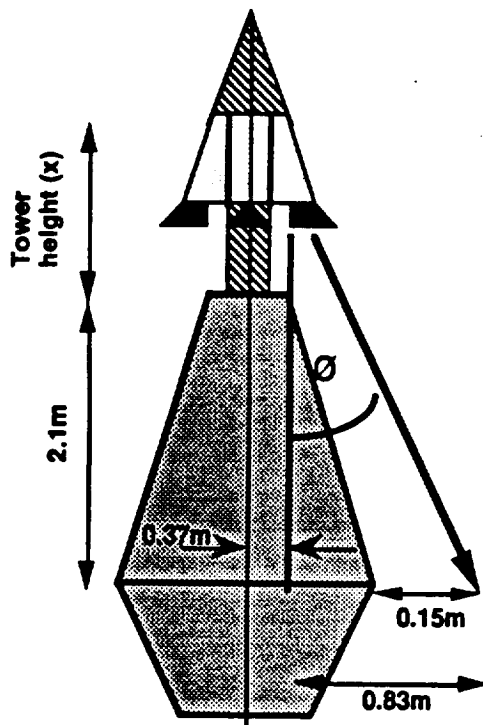


Figure 4.1J: Graph of Motor Nozzle angle vs. Abort Motor Mass

The results from the optimization yielded a motor diameter of 0.2 meters, and a half cone nozzle angle of 12°.

The optimization trade study spreadsheet on the placement of the abort motors on the tower structure was based on the following criteria in figure 4.1K.



- An aerodynamically designed faring will be attached to the tower top to reduce drag.
- The edges of the abort motors were placed at the top radius (0.37m) of the capsule to give room for hardware placement on the tower.
- Two exit nozzle diameters (~0.15m) was added to the centerline of the abort thrust to give the thrust more clearance of the capsule.
- Angle θ was dependent on the tower height (x) by the inverse tangent of $0.83/(2.1 + x)$.
- Thrust, and therefore the motor fuel mass, will be effected by θ .
- Mass of the tower ~5.5 kg per meter in height (Al alloy).

Figure 4.1K Abort Motor Placement vs. Tower Height Criteria

The final optimization data is listed in Appendix I, and is graphically illustrated in figure 4.1L, showing the best tower attachment angle vs. abort motor mass to be an attachment angle of 22°.

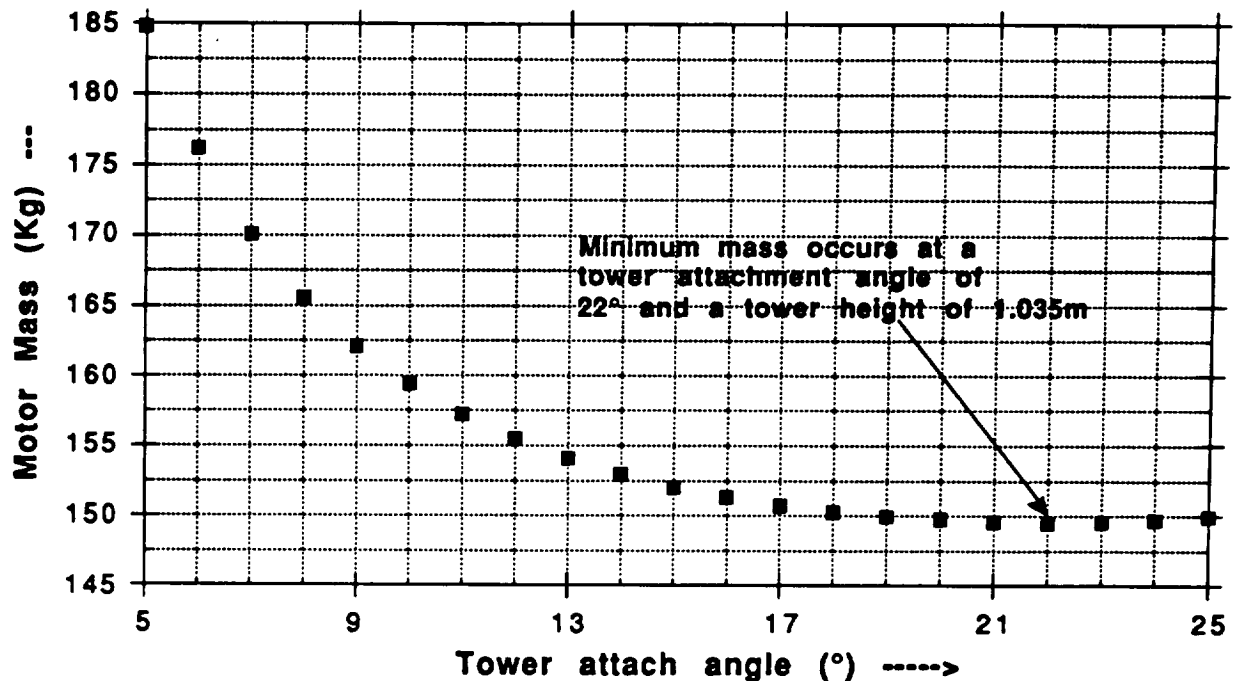


Figure 4.1L: Graph of Tower Attachment Angle vs. Abort Motor Mass

4.1.12 Final Motor Performance Characteristics

The following is a list of the final performance characteristics of the DB/AP-HMX/AL solid fuel motor determined through the optimization trade studies and references (Sutton 1986). Data and equations for these values can be referenced from Appendix I. The slotted tube propellant grain was selected by the values of the web fraction, L/D ratio, and volumetric ratio according to guidelines stated in Sutton's 1986 Rocket Propulsion Elements text.

Three such engines will be used for the abort system. The configuration consists of the three motor casings bonded together at an angle of 22°, and all three engines firing from one igniter system. Figure 4.1M. illustrates the dimensions and internal construction of one of the abort motors, and figure 4.1N. illustrates cross sectional views of the entire abort motor assembly.

Motor Performance
(21°C, Sea Level)

• Average Thrust (n)	23,382
• Chamber Pressure (MPa)	4.90
• Burn Time (sec)	5
• Ignition Delay (sec)	~0.035
• Total Impulse (n-sec)	116,912
• Fuel Specific Impulse (sec)	270
• Temperature Limits (°C)	15 to 27
• Ambient Pressure (MPa)	0.101
• Pressure Ratio	48.36
• Thrust - to - Weight Ratio	45.17:1

Propellant

• Fuel Type, DB / AP-HMX / AL : Double Base, Ammonium Perchlorate, Cyclotetramethylene Tetranitramine, Aluminum	
• Metal Content (%)	20
• Density (kg/m ³)	1799
• Burn Rate at 490 MPa (cm/sec)	1.193
• Burning Rate Exponent, n	0.49
• Flame Temperature (°C)	3707
• Specific Heat Ratio	1.24
• Exhaust Velocity, c (m/sec)	2647.8
• Characteristic Exhaust Velocity, c* (m/sec)	1730.6
• Hazard Classification DOT/MIL	B / 2

Propellant Grain

• Type	Slotted Tube
• Propellant Volume (m ³)	0.0250
• Web (m)	0.05966
• Web Fraction (%)	0.6184
• Sliver Fraction, Estimated (%)	2.0
• Average Burning Area (m ²)	4.035
• Effective Length (m)	1.002
• Volumetric Loading (%)	80.01

Ignition System		
• Type		Pyrotechnic
• Number of Squibs		2
• Minimum Firing Current (A)		~4
Motor Dimensions		
• Overall Length (m)		1.2
• Outside Diameter (m)		0.2
• L/D Ratio		5.193
Motor Casing		
• Material	High Tensile Strength Graphite Epoxy Composite	
• Nominal Thickness (mm)		
• Density (kg/m ³)		1384.93
• Factor of Safety		3.5
• Wall Thickness (mm)		0.995
• Min. Ultimate Strength (MPa)		1723.7
• Min. Yield Strength (MPa)		1436.4
• Case Free Volume (m ³)		0.0112
Casing Insulation		
• Type	Asbestos Phenolic Thermal Shield	
• Density (kg/m ³)		1107
• Thickness (mm)		2.54
Nozzle		
• Number and Type		1, fixed cone
• Expansion Area Ratio		5.9:1
• Throat Area (m ²)		0.00312
• Throat Diameter (m)		0.0315
• Exit Area (m ²)		0.0184
• Exit Diameter (m)		0.0765
• Expansion Cone Half Angle		12
• Throat Insert Material	Pyrolytic Graphite covering ATJ Molded Graphite	
• Shell Body Material	HTS Graphite composite	

Total Abort Motor Mass (kg)	
•Total	147.45
•Total Inert	8.778
•At Burnout	8.548
•Solid Propellant	135.07
•Internal Insulation Liner	5.574
•Igniter	0.0964
•Nozzles	0.375
•Case	2.733
•Miscellaneous (attachments, electronics ~2.5%)	3.596
(Propellant mass Fraction, 0.916)	

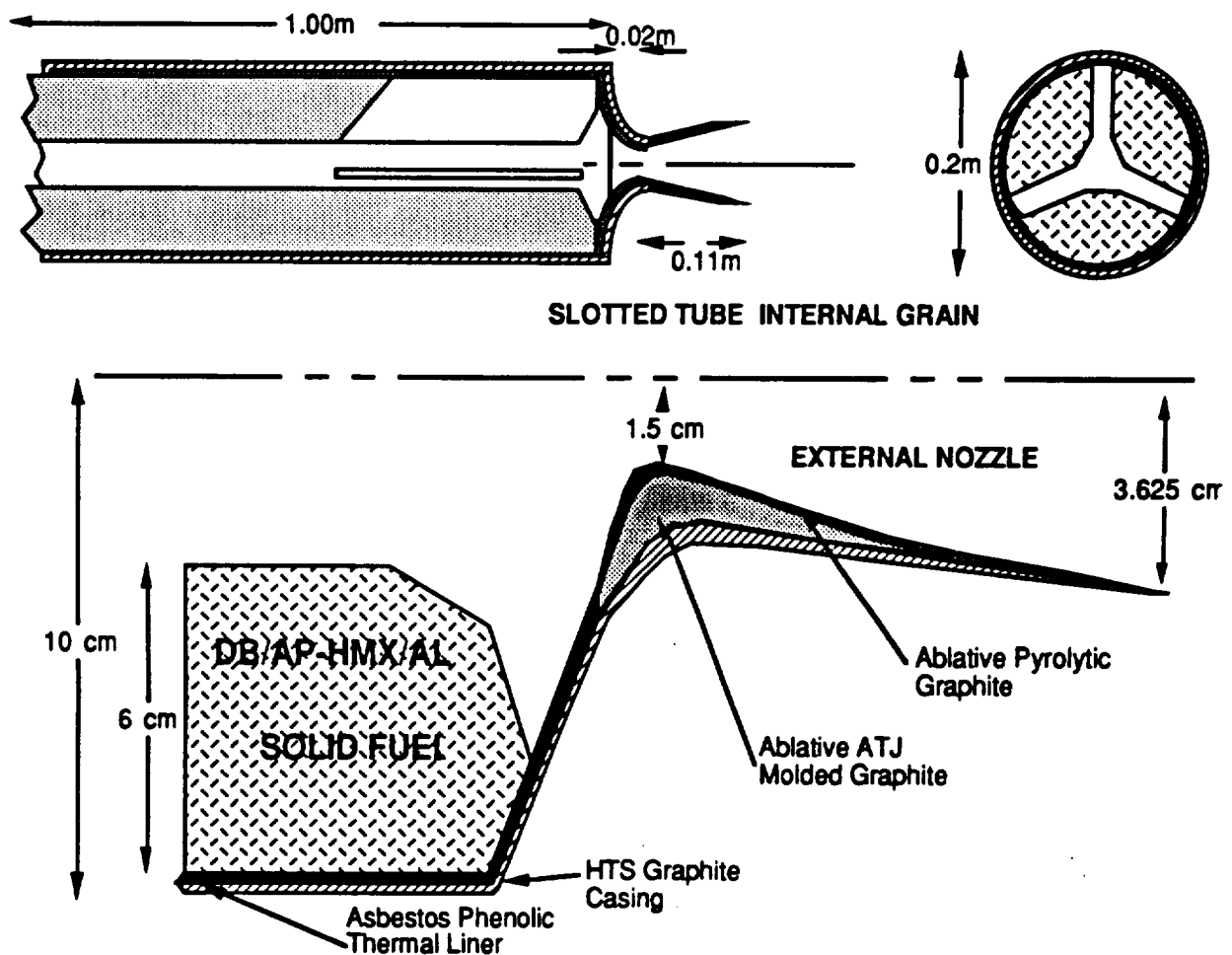


Figure 4.1M: Internal View and Dimensions of an Abort Motor

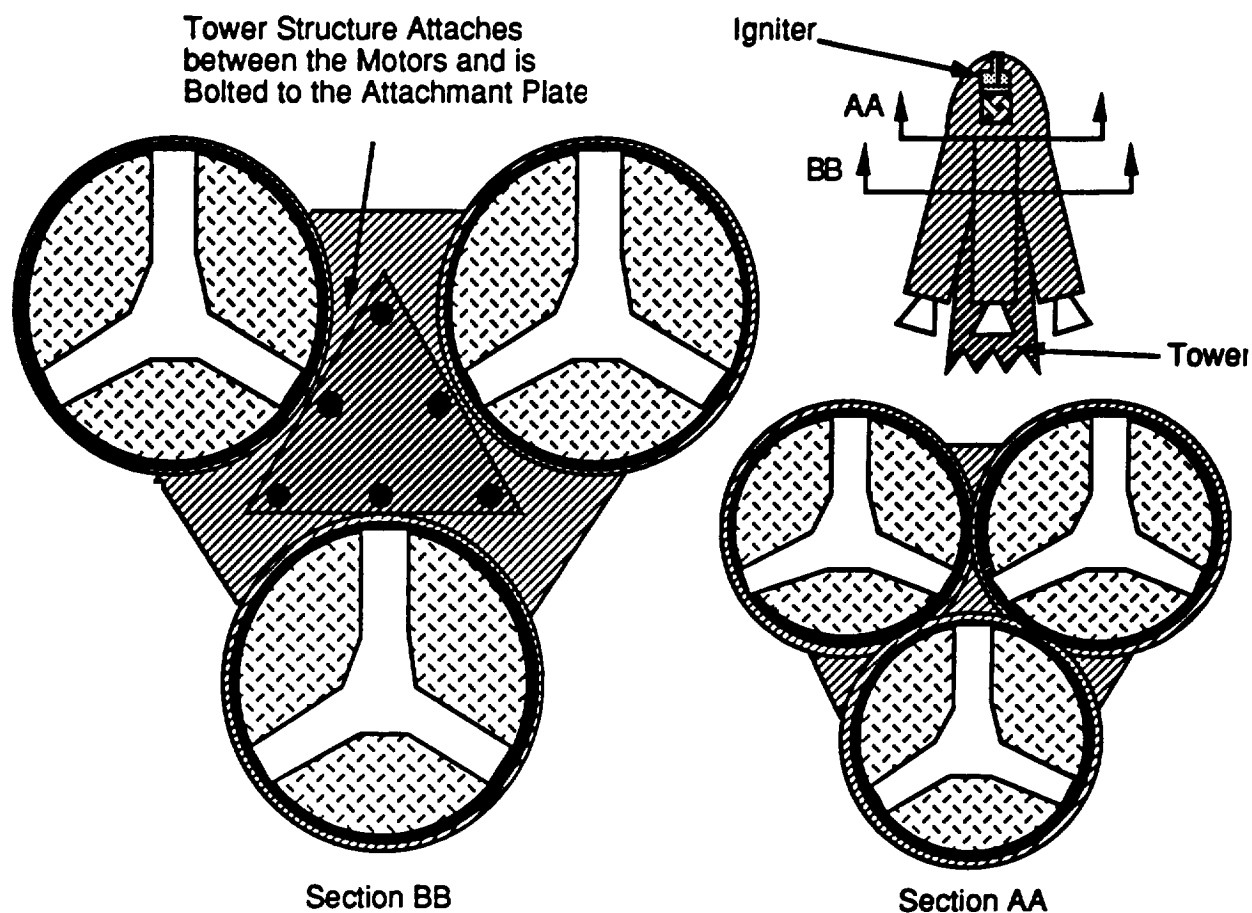


Figure 4.1N: Cross Sectional Views of the Abort Motor System

4.1.13 Thrust Losses Due to Altitude

Due to the fact that the abort motors were designed for sea level operation (P_e), the abort system will experience losses as the abort altitude increases and the air pressure (P_a) decreases. Based on the thrust equation :

- Thrust = Mass flow*Exhaust velocity - ($P_e - P_a$)* Exit Area

For the under-expanded exhaust of the abort motor at altitudes above sea level, Figure 4.1.O. illustrates the percent loss of thrust and the effective acceleration of the Taurus capsule produced by the less efficient motors.

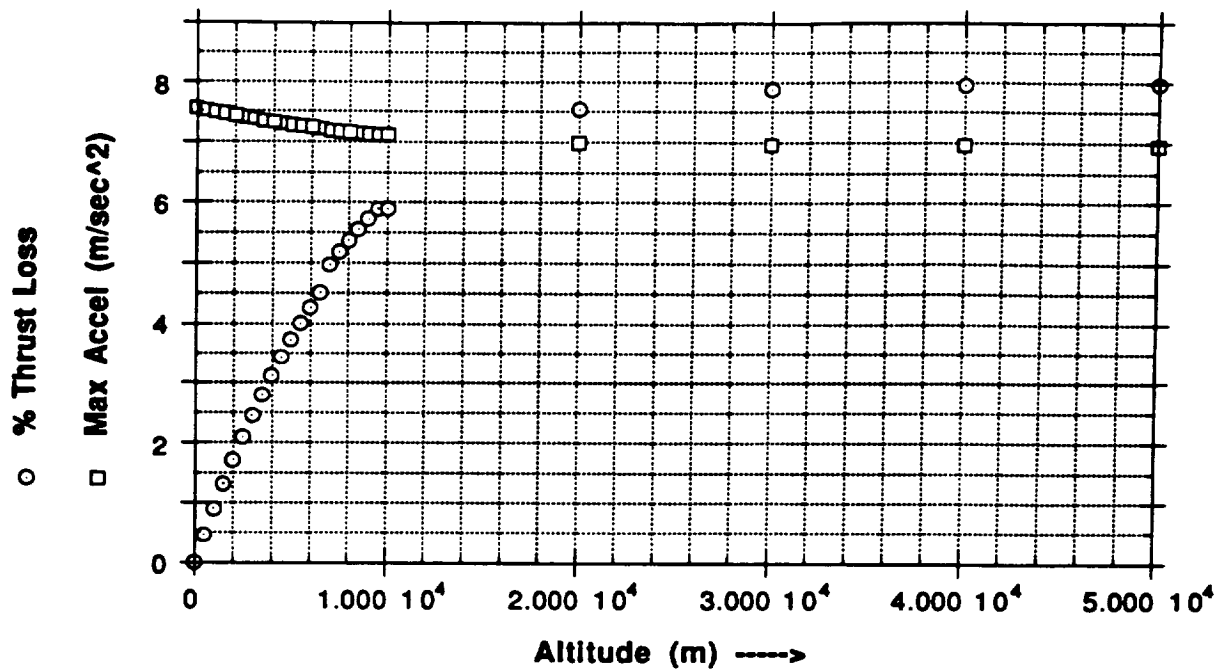


Figure 4.1.O: Graph of Thrust losses and Acceleration vs. Altitude

As the altitude increases, the thrust losses asymptotically approach 8%. Translating this maximum loss into a decrease in the distance the abort system will put the Taurus capsule in five seconds results in a vertical distance of 736 meters. This is a loss of 69 meters or ~8.6% of the abort launch distance, which is an acceptable loss given that the actual amount of abort time could vary more than +/- 1 sec before the booster detonates.

4.1.14 Abort Initiation and Directional Control

Abort initiation will be controlled by two separate systems, one ground controlled and one manually (crew) controlled. After the safe device is removed prior to launch, the abort motors are "armed" for an abort launch. The abort command may be initiated by launch control in the event of a detected malfunction of the Taurus booster or related critical sub-system. In the event that the crew detects a critical malfunction before ground control, the crew can initiate the abort sequence through a manual abort system located in the crew cabin.

The method used to place the Taurus capsule a horizontal distance from the Taurus booster during an emergency abort would be to angle one of the abort motors to provide a horizontal acceleration. The extent of the horizontal distance would be dependent on the angle the abort motor would be placed before launch or having a variable angle nozzle on one or more of the abort motors. An alternate would be one of the motors with a slightly regressive grain pattern burn. This could provide a high initial acceleration to give an off vertical angle and then a matched thrust for the rest of the abort burn time. Exact methods will have to be studied and tested for the best results.

Section 4.2 - Orbital Maneuvering System

Section 4.2.1 Introduction

The following sections present a description of the overall design configuration of the main engine of the orbital maneuvering system for the Taurus LMS. Requirements as well as design objectives and results are established and trade-off studies in propellant selection, chamber pressures, and feed systems are analyzed. The OMS consists of a nonreusable main liquid propellant rocket engine, one tank for the fuel, one tank for the oxidizer, an injector and a gas pressurized system.

Section 4.2.2 Requirements

The propellant mass required to perform the various missions previously outlined is of vital importance due to the mass constraint of the vehicle of approximately 1250 kg. In order to determine how much propellant mass would be required a study of ΔV vs propellant mass was done (Figure 4.2A and Appendix J) using the rocket equation and a constant specific impulse, I_{sp} , of 291.3 sec (this particular choice for I_{sp} will be discussed in the thrust chamber design configuration section). From this study it can be observed that for a ΔV of 240 m/sec a propellant mass of about 100 kg is required, 48.08 kg of fuel and 51.92 kg of oxidizer.

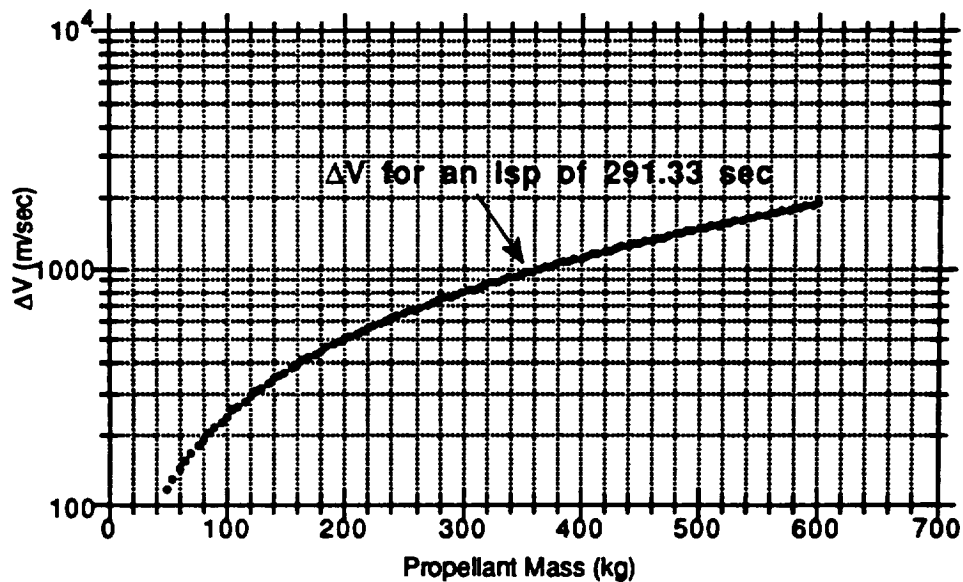


Figure 4.2A- ΔV (m/sec) vs. Propellant Mass (kg)

The OMS must also be capable of restarting numerous times. In addition it must operate in the vacuum conditions of space with a thrust level of 3158 N. This value was determined by assuming an impulsive maneuver of about one minute which is approximately one degree of distance around the orbit. With this assumption an acceleration of a quarter of a gee is obtained.

Section 4.2.3 Design Goals

One main engine will be used to produce the level of thrust required and will be located in the service module. The advantage of this design option is a decrease in structure and hence in mass --a major concern in the design of the Taurus L.M.S. The main engine will be a liquid propellant type. The advantages of using this type of engine over a solid one are: (1) high performance, (2) randomly variable duration for each start, and (3) repeated restarts.

The specific impulse is one of the prime performance parameters. One of the design objectives is to obtain the highest possible value for the specific impulse that would result in a lower system weight. The options for the propulsion system are electric, nuclear and chemical engines. While ion engines (electric engine) have the highest range of Isp values, up to about 5000 sec, the engine weight becomes too high due to the power requirement. Moreover, this is a low thrust type of engine which has not been used in space and thus its reliability at this time is uncertain. Nuclear engines have the second highest Isp values, up to 1000 sec, however, because of much public concern their use has been limited rather significantly. By contrast, chemical engines have the third highest range of Isp values, up to 500 sec, and the selection of a high Isp tends to lower the overall system weight. Furthermore, chemical engines are the most frequently used current technology. Consequently, the orbital maneuvering engine will be chemical.

Once the selection for the type of engine was made, the type of propellant to be used was determined. This selection led to a trade-off study of hypergolic and cryogenic propellants. A summary of this study is presented in Table 4.2A. With cryogenic propellants there is a need for an ignition system which could result in an increase in the weight of the overall OMS. Hypergolic propellants, however, are self-igniting. This property allows for a greatly simplified ignition. Furthermore, since hypergolic propellants ignite smoothly upon contact the accumulation of the mixture of fuel and oxidizer in the combustion chamber does not occur in large quantities. As a result the danger of explosions is minimized and the progress of the various processes in the combustion chamber is more rapid than with cryogenic propellants. Moreover, hypergolics can also be stored for considerable periods of time. The one disadvantage of hypergolic propellants is the fire hazard present during storage. This hazard is no more serious, however, than the explosive hazard created by the accidental mixing of nonhypergolic propellants (Holzmann, 1969). Thus due to the simplicity and ease of propellant maintenance achieved with hypergolics they were preferred over cryogenics.

Propellants type	Hypergolic	Cryogenic
Pros	<ul style="list-style-type: none"> • Self-igniting • Can be contained in small vessels over reasonable temperature ranges for considerable periods of time • Rapid progress of processes in combustion chamber 	<ul style="list-style-type: none"> • High energy
Cons	<ul style="list-style-type: none"> • Present fire hazards 	<ul style="list-style-type: none"> • Usually cannot be stored for any great length of time • Need igniter • Present system complications (e.g. insulation) for small vehicles such as the Taurus L.M.S.

Table 4.2A - Trade-off Study of Hypergolic and Cryogenic Propellants

Section 4.2.4 Selection of Propellant Combination

Once the decision to use hypergolic propellants was made, a trade-off study of various bipropellant combinations was performed. Bipropellants offer a higher performance and safer operation. The factors under consideration in selecting a particular propellant combination were: (1) high density impulse which is the total impulse delivered per unit volume of the propellant. It is defined as the specific impulse times the bulk density or propellant combination specific weight. A high density impulse would minimize the size and weight of the propellant tanks and feed systems, (2) the ability to serve as an effective coolant for the thrust chamber, (3) material compatibility for the design of the tanks, and (4) availability. A comparison of four different combinations is presented in Table 4.2B (Huzel and Huang, 1971)

Hydrazine as a monopropellant, is prone to explosive thermal decomposition. However, when it is combined with nitrogen tetroxide this condition no longer takes place and proves to be very reliable. Fluorine was also considered as a fuel choice given its high Isp value and density impulse. However, because it is very toxic and flammable it would not be safe or reliable. Thus nitrogen tetroxide and hydrazine was selected as the propellant combination to be used in the main engine.

Propellant Combination	*Specific Impulse (sec)	Density Impulse (s-g/cc)	Coolant	Materials Compatibility	Availability
**N2O4/N2H4	341	409	N2H4	Al,Steel,Teflon	Good
**MON/MMH	338	401	MMH	Al,Steel,Teflon	Good
**N2O/MMH	339	407	MMH	Al,Steel,Teflon	Good
F2/N2H4	419	551	N2H4	Al, 300 Series Stainless Steel	Good

Notes: MON = Mixed oxides of nitrogen, 85% N2O4 - 15% NO
MMH = Monomethylhydrazine

*Based upon theoretical shifting equilibrium at 150-psia nozzle chamber pressure

**Propellant technology and application are well established

Table 4.2B - Trade-off Study of Hypergolic Propellant Combinations

Section 4.2.5 Thrust Chamber Design Configuration

The thrust chamber converts the energy of the propellants into thrust. Its basic elements include a combustion chamber section, an expansion nozzle section, and an injector.

For the combustion chamber there are basically three different geometric configurations namely, spherical, near spherical and cylindrical. Ideally a spherical or near spherical chamber has the smallest surface to volume ratio which translates into less cooling surface and a lower mass. However, due to difficulties in its manufacturing such geometric shapes are not practical. Cylindrical configurations on the other hand have proven to perform well and are easily manufactured.

Properties in the combustion chamber are of great importance and relevance to the properties downstream of the chamber. One of these properties is chamber pressure. From the equation of thrust (Hill and Peterson, 1970)

$$T = \left[\frac{A P_0}{\sqrt{\frac{R}{M} T_0}} \right] \sqrt{\gamma \frac{2}{\gamma+1} \left(\frac{\gamma+1}{\gamma-1} \right)} \left\{ \sqrt{\frac{2\gamma R}{(\gamma-1)M}} T_0 \left[1 - \left(\frac{P_e}{P_0} \right)^{\frac{\gamma-1}{\gamma}} \right] \right\} + (P_e - P_a) A_e$$

it can be observed that the higher values of chamber pressures increase thrust levels. This seems to indicate that high chamber pressures are desirable for they not only increase thrust but could decrease the value of the throat area as well. However, very high chamber pressure values will increase thrust chamber stress and heat transfer rates. As a result, the chamber walls would have to be thicker and tank weights for gas pressurized systems would increase rather significantly.

The chamber pressure was obtained by performing a study of the variation in chamber pressure and its effect on the thrust coefficient. A graph of the results is presented in Figure 4.2B. Equations used to obtain the given results are explicitly presented in Appendix J.

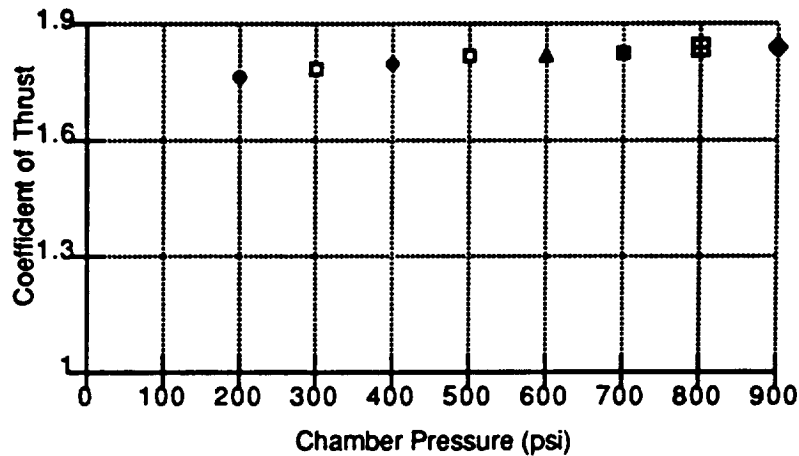


Figure 4.2B - Coefficient of Thrust vs. Chamber Pressure

From the graph it can be observed that the curve starts to level off at a chamber pressure of about 300 psi or 2.069 MPa. This result agrees with the claim that the effects of increasing chamber pressure on thrust levels are slight especially at chamber pressures above 300 psi (Huzel and Huang, 1971). Moreover, a chamber pressure of 300 psi is the technology limit for small engines. Since the orbital maneuvering engine is indeed small (the dimensions are presented at the end of this section) a chamber pressure of 300 psi was chosen.

The combustion chamber parameters for the design options considered thus far can be summarized as follows (Sutton, 1986)

Propellants:	N_2O_4/N_2H_4
Mixture Ratio:	1.08
Chamber Pressure:	300 psia
Chamber Temperature:	2857 oK
Specific Heat Ratio:	1.26
Mean Molecular Weight of Exhaust Gases:	19.5 kg/mole

The two nozzle shapes considered in the design were conical and bell shaped nozzles. A trade-off study was performed in order to determine which shape would provide the best results. Given an expansion area ratio of 23.56 (calculated in Appendix J) a conical nozzle with a half angle of 15 degrees provided a coefficient of thrust of 1.69, a nozzle length of 24.20 cm and a thrust loss of 1.71%. A similar study was done for a bell shaped nozzle with identical expansion area ratio using the MIT Project Athena (Todor Package). The bell

shaped nozzle had a coefficient of thrust of 1.71 and a nozzle length of 86 cm. The results obtained indicate that the conical nozzle is shorter and hence lighter than the bell shaped nozzle. This is an important result given the Taurus LMS. mass restriction. Furthermore, the conical nozzle provided almost as good coefficient of thrust as the bell shaped nozzle. These results along with the ease of manufacturing of conical nozzles and the ability of modifying an already existing design by simply altering the expansion area ratio without the need of redesigning the entire contour of the nozzle make the conical nozzle the choice for the orbital maneuvering engine. Consequently, the nozzle was designed to be conical with a 15 degree divergent half angle.

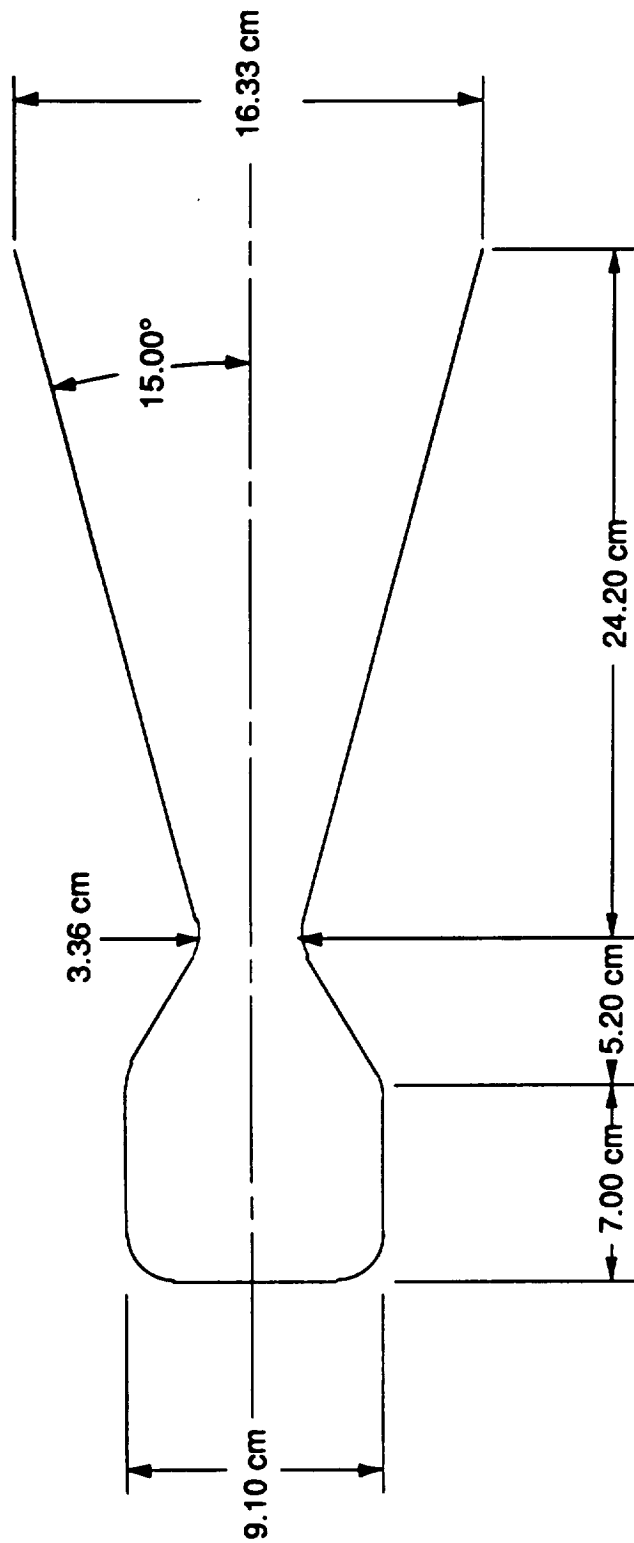
At this point in the analysis geometrical configurations of the two major sections in the thrust chamber as well as combustion chamber parameters have been presented. It is now time to combine all these results in order to come up with the thrust chamber specifications.

Using the standard nozzle design equations explicitly presented in Appendix J and assuming a one dimensional, compressible flow and isentropic nozzle region a spreadsheet was set up to determine area, diameters, exit velocity, I_{sp} value, exit pressure, and thrust coefficient of the orbital maneuvering engine for a chamber pressure of 300 psi. A summary of the engine's dimensions as well as a sketch of it is presented in Figure 4.2C

Section 4.2.6 Heat Transfer

The techniques studied to cool the thrust chamber were heat sinks and ablative cooling. The simplest method is the heat sink. It provides a sufficiently thick chamber or nozzle wall with the necessary heat capacity to soak up the heat transferred during a prescribed firing duration. Nonetheless, for durations greater than 10 to 20 seconds (Holzmann, 1969) the thickness of the walls becomes increasingly greater resulting in a weight penalty. This would be disadvantageous in the design of the vehicle under study due to the set mass allotment. By contrast, ablative cooling proves to be effective for longer durations without the weight penalty. Although this technique was initially used for solid propellant systems it has since proved to be quite successful for engines with chamber pressures of 300 psi or less and pressure-fed systems. This process involves melting and subsequently vaporizing the wall material in order to dissipate heat allowing for a cooler gas flow over the wall surface. The advantages of ablative cooling are low cost, and exterior wall temperatures can be held to a minimum (Huzel and Huang, 1971).

The char depth, or thickness, will vary along the thrust chamber being greater at the combustion chamber and throat and decreasing to a constant thickness along the rest of the nozzle. From equations in Appendix J and using



Chamber	Throat	Exit
P = 2.069 MPa	P = 1.144 MPa	P = 6894 Pa
T = 2857 K	T = 2528 K	T = 1880 K
A = 65.1 cm ²	A = 8.9 cm ²	A = 209.3 cm ²

Mass :	16 kg	Mixture Ratio :	1.08
Thrust :	3158 N	Specific Heat Ratio :	1.26
Isp :	291.3 sec	Wall Thickness (chamber and throat):	1.54 cm
Propellants :	N2H4/N2O4	Wall Thickness (Nozzle) :	0.71 cm

Figure 4.2C - Engine Specifications

Refrasil phenolic as the ablative material the calculated thicknesses are as follows: for the combustion chamber and throat a thickness of 1.54 cm is required for a firing of 90 seconds; for the rest of the nozzle the thickness needed is 0.71 cm. Figure 4.2D shows the ablatively cooled thrust chamber (Huzel and Huang, 1971).

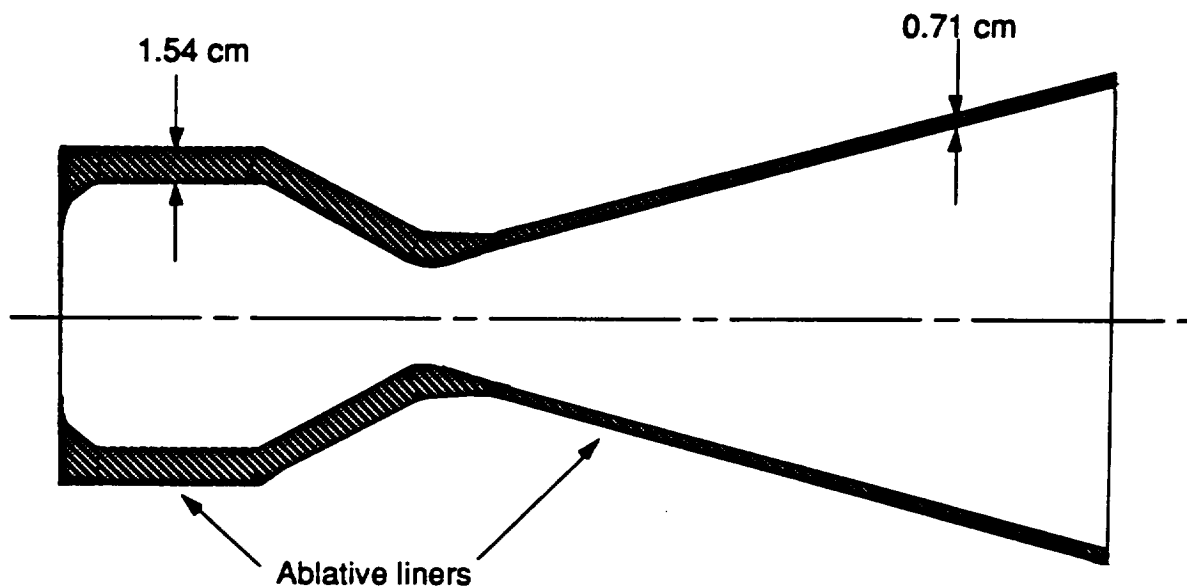


Figure 4.2D - Ablatively Cooled Thrust Chamber

Section 4.2.7 Injector

In order to introduce and meter the flow into the combustion chamber the presence of an injector is required. The injector breaks up the fuel and the oxidizer into very fine droplets which produce an increase in the surface of the liquid leading to an effective rapid mixing of the bipropellants and their rapid vaporization. Rapid mixing of the propellants is of vital importance for a more complete combustion. In the event that this does not take place some portion of the oxidizer may not come into contact with the fuel. This would lead to a loss in efficiency of the engine and hence to an incomplete combustion. Thus the main goal is to design an injector that will carry out the stated processes to the fullest.

The type of injector used is an impinging stream type. This type of injector has been extensively used and proven to be very reliable. The process is to inject the propellants through a number of separate orifices so that the fuel and oxidizer streams impinge upon each other. This impingement contributes enormously to the break down of the liquid. Figure 4.2E shows a sketch of the injector and Table 4.2C summarizes the injector design parameters for the fuel and oxidizer (for a detailed calculation of the design parameters refer to Appendix J).

Injector Design Parameters	Fuel	Oxidizer
Flow Rate	0.24 kg	0.26 kg
Volume Flow Rate	2.36E-4 m ³ /s	1.79E-4 m ³ /s
Pressure Drop Through Injector	60 psi	60 psi
Injector Velocity	21.5 m/s	17.9 m/s
Number of Orifices	8	8
Diameter of Each Orifice	0.133 cm	0.126 cm
Angle of Orifice with Nozzle Axis	17.9 degrees	-20.0 degrees
Total Injection Area	0.09 cm ²	0.11 cm ²

Table 4.2C - Injector Design Parameters

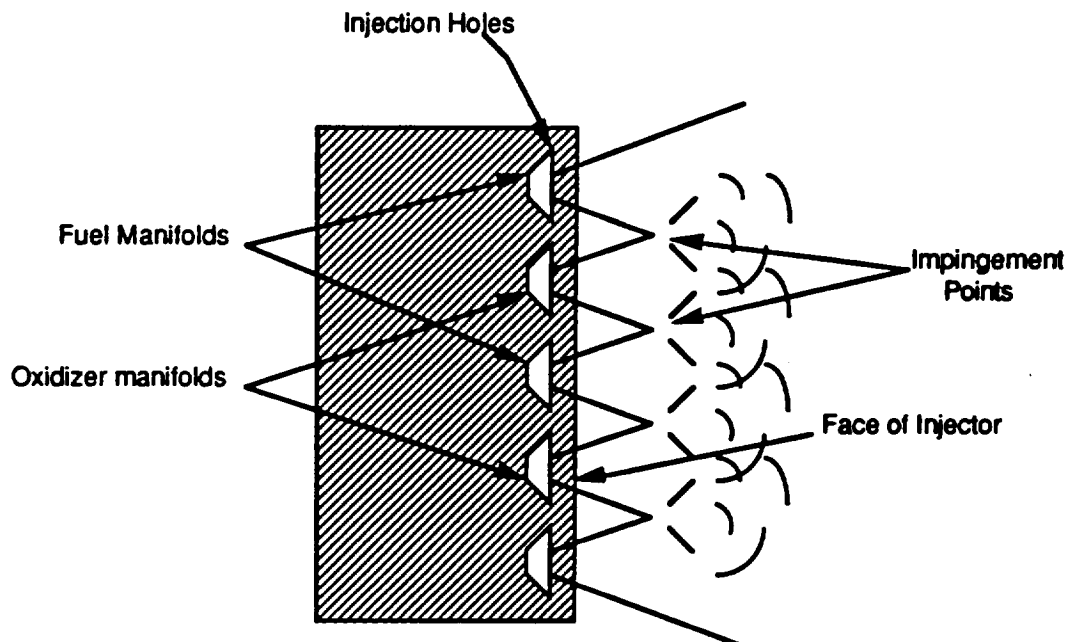


Figure 4.2E - Impinging Stream Pattern Injector

Section 4.2.8 Feed System

Pressurized-gas and turbopumps are the two options for the feed system. A turbopump system, consists of propellant pumps, turbines to drive them, a power source for the turbines, speed reduction gear transmissions, lubrication system for bearings and gears, shaft-speed pickup for instrumentation and for safety purposes, accessory drives, propellant inlet and discharge ducts, and turbopump mounts (Huzen and Huang, 1971). The pressurized-gas system mainly consists of a high pressure storage tank, a start and shutoff valve, and a pressure regulator.

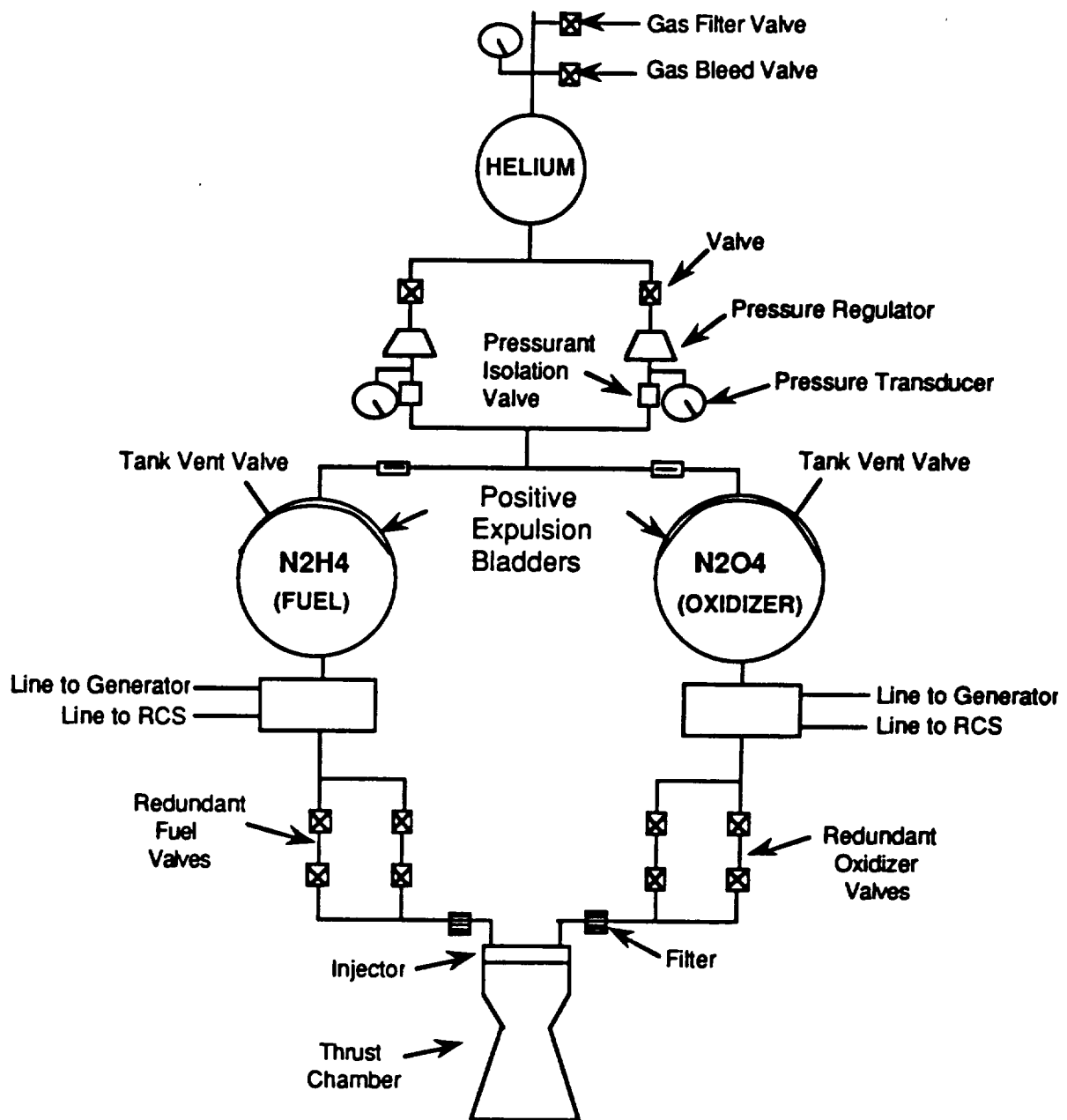
A pressurized-gas feed system will be used for the Taurus LMS. One of the main advantages of this system is its simplicity and reliability. The oxidizer and fuel are fed into the combustion chamber by the displacement of a gas at high pressure. The gas will be helium and it will be stored at a pressure of 4000 psi or 27.579 MPa in order to keep the storage vessel small.

To assess if a reheating system would be needed for the gas a comparison between an isothermal and adiabatic expansion analysis was performed. The results (see Appendix J) reflected a difference of only 0.2 kg which does not justify the need of a reheating system and its inherent complications.

Once the helium is ducted to the pressure regulator its pressure is decreased and the gas pressurizes the propellants within their storage tanks. The propellants are then expelled from their tanks to the injector and eventually to the combustion chamber with the aid of a positive expulsion bladder. Positive expulsion bladders have been extensively used with a propellant expulsion range of 96% to 99% (Sutton, 1986). A schematic of the system is shown in Figure 4.2F.

The plumbing in the OMS was designed so that any active systems (e.g. pressure regulators, transducers and valves that open and close) are double stringed to provide redundancies while passive systems (e.g. check valves) are single stringed. The set of valves located below the tanks are double-double stringed. If one of the valves in one string fails "on" or "off" a valve from the other string can be used thus making the configuration completely redundant.

The two tanks shown in Figure 4.2F contain the necessary amounts of fuel and oxidizer for the orbital maneuvering system, the reaction control system, and the power system to operate. This design enables any one of the aforementioned systems to draw more propellant from a common tank in the event of an emergency. The tanks will be kept at a pressure of 500 psi or 3.447 MPa. This pressure value accounts for pressure drops in the pipes, connections, and valves. Approximate values for such pressure drops are shown in the schematic of the OMS along with the mass and dimensions of the tanks. Details of the design of the tanks are presented in Chapter 6, Section 6.7 and calculations performed in Appendix O.



Tank Dimensions, Mass and Pressure

	He	N2H4	N2O4
Radius :	18 cm	27 cm	26 cm
Mass :	4.73 kg	85.64 kg	106.58 kg
Pressures :	4000 psi	500 psi	500 psi

Approximate Values for Pressure Drops

Pipe :	4 psi
Connections :	5.86 psi
Oxidizer Valve :	30.24 psi
Fuel Valve :	21.21 psi

Figure 4.2F - Schematic Diagram of the Orbital Maneuvering System

Section 4.3: Reaction Control Systems

4.3.1 Introduction

During the spacecraft mission, it will experience a variety of forces which will cause it to rotate and/or translate. The purpose a Reaction Control System (RCS) of a spacecraft vehicle is to measure, correct, and counteract the adverse motion (yaw, roll and pitch). Besides responding to forces and moments, the RCS of a spacecraft will maneuver the vehicle in the following activities. They are: altitude control, position keeping, and re-entry.

Forces that will cause the spacecraft to rotate or translate can be categorized as short-term or long-term. The daily or orbital period oscillating forces are called *diurnal* and the long periods are called *secular*. For a medium altitude mission profile (500 to 3500 km), the vehicle will experience perturbations due to the earth oblateness. Since the earth bulges in the vicinity of the equator, the cross section through the pole is not circular. Depending on the inclination of the orbit plane to the equator and the altitude of the orbit, the spacecraft will experience two kinds of perturbation. They are as follows: the regression of the nodes (Figure 4.3A) and shifting of the apsides line (major axis, Figure 4.3B). Regression of the nodes is an affect which cause the vehicle to change its angle plane of orbit. The plane of the orbit can change as much as 9 degrees per day . However, regression theoretically does not occur in equatorial orbits and therefore is dependent on the orbit. Figure 4.3A shows an exaggerated shift of the apsidal line with the center of the earth remaining the focus point (Sutton,1986.). This perturbation may be visualized as the movement of the predetermined elliptical orbit. The change in apogee and perigee position is a function of the vehicle altitude and plane of inclination.

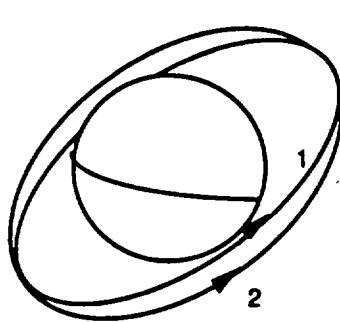


Figure 4.3A Regression

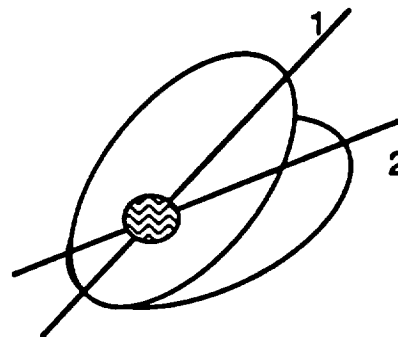


Figure 4.3B Apsidal Shifting

There are other forces that the spacecraft will experience throughout its mission. The principal forces are as follows: solar radiation, aerodynamic drag, and internal acceleration. Solar radiation is not significant factor at altitude less than 800 km and will not be considered. Aerodynamic drag is only significant for orbits below 500 km, and internal acceleration will occur in deployment of solar array panels, the shifting of propellant, movement of the astronauts or other mass within the spacecraft.

Other needs for a RCS on a spacecraft is for attitude control, station keeping, repositioning, and reentry assist.

With the above requirements in mind, the RCS will be analyzed by the following criteria. It must meet the vehicle operational requirements in mass and size, thrust level and duration, space available, and reliability.

4.3.2 Thruster System

The simplest and most common means of pressurizing the propellant is to force them out of their respective tanks by displacing them with high-pressure gas. This gas is fed into the propellant tanks at a controlled pressure, thereby giving a controlled propellant discharge.

For low thrust and/or short duration, such as for space vehicle attitude control, a feed system of this type is preferred. Although the propellant tanks in a gas-pressure feed systems have to be heavy to withstand the high internal pressure, the overall system weight is lower than that of a turbo pump system (Sutton, 1986). Because of their relative simplicity, the rocket engines with pressured feed systems can be reliable. A typical pressured-fed liquid propellant rocket engine is schematically shown in figure 4.3C.

The pressure-fed system consists high-pressure gas tanks, gas shutoff and starting valves, pressure regulators, propellant tanks, propellant valves, and feed lines. Additional components, include filling and draining provisions, check valves, filters, flexible elastic bladders for separating the liquid from the pressurizing gas, and pressure sensors or gages. For more details refer to Section 4.2 of this report.

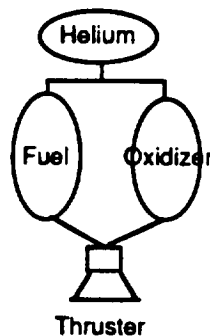


Figure 4.3C. Propulsion System

By using $C^* = P_o A^* / \dot{M}$, $C_t = T / P_o A^*$, and data given by "a past to build on", by Rockwell International, thrust, weight, chamber pressure and A_e / A^* for each thruster were determined. Refer to Table 4.3A for thruster data.

Table 4.3A. Thruster Data

Section	Thrust (N)	Mass (kg)	Po (MPa)	Ae/A*	Dimension (cm)
Reentry RCS	42.0	1.090	0.689	150:1	17.0 long/6.6 wide
Main RCS	110.0	1.260	0.689	40:1	23.1 long/7.8 wide
Main RCS	42.0	1.090	0.689	150:1	17.0 long/6.6 wide

4.3.3 Spacecraft Dynamics

The moment of inertia was determined to calculate the maximum rotational angular velocity. From this a RCS thrust was calculated to adequately counter react the angular moments about all major axis.

$$I_{YY} = I_{xx} = 1687.4 \text{ KgM}^2$$

$$I_{zz} = 687.1 \text{ KgM}^2$$

If the forces which causes rotation are external, the moment of the spacecraft can be calculated by taking the angular momentum and dividing it by a time derivative. The equation use are:

$$M = [h / dt] + W \times h$$

where: $h = (I_{xx}W_x - I_{xy}W_y - I_{xz}W_z)i + (I_{yy}W_y - I_{yz}W_z - I_{xy}W_x)j + (I_{zz}W_z - I_{zy}W_x - I_{yz}W_y)k$

Angular Velocity

The angular velocity of a spacecraft is dependent on total impulse $I(\text{total}) = \int F dt = M(u_2 - u_1)$. Assuming that the initial velocity is zero, the final velocity $u_2 = \int F dt / M$. This is true if the mass expel out of the thruster nozzle is assumed to be negligible. For each axis, a pair of thrusters are coupled to produce angular velocity $W = u / r$ where u is the final velocity and r is the location of the thruster. The external moments is then related to the the angular velocity by Torque = $W \cdot I$, where I is the moment of inertia about a given axis.

4.3.4 Propellant Selection

In choosing a propellant, criteria such as economics, performance, hazards, and physical properties have to be meet. The economics of a good fuel are availability and costs. If the production process is simple and the raw materials required are easily obtain, then the fuel is economical. Listed below are studies on performances, hazards, and physical properties of propellants.

Table 4.3B Performance

Oxidizer	Fuel	Specific Impulse(Isp) sec
Oxygen	Hydrazine	301
	Hydrogen	388
	UDMH	295
Fluorine	Hydrazine	334
	Hydrogen	398
Nitrogen Tetroxide	Hydrazine	
	50% UDMH- 50% Hydrazine	278

Table 4.3C. Hazards

Characteristics	Fuel	Oxidizer
Explosive	Nitromethane Hydrogen	Hydrogen Peroxide
Fire		Nitric Acid Nitrogen Tetroxide Hydrogen Peroxide
Toxicity	Hydrazine*	Fluorine Nitric Acid
Corrosive	Hydrazine*	Fluorine Nitric Acid

* Includes all forms of hydrazine.

Table 4.3C Physical Properties

	Monomethylhydrazine	Nitrogen Tetroxide
Molecular Mass	46.08	92.016
Melting Point	220.7 K	261.5 K
Specific Gravity	0.8788 g/cm ³	1.447 g/cm ³
Vapor Pressure	0.0069 Pa	0.00689 Pa
	Fluorine	Oxygen
Molecular Mass	38.0	32.0
Melting Point	53.7 K	54.4 K
Specific Gravity	1.66 g/cm ³	1.26 g/cm ³
Vapor Pressure	0.158 Pa	0.0052 Pa

From the equation of $U_e = \sqrt{\left(\frac{2 \cdot \psi R}{(\psi - 1) M} \right) T_o [1 - (P_e / P_o) (\psi - 1) / \psi]}$.
 High performance thruster should have high energy content of chemical energy per unit of propellant mixture is desirable because it permits a high chamber temperature. A low molecular mass of the product gases of the propellant combination is also desirable.

Overall hydrazine is the best fuel and nitrogen tetroxide is the best oxidizer. The combustion of hydrazine and nitrogen tetroxide produces a chamber temperature of 2857° K. Both hydrazine and nitrogen tetroxide was chosen for the reaction control system because it is storable in room temperature of 288 ° K. Hydrazine and nitrogen tetroxide are relatively dense and therefore reduces propellant tank mass.

4.3.5 Propellant Mass

The propellant mass was determined by the mission profile of 24 hours. Therefore a worst case scenario of 3 hours continuous impulse was determined to be 10,800.0 sec. But the thrusters will be fired at 24 second interval with pulse time of one second. Since two thrusters will be burning at any one time, the total impulse is reduced to 225.0 seconds for each thruster cluster. From the equation $\text{thrust} = \text{mass flow} \cdot U_e$, the mass of propellant required for this mission is 70.686 kg. The total impulse of the RCS is 110,626.6 N-Sec.

The propellant fuel and oxidizer for the main RCS, attached to the service module, will be stored in the main propulsion tanks located in the service module. The required amount of propellant for the RCS will be combined with the propellant of the OMS and power generation engine. This system reduces the mass of having individual tanks and provides an additional safety feature of "fuel crossfeed" for emergency fuel requirements for any of the three systems requiring fuel and oxidizer.

Section 4.4: Electrical Power Generation

4.4.1 Introduction

The electrical power system is one of the most important systems in a spacecraft. It provides the required power to the avionics and other instruments at all times. It is very necessary to have two different sources of electrical power to satisfy all the requirements of the spacecraft and to provide a high reliability to the entire system. The mission requirements and the configuration of the spacecraft are the main elements to be considered when designing an electrical power system. There are many sources that can provide electrical power in a spacecraft. Some of these sources are nuclear, chemical, and solar. Their advantages and disadvantages are discussed in the following section.

4.4.2 Energy Sources

Source	Type	Pros	Cons
Nuclear	Reactors	Reliable Insensitive To Space Conditions	Shielding Is Needed To Protect From Radiation
Solar	Solar Cells	Usefull In Long Missions Relatively Light Weight	Low Efficiencies. Work Only With Sun Light
Chemical	Batteries Ni-Cd, Ni-H2, Ag-Zn	Reliable Compact	Additional Power Supply Is Needed. Weight Increases
	Fuel Cells	Reliable	Large Heat Loads. Radiators Are Needed

Table 4.4.A. : Energy Source Alternatives

Solar Energy

The sun is the most reliable source of energy available, its radiation can be used to generate the power needed to maintain a spacecraft working. The sun produces $1.35 \text{ Kw} / \text{m}^2$ of power in space (Rauschenbach,80). This power is collected and converted to electricity by solar cells. Solar cells are made of different materials but the most common are silicon, gallium, and cadium cells. Inside the cells a photovoltaic effect takes place, converting the solar radiation into useful electrical power. Each of these cells are approximately $0.02 \times 0.02 \text{ m}$ and produce 75 to 84 mW of power (Agrawal,85). To achieve high power demands, large arrays of solar cells are needed.

Chemical Energy

Rechargeable batteries are the most common source of electrical power. Electricity is generated as a result of a chemical reaction. There is a wide variety of rechargeable batteries, each with its own application in aerospace. Batteries are characterized by their energy density, weight, and life expectancy. The most used and reliable batteries in a spacecraft are: Nickel-Cadium (Ni-Cd), Nickel-Hydrogen (Ni-H₂), Lithium-Hydried (Li-H), and Silver-Zinc (Ag-Zn). Nickel-Hydrogen batteries are very efficient and posses a long cycle-life of approximately 12,500 cycles. Their energy density is relatively low, close to 40 Whr / Kg. Nickel-Cadium batteries are very similar to the Nickel-Hydrogen batteries, they also have a relative long life, close to 10,000 cycles. These batteries have even lower energy densities, around 22 to 26 Whr / Kg. Because of their low power densities, Ni-Cd, and Ni-H₂ batteries are not recommended for use in short missions where high power densities are a must. Lithium -Hydried batteries have very high energy densities (600 Wh / Kg), but as a result of their chemical reactions, great amounts of heat are released. Finally, Silver-Zinc batteries also have high energy densities, but very low life-cycles. They produce around 152 Wh / Kg, and they sustain a life of 20 to 200 cycles. These batteries are used in short missions where weight is a primary concern. (Agrawal,85).

Fuel cells were also considered, they were a very competitive option because of their high energy-weight ratios. Although fuel cells are very efficient sources of power, they create very high heat loads which are difficult to control and dissipate. Because of the size of the spacecraft, reduction of heat is very difficult to achieve. Almost every single instrument placed in the spacecraft produces heat which is accumulated inside the cabin. For this reason additional heat loads from the fuel cells would had been almost impossible to manage. Also, an additional weight restriction would had come as a result of using fuel cells because bigger radiators would have been needed to dissipate the heat.

Besides fuel cells and batteries, gas engines were also considered for the Taurus power supply system. A Hydrogen-Oxygen engine was analyzed and it was found to be very reliable and of minimal weight. This engine produces electrical power from a chemical reaction which takes place when the Oxygen and the Hydrogen are pumped together. A very interesting and useful thing was found, the engine can be modified, without any difficulties, to work with any other fuel and oxidizer, (N.E. Morgan & W. D. Morath). This can be very useful since the engine can be modified to work with the same fuel used for the propulsion system. Also, this engine is capable of producing the power needed by a small spacecraft. The average weight of an engine of this kind is very small compared to the weight of fuel cells and rechargeable batteries. Since the engine can be modified to consume the fuel from the propulsion system, no additional tanks or extra fuel will be needed to work the engine. This is very desired for a small spacecraft such as the Taurus where weight is a main concern.

Nuclear Energy

Radioisotopes are being successfully used as a thermal source for space power supply. Compact nuclear reactors can be designed to supply the required electricity and propulsion for the spacecraft. These reactors are reliable, rugged, insensitive to space environment, and they have large specific thermal power. Because of dangerous radiation, nuclear reactors require large amounts of shielding; thus, extra weight. It will be impossible for a nuclear reactor to supply power to a small spacecraft where weight is a very important consideration.

4.4.3 Power Requirements For The Taurus Spacecraft

The Taurus spacecraft must be able to produce the amount of power required by the avionics, electronics, and all other systems that need some form of electrical power. The power demand is also controlled by the mission duration, the energy needed is determined from the time of the mission. For the Taurus spacecraft the mission will be 24 hours. The power demand for the Taurus has been set at 800 Watts of continuous electrical power, most of this electrical power goes to the avionics and human factors systems. Besides these primary requirements, the electrical power system must also meet the weight and size limitations imposed by the spacecraft. After a conscious and extensive study, it was decided that for such a short mission with a relatively low power demand, a reciprocating engine modified to work with hydrazine and nitrogen tetroxide as fuel and oxidizer, will serve as the primary power supply. The secondary power supply will be a system of Silver-Zinc rechargeable batteries. These are the best sources of electrical power that can be fitted into the Taurus spacecraft. They are compatible with the other systems and are light in weight and proven to have very high reliabilities.

4.4.4 Primary Power Supply

As mentioned before, the primary power supply will be a single reciprocating Hydrogen-Oxygen engine modified to work with Hydrazine-Nitrogen Tetraoxide, the same fuel and oxidizer used by the Reaction Control System and Orbital Maneuvering System. The Taurus spacecraft will perform a mission of twenty four hours, it will need 800 Watts of continuous power. This means that the total energy needed can be calculated by:

$$(24 \text{ hours}) \cdot (800 \text{ Watts}) = 19,200 \text{ W-hr.}$$

This energy will come from a Hydrazine-Nitrogen Tetraoxide engine. The mass and size of the engine was scaled down from an existing engine used in missions similar to the one performed by the Taurus. (N.E. Morgan & W. D. Morath). Full description of this process of obtaining the size and weight of the engine is included in appendix L. For the required energy of 19.2 KW-hr, the weight of the engine was scaled down to 25.2 Kg. This includes the weight of the compressor, alternator, cooling system, and plumbing. This engine has a volume of 0.0973 m³. The minimal dimensions are: 0.519m X 0.405m X 0.463m.

As mentioned before, the engine was modified to work with Hydrazine and Nitrogen-tetraoxide. The energy produced by the mixture of Hydrazine and Nitrogen-tetraoxide in a 1 to 1.34 ratio, produces 0.5038150 KW/Kg. This means that in order to produce the 19.2 KW-hr of energy, with an engine efficiency rating of 0.65, the mass of the Hydrazine will be 25.08 Kg and of the Nitrogen-tetraoxide will be 33.54 Kg. The density of the Hydrazine is 1025 Kg/m³, and of the Nitrogen-tetraoxide is 1450 Kg/m³. This gives a volume of 0.02447 m³ for the Hydrazine and 0.02313 m³ for the Nitrogen-tetraoxide.

4.4.5 Secondary Power Supply

A system of high energy density rechargeable batteries was chosen as the secondary power supply. Silver-Zinc (Ag-Zn) batteries were selected because of their high energy density, 152 Wh / Kg, and proven reliability. These batteries will be used for reentry power when the service module containing the primary power system is detached, and whenever the demand for power rises above the primary power supplies output capability. For the needed 19.2 KW-hr of energy, the weight of the batteries will be:

$$(19.2 \text{ KW-hr}) + (152 \text{ W-hr/Kg}) = 126.32 \text{ Kg.}$$

This would be the weight of the batteries if they were to continuously discharge only once throughout the mission. But since Ag-Zn batteries have a cycle life of 20 to 200 cycles, they can be recharged using the engine's electrical power output. For a discharge rate of four hours, the total weight of the batteries will be reduced to 21.05 Kg. This means that if the need arises, the batteries will be recharged six times during the entire mission. The charge-recharge cycles must be kept as low as possible to avoid an efficiency reduction of the batteries. As the charge-recharge cycles increase, the efficiency of the batteries decreases. Above 10 cycles, the efficiency drops very fast. The batteries are composed of 45 to 50 cells or plates which are connected together and stored inside a sealed box to prevent leakage and to protect them against the space environment. A selection of two batteries was made to add redundancy and reduce the risks of a malfunction. In this way if one battery fails the other will take over without any danger or noticeable losses. For a system of batteries with a total weight of 21.05 Kg, each battery will weight 10.5 Kg. The total volume of the battery system will be 0.03146 m³. These batteries can be stocked or piled up one over the other, or one next to the other. They are placed in the rear of the pressurized cabin to save space inside. When the mission is completed and the spacecraft is ready for reentry, the batteries will provide the primary power and be discharged at the lowest power output required during this time.

4.4.5 Power Distribution System

The functions of the power distribution system are to control the output of the engine and of the batteries. Since there are many instruments that work with different voltages and frequencies, regulators and inverters must be used to deliver the correct voltage to the instruments. The Electric Power System (EPS) is designed to meet the requirements imposed by the spacecraft, these requirements are: load profile, orbit mission, and system configuration. The EPS basically takes the electrical power from a source, and distributes it to each of the instruments inside.

Most aerospace instruments work at 28 V dc (direct current is preferred because of vehicle size and weight restrictions) so that the voltage output must be designed for this desired voltage. Alternate current will also be needed for separate systems, so that an inverter will be used in order to change dc to ac. Also, due to the extreme conditions in space and to the sudden changes in voltage, some devices must be used to regulate these changes. This means that regulators must be used to provide the required voltage and must protect the sensitive electronics from power surges. The same problem arises during battery recharging, high charge currents go into the battery and overheat it; thus, reducing the battery life.

Two bus-voltage systems will be used to provide equal battery discharge rate and to protect against single point faults. The main bus will be connected directly to the primary power source, the reciprocating engine, and it goes directly connected to the main electronics. The main electronics are used 100% of the time and are essential for the mission. The inverter providing alternate current to the Environmental Control System (ECS) is also connected to the main bus. The secondary bus is connected in series to the primary bus to add redundancy and to use the engine to recharge the batteries if needed. The non-essential avionics and other instruments are connected to the secondary bus. Another inverter providing alternate current to the Stabilization Control System (SCS) is also connected here. The following is a list of the avionics used in the Taurus spacecraft:

- C/S Band Tx/Rx
- Switch
- Antenna
- Intercoms
- Audiomixer
- Crew Interface
- Sound Tapes
- Recorders
- Main Computers

Besides these avionics there are other instruments from guidance and navigation and from human factors. All add up together requires a maximum power of 800 Watts.

Protection devices must be added to prevent short circuits and other failures. Circuit breakers and fuses are excellent choices. The following schematic is a diagram of the spacecraft electrical system. This diagram shows the main connections among the power generators and the instrumentation.

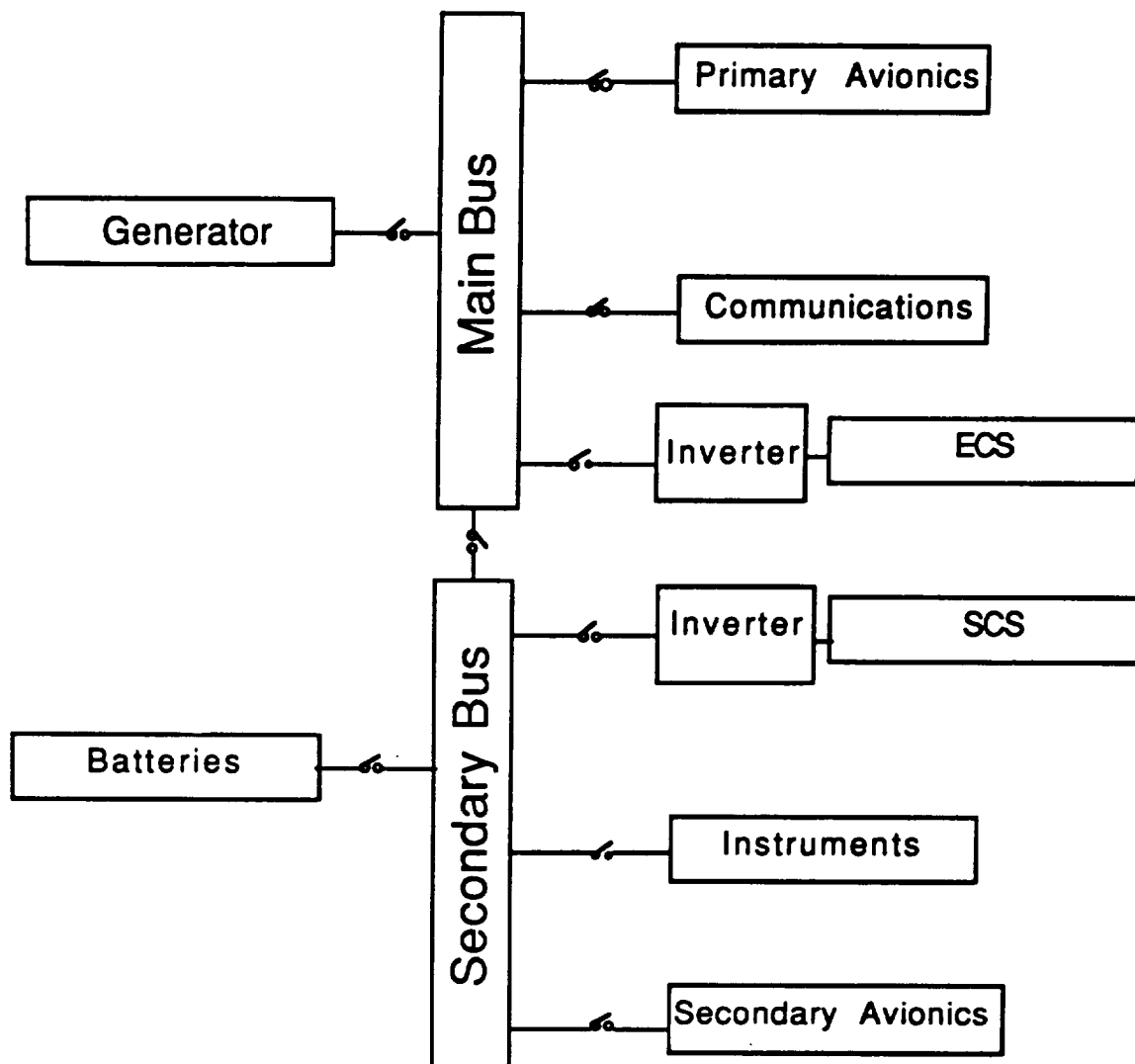


Figure 4.4.A. : Spacecraft Electrical Control System

CHAPTER 4 REFERENCES

- Agrawal, B.N., *"Design of Geosynchronous Spacecraft."* John Wiley & Sons, Inc., New York. 1985
- Akin, David, PhD., Interview with Professor, Personal Communication. University of Maryland, College Park, MD, 11 Feb 1991.
- Center, Allan M., Capt, USAF. Interview with Missile Launch Instructor, Personal Communication. Vandenberg AFB, California, 2 Aug 1990.
- Collins, W. B. and D. R. Newell, *"Power Conditioning Requirements and Tradeoff Considerations for the Space Shuttle."* IEEE 1971 Power Conditioning Specialists Conference.
- Empell, C.M., *"Multirole Capsule An Introduction."* Journal of the British Interplanetary Society Vol#2, 1989. York. 1986.
- Gross, S. , *"Battery Design and Optimization,"* Electrical Society, Princeton, NJ. 1979.
- Hill, P.G and C.R. Peterson, *"Mechanics and Thermodynamics of Propulsion,"* Reading, Mass: Addison-Wesley ,1970.
- Huzel K. Dieter and Huang H. David, *"Design of Liquid Propellant Rocket Engine,"* NASA Scientific and Technical Information Office, Washington DC, 1971.
- Manzo, M. and N. R. Schulze, *"NASA Aerospace Battery System Program Update."* 1989 24th Intersociety Energy Conversion Engineering Conference.
- Morgan, N.E. and W. D. Morath, *"Development of a Hydrogen-Oxygen Internal Combustion Engine Space Power System."*
- Rausenbach, H. S., *"Solar Cell Array Design Handbook,"* New York: Van Nostram Reinhold Co. 1980.
- Sutton, G. P., *"Rocket Propulsion Elements,"* John Wiley & Sons, Inc., New York. 1986.
- Thompson, T. William, *"Introduction to Space Dynamics,"* Dover Publishing, New York, 1985

Chapter 5: Avionics

Section 5.1 Navigation and Guidance

5.1.1 Positioning, Tracking, and Time Keeping

To navigate a spacecraft, three things are required; the spacecraft's position, a tracking method, and a way to keep accurate time between the spacecraft and the navigational system. While in orbit, periodic fixes will be measured by the on board and satellite based navigational systems. Continuous fixes are not necessary because once in orbit, the trajectory is predictable to within hundreds of meters for several revolutions of low orbit.

The Inertial Navigation System (INS) on board the Taurus LMS will give instantaneous data to the astronaut. The system is built by Delco Electronics and is named the LCINS (Low Cost Inertial Navigation System). The main reason for choosing this INS is because of its low mass, which also accounts for its somewhat less accurate information. The LCINS is a strapdown configuration with two degrees of freedom gyros. The inertial reference assembly is reduced in size. A digital microprocessor performs all the measurement data processing, instrument torquing computation, scaling, attitude, and navigation functions. Steering commands as well as other autopilot interfaces are provided. The LCINS is believed to have a factor of two inaccuracy compared to other systems. The factor of two came from comparing the LCINS with more accurate systems available today.

Dimensions: 152 X 152 X 215mm
Weight: 3.0kg
Power: 35W (+12 and +5VDC)
Accuracy: 7.408km/h

The above characteristics about the LCINS makes it the ideal system to use in a heavily mass constrained space vehicle like the Taurus.

5.1.2 Dynamic Stability and Control

Because the LCINS has been used and proven to be reliable, gyroscopic motion tests have already been performed. Most likely, Lagrange's equations were used for formulating the differential equations for rotational motion about principal axes and free motion. If the Taurus LMS had built its own INS, these equations would have been implemented to give the necessary equations of motion.

5.1.3 Updating the INS

Because the positional error of the LCINS increases every hour (see figure 5.1A), it will have to be updated by another navigation system. The primary satellite navigational system considered for updates is the Global Positioning System. GPS is a satellite based navigational system which will give continuous worldwide coverage by the year 1992, when there are 21 operational satellites in orbit. The satellites orbit once every 12 hours and transmit two L-band signals, L1 at 1575.42MHz and L2 at 1227.60MHz. This system of orbits ensures at least four satellites in view at all time. GPS will provide an accuracy better than 30m using the public available coarse acquisition code (C/A code called "standard positioning."). This type of accuracy will be sufficient when the spacecraft is in orbit and only periodic fixes are taken.

There are also times when more precise accuracies will be required by GPS, for example, change of orbit. Using the P code (military code), GPS will be able to give an accuracy of 1 to 10m, depending on the position of the satellites. Permission from the military will be necessary to use the P code. When a change of orbit is desired, fixes will be measured by accelerometers to guide an orbit change maneuver.

On board computers will calculate the instantaneous orbit while the spacecraft is thrusting, using the integrated accelerometer outputs. The position of each satellite will be known with a high degree of accuracy and each satellite is equipped with four atomic clocks called hydrogen masers for redundancy. Accurate satellite position data and accurate clocks are essential for accurate, three-dimensional position determination. Three satellites will determine the latitude, longitude, and altitude of the spacecraft at any positioning update.

Because the clock on the craft is not atomic, a time bias occurs. To correct it, a fourth satellite is used to provide a fourth line of position (LOP), which eliminates the time bias and reduces the area fix to a point in space. Thus, the fourth satellite acts as the spacecraft's atomic clock.

To navigate and guide, a C/A code sent at 1,023,000 bits/s is repeated every millisecond. The P code can be also sent at 10,230,000 bits/s and takes a week to repeat itself. A GPS receiver has the same program for generating the C/A and P codes as the satellites. By matching the two patterns, the satellite and receiver can be synchronized, all in a matter of seconds. Once synchronized, the satellite can measure the elapsed time since transmission by comparing the phase shift, or remaining difference between the two codes. The more the two disagree, the greater the length of time since transmission, and length of time since transmission multiplied by the speed of light equals distance. Thus by measuring phase shifts in the code, distance between satellite and receiver can be computed. For example, if the closest the two are synchronized is 0.07 seconds, then multiplying by the speed of light (3×10^8 km/s) the distance is 21000km.

If the distance from a satellite is known, then it follows that the spacecraft must be located somewhere on the surface of a sphere with a radius of that distance, centered on that point. Three satellites make three surfaces and intersect at one point. This is a point in space based on the distance. By knowing how far the spacecraft is from each satellite and the satellite's position, the on board computer can calculate its position (Figure 5.1A).

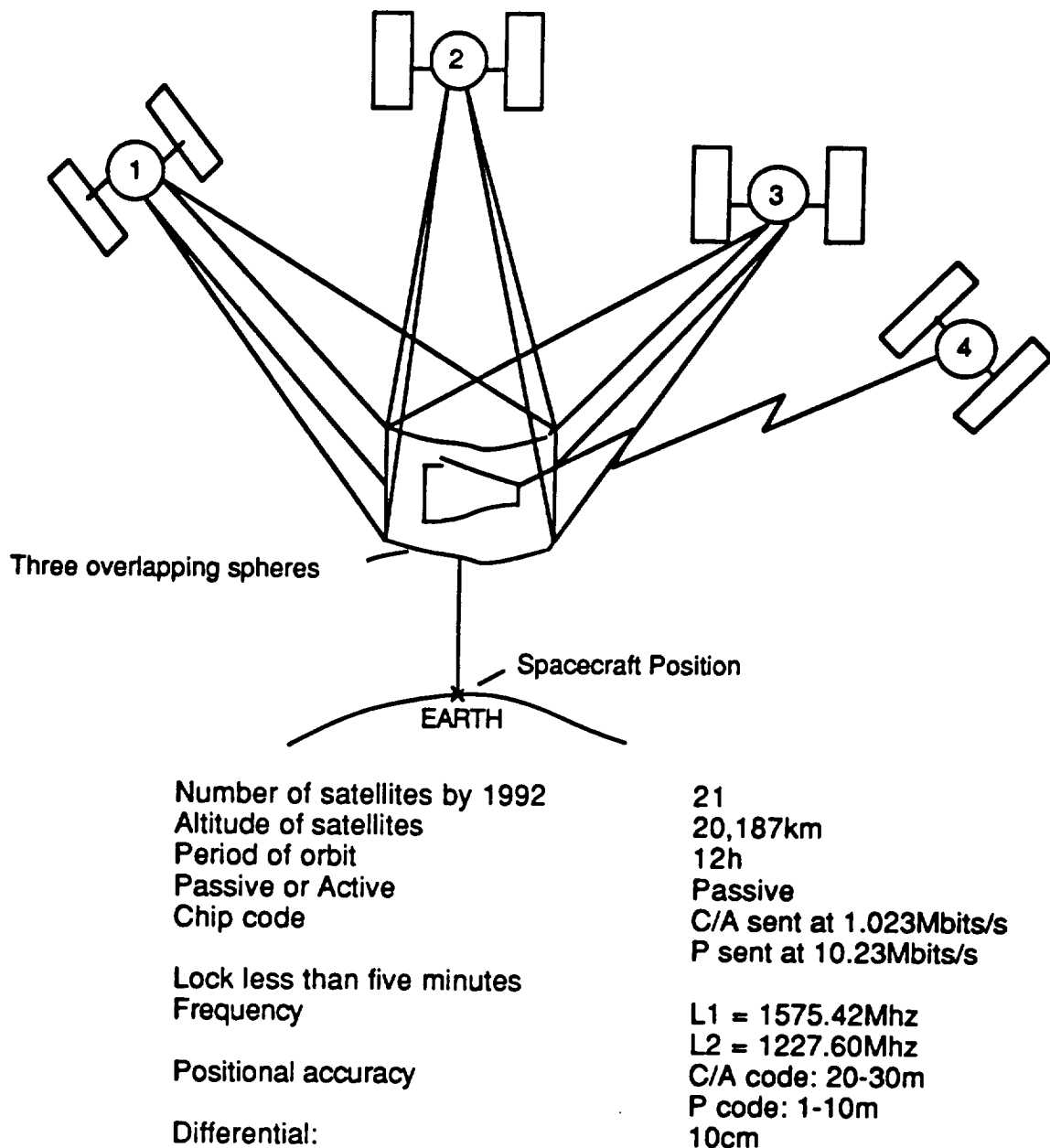


Figure 5.1A. The Global Positioning System (Ref. 1)

5.1.4 GPS Vs. Other Systems

GPS is the best choice for the navigational system to update the INS. With the accuracy of 1-10m and a 100% coverage, GPS is guaranteed to give good accuracy at any time. No signal is required from the spacecraft to receive the position data because GPS is a passive system. One disadvantage of GPS is the fact that four satellites must be used for accuracy including the time bias, but with

the number of satellites at their altitude, this should not be a problem.

The Tracking Data Relay Satellite System (TDRSS) is another major satellite system. It provides close to 85% continuous unified S-band coverage to as many as 24 satellites at once below 3700km altitude. The same dish used for communication (its primary use) can be used for navigation because they both work on the same band (Ku). A downfall for TDRSS is that all transmissions must pass through a ground terminal in White Sands, NM. This puts the dependency for information on one station. Also, as of 1983, numerous system outages have occurred, lasting from a few minutes to several hours or more. When this occurs, the spacecraft has to rely on ground stations for all communications. Single points of failure exist throughout the computer and communication systems and can cause system outages.

Another downfall is the 15% unavailable coverage. If TDRSS was to be used as the primary navigation system, there would always be the 15% chance where only the INS could give the spacecraft position, where accuracy decreases with time. Performing orbital maneuvers during the 15% unavailable coverage would not be very accurate.

NASA is in the process in constructing a second TDRSS ground terminal at White Sands because of concerns about the reliability of the first one. The second terminal will provide backup to the first and eliminate it as a single point of failure. When the second terminal is completed in 1993, the original terminal will be completely overhauled to be identical with the new terminal.

Another form of navigation is ground based. A ground system can use simple and inexpensive quartz oscillators to time the interval between the start of a signal and the receipt of the return pulse.

Ground based systems (active) require a signal from the user, which can be intercepted, and disrupted by unfriendly opposition. Also, ground clutter and precipitation often mask return signals. A ground based station can only be used when the spacecraft is flying in the range of the station which would require many different stations to navigate a mission. Ground station navigation would be used only in conjunction with another form of a navigational system.

5.1.5 Sensors

The guidance system will, in general, consist of sensors and satellites for measuring various dynamic variables such as acceleration, velocity, position, and angular velocity. Transducers will process the sensor information, then the computer will interpret the transducer information. The computer will give commands to the actuators whose function it is to develop and apply forces and moments to the vehicle in the manner directed by the computer's outputs.

Trajectories influence the guidance and control of the vehicle. The resulting optimum trajectory dictates the path along which the guidance and control must direct the aerospace vehicle.

The gyro of the INS will be used for inertial sensing. The purpose of the gyro is to provide a physical element, arranged either to preserve angular fixes in inertial space about all axes, regardless of spacecraft motion, or to precisely measure angular motions of the craft relative to inertial space. The gyro will be as insensitive to vehicle motion as possible.

Accelerometers will be used to measure changes in vehicle speed. The

orientation of the accelerometers will be established with help from the gyro system so gravity is taken into account as well as components of vehicle velocity changes, due to thrust, drag and other non-gravitational forces when determining velocity and displacement.

5.1.6 Rendezvous

Because of the large mass constraints placed on the Taurus LMS vehicle, rendezvous was determined to be unlikely due to the maneuvering fuel constraints. Future rendezvous guidance was examined as a mission expansion possibility for the LMS. A typical Star Tracker may have a mass of about 13-14kg and Rendezvous Radar (along with its supporting equipment) may have a mass over 70kg. A COAS (Crew Optical Alignment Sight) would only have a mass of about 1kg and could be included within the capsule. The ground could uplink the position of the target and also uplink the burns to place the LMS close to the target. This was a method used by the Gemini crew (which also had a rendezvous radar).

A COAS can have a range of about 185km. Once the ship would get inside the range, the astronaut could look through the COAS to see how the target was moving relative to the spacecraft. The COAS has an advantage of looking through it rather than a window because a window doesn't have any way of letting one know how much the target is moving left, right, up, or down relative to the ship. The COAS has marks which would let the astronaut know which way the target was moving.

Overall, if there was enough fuel, rendezvous would have been possible, but not very accurate. Another guidance sensor, such as rendezvous radar, would make a potential rendezvous much more accurate and safe.

5.1.7 The Role of Orbital Mechanics

Orbital mechanic equations were used to determine the required accuracies for positional accuracy and flight angle. It was determined that for a survivable re-entry, the Taurus LMS needed an accuracy of about 100km in position and 2 degrees in flight path angle. A positional accuracy of 10m would give the Taurus LMS a negligible landing site. A flight path angle accuracy of 0.20 degrees would give the Taurus LMS a landing site error of 7.7 km. The orbital mechanic equations used to find these accuracies can be found in Appendix M.

Section 5.2 Attitude Determination and Control

As mentioned in section 5.1, the inertial navigation system requires periodic updating to correct the inherent errors which accumulate over time. These correction updates are provided by additional sensors on the capsule. This section discusses different types of attitude determination sensors used on spacecrafts and provides their advantages and disadvantages. Attitude control techniques will be discussed as well.

5.2.1 Requirements

The attitude requirements for the Taurus LMS capsule are set forth by the missions it will perform. From the limited number of missions available, the reentry requirements are the most stringent in terms of attitude. From these requirements, an accuracy of better than one-quarter degree will be needed for both attitude determination and control. Hence, the sensors therefore must provide an accuracy of 0.20 degrees or better to insure accuracy between the periodic updates. These requirements, as well as mass and volume constraints, set the guidelines to determine which techniques to implement.

5.2.2 Overview

Various techniques to determine a spacecraft's attitude were studied. These studies involved analog and digital sun sensors, horizon sensors, magnetometers, star sensors, and various types of gyroscopes. Each technique was evaluated on its accuracy, its typical mass, volume and power requirements, and its costs and complexity.

5.2.3 Sun Sensors

Sun sensors are the most widely used sensor in space applications today due to its many advantages. Since the angular radius of the sun is fairly constant for an orbit around the earth, and appears small enough at this distance, the simplification of the sun as a point source can be made without loss of accuracy. This, in turn, simplifies the sensor itself and the algorithm associated with the attitude determination. Also, due to the brightness of the sun, it is easily distinguishable from other bodies in space. Hence, the sensor does not require additional distinguishing mechanisms, and will require less power. Another factor for this type of sensor is that other equipment such as solar panels need to face the sun, so no special orientations are needed just for the sensor.

Sun sensors come in single-axis and two-axis configurations. The single-axis system provides the angle of the sun in reference to the spacecraft. Meanwhile, the two-axis system provides the vector to the sun from the spacecraft.

Two types of sun sensors were examined - analog and digital. Analog sensors use a photocell whose output current indicates the angle of incidence of the solar radiation. Analog systems require no input power or control electronics, but have only a fair accuracy rating. Digital sun sensors, however, can have very

good accuracies (better than 0.1°), with the costs of power required and additional electronics. The digital sensors use a number of photocells, which represent the specific bit used to generate a digital output signal representing the angle of the sun to the spacecraft. Although digital sun sensors require slightly more power, mass and volume, their improved accuracy outweighs these disadvantages. Therefore, the Taurus capsule will use the two-axis digital sun sensors system to obtain the given sun vector.

5.2.4 Horizon Sensors

Horizon sensors are the most common method of determining the orientation of the spacecraft with respect to the earth. Present-day sensors make use of the infrared spectra band to limit errors associated with visible light sensors, allow night determination, and reduce the effects of reflected sunlight off the spacecraft. Disadvantages with these infrared sensors include higher costs, slower response times (on the order of milliseconds instead of microseconds) and lower signal-to-noise ratios in comparison to the visible light sensors.

Horizon sensors require some type of scanning mechanism to search across space. For a spinning spacecraft, mounting the sensor on the body is sufficient. But since the Taurus capsule will not be spinning while in orbit, some type of mechanical device must be used. Methods such as attaching the sensor to a momentum wheel are inadequate on the Taurus LMS because of the extra mass required. A system similar to the panoramic attitude sensor (manufactured by Ball Brothers Research Corporation) therefore, is desirable. This type of system can be used on a rotating spacecraft or can use internal scanning when the spacecraft is not rotating.

Horizon scanners provide good accuracy (in the 0.05° range) during both day and night. Some limitations on these sensors are that they are orbit dependent (but since the Taurus LMS will maintain a somewhat constant orbit, this is not a major concern) as well as being poor in yaw. Also they are somewhat heavier in comparison to sun sensors and magnetometers (to be discussed next) and require more complicated mechanisms for spanning. But as with sun sensors, this improved accuracy outweighs these disadvantages and therefore will be used on the Taurus capsule.

5.2.5 Magnetometers

Magnetometers are also widely used in spacecraft today because of their many advantages including low mass, low cost, high reliability (mainly because of the need for few moving parts), low power requirements, and supplying continuous coverage. Also, they are vector sensors, determining the direction and magnitude of the magnetic field of the earth. However, since they depend on the little known magnetic field and the models used to predict the field's strength and direction, they are subject to significant errors and therefore poor accuracy(in the 1.0° range). Hence, this poor accuracy prevents their use on the Taurus capsule.

5.2.6 Star Sensors

Star sensors provide vectors to stars with respect to the spacecraft. Using

known star positions, the attitude of the spacecraft can be determined. Star sensors are the most accurate attitude sensor (in the 0.005° range). But for the Taurus capsule, this excellent accuracy is outweighed by the costs associated with this sensor. Star sensors are expensive, heavy, sensitive to light, and require more power than any other previously described sensor. Also the computer processing requirements are much more extensive. For these reasons, star sensors are presently not part of the capsule design.

5.2.7 Gyroscopes

Gyroscopes are the primary attitude determinate technique when there exists gaps in which other sensors can not obtain readings. Gyroscopes provide updated attitude angular displacements and/or rates. When the attitude system is designed with gyroscopes, the spacecraft is essentially using the gyros for its attitude reference and these gyros are updated periodically by the other sensors to insure accuracy and correct for integration errors. The accuracy of gyroscopes is in the range of 0.01° per hour drift.

There are two types of attitude determination gyroscopes, rate gyros and rate-integrating gyros. Rate gyros measure the angular rates of the spacecraft while the rate-integrating gyros measure the spacecraft's angular displacements directly. Both types may be used for spin rate control and attitude stabilization. For these functions, rate-integrating gyros are usually more accurate than rate gyros, but usually cost more.

As mentioned in section 5.1, gyroscopes are utilized in the INS. The use of laser fiber-optic gyroscopes provide many advantages such as having few moving parts, high levels of reliability and are able to withstand harsher conditions. Fiber-optic gyros also have the ability to be very compact and light.

Table 5.2A provides a summary of the characteristics of these previously discussed attitude determination sensors. (Ref. 2)

Table 5.2A Sensor Characteristics

<u>Sensor</u>	<u>Accuracy</u>	<u>Mass(kg)</u>	<u>Vol.(m³)</u>	<u>Power(W)</u>
Digital Sun Two-Axis Sys.	.01°-.05°	.4 - 1.7	.001 - .01	~1.8
Analog Sun Two-Axis Sys.	.03°-2°	.05 - .1	< .001	none
Horizon Scanwheel	.02° - .05°	3. - 6	~ .02	~ 5.5
Panoramic	.02° - .05°	~ 1.0	< .01	~ 5.5
Magnetometers	.25° - 1.°	.1 - 1.	.001 - .005	< 1.0
Star Sensors	.001° - .02°	13.0	~ .03	~ 2.0
Gyroscopes	.01° / hr	< .3	< .001	< 1.0

5.2.8 Attitude Control

Five different systems were studied for the attitude control system. These five systems include reaction wheels, momentum wheels, reaction jets (thrusters), control moment gyros, and magnetic torquers. From these, reaction jets were chosen as the technique to be used for attitude control. This is due mainly to their quick, high force response ability and good accuracy. Although reaction and momentum wheels, as well as control moment gyros, provide a quick and accurate response, the mass required for these systems to be effective control techniques is well beyond the limits set for the Taurus spacecraft. (This conclusion comes from a design study to determine the needed sizes of reactions and momentum wheels for effective torque on the Taurus capsule.) As for magnetic torquers, they are lightweight, but provide only a slow response with poor accuracy (Jane's, All the World's Avionics, 1990). Hence thrusters are the focus of the control model. See section 4.3 on propulsion for complete details on the design of the reaction control system.

Section 5.3 Data Processing

5.3.1 Introduction

The primary function of the data processing system is to monitor all equipment on the Taurus LMS capsule. Through the use of sensors (discussed in section 5.4) and output devices, this system will keep the astronaut informed about the present condition of all aspects of the spacecraft.

Another function of the data processing system is to perform necessary navigation, guidance and attitude and flight control computations. The goal of this system is to allow for as many on-board processing capabilities as possible and thereby relying less on ground-based computations. Also, with recent technologies, the goal is to obtain much faster computation speeds, much larger memory capability, and better display units, thus reducing the need of the astronaut for maintenance and computer administration functions.

5.3.2 Requirements

The basic requirements for the data processing system is to be able to handle all sensor inputs and present this information to the astronaut in a concise form. The processing of this data involves reading in the sensor data and comparing the value with the limits set for that sensor. If the value is not within the specified range, a warning is sent to the astronaut and action is taken to try to correct the problem while auxiliary equipment is used in place of the malfunctioning object. (Note that additional sampling from the sensor will be performed to insure that the data is correct and was not corrupted.) Along with reading the sensor data, the processor must update certain sensors with information from other sensors. For example, the INS is updated by the attitude sensors and the GPS (as discussed in sections 5.1 and 5.2).

Another requirement of the data processing system is to make the necessary computations for the guidance and navigation system (OMS) and the attitude and flight control systems (RCS). These computations involve determining the directional vector to the target position, number and duration of OMS engine burns and the required thruster firings for attitude control. Also, these computations must be adaptive to possible failures of any system at any time.

The data processing system is also required to interact with other external systems on the spacecraft. For example, the communication system must be linked to the processors to allow for data uplink and downlink. (New code may be uplinked in the case of changes to the predefined mission.) Also, the astronaut must be able to enter commands and perform any necessary changes.

The final requirement of the data processing system is to provide a 95% mission success rate. For the Taurus spacecraft, mission success is not as dependent on onboard computation as does other spacecrafts such as the shuttle. Therefore, even though it may be difficult on the astronaut, manual control capabilities must be provided in case of computer malfunction. In other words, this system must be designed to control all systems of the spacecraft in case the astronaut is unable to perform his duties, allow for dual control when both the computer and astronaut are functioning, and allow for manual control if the computer malfunctions.

5.3.3 System Architecture

Three major types of architecture were studied for the Taurus capsule design: centralized, federated, and distributed. A distributed system has multiple processors throughout the spacecraft performing specific tasks. This type of system allows for short, quicker buses, and faster program execution. However, this design allows for different processors and requires more software development. It also restricts the amount of shared information, which is a primary requirement for the spacecraft. The federated system has each major system sharing input and sensor data over common data buses. This system allows for independence of the major systems while insuring a common data base. One disadvantage of this type of system is partitioning (limiting the spread and effects of a subsystem's failure is difficult). The centralized system has all processors together, making design and software development simpler. But this design leads to long buses for data and command communications.

For the Taurus design, a centralized system will be used. As can be seen in figure 5.3A (layout similar to Rockwell's block diagram for the shuttle's data processing system), this design will consist of two general purpose processors for guidance, navigation, and control, one as the primary processor and one as a backup computer. From these central processors will be links to main memory, the sensors, display controls, engine interfaces, and other external interfaces.

The choice of using two processors was determined after looking at different systems consisting of one to four processors. For the case of just one processor, it was determined that this was not a desirable choice. Even though the use of only one processor reduces the required mass for the system, it forces the sole computer to be a single point of failure. Although the capsule can be manually controlled, the mass penalty of adding an additional backup computer is outweighed by the reliability a second computer adds. Therefore a minimum of two processors was specified. After this minimum was set, choosing the optimal number was determined by comparing the mass required for multiple processors to the amount of reliability another processor would add. Using estimates of 5 kg of mass and 20 W of power required for each processor and its associated RAM (Morgan and Gordon, 1989), it was decided that two processors is all that is needed. The use of three or four processors seemed unnecessary for such limited mission capabilities.

As previously mentioned, each processor will have its own RAM associated with it. The size of the RAM will be 16 Mbyte. This size allows for an estimated 1 Mbyte of software, 8 Mbytes reserved for runtime memory and 7 Mbyte for temporary data storage and space for uplinked code if needed. In case this memory gets corrupted, the capability to reload the software from the mass memory will exist. The decision to go with individual RAM was made to allow for quicker and more independent execution.

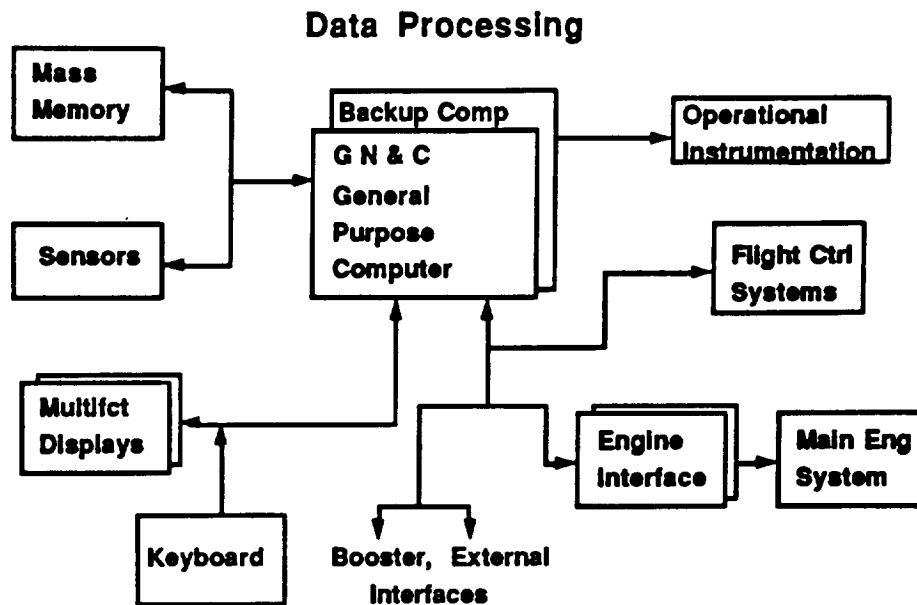


Figure 5.3A Avionics System Design

Associated with each processor will also be an I/O processor to handle all the required sensor input. After looking at the amount of sensor data to be handled (discussed in section 5.3.3.4) and the amount of computations for other systems, a processor with at least a 1 MHz capability is required.

5.3.4 Data Bus Design

The design of the data bus consists of a two-way linear bus configuration. The linear configuration is used due to its ease and simplification for design and modifications. Although the bus controller is a single point of failure, having dual redundancy and well partitioned buses will increase reliability. Six busses will be used on the Taurus capsule, two for sensors and mass memory, two for engine and external interfaces, and two for displays and keyboard (all connected to the CPUs).

5.3.5 Displays

The choice of the type of display equipment for the system involves three types: CRT's, liquid crystal displays (LCD) and luminous flat panels. For CRT's, reliability and versatility are its main advantages, but its size is a significant disadvantage. Its depth requirement is up to ten times more than that of the other two types (approximately 10 to 75 cm). LCDs, on the other hand, require little depth space (approx. 2.0 cm), low power and are digitally compatible. But they do require some type of external backlight. Both of these types have good resolution (approx. 80 lines/cm) and full color capability. Luminous flat panels have the advantage of being very rugged and having uniform resolution and brightness. They are also compact in depth and like LCDs, are digitally compatible. But these displays have been limited in resolution (only 25 lines/cm) and size in the past (approx. 8.0 cm depth). For these reasons, the Taurus capsule will use LCDs for their two displays (Spitzer, 1987)

5.3.6 Mass Memory

Mass memory is required to store a backup copy of all software needed by the processors in the case of memory error on the RAM. It is also needed to store data while communications downlink is not available. The amount of this data storage is dependent on the input cycle rates of the sensors and the downlink rate of the communication system (8 Kbyte/sec). Table 5.3A provides a breakdown of the input cycle rates for the different sensors. These rates were determined based on the importance of the system and on possible fluctuations with the sensor values. (These rates are for the time when the OMS or RCS engines are firing and main life support is functioning.) From this data, it can be seen that 310 sensors are processed 12.5 times per second, 120 sensors at 25 times per second and 22 at 100 times per second. This gives a total of 9075 inputs per second. With an average of 2 bytes per sensor input, the total is 18.2 Kbytes per second. For the worst case of 30 minutes without the capability of downlink, and if every other data value was saved, the mass memory would be required to have at least 16.4 Mbytes of space free for data. Therefore, to allow for software, data storage and auxiliary space, the mass memory needs to be at least 40 Mbytes.

Table 5.3A Sensor Cycle Rates (at time of engine firing)

<u>System</u>	<u>Sensor Type</u>	<u># Sesnors</u>	<u>Cycle Rate (input/sec)</u>
Propulsion	Temperature	8	12.5
	Pressure	20	25
	Flow	4	100
	Valve	56	12.5
Main Life Supp	Temperature	10	25
	Pressure	18	25
	Flow	18	100
	Valve	56	12.5
	Level	12	25
Secondary Life	Temperature	12	12.5
	Pressure	26	12.5
	Flow	20	12.5
	Valve	72	12.5
	Level	4	12.5
RCS	Temperature	12	12.5
	Pressure	56	25
	Valve	30	12.5
Abort	Electro/Static	2	25
	Pressure	2	25
	Control	6	12.5
Miscellaneous		8	12.5

(Main Life
Support
Functional)

5.3.7 Summary

Table 5.3B lists estimated characteristics of the data processing system's components (Jane's, All the World's Avionic's, 1990)

Table 5.3B Component Characteristics

<u>Component</u>	<u>Mass (kg)</u>	<u>Volume(m³)</u>	<u>Power (W)</u>
(2) Processors	10	0.015	40
(2) Displays	6	0.010	60
Mass Memory	8	0.011	20
Keyboard	3	0.010	3
(2) Engine Interfaces	6	0.010	20
(6) Bus Controllers	<u>12</u>	<u>0.020</u>	<u>50</u>
Totals:	45 kg	0.076 m ³	193 W

Section 5.4 Sensors

5.4.1 Introduction

In order for the Taurus LMS to operate through computer and/or manual control sensors are required. The sensors return information concerning all operational systems on the Taurus Capsule to the astronauts for updates as well as corrections. For this reason, sensors will be applied to the following systems: propulsion, main life support, secondary life support, reaction control, and abort .

5.4.2 Propulsion

For the propulsion system, it will be necessary to measure the conditions of the pressurant, oxidizer, and propellant tank as well as the conditions of the plumbing and rocket combustion chamber. Conditions which will be measured are temperature, pressure, flow rate, and valve openings.

Temperature measurements will consist of tank temperatures of the pressurant, oxidizer and propellant as well as the temperature of the rocket combustion chamber. The tank temperature measurements will determine the necessity of abort based on an increase of the temperatures based on a maximum set by design. The measurement of the temperature of the rocket combustion chamber will determine the necessity for adjustments in the plumbing or tank system for its proper operation. A total of eight temperature sensors ranging from 20 to 3000 Kelvin will be required in the system (See Table 5.4A)

Pressure measurements consist of transducers installed inside of each tank as well as claibration gauges outside of each tank. There will also be pressure transducers installed at the pressurant filter and regulator as well as at the pressurant bleeder valve. Pressure measurements will also be taken inside of the combustion chamber of the rocket to determine the need to increase flow of either the propellant and oxidizer. A total of twenty pressure sensors ranging from 1 to 30 MPa will be required in the system (See Table 5.4A).

The rate of flow from the propellant tank and the oxidizer tank will also be measured. These sensors will determine if the flow rate from the tanks remains consistent with the flow/propellant ratio set by design. For the plumbing and tanks, a total of approximately twenty flow rate sensors ranging from 100 to 300 cm³/sec will be required in the system (See Table 5.4A).

Valve sensors throughout the plumbing system as well as on the tank fill and bleeder lines will determine proper operation of the valves. The ammount of valve sensors will approximately be fifty-six on the plumbing and tanks of the propulsion system (See Table 5.4A).

The total ammount of propulsion sensors required will be approximately eighty-eight (See Table 5.4A).

Table 5.4A: Propulsion Sensors

<u>Type</u>	<u>Range</u>	<u>Quantity</u>
Temperature Sensors		
Pressurant Tank (1 Tank)	20-100 Kelvin	2
Oxidizer Tank (1 Tank)	100-400 Kelvin	2
Propellant Tank (1 Tank)	100-400 Kelvin	2
Rocket Cmbstn. Chamber (1 Rocket)	2000-3000 Kelvin	<u>2</u>
Total Temperature Sensors		8
Pressure Sensors		
Pressurant Transducer (1 Tank)	10-30 MPa	2
Oxidizer Transducer (1 Tank)	1-4 MPa	2
Propellant Transducer (1 Tank)	1-3 MPa	2
Pressurant Calibration Gauge (1 Tank)	10-30 MPa	2
Oxidizer Calibration Gauge (1 Tank)	1-4 MPa	2
Propellant Calibration Gauge (1 Tank)	1-3 MPa	2
Pressurant Bleeder Valve Gauge (2 Lines)	10-30 MPa	4
Pressurant Regulator Gauge (1 Tank)	10-30 MPa	2
Combustion Chamber (1 Rocket)	1-5 MPa	<u>2</u>
Total Pressure Sensors		20
Flow Rate Sensors		
Propellant Flow	100-200 cm ³ /sec	2
Oxidizer Flow	100-300 cm ³ /sec	<u>2</u>
Total Flow Rate Sensors		4
Valve Sensors		
Tank Pressure Relief Valve (3 Tanks)	open/close	6
Tank Vent Valve (3 Tanks)	open/close	6
Tank Fill Valve (3 Tanks)	open/close	6
Tank Pressure Regulation Switch (3 Tanks)	open/close	6
Tank Supply Valve (3 Tanks)	open/close	6
Gas filter Valve (2 Lines)	open/close	4
Pressurant Bleeder Valve(2 Lines)	open/close	4
High Pressure Gas Valve (2 Lines)	open/close	4
Pressurant Isolation Valve (2 Lines)	open/close	4
Check Valve (2 Lines - 4 Check Points)	open/close	8
Rocket Ignition Switch (1 Rocket)	open/close	<u>2</u>
Total Valve Sensors		56
Total Propulsion Sensors		88

5.4.3 Human Factors - Main Life Support System

For the main life support system on the Taurus LMS it will be necessary to measure the conditions of the pressurant, nitrogen, and oxygen tanks as well as the heat exchanger and cabin conditions.

Temperature measurements will be made in each of the tanks and also in the cabin. Temperature measurements on the nitrogen and oxygen tanks range from 50-90 Kelvin while measurements in the cabin range from 330-370 Kelvin. Ten temperature sensors will be required (See Table 5.4B).

Pressure sensors are similar to those in the propulsion system where it will be necessary to measure the pressure in each tank: pressurant, oxygen, and nitrogen. It will also be necessary to measure the pressure in the crew cabin as well. The total number of pressure sensors required is eighteen (See Table 5.4B).

Flow rates of nitrogen and oxygen will also be measured in order to determine the amount left in each tank during the flight. The same holds true for the lithium hydroxide tank which will be changed regularly during the flight (See Table 5.4B).

Valve sensors will be placed in all the tanks as well as the heat exchanger, fan, heater, coolant pump, LiOH canister, intake screen and exhaust screen. These sensors will determine the operation of each element (See Table 5.4B).

It is also necessary to measure the levels of nitrogen, oxygen, and carbon dioxide in the cabin. Measurements of humidity, radiator power output and cabin radiation will also be taken into account (See Table 5.4B).

Table 5.4B: Human Factors - Main Life Support System

<u>Type</u>	<u>Range</u>	<u>Quantity</u>
Temperature Sensors		
Pressurant Tank (2 Tanks)	20-100 Kelvin	4
Nitrogen Tank (1 Tank)	50-90 Kelvin	2
Oxygen Tank (1 Tank)	50-90 Kelvin	2
Cabin	280-320 Kelvin	<u>2</u>
Total Temperature Sensors		10
Pressure Sensors		
Pressurant Transducer (2 Tanks)	????	4
Oxygen Transducer (1 Tank)	????	2
Nitrogen Transducer (1 Tank)	????	2
Pressurant Calibration Gauge (2 Tanks)	????	4
Oxygen Calibration Gauge (1 Tank)	????	2
Nitrogen Transducer (1 Tank)	????	2
Cabin	0-0.2 MPa	<u>2</u>
Total Pressure Sensors		18
Flow Rate Sensors		
Nitrogen Flow Rate	????	8
Oxygen Flow Rate	????	8
LiOH Flow Rate	????	<u>2</u>

Table 5.4B: Human Factors - Main Life Support System (Continued)

<u>Type</u>	<u>Range</u>	<u>Quantity</u>
Valve Sensors		
Pressurant Tank		
Relief Valve (2 Tanks)	open/close	4
Tank Vent Valve (2 Tanks)	open/close	4
Fill Valve (2 Tanks)	open/close	4
Regulation Switch (2 Tanks)	open/close	4
Oxygen Tank		
Supply Valve (1 Tank)	open/close	2
Vent Valve (1 Tank)	open/close	2
Fill Valve (1 Tank)	open/close	2
Regulation Switch (1 Tank)	open/close	2
Nitrogen Tank		
Supply Valve (1 Tank)	open/close	2
Vent Valve (1 Tank)	open/close	2
Fill Valve (1 Tank)	open/close	2
Regulation Switch (1 Tank)	open/close	2
Heat Exchanger		
Air Intake Valve	open/close	2
Air Outtake Valve	open/close	2
Ethylene Glycol Intake Valve	open/close	2
Ethylene Glycol Outtake Valve	open/close	2
Heater Operation	on/off	2
Screened Intake	open/close	2
Fan Operation	on/off	2
Electrical Heater	on/off	2
Radiator	on/off	2
Coolant Pump	on/off	2
LIOH Valve	open/close	2
Exhaust Valve	open/close	2
Total Valve Sensors		56
Level Sensors		
Cabin Nitrogen	75-85%	2
Cabin Oxygen	15-25%	2
Carbon Dioxide	Amount Extracted	2
Radiation	17-140mrems	2
Humidity	40-60%	2
Radiator Power Output	200-400 Watts	2
Total Level Sensors		12
Main Life Support System Total		106

5.4.4 Human Factors - Secondary Life Support System

The sensors for the secondary life support system are similar to those in the main life support system due to their similar design. The only difference comes into account with the addition of a water tank. Once the secondary life support system is initiated, it will no longer be necessary to measure the conditions in the cabin. The total number of sensors required is one hundred thirty-four (See Table 5.4C).

Table 5.4C: Human Factors - Secondary Life Support System

<u>Type</u>	<u>Range</u>	<u>Quantity</u>
Temperature Sensors		
Pressurant Tank (3 Tanks)	20-100 Kelvin	6
Nitrogen Tank (1 Tank)	50-90 Kelvin	2
Oxygen Tank (1 Tank)	50-90 Kelvin	2
Suit Temperature	280-320 Kelvin	2
Water Tank (1 Tank)	????	<u>2</u>
Total Temperature Sensors		12
Pressure Sensors		
Pressurant Transducer (3 Tanks)	????	6
Oxygen Transducer (1 Tank)	????	2
Nitrogen Transducer (1 Tank)	????	2
Pressurant Calibration Gauge (3 Tanks)	????	6
Oxygen Calibration Gauge (1 Tank)	????	2
Nitrogen Transducer (1 Tank)	????	2
Suit Pressure	0-0.2 MPa	2
Water Tank Transducer (1 Tank)	????	2
Water Tank Calibration Gauge (1 Tank)	????	<u>2</u>
Total Pressure Sensors		26
Flow Rate Sensors		
Nitrogen Flow Rate	????	8
Oxygen Flow Rate	????	8
Water Flow Rate	????	2
LIOH Flow Rate	????	<u>2</u>
Total Flow Rate Sensors		20
Valve Sensors		
Pressurant Tank		
Relief Valve (3 Tanks)	open/close	6
Tank Vent Valve (3 Tanks)	open/close	6
Fill Valve (3 Tanks)	open/close	6
Regulation Switch (3 Tanks)	open/close	6

Table 5.4C: Human Factors - Secondary Life Support System (Continued)

<u>Type</u>	<u>Range</u>	<u>Quantity</u>
Oxygen Tank		
Supply Valve (1 Tank)	open/close	2
Vent Valve (1 Tank)	open/close	2
Fill Valve (1 Tank)	open/close	2
Regulation Switch (1 Tank)	open/close	2
Nitrogen Tank		
Supply Valve (1 Tank)	open/close	2
Vent Valve (1 Tank)	open/close	2
Fill Valve (1 Tank)	open/close	2
Regulation Switch (1 Tank)	open/close	2
Water Tank		
Supply Valve (1 Tank)	open/close	2
Vent Valve (1 Tank)	open/close	2
Fill Valve (1 Tank)	open/close	2
Regulation Switch (1 Tank)	open/close	2
Heat Exchanger		
Air Intake Valve	open/close	2
Air Outtake Valve	open/close	2
Ethylene Glycol Intake Valve	open/close	2
Ethylene Glycol Outtake Valve	open/close	2
Heater Operation	on/off	2
Screened Intake	open/close	2
Fan Operation	on/off	2
Electrical Heater	on/off	2
Radiator	on/off	2
Coolant Pump	on/off	2
LIOH Valve	open/close	2
Exhaust Valve	open/close	<u>2</u>
Total Valve Sensors		72
Level Sensors		
Radiation	17-140mrems	2
Radiator Power Output	200-400 Watts	<u>2</u>
Total Level Sensors		4
Secondary Life Support System Total		134

5.4.5 Reaction Control System

The reaction control system consists of 2 sets of tanks located at the upper and lower sections of the Taurus LMS. The pressures and temperatures of each of these tanks will be measured in the system. The pressure of each thruster in the reaction control system will be taken into account in order to allow the computer to reroute required thrust and compensate for any malfunctions in the system. The total number of sensors required in the reaction control system equals ninety-eight (See Table 5.4D).

Table 5.4D: Reaction Control System

<u>Type</u>	<u>Range</u>	<u>Quantity</u>
Temperature Sensors		
Pressurant Tank (2 Tanks)	200-280 Kelvin	4
Oxidizer Tank (2 Tanks)	250-300 Kelvin	4
Propellant Tank (2 Tanks)	250-300 Kelvin	<u>4</u>
Total Temperature Sensors		12
Pressure Sensors		
Chamber Pressure (32 Rockets)	0-0.6 MPa	32
Pressurant Transducer (2 Tanks)	8-12 MPa	4
Oxidizer Transducer (2 Tanks)	1-1.5 MPa	4
Propellant Transducer (2 Tanks)	1-1.5 MPa	4
Pressurant Calibration Gauge (2 Tanks)	8-12 MPa	4
Oxidizer Calibration Gauge (2 Tanks)	1-1.5 MPa	4
Propellant Calibration Gauge (2 Tanks)	1-1.5 MPa	<u>4</u>
Total Pressure Sensors		56
Valve Sensors		
Tank Pressure Relief Valve (3 Tanks)	open/close	6
Tank Vent Valve (3 Tanks)	open/close	6
Tank Fill Valve (3 Tanks)	open/close	6
Tank Pressure Regulation Switch (3 Tanks)	open/close	6
Tank Supply Valve (3 Tanks)	open/close	<u>6</u>
Total Valve Sensors		30
Total Reaction Control System Sensors		98

5.4.6 Abort Systems

The abort system is made up of the abort tower and solid fuel motor located on top of the Taurus command module. Measurements throughout the system include electro/static buildup, chamber pressure of the motor, and ignition controls. The abort control sensors will be placed on the system to guarantee that the tower has been armed before launch (See Table 5.4E).

Table 5.4E: Abort System

<u>Type</u>	<u>Range</u>	<u>Quantity</u>
Solid Fuel Motor		
Electro/Static Buildup	????	2
Chamber Pressure	1-5 MPa	2
Ignition Control	on/off	2
Ejection Control	on/off	2
Abort Control (Arm/Disarm)	on/off	<u>2</u>
Total Solid Fuel Motor Sensors		10

5.4.7 Miscellaneous Sensors

Extra sensors added to the Taurus system include hatch and ejection determinations. It is necessary to guarantee that the astronaut entry hatch and the parachute deployment hatch are secure prior to launch and open when needed. The determination of the abort tower ejection as well as the service module ejection will also be checked after launch and prior to re-entry.

Table 5.4F: Miscellaneous Sensors

<u>Type</u>	<u>Range</u>	<u>Quantity</u>
Astronaut Entry Hatch	open/close	2
Parachute Deployment Hatch	open/close	2
Service Module Ejection	on/off	2
Abort Tower Ejection	on/off	<u>2</u>
Total Miscellaneous Sensors		8

5.4.7 Conclusion

Contained on the Taurus LMS will be four hundred twenty-eight sensors making checks on all systems to guarantee proper functioning and allowing for necessary changes if malfunctions occur.

Based on the weight constraint of the Taurus system, only those sensors necessary for the proper operation have been taken into account. Any other extraneous sensor (example: propulsion flow sensors placed along all lines of plumbing) have been removed. This brings the total weight of the sensors to be approximately twenty-five kilograms. The use of optical fiber wiring in the Taurus LMS system contains the very minimum ammount of heat and radiation shielding. The entire mass of the sensors system on the Taurus service module is approximately fifty kilograms.

All sensors have been made double redundant and are 99.999% reliable.

Section 5.5 Communications

5.5.1 Introduction

Communications are needed for video and voice contact, data transmissions for rendezvous and navigation and in conducting experiments. It is also needed if there are any changes in the mission plan due to failures in equipment or on ground procedures. Communications adds safety to the situation of being a long way from the natural environment of earth. Other systems under communications are radar and EVA communications and telemetry.

On the Taurus LMS spacecraft, the avionics received an initial mass budget of 75 kg. This budget limited the avionics to just the basics, however due to the spacecrafts overall mass restriction the missions were mostly eliminated thus resulting in few communications inflicted equipment cuts. This left only the requirement of voice and data relay. The following is the composition of the communications package onboard the Taurus LMS spacecraft.

5.5.2 Receiving Stations

In order to insure communications are reliable two modes of communication have been chosen. One communication path through TDRSS and one directly to earth stations.

The primary receiving station will be the Telemetry Data Relay Satellite System better known as TDRSS. It consists of two satellites that enable communications for 80 minutes of the 95 minute orbit. This is how the system exists now, however by the year 1995 there should be at least three or up to five total satellites in the system. Having more satellites would enable constant communication capability. In order to communicate through TDRSS frequencies must be chosen from the S, C or Ku bands. These bands are chosen for their few atmospheric losses in transmission to earth. The range of 1 to 10 GHz is the only range with these few losses.

If communications cannot be made through TDRSS for whatever the reason the second choice for a receiving station will be direct transmission to earth. The number of earth stations is limited, however there exists enough to say there could be at least three used per orbit which would account for about 30 minutes of transmission time per 95 minute orbit.

The capsule will also receive transmissions from the Global Positioning System (GPS). These communications are used for navigation as discussed in section 5.1. The capsule is passive in its communications with GPS. Its communication requirements are as follows: the system is an off-the-shelf item consisting of an antenna and a receiver. The system operates on two frequencies, one at 1.575 GHz and one at 1.228 GHz. The systems mass, volume and power are as discussed in section 5.1. The antenna is placed on the capsule's surface facing outwards to GPS, which can be seen in the exterior layout in earlier chapters. These are the modes of communications for the capsule.

5.5.3 Frequency Assignments

The frequency assignments are based in the S band and are spaced so that not more than 500 MHz will be assigned for any one transponder as suggested by Morgan and Gordon in the Communications Satellite Handbook. The base frequencies were chosen to model the system and to calculate the quality of system. The frequencies may change slightly for exact system compatibility later in production, but will not change the calculations significantly.

The bandwidth for these base frequencies are determined from the amount of data that must be transmitted each second and the clarity that the data must have in order to be receivable. For this reason data requires a larger bandwidth than voice for approximately the same data rate. The bandwidth is limited by the systems power and gain. For the systems frequency assignments see Table 5.5A.

Table 5.5A Frequency Assignments

Component	Frequency	Data Rate	Bandwidth
Voice Uplink	2.1 GHz	56 Kbit/s	4 KHz
Voice Downlink	2.2 GHz	56 Kbit/s	4 KHz
Command Uplink	2.15 GHz	64 Kbit/s	36 KHz
Data Downlink	2.25 GHz	64 Kbit/s	36 KHz

5.5.4 Link Budgets

The link budgets are used to determine whether or not a signal will be receivable. The method used in this analysis was taken from Communications Satellite Handbook. This process looks at the transmitters qualities and the losses in going to the receiver and then the receiver's ability to clearly interpret the signal.

For the purpose of calculating the capsule's system two models were made to qualify the communications onboard. The first model was for the earth station. It has a 10 meter diameter antenna with a gain of 316K times that of the isentropic reception and an amplification power of 1000 watts. The TDRSS model has a 4 meter diameter antenna with a gain of 4K to 141K times that of isentropic reception and an amplification power of 200 watts. These values as well as all others are converted to decibels for the link budget calculations.

The overall qualifying figure in the link budget determination is the carrier to noise ratio. In the Communications Satellite Handbook this ratio must be positive and be at least 10 to 12.5 dB in order for the signal to have good reception. For the results of the link budget calculations see Tables 5.5B,C,D,E.

Table 5.5B Uplinks from TDRSS

Frequency Band, GHz	2.1	2.15
Satellite antenna dia., m	4	4
Satellite Station		
Transmitter power, dBw	23	23
Feed losses, dB	-2.1	-2.1
Antenna gain, dBi	36.29	36.49
EIRP, dBw	57.19	57.39
Satellite to Capsule		
Path losses	191.76	191.97
Capsule		
Antenna gain, dBi	2.15	2.15
System noise temp., dBK	0.15	0.15
G/Ts, dBw/K	2	2
Illumination level, dBw/m ²	-67.79	-67.59
(C/T) _u , dBw/K	-93.73	-93.73
1/Boltzmann const., dBHz	228.6	228.6
C/kT, dBHz	134.87	134.87
1/ bandwidth, dBHz	-36.02	-45.56
(C/N) _u , dB	98.85	89.31

Table 5.5C Uplinks from Earth

Frequency Band, GHz	2.1	2.15
Earth station antenna dia., m	10	10
Earth Station		
Transmitter power, dBw	30	30
Feed losses, dB	-3.5	-3.5
Antenna gain, dBi	55	55
EIRP, dBw	81.5	81.5
Earth to Capsule		
Path losses	153	153
Capsule		
Antenna gain, dBi	2.15	2.15
System noise temp., dBK	0.15	0.15
G/Ts, dBw/K	2	2
Illumination level, dBw/m ²	-43.48	-43.48
(C/T) _u , dBw/K	-69.42	-69.63
1/Boltzmann const., dBHz	228.6	228.6
C/kT, dBHz	159.18	158.97
1/ bandwidth, dBHz	-36.02	-45.56
(C/N) _u , dB	123.16	113.41

Table 5.5D Downlinks from TDRSS

Frequency Band, GHz	2.2	2.25
Capsule beam type	omni.	omni.
Satellite antenna dia., m	-	-
Capsule		
Transmitter power, dBw	14.7	14.7
Feed losses, dB	-1.7	-1.7
Antenna gain, dBi	2.15	2.15
EIRP, dBw	15.15	15.15
Capsule to Satellite		
Path losses	191.76	191.97
Illumination level, dBw/m ²	-148.72	-148.72
Satellite		
Antenna gain, dBi	36.29	36.49
System noise temp., dBK	-30	-30
G/Ts, dBw/K	6.29	6.49
(C/T)d, dBw/K	-170.78	-170.77
1/Boltzmann const., dBHz	228.6	228.6
C/kT, dBHz	57.82	57.83
1/ bandwidth, dBHz	-36.02	-45.56
(C/N)d, dB	21.80	12.27

Table 5.5E Downlinks to Earth

Frequency Band, GHz	2.2	2.25
Capsule beam type	omni.	omni.
Satellite antenna dia., m	-	-
Capsule		
Transmitter power, dBw	14.7	14.7
Feed losses, dB	-1.7	-1.7
Antenna gain, dBi	2.15	2.15
EIRP, dBw	15.15	15.15
Capsule to Earth		
Path losses	-153	-153
Illumination level, dBw/m ²	-109.83	-109.83
Earth Station		
Antenna gain, dBi	50	50
System noise temp., dBK	-21	-21
G/Ts, dBw/K	29	29
(C/T)d, dBw/K	-109.18	-109.37
1/Boltzmann const., dBHz	228.6	228.6
C/kT, dBHz	119.42	119.23
1/ bandwidth, dBHz	-36.02	-45.56
(C/N)d, dB	83.40	73.67

The link equations used are:

EIRP (equivalent isotropic radiated power) dBw

$$\text{EIRP} = 10 \log G + 10 \log W$$

W - amplification power, watts

Path loss dB

$$L = 92.45 + 20 \log S + 20 \log f$$

S - path length, Km

f - frequency, GHz

Gain to system noise ratio dB/K

$$G/T_s = 10 \log G - 10 \log T_s$$

G - gain

T_s - system temperature, K

Illumination level dBw/m²

$$W = \text{EIRP} - 20 \log S - 70$$

Carrier to noise ratio dB

$$C/T = W + G/T_s - 21.5 - 20 \log f \quad (\text{dBw/K})$$

$$C/kT = C/T - 10 \log k$$

k - Boltzmann constant

$$C/N = C/kT - 10 \log B$$

B - bandwidth, Hz

The weakest link is the downlink to TDRSS. In this link the carrier to noise ratio have been reduced to the minimum needed for good reception. This gave a dipole antenna with the standard gain of 1.64 and 30 watts of amplification power. The path length of transmission was used as a worst case of 3000 Km to earth and 50000 Km to TDRSS in order to calculate the path losses. The results will only vary slightly if fine tuning of the base frequencies needs to be done. All not calculated were estimated using the graphs given throughout the Communications Satellite Handbook for system modelling.

5.5. 6 Antennas

In order to transmit and receive the desired frequencies different antennas are needed to cover the gaps in the bands used. Each band requires a different

type of antenna based on the necessary bandwidth .

For the S - band a dipole antenna will be implemented and housed under a skin blemish to avoid the need for mechanical deployment. There will be two of these antennas, one facing earth and one facing space. The two antennas supply a mode af redundancy and make serving earth stations and TDRSS efficient during orbit. Skin and whip antennas were also considered for this application, however due to deployment being necessary dipoles were chosen. The dipoles give higher gain and take up less space.

The L - band antenna will be mounted on the skin in the same fashion as the S-band antennas but only on the surface facing GPS satellites.

5.5.7 Equipment

The equipment used onboard the capsule was based on the equipment outline presented for the British Multi-Role Capsule. This was done because of its similar mission capability and capsule size similarity. Using this outline the volumes and masses were also estimated. For the summary of equipment on board see Table 5.5F.

Table 5.5F Equipment Summary

Unit	Equipment	Quantity	Total mass Kg	Volume mm mm x mm x mm	Power watts
Data	S-Band Tx/Rx	2	6	195 x 188 x 122	30
	Switch	1	0.5	-	
	RF Harness	1	1	-	
	Dipole antenna	2	1	300 x 175 x 80	
Audio	Intercom	1	1	-	
	Audiomixer	1	2	200 x 190 x 130	
			Total = 11.5 Kg		50 % efficiency Total = 60 watts

5.5.8 Redundancy / Reliability / Costing

The voice and data relay components (the S-band system) has two complete systems for redundancy. All other systems are singular and need to be made reliable enough for mission success. For the data and voice system the table on reliability in the Communications Satellite Handbook gave a value of 0.9919 and all the singular systems a value of 0.91.

The estimated DDT & E cost for the communications package based on 11.5 Kg was 24.817 \$M91 and the first unit cost of 1.991 \$M91.

Chapter 5 References

- Clausing, D.J., *"The Aviator's Guide to Modern Navigation,"* TAB Books Inc., 1987.
- Griffin, M. D. and J. R. French, *"Space Vehicle Design,"* New York: AIAA, 1991.
- "Jane's, All the World's Avionics,"* IEEE, 1990.
- Morgan, Walter I. and Gordon, Gary D. *"Communications Satellite Handbook,"* John Wiley & Sons, New York, 1989.
- Spitzer, C. R., *"Digital Avionics Systems,"* New Jersey: Prentice Hall Inc., 1987.
- Wertz, J. R., *"Spacecraft Attitude Determination and Control,"* Boston: D. Reidel Publishing Co., 1986.

CHAPTER 6: TAURUS STRUCTURES

Section 6.1 Selection of Materials

Due to the critical mass restriction the Taurus LMS requires effective material choices, so that the structures group can achieve the mass limit of 475 kg allotted by systems integration. A trade study was done for specific properties and characteristics of fiber composites and metal alloys.

The following table shows the findings of this study.

Table 6.1A: Trade Study of Material Properties

<u>MATERIAL</u>	<u>ADVANTAGES</u>
FIBER COMPOSITES	HIGH STRENGTH AND STIFFNESS FATIGUE RESISTANT LOW COEFFICIENT OF THERMAL EXPANSION CHOICE OF MANUFACTURING PROCESSES
METAL ALLOYS	AL AND TI HIGH STRENGTH/WEIGHT EASE OF FABRICATION TITANIUM GOOD FOR HIGH TEMPERATURES RESISTANT TO CORROSION
	<u>DISADVANTAGES</u>
FIBER COMPOSITES	EXPENSIVE TEMPERATURE DEGRADATION
METAL ALLOYS	WEIGHT PENALTIES TEMPERATURE DEFORMATIONS

While working with Dr. A. Vizzini of the University of Maryland on the use of composites materials it became evident that the exact analysis methods were far beyond our present base of knowledge. However, the use of composites in specific areas where the analysis is trivial (e.g. fuel and life support tanks) was completed using the assumption that the composite layup is very similar to that of an isotropic material. The following table shows some of the properties of both

composites and metal alloys. Graphite epoxy was included in the metal alloys table for ease of comparison of the two materials. Note the compression yield stresses of the materials in the table. Also note the differences in specific gravity which is a direct reflection of the mass savings encountered when using composites.

Table 6.1B: Material Property Comparisons (Vizzini, 1991)

Compasrison of Metal Alloy:					
Material Designation	Tensile Ultimate MPa	Comp. Yeild MPa	Modulas GPa	Specific Gravity	Specific Modulus
2024-T3 Al	426	290	74	2.77	27
7075-T3 Al	586	531	72	2.80	26
7175-T73 Al	504	436	70	2.80	25
Ti6 A I-4 V	923	909	110	4.43	25
300M Steel	1931	1703	200	7.84	25
Graphite/ Epoxy	1661	1698	130	1.61	81

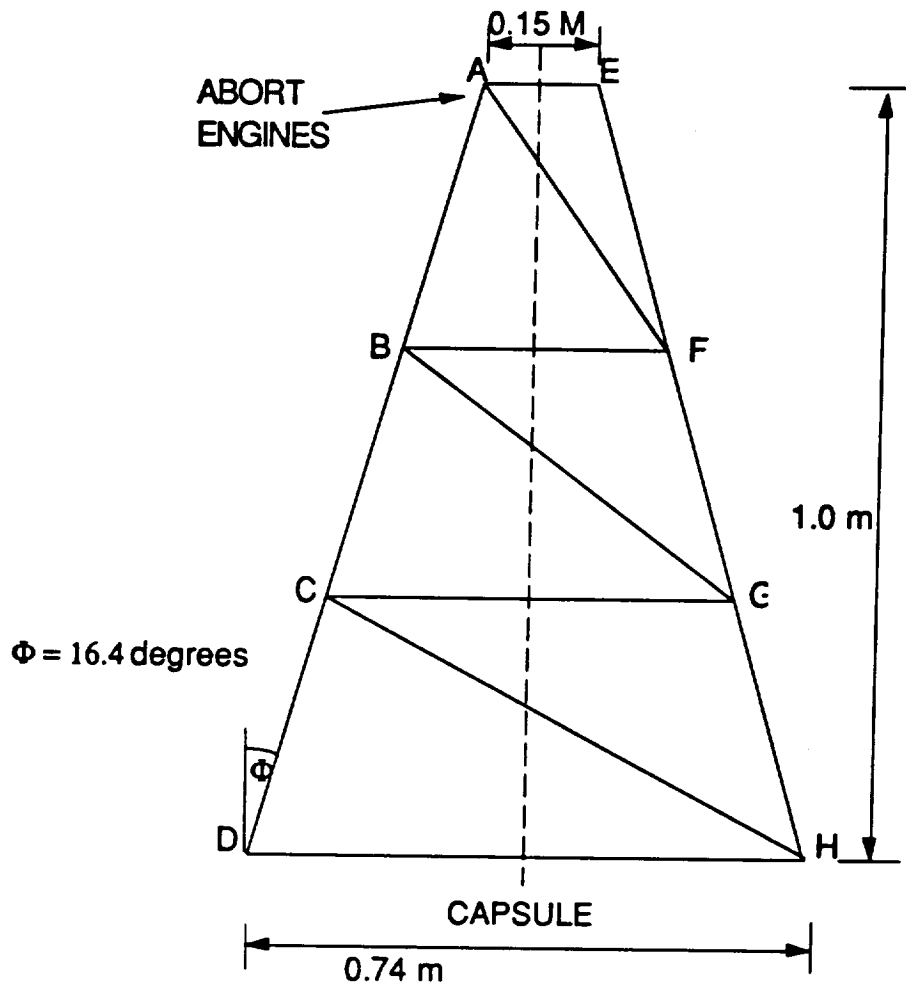
6.2 Design of the Abort Escape Tower

This tower or truss will act as the connection between the abort system and the capsule. The loads on the tower will be different for the two possible situations encountered. The first will be the compressive loading due to the 150 kg inertia load of the abort system when the booster has fired properly. The rocket provides a 10g axial acceleration, and a 1g sideways acceleration. The second situation involves the aborted launch which places a 500 kg inertia loading due to the capsule. The abort rockets provide an axial acceleration of 7.565g. This loading should be the critical load on the structure as it will try to pull the tower apart in response. The design requirements were received from systems integration (base=.74 m), and propulsion (top=.15m and height=1.0 m). The truss designed resembles that used for Project Mercury (Project Mercury, 1963) as it consists of a three-sided symmetric structure as shown in Figure 6.2A. The structure will consist of a total of 24-members made of 6061-T6 aluminum. The longitudinal members carry more of the load than the cross members do and therefore have a larger cross-section area. The cross-section was chosen to be homogeneous round bars. The critical loadings are shown in Figure 6.2A and the bars were designed for these conditions. The abort engines are covered in a graphite/epoxy casing which will bolt directly to the top of the tower. The base will connect to the capsule in a manner similar to that of Project Mercury. Each longitudinal member will be connected to the capsule by two short members which will be fastened to the capsule by explosive bolts. Therefore, the tower and abort system can be jettisoned so that the extra mass isn't carried into space. The final design consideration was possible burn thru of the truss due to the plume of the abort engines. Due to the short burn time of just 5-seconds it was recommended by Dr. Donaldson of the University of Maryland (B. Donaldson, 1991) that heat shielding for the tower will not be necessary. The following table is the final configuration for one side of the truss giving lengths and masses for all members

Table 6.2A: Dimensions and Masses for Tower Members

MEMBER TYPE	LENGTH, m	RADIUS, m	MASS, kg
DH	0.74	0.0031	0.181
CG	0.542	0.0031	0.133
BF	0.349	0.0031	0.085
AE	0.15	0.0031	0.037
AD	1.043	0.01	2.654
CH	0.727	0.0031	0.178
BG	0.55	0.0031	0.134
AF	0.42	0.0031	0.103
<u>Total Mass</u>			<u>3.505</u>

The final design configuration for the abort tower is shown in Figure 6.2A



ABORT LAUNCH
INERTIAL LOADING = 37106 N
MATERIAL: 6061-T6 AL
TENSILE STRENGTH = 480 MPA
LOADING AT CH = 4305.2 N
LOADING AT GH = 9342.4 N

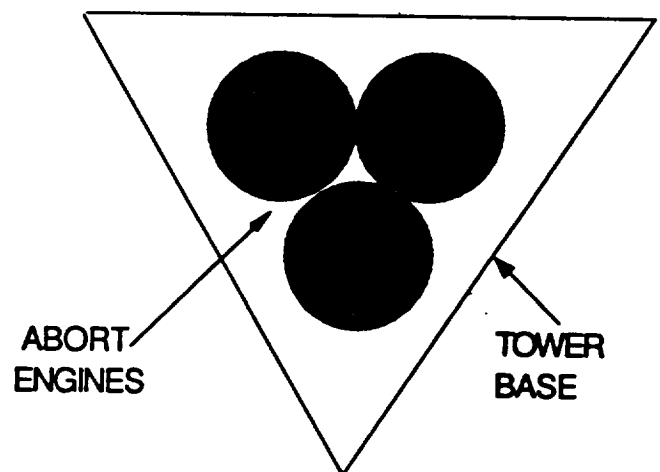


Figure 6.2A: Abort Tower Configuration and Design

Section 6.3 The Capsule Structure

6.3.1 The Framework

The sophistication of the structural analysis was limited to mainly approximations, and any further studies done on the LMS would certainly involve the creation of finite element model for the entire structure. Therefore, the following analysis will be more of a systems integration study of the structure. Figure 6.3A displays the major members of the framework for the capsule.

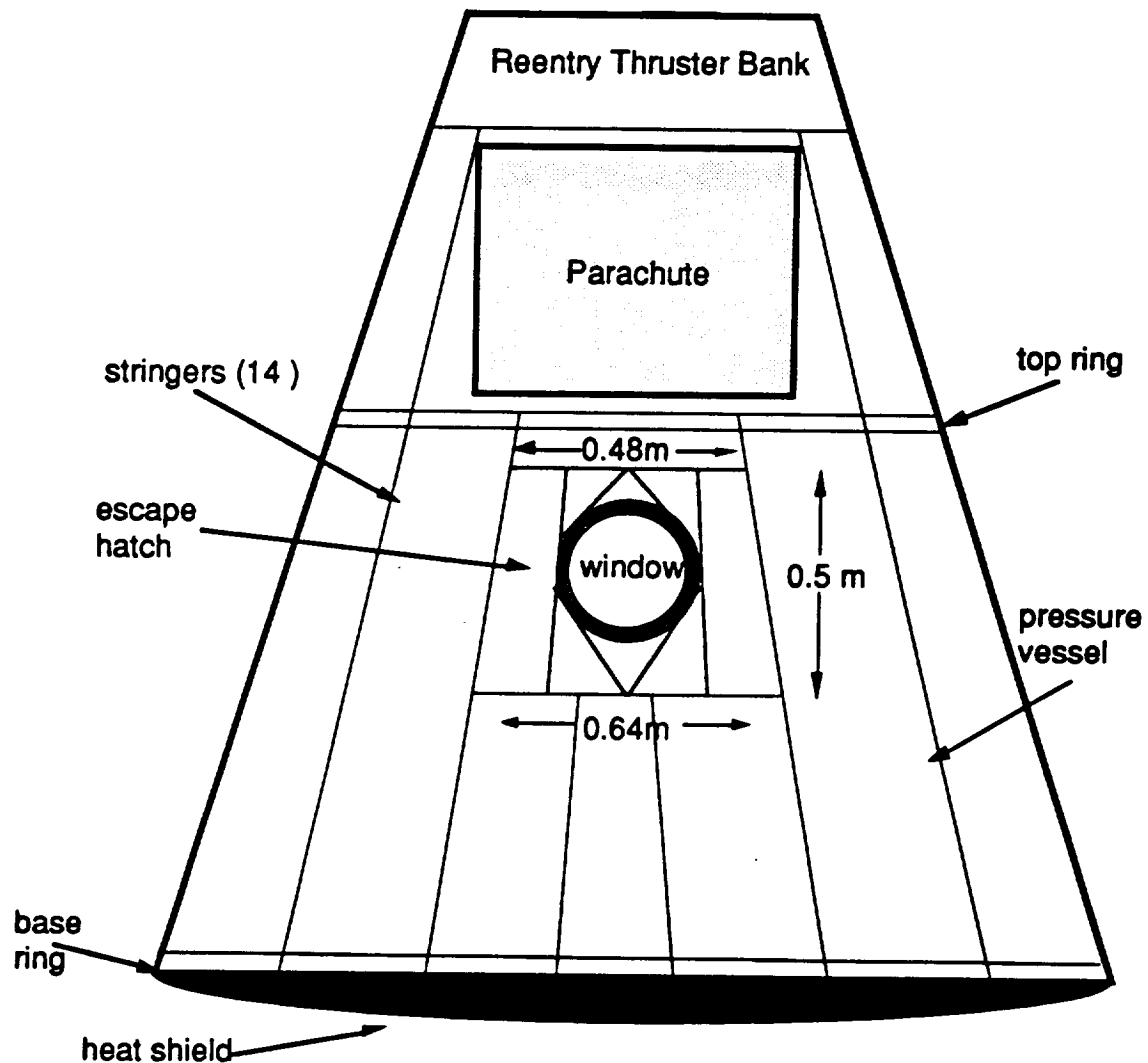


Figure 6.3A: Structural Framework of the Capsule

It was found that no rings were necessary to strengthen the capsule. The stringers will be strong enough to support the axial or buckling loads encountered. The design uses 14-stringers, and each carrying an axial loading of approximately 5000 Newtons. The stringers were chosen as I-beams for two reasons:

- Flanges allow for easy fastening of the skin and pressure vessel
- I-beams are very resistant to bending

Each stringer will have a cross-sectional area of 0.00012 sq. meters and its dimension can be seen in figure 6.3B.

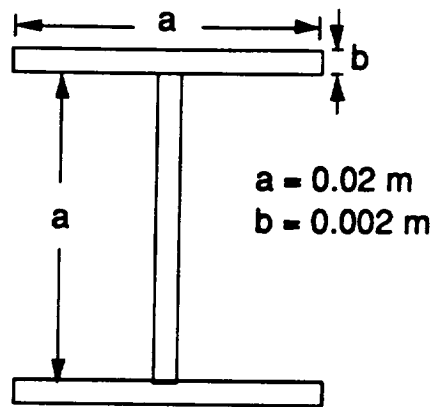


Figure 6.3B: Stringer Cross-Section

The hatch was designed to hold the small navigation window. The window and its mounting structure is similar to that used in Project Mercury (NASA SP-4001, 1963). Both the hatch and the window will be areas of high stress concentrations and will need to be reinforced as shown in Figure-6.3.A.

The skin thickness was estimated to be 4.8 mm as suggested by Dr. Donaldson of the University of Maryland (Donaldson, 1991) from his personal knowledge of fuselage construction. This value was then used to calculate the mass of the skin.

6.3.2 Mass Breakdown of the Capsule

The following table will give a mass breakdown for the capsule. It should be noted that many values are estimated using scaling factors designed to coincide with masses used in Project Mercury (NASA SP-4001, 1963). Calculations of the known masses and the estimating procedures used for scaling the unknown masses may be seen in Appendix N. This section was designed to show that the feasibility of the L.M.S capsule from the structural standpoint is excellent. The masses while often estimated were done so conservatively, so the actual structure should fit into the overall mass budget for this project.

Table 6.3A: Mass Breakdown for the Capsule

MEMBER	STATUS	MASS, kg
STRINGERS	KNOWN	10.62
BASE RING	ESTIMATE	7.85
TOP RING	ESTIMATE	5.5
DOOR	ESTIMATE	7.5
SKIN	KNOWN	42.41
PRESSURE VESSEL	ESTIMATE	40
HARDWARE	ESTIMATE	20
<u>TOTAL MASS</u>		<u>133.88</u>

Section 6.4 Service Module Structural Design and Analysis

6.4.1 Introduction

The designs and analyses of the service module structures are presented in this section in four categories. They are the explosive bolts for the capsule and service module, the longitudinal stringers and transverse rings, shear flow, and capsule supporting truss. Many simplifications and assumptions are made for easy calculations. The structures are designed to sustain a 10 gee axial acceleration and a 1 gee sideways acceleration. Due to the weight constraint, the factor of safety of 1.2 is used throughout the analysis. Temperature effects on the structure are neglected. All calculations are shown in Appendix U.

6.4.2 Explosive Bolt

Four equally spaced explosive bolt joints connect the capsule and the service module. (see Figure 6.4A) There are four joints with two explosive bolts on each joint. The four joint design is selected to reduce the chance of bolt failure. The two explosive bolts per joint design is for high redundancy. The bolts are designed to explode at the same time for separation.

- Assumptions
- 1) C.G. is located on the center line
 - 2) The joint is designed so that the bolts are in equal strength in shear, tension and compression. No moments on the bolts
 - 3) Aluminum Alloy: 1100-H14

Design Guidelines:

- 1) Riveted type butt joint is selected (see fig 6.4B)
- 2) The butt joint should be at least as thick as the main Plate
- 3) The space between the bolts and the edges should be at least equal to 1.5 times the diameter of the bolt

The load P-sum moment at point A was determined to be $P=5112.1$ N (see Appendix U.1). By applying the shearing stress formula, the calculated diameter of the bolt is 7.70 mm. This number is very small because there is only 1 gee in lateral acceleration. Therefore, the standard bolt size of 25 mm can be used in this design.

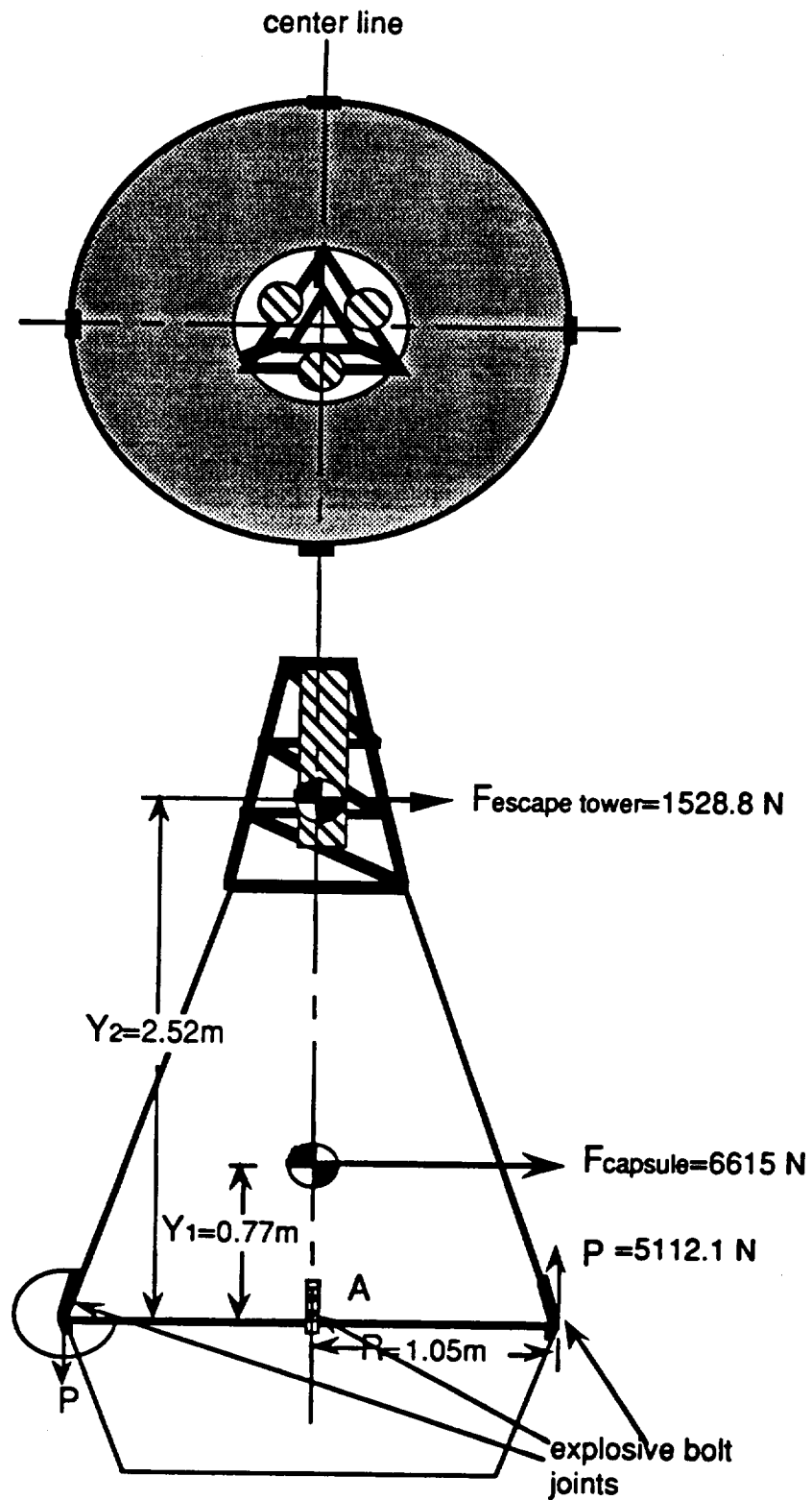


Figure 6.4A Top and Side View of the Location of the Explosive Bolt Joints

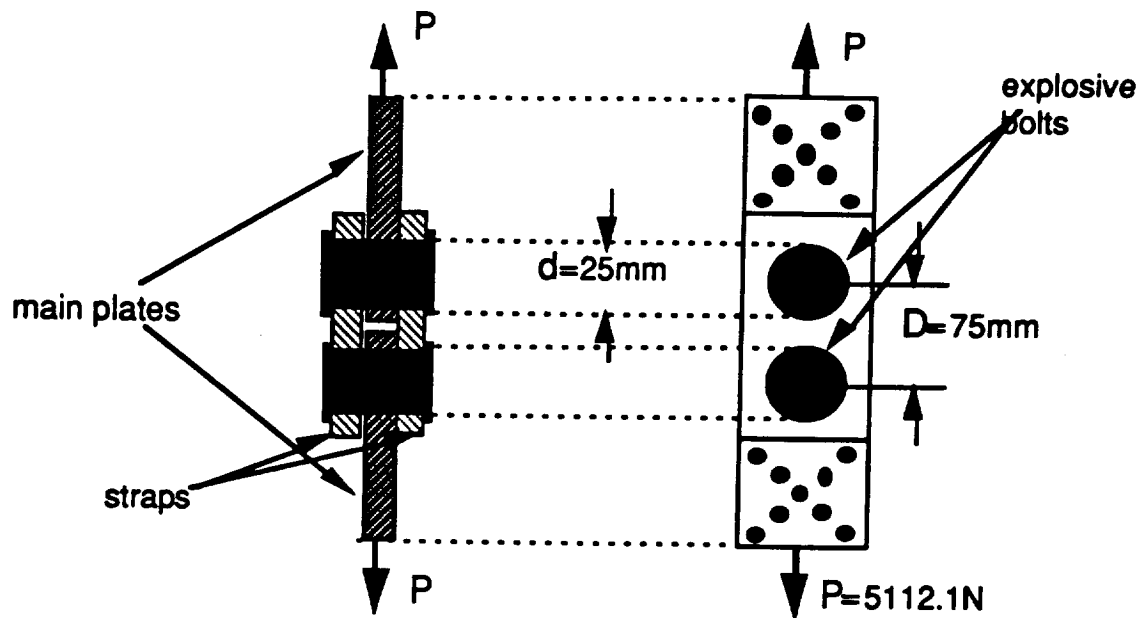


Figure 6.4B: Side and Top View of the Butt Type Explosive Bolts

6.4.3 Stringer and Ring

In analyzing bending instability and failure of the longitudinal stringers, the Rayleigh-Ritz method can be used with the principle of the stationary value of the total potential to obtain approximate solutions for the buckling load.

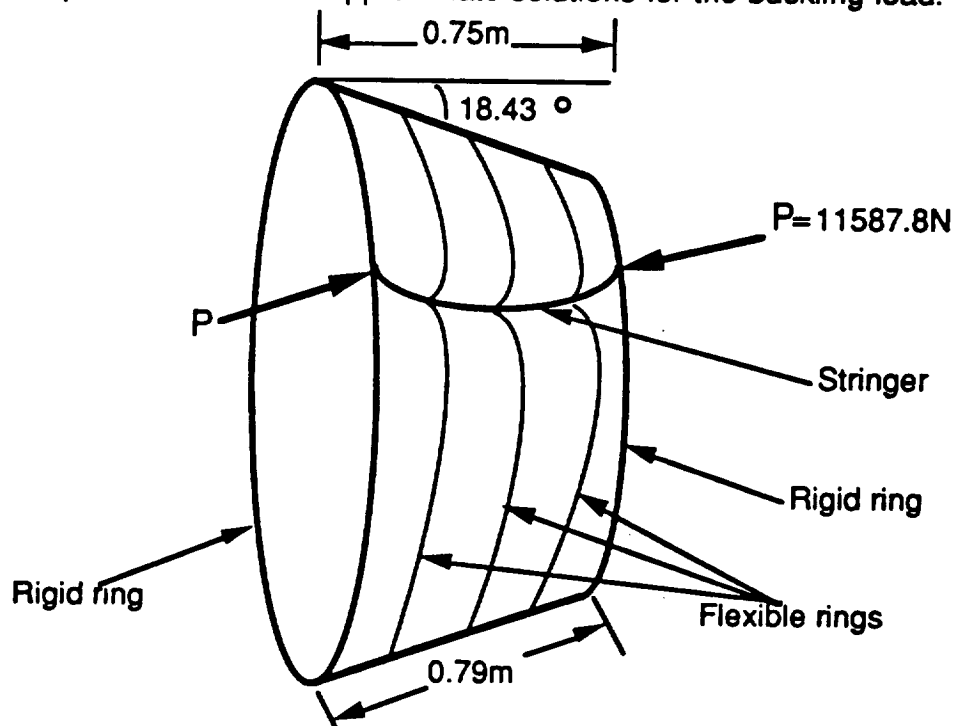


Figure 6.4C Stringer under Compressive Load P

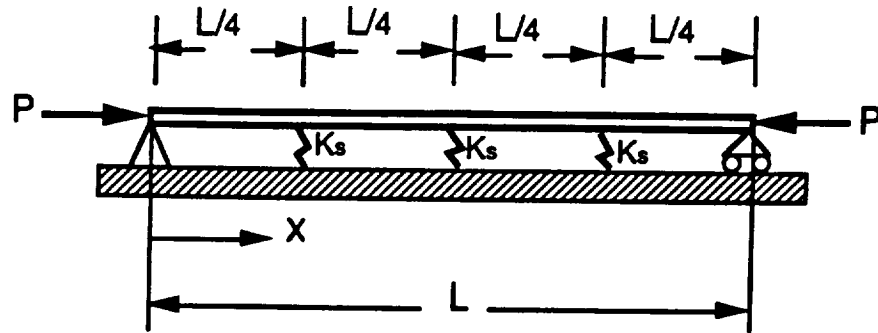


Figure 6.4D Idealization of the Stringer under Load P

Assumptions:

- 1) Eight longitudinal stringers are chosen due to symmetry and only carry axial load.
- 2) Five transverse rings; the stiff end rings provide rigid support against lateral displacement, while the three relatively flexible intermediate rings give elastic lateral support (see Fig 6.4C)
- 3) Idealization of the stringer and rings (see Fig 6.4D), where the intermediate rings are shown as elastic supports of stiffness k_s . k_s is constant for those three rings.
- 4) The deflection shape of the buckled stringer (see Fig 6.4E)
- 5) Euler's buckling equation. Although it works better for long beams, it is applicable in this analysis.

The deflection shape of the buckled stringer can be presented by the series:

$$w = \sum_{j=1}^n C_j \sin \frac{j\pi x}{L}$$

which satisfies the displacement boundary conditions $w(0)=w(L)=0$. To simplify the calculations, let $n=4$, the smallest value of n that permits the stringer to buckle between intermediate rings without deforming them.

In this analysis the Rayleigh-Ritz method must satisfy $\delta U - \delta W = 0$, where

$$a_{ij} = \frac{j^2 \pi^4 EI}{L^4} \int_0^L \sin \frac{i\pi x}{L} \sin \frac{j\pi x}{L} dx + k_s \left(\sin \frac{i\pi}{4} \sin \frac{j\pi}{4} + \sin \frac{i\pi}{2} \sin \frac{j\pi}{2} + \sin \frac{3i\pi}{4} \sin \frac{3j\pi}{4} \right)$$

$$b_{ij} = \frac{ij\pi^2}{L^2} \int_0^L \cos \frac{i\pi x}{L} \cos \frac{j\pi x}{L} dx$$

With the aid of the following integration formula

$$\int_0^a \sin \frac{m\pi x}{a} \sin \frac{r\pi x}{a} dx = 0 \text{ if } m \neq r$$

$$= \frac{a}{2} \text{ if } m = r$$

the result obtained is given by

$$a = \frac{\pi^2 EI}{2L^3} \begin{bmatrix} 1 & 0 & 0 & 0 \\ 0 & 16 & 0 & 0 \\ 0 & 0 & 81 & 0 \\ 0 & 0 & 0 & 256 \end{bmatrix} + 2k_s \begin{bmatrix} 1 & 0 & 0 & 0 \\ 0 & 1 & 0 & 0 \\ 0 & 0 & 1 & 0 \\ 0 & 0 & 0 & 0 \end{bmatrix}, \quad b = \frac{\pi^2}{2L} \begin{bmatrix} 1 & 0 & 0 & 0 \\ 0 & 4 & 0 & 0 \\ 0 & 0 & 9 & 0 \\ 0 & 0 & 0 & 16 \end{bmatrix}$$

The nontrivial solution of, $a-Pb=0$, is the following characteristic equation :

$$\frac{\pi^4 EI}{2L^3} \left(1 + \beta - \frac{P}{P_E} \right) \left(16 + \beta - 4 \frac{P}{P_E} \right) \left(81 + \beta - 9 \frac{P}{P_E} \right) \left(256 - 16 \frac{P}{P_E} \right) = 0$$

where the dimensionless parameters are $\beta = \frac{4k_s L^3}{\pi^4 EI}$; $P_E = \frac{\pi^2 EI}{L^2}$

and the rest of the characteristic equation is $\frac{P}{P_E} = 1 + \beta$, $\frac{P}{P_E} = 4 + \frac{\beta}{4}$, $\frac{P}{P_E} = 9 + \frac{\beta}{9}$, $\frac{P}{P_E} = 16$

These equations are plotted in Fig 6.4E.

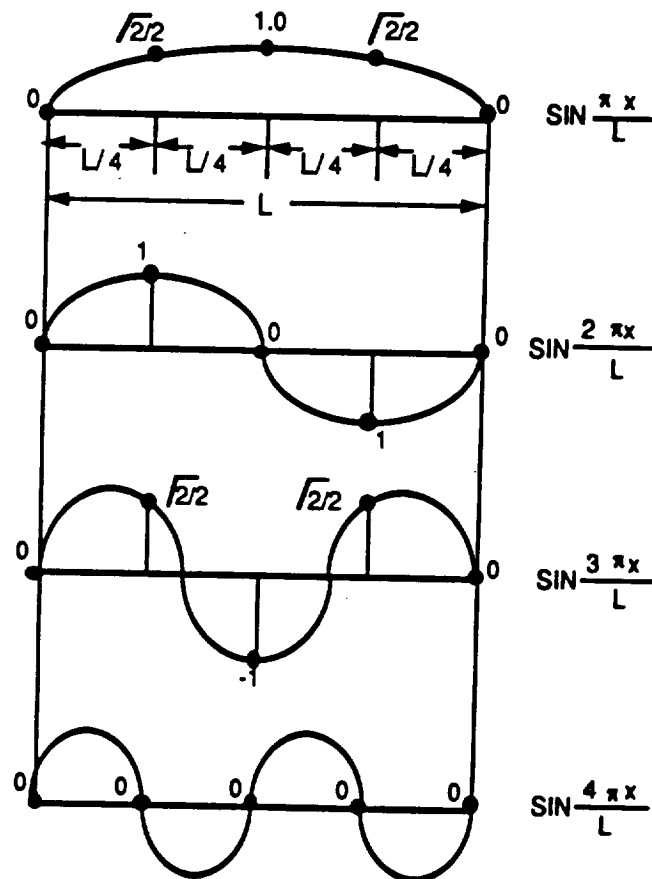


Figure 6.4E Four Assumed Functions

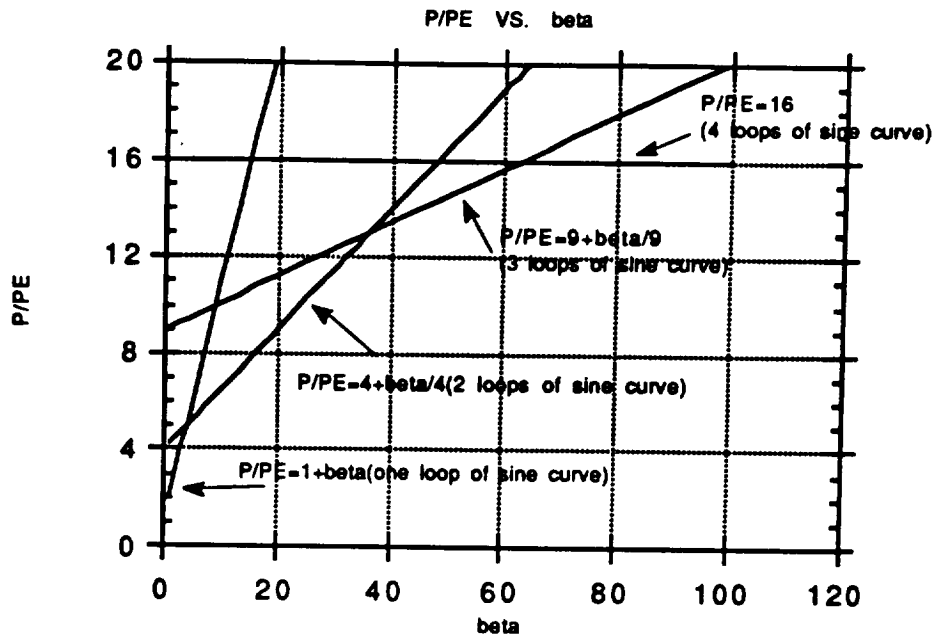


Figure 6.4F P/Pe Vs Beta Graph

It is seen that the intermediate rings prevent lateral displacements at the supports if $\beta > 63$, that is, if $K_s > 1535EI/L^3$. In this case, P/PE is under the solid line and hence the structure of the service module is safe under the given load. It can sustain 160gee of axial load. For $K_s = \text{constant} = EA/I$, where I is the segment between stringers, the cross-section area of the ring is smaller for the bottom ring and bigger for the top ring.

The aluminum alloy 6061-T6 is chosen for the stringers and the rings, the load P acting on each stringers is:

$$P/8 = 10g(675 + 156)Kg(1.2)(\cos 18.43)$$

$$P = 11587.8N = \pi^2 EI/L^2, \text{ solve for moment of inertia } I_r, \text{ in radial direction.}$$

$I_r = 10600\text{mm}^4$, I-beam is selected due to its high stiffness in buckling and bending.

By iterating, the cross-section area of the stringer, A is illustrated on Figure 6.4G.

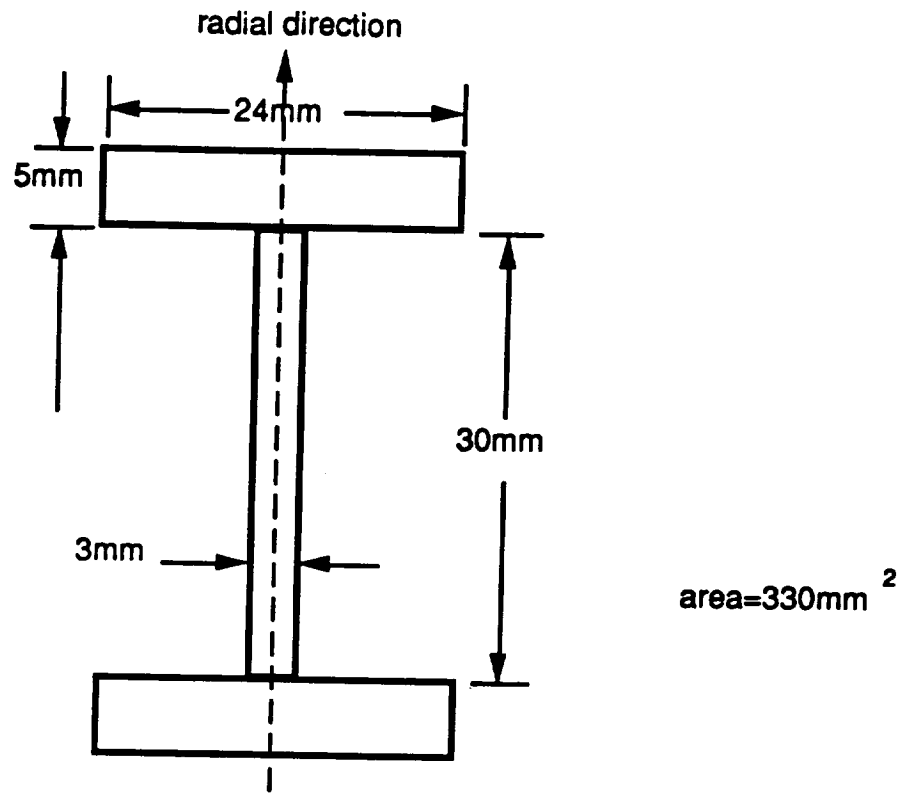


Figure 6.4.G Stringer Cross-Section Area

6.4.5 Shear Flow Analysis

The assumptions for this analysis are :

- 1) The shear flow only carried by the skin
- 2) The stringers do not carry shear flow

Aluminum alloy 6061-T6 was chosen for the skin material. The shear flow is maximum at the bottom of the service module because it has the smallest diameter. The thickness of the skin is calculated to be 0.06mm. This is due to the small lateral force acting at the center of gravity. Therefore, a skin thickness of 2mm was chosen for the actual handling of the module as a more realistic estimate. For the forces on the stringers and the shear flow on the skin refer to Fig 6.4H.

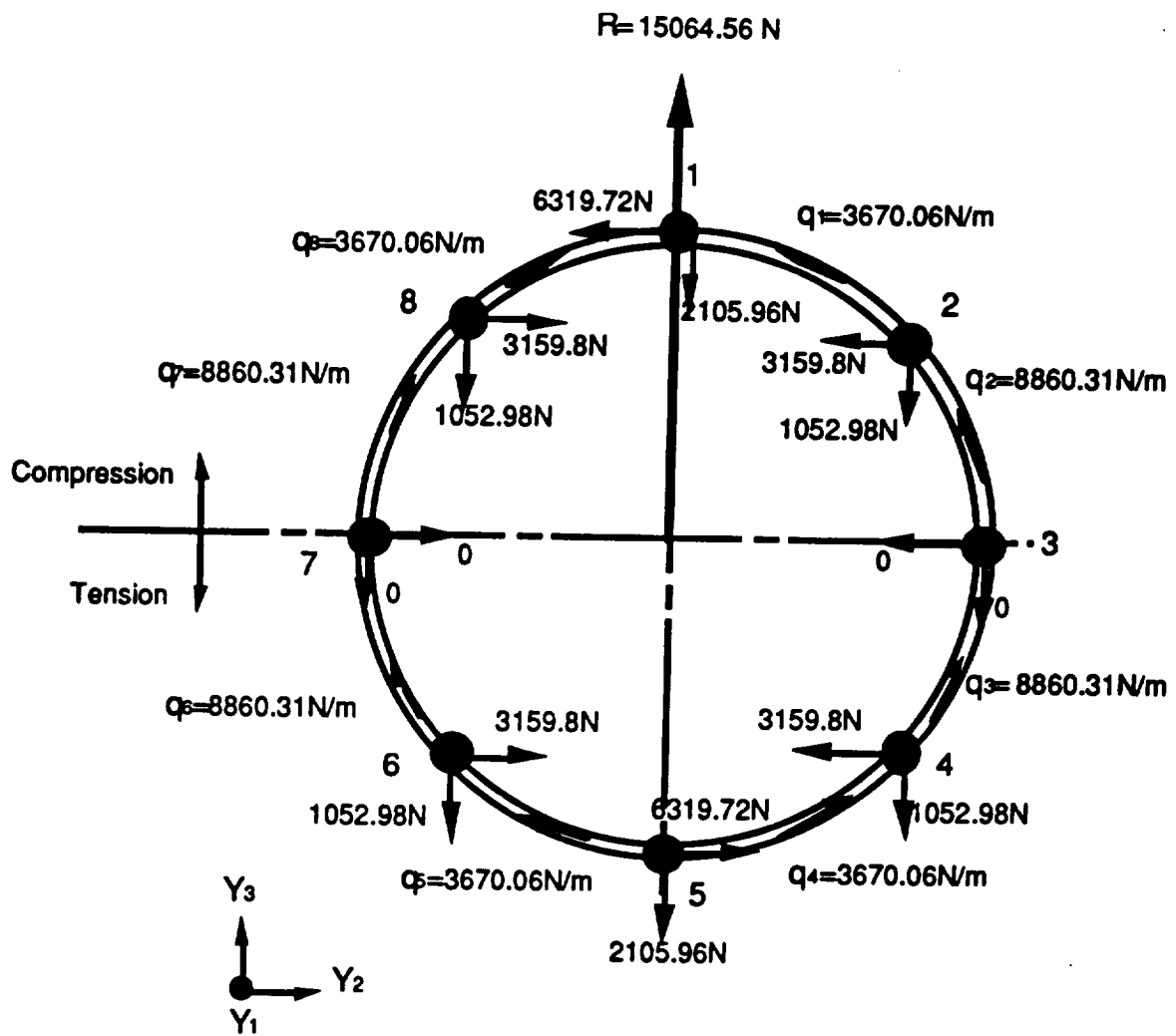


Figure 6.4 H Forces and Shear Flow Carried by the Stringers and Skin

Due to the symmetry of the stringer locations the forces acting on the stringers 2, 4, 6, and 8 are equal. Similarly, stringers 1 and 5 also carry the same loadings. Finally, stringers 3 and 7 carry no forces.

Section 6.5: Structural Interface

6.5.1 Summary

A truss structure will interface the Taurus L. M. S. and the Taurus booster. The design constraints for this structure are prescribed by the dimensions of the service module and the mechanical interface of the Taurus booster. These dimensions are shown in Figure 6.5A at the end of this section. In addition, the structural interface is designed to take a vertical force of 8 gees and a horizontal force of 1.7 gees. The interface structure is designed to meet these constraints with the lowest weight.

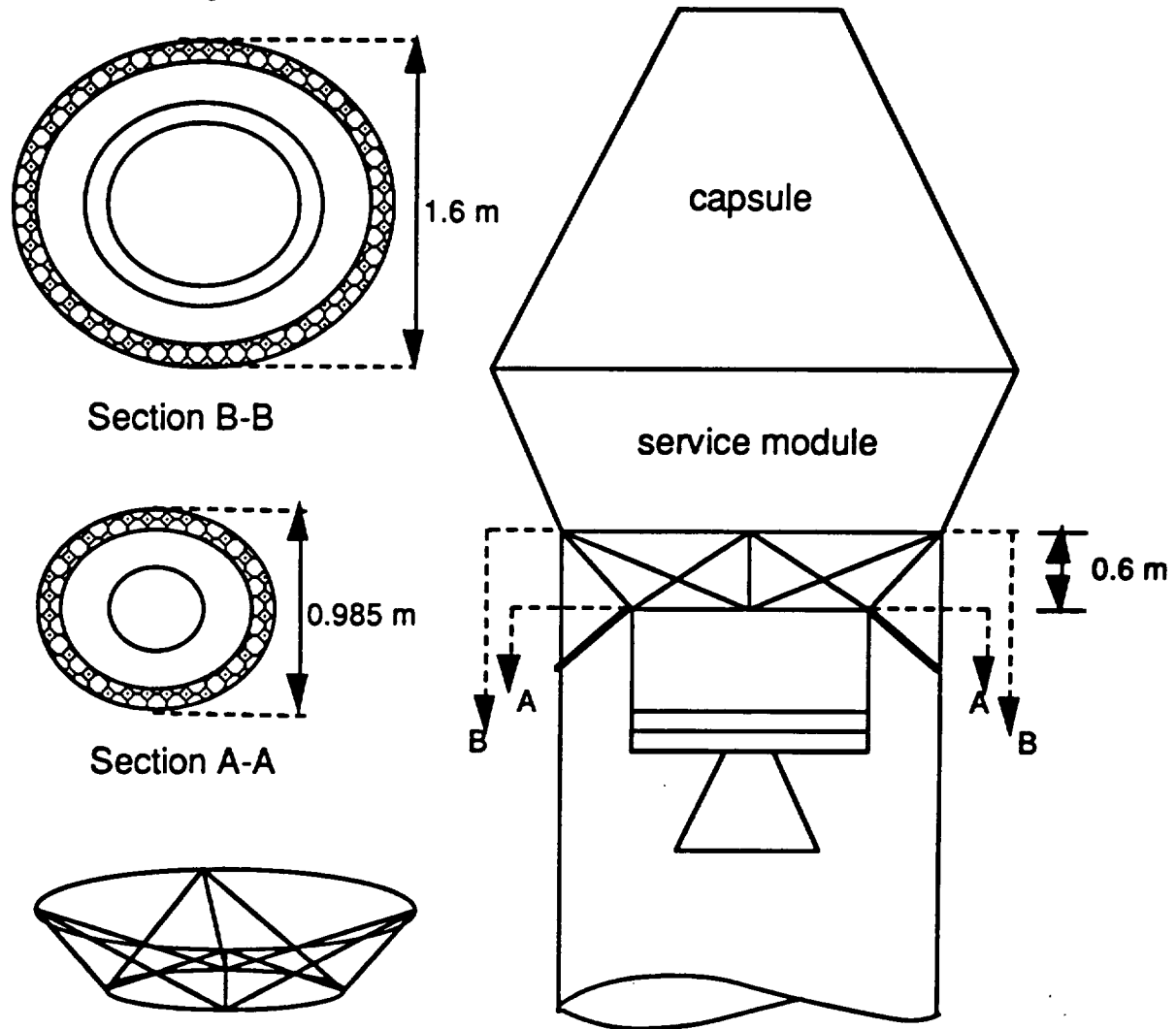
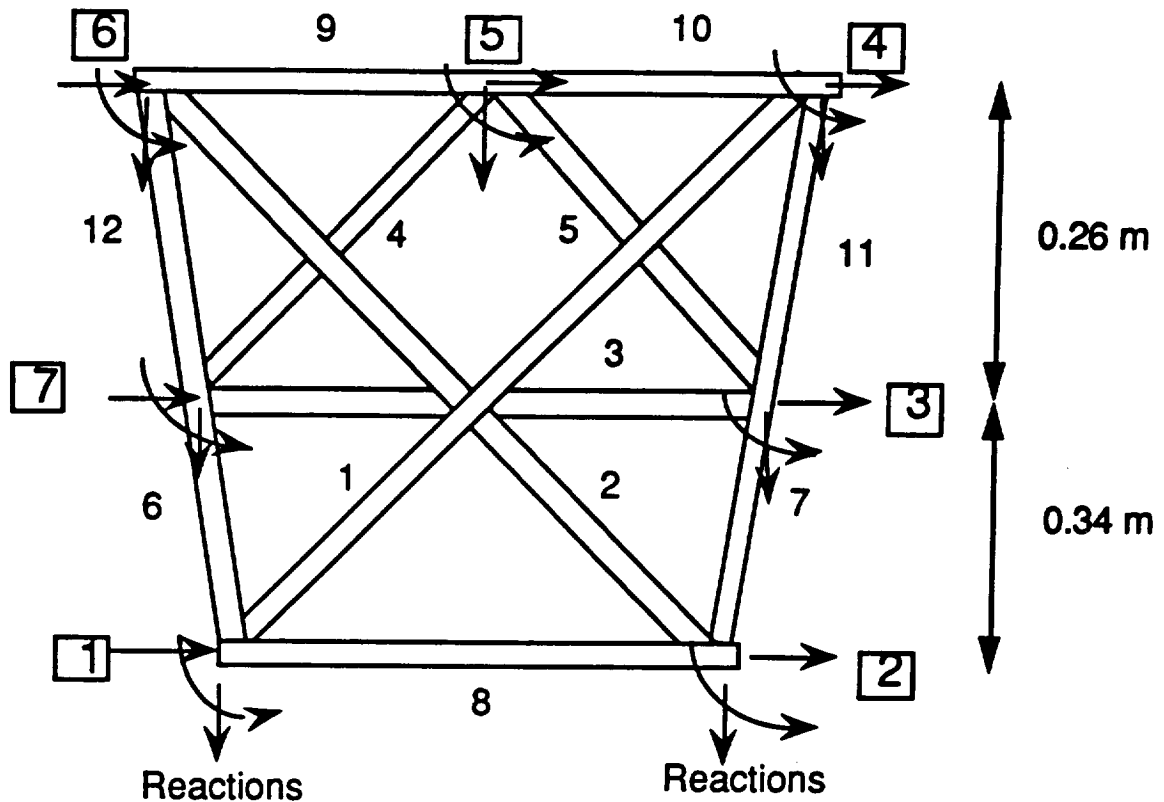


Figure 6.5A: Capsule Configuration and Interface Dimensions

The design of one of the four trusses that form the interface structure and the finite element model are shown in Figure 6.5B. The height of the structure is 0.6 m.

The structure weighs approximately 30 kg and the material is 7075-T6 aluminum alloy. The stresses in the force members of the truss are within the yield stress of this alloy (542 MPa).



Nodes are represented with boxes. Forces at nodes 3,4,6, and 7 are constrained

Figure 6.5B: Finite Element Model

6.5.2 Truss Design

The diameter of the top ring of the interface is 1.6 m and the diameter of the lower ring is 0.986 m. The height of the interface is 0.6 m. This value was determined by calculating the height dimension that would be needed for a 45° angle between most of the force members. With a height of 0.6 m, the angles between force members ranged from 40° to 50°. For example, the angle, Φ , between elements 8 and 1 in Figure 6.4B is determined by:

$$\bullet \Phi = \arctan (60 + 72) = 39.8^\circ \approx 40^\circ$$

The angle, Ψ , between element 4 and the z axis is:

$$\bullet \Psi = \arctan (33 + 26) = 51.7^\circ \approx 50^\circ$$

The angle of inclination of elements 11 and 12 is approximately 21°.

6.5.3 Structural Loads

The maximum design loads for the interface structure are:

- In the vertical direction:

Gee Load x Safety Factor x Gravity x Mass of Taurus L. M. S.
where:

Gee Load (including vibrations and shock) = 8.0

Safety Factor (for yield stress limit analysis) = 1.25

Gravity = 9.81 N/kg

Mass of Taurus L. M. S. = 1100 kg

Force vertical = $8 \times 1.25 \times 9.81 \text{ N/kg} \times 1100 \text{ kg} = 108 \text{ kN}$

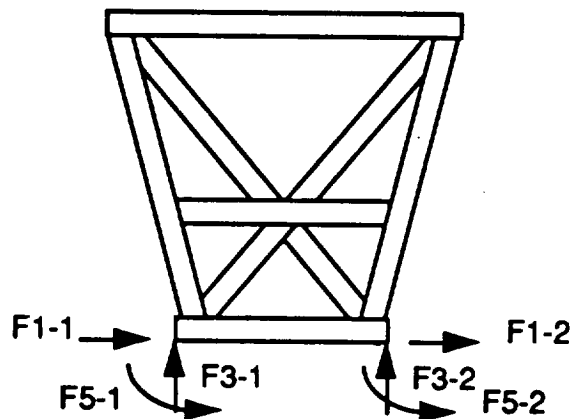
- In the horizontal direction:

Gee Load (including vibrations and shock) = 1.7

Force horizontal = $1.7 \times 1.25 \times 9.81 \text{ N/kg} \times 1100 \text{ kg} = 23 \text{ kN}$

6.5.4 Structural Analysis

A NASTRAN analysis of the interface structure yielded the reaction forces due to the applied design loads. The forces on one of the four truss structures that form the interface are shown in Figure 6.4C.



The reaction forces are:

F1-1 = -14 kN

F3-1 = 18 kN

F5-1 = -0.106 N-sq. m.

F1-2 = 5.4 kN

F3-2 = 22.5 kN

F5-2 = -0.907 N-sq. m.

Figure 6.5C: Reaction Forces on the Truss Structure

The volume of the material used in the interface structure is 0.0112 m^3 . Two factors were used to determine the best material: density and yield stress. The primary consideration for choosing a material is mass. Therefore, the resulting mass of an aluminum, steel, and titanium structure was determined. The results are shown below.

Material	Density (kg / m3)	Mass (kg)
7075-T6 Aluminum	2795	31.3
Low Alloy Steel	7805	84.7
Titanium	4705	53.7

The stresses in each member were also determined by NASTRAN. Each stress was multiplied by a safety factor of 1.25. The yield stress for aluminum, steel and titanium are shown below.

Material	Yield Stress (MPa)
7075-T6 Aluminum	542
Low Alloy Steel	1517
Titanium	1103

The values of the calculated axial stresses and the magnitude of the stresses, including the safety factor, are shown in below.

Element	Axial Stresses (MPa)	Axial Stressesx1.25 (MPa)
1	-44.84	-56.05
2	-71.57	-89.47
3	-93.19	-116.49
4	-132.00	-165.00
5	-145.60	-182.00
6	-202.80	-253.50
7	-243.80	-304.75
8	0.0	0.0
9	120.00	150.00
10	116.70	145.88
11	-160.60	-200.75
12	-141.10	176.38

Therefore, all of the axial stresses in the force members are within the yield stress of these materials. Due to the mass savings, cost, and ease of manufacturing, the structure will be aluminum.

The structure will have a "L-shape" cross section for ease in riveting. The cross-sectional area is:

$$\bullet \text{ Area} = 200 \times 200 \times 20 \text{ mm} = 0.008 \text{ m}^2$$

6.5.5 Final Results

The truss structure that will interface the Taurus L.M.S. with the Taurus booster will be made of 7075-T6 aluminum and will weigh approximately 31 kg. The axial stresses in each member of the truss are below the yield stress of this material (542 MPa). The design loads with a margin of safety are: 108 kN in the vertical direction and 23 kN in the horizontal direction. The volume of the material used in the structure is 0.0112 cu. m. The interface will be equipped with explosive bolts around both the upper and lower circular perimeter. The bolts will be equipped with springs to allow for separation from the service module once the orbit is circularized.

Section 6.6: Thermal Protection System (TPS)

The thermal protection system of the capsule is one of the most important systems for reentry. In designing the TPS, two alternatives were considered, reflective and ablative. The reflective system is a reusable heat shield, that radiates heat as fast as it absorbs heat. The shield consists of a highly insulative tile with a high emissivity. These systems generally can dissipate varying amounts of heat, dependent on flight path; but the weight is fairly constant for a given shape vessel and a specific maximum temperature. The ablative system, however, is a non-reusable heat shield that dissipates heat by ablation, the sublimation of the solid ablative material into the ambient atmosphere. The high heat of ablation absorbs as much heat as is needed, at the expense of the material. Ablative heat shields can absorb any amount of heat if they are made heavy enough.

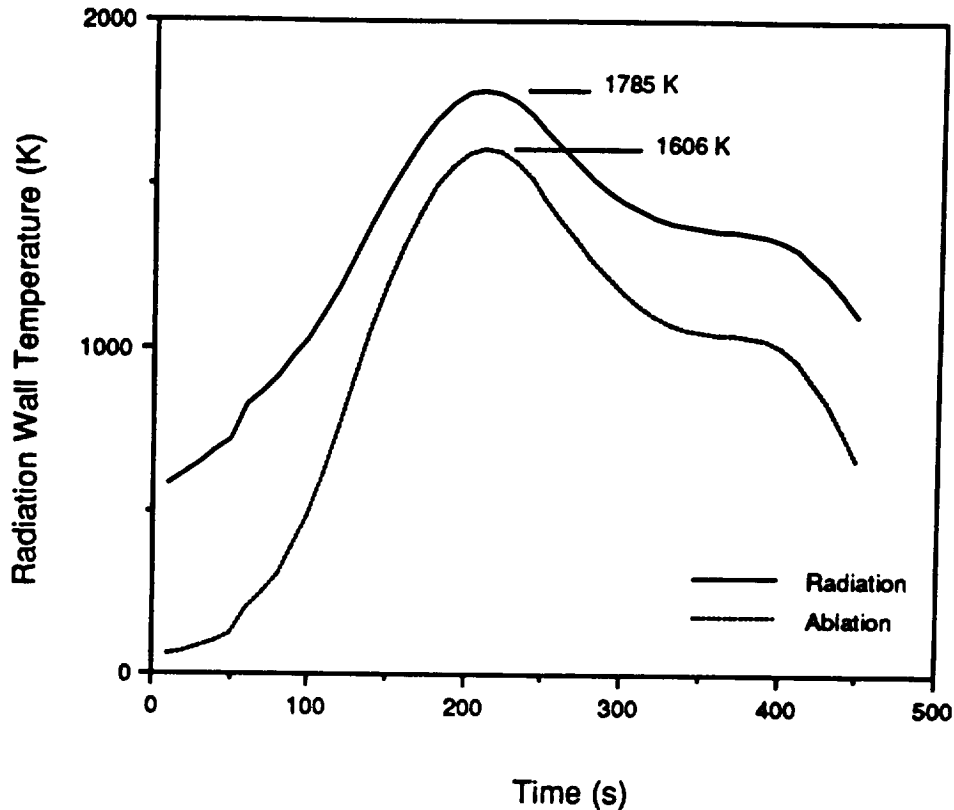
6.6.1 Primary TPS Trade Study

The primary consideration in design of the heat shield was determining the type of heat shield to be used. The radiative heat shield was the first system examined. Analysis of this type of shield is fairly straightforward. The ablative term is simply set to zero in the thermal equilibrium equation, as described in appendix D. The equation is then solved for the equilibrium wall temperature. The only real design constraints are that the shield material be able to withstand this heat level, and that there be sufficient insulation to withstand the total heat absorbed by the shield.

The ablative type of shield was a bit more difficult to analyze. First, the type of ablative material had to be selected. After the selection of the material, and the determination of its ablation rate curve, as described in appendix D, the ablative heating rate term was plugged into the equilibrium equation. The maximum wall temperature was then examined to determine if the material could withstand this temperature. After a number of tries, the material was chosen to be low density phenolic - nylon. This material has a heat of combustion of 12 MJ/kg, and a mass flow rate at 1800 K of 1.52×10^{-2} kg/m²s (Clark, 1973). Assuming a linear ablation rate curve, the rate varies as $101.23T$.

With both sets of equilibrium equations complete, the wall temperature profile can be determined by use of the program in Appendix C. These results are shown in figure 6.6A. As expected, the wall temperatures for the radiative heat shield are higher than those of the ablative type. The maximum temperature of the radiative heat shield is 1785 K, compared to 1606 K for the ablative shield. It is also notable that the radiative TPS has a much higher average temperature.

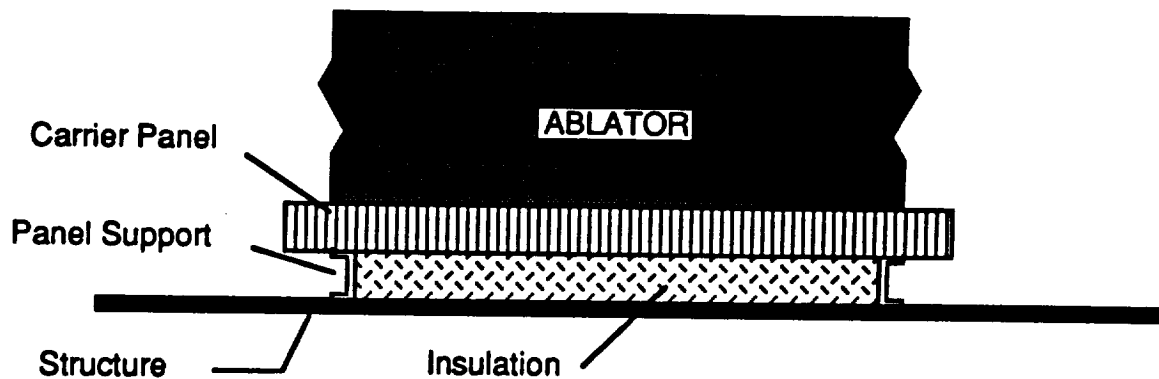
Figure 6.6.A: Surface Temperature Comparison



The total heating load for the ablative TPS under consideration was determined in section 1.5 to be 148.6 MJ. Considering a factor of safety of 1.2 and the heat of ablation of 12 MJ/kg, the mass of ablative material for the primary heat shield is 14.86 kg. The ablative material also needs a structure to support the aerodynamic loads, and to insulate the capsule from any heat that is conducted through the shield. The standard type of heat shield support structure is shown in figure 6.6B. The shield itself is bonded to a carrier support panel. This panel is used to evenly distribute the aerodynamic loading to the panel supports. These supports are then mounted onto the skin of the capsule. In between the supports and the panel is a layer of insulation to protect the capsule from the higher temperature support panel. The insulation is relatively soft, creating a need for the panel supports. The carrier panel and supports have a mass of 3 kg/m² while the insulation required weighs 1.5 kg/m² (Dow and Tompkins, 1972). This brings the total weight of the ablative heat shield to 30.45 kg.

For a radiative TPS, the shield must be able to withstand the highest temperature. From historical data, the mass of a TPS able to operate at temperatures up to about 2000 K will weigh between 18 and 22 kg/m². Over the capsule heat shield area of 3.46 m², this shield will weigh from 62 to 76 kg. Clearly on the basis of weight, the ablative TPS is vastly superior.

Figure 6.6B: Heat Shield Construction



Dow and Tompkins, 1973

The primary advantage of the radiative TPS is that it is reusable. The ablative type is not reusable. If the craft is to be reused an entirely new ablative heat shield must be installed after every flight. The radiative type is reusable for up to 100 flights. The Taurus LMS, however, is not a reusable spacecraft, again making the ablative TPS more attractive, due to its lower unit cost. It was mainly on the basis of mass that the heat shield was selected. The final TPS will be an ablative heat shield composed of low density phenolic - nylon. The structure will be composed of a carrier support panel, mounted to the capsule structure via channel beam panel supports, with a layer of insulation between the panel and the skin of the capsule.

6.6.2 Secondary TPS

The walls of the capsule will also be subjected to high temperature flow. This flow, however, is much more difficult to model, since it is mainly separated. Heat transfer along the windward side of a flat plate is proportional to the inverse root of the distance from the leading edge. To model the heat transfer on the leeward edge, the transfer rate close to the primary heat shield was assumed equal to that on the primary heat shield. The rate was also assumed to vary the same as for the windward side of the plate.

A value of 0.025 meters was chosen as the position of transfer to plate theory. At this locale the mass of the TPS was assumed to be the same as that for the primary heat shield. From here, the transfer rate varies proportional to the inverse root of the distance along the plate. The constant of proportionality was determined to be $0.936 \text{ kW/m}^{1.5}$. Summing these values over the length and height of the capsule, the total mass of the secondary heat shield was determined to be 9.065 kg. As the secondary heat shields are not exposed to the high aerodynamic forces that the primary shield is, the ablative material was bonded directly to the skin of the spacecraft. This gives a total TPS weight of 39.52 kg.

SECTION 6.7 Tank Design

6.7.1 Cryogenic Life Support Tanks

Gases which are difficult to liquefy can be stored in the liquid state for a long time in a double-walled flask known as a Dewar flask (Barnes and Noble, 1968). The following is a sectional view of the flask designed for the storage of liquid nitrogen and liquid oxygen.

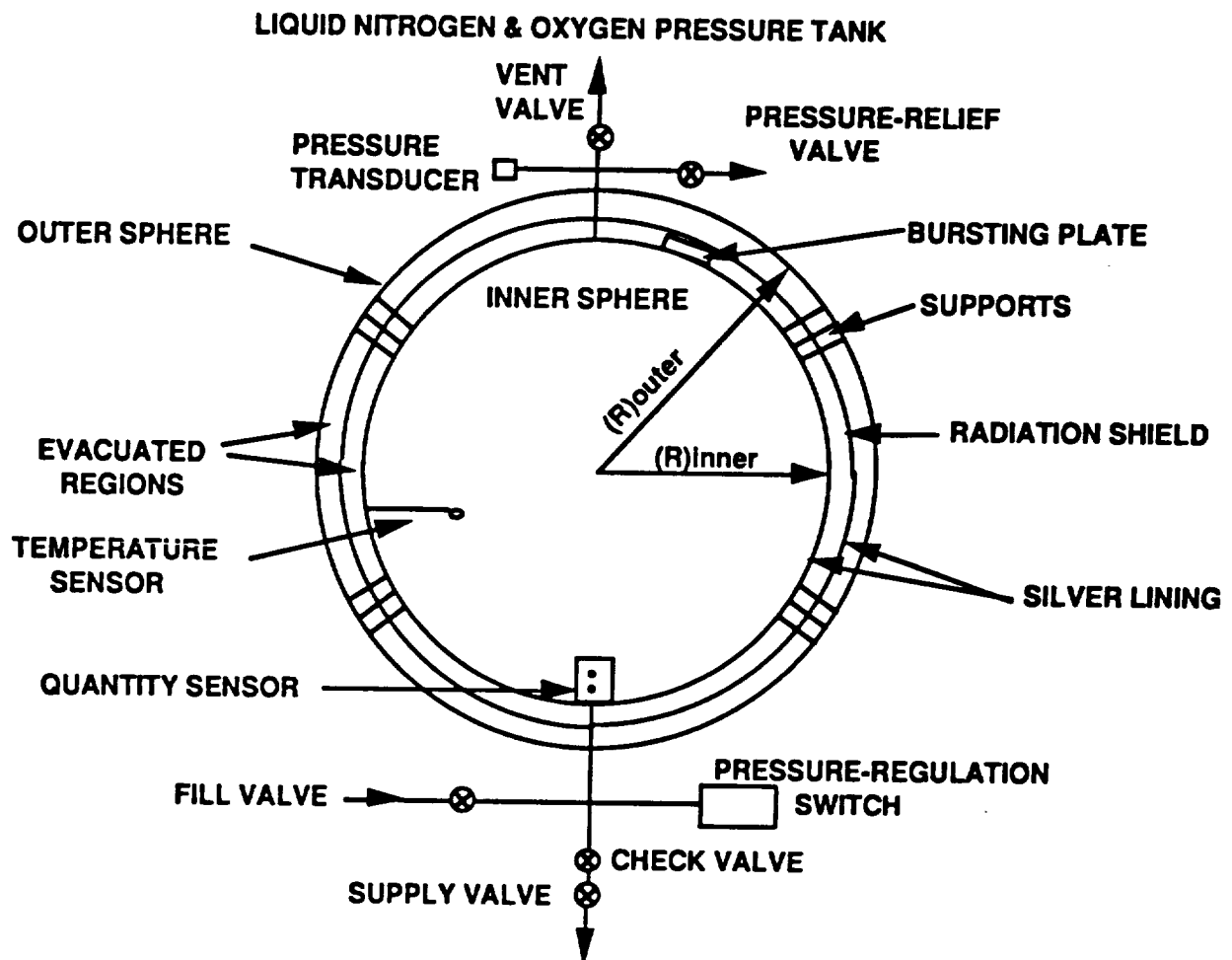


Figure 6.7A: Configuration of Cryogenic Life Support Tanks

The space in between the walls is evacuated. The vacuum prevents heat from being convected inwards or outwards. This basically is the same idea of the ordinary thermos bottle. The radiation shield is used to help prevent heat transfer by radiation. The silver surface applied during manufacturing is placed on the outside of the inner sphere and tank to further prevent heat absorption by radiation. Silver linings are used because it has a low emissivity. A bursting plate is fitted to prevent the internal pressure from exceeding the critical pressure for the tank. In Figure-6.7.A a portion of the avionics that will be used for these tanks is shown. A

brief outline of these are a pressure transducer to monitor the tank pressures continuously, a temperature sensor to ensure that the liquid doesn't boil off, and a pressure regulation switch to monitor the exit pressure of the liquid as it enters the life support system. Details on the aforementioned items can be found in the Avionics section of this report. To make a brief mention of some of the plumbing involved again Figure-6.7A shows numerous valves leading to or away from the tank. The pressure-relief valve can be used to lower the pressure of the tank by the pilot or by computer if that pressure becomes too great, the vent valve is for excess vapor to escape. There is an external fill valve for filling the tank just before launching, and finally a check and supply valve leading to the life support system (NASP-247, 1970). The concentric sphere idea was used because of the excellent known strength of the spherical shape, and for the ease of initial analysis of the hoop and longitudinal stresses. A factor of safety of 4.0 will be used in accordance with NASA specifications for pressure vessels. Shown below are the aforementioned equations

$$\text{HOOP STRESS: } \sigma_{\text{YIELD}} = \frac{Pr}{t_{\text{min}}}$$

$$\text{LONGITUDINAL STRESS: } \sigma_{\text{YIELD}} = \frac{Pr}{2t_{\text{min}}}$$

where P is the internal pressure of the tank, r is the radius of the inner tank and t is the wall thickness needed when using the compressive yield stress of a particular material. The tank was analyzed for being made from 6061-T6 aluminum. Later in section 6.7.2 it will be shown that in designing the storage tanks for the propulsion system for the vehicle that composite materials were used. Composite materials were not considered for the cryogenic tanks simply because no evidence was found that composites were ever used for these tanks previously, and because in the forthcoming analysis there was some comparison scaling done to that of tanks used in Project Mercury. The results of the analysis done in Appendix O can be seen in Table 6.7.A.

TANK STYLE	INNER RADIUS cm	OUTER RADIUS cm	MASS kg	TOTAL MASS kg
PRIMARY:				
NITROGEN	10.62	13.5	2.5	6.555
OXYGEN	8.29	11.2	1.78	3.846
SECONDARY:				
NITROGEN	6.68	9.56	1.27	2.27
OXYGEN	6.47	9.37	1.24	2.224

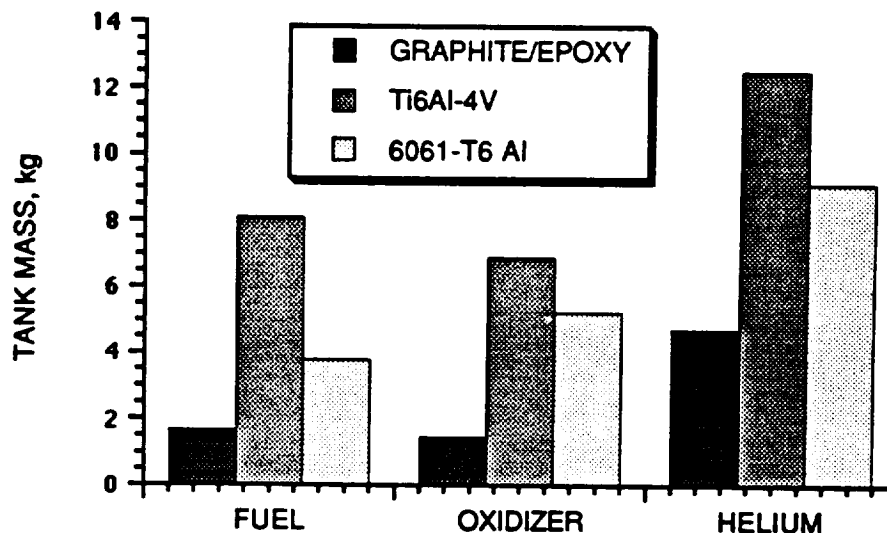
Table 6.7.A: Cryogenic Tank Dimensions and Masses

It should be noted that the total mass column consists of the tank mass plus the mass of the liquid contents. Further dimensions of the tanks including wall thicknesses can also be found in Appendix O.

6.7.2 Propulsion Tank Design

Several hours were spent working with the propulsion group on the design of the fuel tanks and the fuel pressurant system. While the propulsion group is more concerned with the propulsion side of these tanks the structures group is concerned with the mass of the tanks, sizes, and material choices. In the Appendix O the information for a single case is carried to completion. In addition, spreadsheets for both the fuel and pressurant tanks were used to create Figure 6.7.B which graphically displays the mass savings encountered when using composite materials. The analysis was done for three materials: Ti6Al-4V, 6061-T6 Al, and for Graphite/Epoxy. The titanium alloy was recommended (NASA -SP125) as a popular choice for high pressure storage vessels that are lightweight too. The composite material was used after talking with Dr. Vizzini (A. Vizzini, 1991) about popular materials for pressure vessels, and also because data was available for a layup that was approximately equal to that of an isotropic material.

FIGURE-6.7.B: FUEL TANK TRADE STUDY



The composite material was chosen due to nearly 5:1 mass savings encountered. Both cylindrical and spherical tanks were studied. The spreadsheets provided a wide variety of choices for length, radius, and wall thickness for the cylindrical tanks. Once the entire spectrum of data was available the decision was made using the following guidelines (NASA SP-125):

- minimum overall weight
- maximum storage volume in a given vehicle design
- least possibility of propellant mixing
- clean aerodynamic vehicle shape
- ease of installation of ducts and lines
- ease of insulation
- ease of fabrication and handling
- minimum trapped (unusable) propellants

However, the final choice was made to use the spherical tanks because the space was available in the service module, they provided a highest strength vessel with the smallest mass. The propulsion scheme uses a helium pressurant feed system for the various systems working off of the main fuel and oxidizer tanks. The installation of a bladder for the fuel and oxidizer tanks will be required, and will complete the positive expulsion system. The bladder is shown in Figure 6.7C and is oriented in before the launch position. The bladder is a flexible material connected to the equator of the tank which creates a hemisphere shape which fills the top of the fuel/oxidizer tank. Once the helium pressurant is applied it begins to use the bladder as surface to help push the fuel into whatever system is requiring it. As the fuel/oxidizer level decreases the bladder pushes out to help keep the pressure constant. Eventually, the bladder position is opposite to that of which it started. The reactivity of the materials with the propellants will require the installation of a liner. Aluminum was found to be a compatible material. In addition, if the tanks would begin to expand the liner would reach its yielding point earlier than the composite tank, so the liner will be corrugated. This process allows the liner to expand to fill the tank without reaching its own failure point. Figure 6.7C also shows a shut off valve at both the entrance and the exit of the tank.

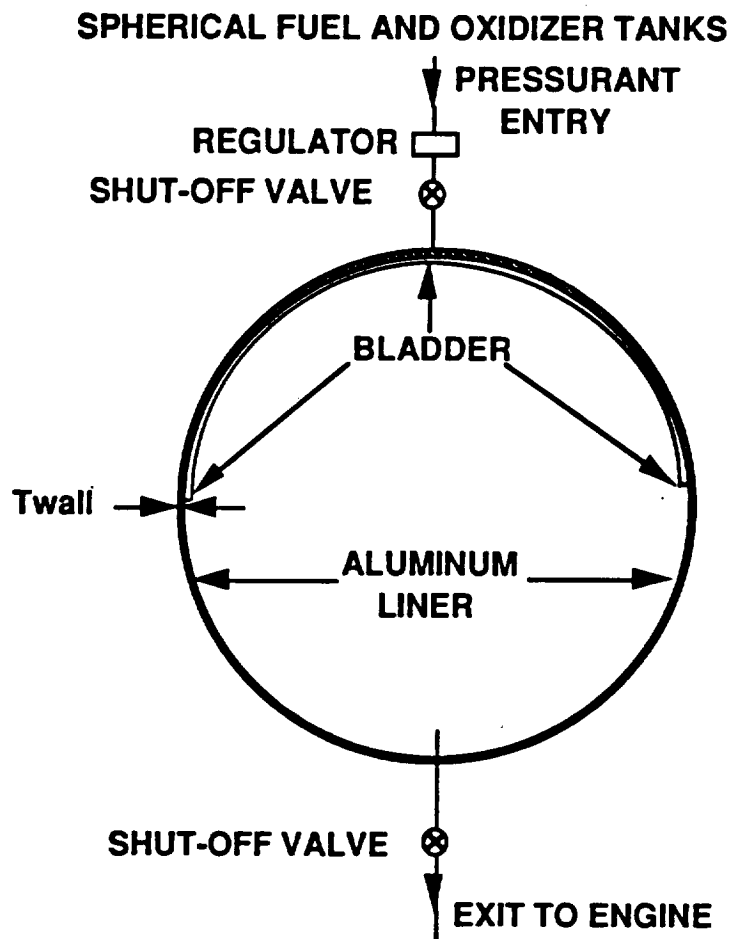


Figure 6.7C Tank layout and Bladder design

The regulator shown helps to reduce the pressure of the helium down to the level desired for pressurizing the fuel/oxidizer tanks. In the avionics section there is mention of the different sensors used to monitor fuel pressure and temperature. Table 6.7B displays the specifics of these tanks.

TANK TYPE	RADIUS	THICKNESS	TANK MASS
	cm	mm	kg
FUEL	27.25	1.106	1.66
OXIDIZER	26.1	1.06	1.46
HELIUM	17.58	5.71	4.73

Table 6.7B: Dimensions and Masses for Propulsion Tanks

6.7.3 Reentry Control Thruster Tanks

The design of these tanks is analogous to that of the main propulsion system. These tanks are located in the small area located at the top of the capsule, and used only for adjusting the reentry path. Therefore, the tanks are very small and the contents actually act as part of the structure to help the tanks keep their shapes. Table 6.7.C gives a breakdown of the specifics for these tanks.

TANK TYPE	RADIUS	THICKNESS	TANK MASS
	cm	mm	kg
FUEL	5	0.21	0.535
OXIDIZER	5.2	0.21	0.86
HELIUM	11.45	3.72	0.971

Table 6.7C: Dimensions and Masses for Reentry Control Tanks

Chapter 6 References

- "Aerospace America,"* January 1991.
- Akin, David, personal interviews/ Class Lectures, University of Maryland, 1991.
- Anton., *"Elementary Linear Algebra,"* John Wiley & Sons, 1973.
- Beer & Johnson, *"Mechanics of Materials,"* McGraw Hill, Inc., 1981.
- Bruhn, E., *"Analysis & Design of Flight Vehicle Structures,"* Tri-Offset Co., 1965.
- "Chemical Technology,"* Barnes & Noble, Inc., 1968.
- Clark, R.K., *"An Analysis of a Charring Ablator with Thermal Nonequilibrium, Chemical Kinetics, and Mass Transfer,"* NASA TN D-7180, 1973.
- "The Development of Cryogenic Storage Systems for Space Flight",* NASA SP-247, 1970.
- Donaldson, Bruce K., *"An Introduction to The Analysis of Aerospace and Other Vehicular Structures,"* Unpublished.
- Donaldson, Bruce K., Personal Interview, University of Maryland at College Park, 1991.
- Dow, M.B., and Tompkins, S. S., *"Materials and Design for Ablative Heat Shields,"* NASA TM X-2570, 1972.
- Project Mercury, A Chronology,* NASA SP-4001, 1963.
- Rivello, *Theory And Analysis Of Flight Structures,* 1969.
- "Space Materials Handbook,"* NASA SP-3051, 1969.
- "Structural Design Concepts, "* NASA SP-5039, 1967.
- "Thermal Insulation Systems,"* NASA SP-5027, 1967.
- Varisco, A., Wolter, W., and Bell, P., *"Design and Fabrication of a Super Alloy Thermal Protection System,"* NASA CP-2065, September, 1978.
- Vizzini, A., *"Composite Materials,"* Unpublished.
- Vizzini, A., Personal Interview, University of Maryland at College Park, 1991.
- Young, W., *"Roark's Formulas for Stress and Strain,"* McGraw-Hill, Inc., 1989
- Younger, *"Mechanics Of Aircraft Structures,"* 1942.

Bibliography

"Aerospace America," January 1991.

Agrawal, Brij N., "Design of Geosynchronous Spacecraft," Prentice-Hall, Inc., Englewood Cliffs, New Jersey, 1986.

Akin, David, personal interviews/ Class Lectures, University of Maryland, 1991.

Anderson, John D. Jr., "Introduction to Flight: Its Engineering and History," McGraw Hill, New York, 1978.

Anderson, John D., "Introduction to Flight ," McGraw-Hill, Inc., New York, 1985.

Anderson, John D., "Modern Compressible Flow With Historical Perspective," McGraw-Hill, Inc., New York, 1990.

Anderson, John D., "Hypersonic and High Temperature Gas Dynamics," McGraw-Hill, Inc., New York, 1990.

Anderson, J. D. Jr., personal interviews, University of Maryland, 1991.

"Anthropometry for Designers." ed. Staff of Anthropology Research, Webb Associated, NTIS, Springfield, VA, 1978.

Anton., "Elementary Linear Algebra," John Wiley & Sons, 1973.

Bate, R.R., D.D. Mueller, and J.E. White, "Fundamentals of Astrodynamics," Dover Publications, New York, 1971.

Beer, F.P. and E.R. Johnson, "Mechanics of Materials." New York: McGraw-Hill, 1981.

Bruhn, E., "Analysis & Design of Flight Vehicle Structures," "Tri-Offset Co., 1965.

"Chemical Technology," Barnes & Noble, Inc., 1968.

Center, Allan M., Capt, USAF. Interview with Missile Launch Instructor, Personal Communication. Vandenberg AFB, California, 2 Aug 1990.

Clark, R.K., "An Analysis of a Charring Ablator with Thermal Nonequilibrium, Chemical Kinetics, and Mass Transfer," NASA TN D-7180, 1973.

Clausing, D.J., "The Aviator's Guide to Modern Navigation," TAB Books Inc., 1987

- Collins W. B. And D. R. Newell: *"Power Conditioning Requirements and Tradeoff Considerations for the Space Shuttle."* IEEE 1971 Power Conditioning Specialists Conference.
- The Development of Cryogenic Storage Systems for Space Flight", NASA SP-247, 1970.*
- Donaldson, Bruce K., *"An Introduction to The Analysis of Aerospace and Other Vehicular Structures,"* Unpublished.
- Donaldson, Bruce K., Personal Interview, University of Maryland at College Park, 1991.
- Dow, M.B., Pittman, C.M., and Croswell, W.F., *"Thermal Protection and Radio-Frequency Transmissivity of Several Ablation Materials,"* NASA TN D-1896, 1964.
- Dow, M.B., and Tompkins, S. S., *"Materials and Design for Ablative Heat Shields,"* NASA TM X-2570, 1972.
- Ellis, Robert and Denny Gulick, *"Calculus with Analytic Geometry, 2nd Edition,"* Harcourt Brace Gianovich, New York, 1982.
- Empell C.M., *"Multirole Capsule An Introduction."* *Journal of the British Interplanetary Society* Vol#2, 1989.
- Feaser, Thomas A., *Facilities at John F. Kennedy Space Center, NASA and Cape Canaveral Air Force Station,* NASA, 1981.
- Fleischer A., *"Silver-Zinc Batteries."* *Symposium on Silver-Zinc Batteries"* New York, J Wiley & Sons, 1968.
- Foch, Richard, personal interview, Naval Research Laboratory, 1991.
- Fraas, Arthur P. , *"Heat Exchanger Design,"* John Wiley and Sons, New York, 1989.
- Furniss, T., *"Manned Spaceflight Log",* Janes Publishing Company Limited, London, 1983.
- Griffin, M. D. and J. R. French, *"Space Vehicle Design,"* New York: AIAA, 1991.
- Gross S., *"Battery Design and Optimization,"* Electrical Society, Princenton, NJ. 1979.
- Hagar, H., Lecture Notes from ENAE 488A *"Astronautics",* University of Maryland, College Park, MD, Fall 1990.

- Hallion, Richard P., and Tom D. Crouch, *"Apollo: Ten Years Since Tranquility Base."*
- "Handbook of Astronautical Engineering"*: ed. Heinz Hermann Koelle, McGraw-Hill Book Company, New York, 1961.
- Hansen, C.F., *"Approximations for the Thermodynamic and Transport Properties of High-Temperature Air,"* NASA TR R-50, 1959.
- Harvey, B., *"Race into Space - the Soviet space programme,"* Ellis Horwood Limited, West Suffex, England, 1988.
- Heisenrath, J., and Klein, M., *"Tables of Thermodynamic Properties of Air in Chemical Equilibrium Including 2nd Viral Corrections from 1500K to 15000K,"* AEDC TR-65-58, 1965.
- Helfrick, Albert. *"Modern Aviation Electronics."* Prentice-Hall, Inc. Englewood Cliffs, NJ 1984.
- Hempsell, C. M., *Multi-Role Capsule System Description,* Journal of the British Interplanetary Society, 1989.
- Hibbeler, R.C., *"Engineering Mechanics Statics and Dynamics Forth Edition,"* Macmillian Publishing Co., New York, 1986.
- Hill, P.G and C.R. Peterson, *"Mechanics and Thermodynamics of Propulsion."* Reading, Mass: Addison-Wesley ,1970.
- Hord, R. Michael. *"Handbook of Space Technology: Status and Projections."* CRC Press Inc. Boca Raton, FL 1985.
- "Human Factors in Long-Duration Spaceflight."* National Academy of Sciences Washington, D.C. ,1972.
- Huzel K. Dieter and Huang H. David, *"Design of Liquid Propellant Rocket Engine,"* NASA Scientific and Technical Information Office, Washington DC, 1971.
- Institute for Strategic Defense Studies, *"U.S. Defense Issues,"* 1989-1990.
- "Jane's, All the World's Avionics,"* IEEE, 1990.
- Jasinski R., *"High Energy Batteries",* New York, Plenum Press. 1967.
- Kayton, M., *"Navigation: Land, Sea, Air, and Space",* IEEE., Press, 1989.
- Kendal, Brian. *"Manual of Avionics: Second Edition."*, BSP Professional Books Oxford: 1987.

- Kent, A. and J. G. Williams, *"Encyclopedia of Computer Science and Technology,"* Marcel Dekker, Inc.
- Kiker, John W. and Campbell, Carlisle C. Jr., *"Spacecraft Landing Systems-Design Criteria and Components",* Manned SpaceCraft, 1964.
- Lambert, Mark., *"Jane's All the World's Aircraft 1990-91",* New York, 1990.
- Lewis, Mark, personal interviews/ Class Lectures, University of Maryland, 1991.
- Lewis, Richard S., *"Space Exploration,"* Salamander Books Limited, London, 1983.
- Leondes, C.T., *"Guidance and Control of Aerospace Vehicles,"* McGraw-Hill Book Company, Inc., 1963.
- Loh, W.H., *"Re-entry and Planetary Entry Physics and Technology,"* Springer-Verlag, New York, 1968.
- Long, Lawrence P., personal interviews, University of Maryland at College Park, 1991.
- "Manned Spacecraft: Engineering Design and Operation":* ed. Paul E. Purser, Maxime A. Faget, and Norman F. Smith, Fairchild Publications, Inc., New York, 1964.
- Manzo M. and N. R. Schulze: *"NASA Aerospace Battery System Program Update."* 1989 24th Intersociety Energy Conversion Engineering Conference".
- McLean, Ian S. *"Electronic and Computer-Aided Astronomy: From Eyes to Electronic Sensors,"* Ellis Horwood Limited New York, NY : 1989
- Morgan N.E. and W. D. Morath. *"Development of a Hydrogen-Oxygen Internal Combustion Engine Space Power System."*
- Morgan, Walter I. and Gordon, Gary D. *"Communications Satellite Handbook,"* John Wiley & Sons, New York, 1989.
- NASA, *"Satellite Acquisition: Global Positioning System Acquisition Changes After Challenger's Accident,"* 1987.
- NASA, *"Space Operations: NASA's Communications support for Earth Orbiting Spacecraft,"* 1989.
- National Aeronautics and Space Administration (NASA), *"JSC Cost Model Summary,"* 1991 (converted by D. Akin).

- National Space Transportation System Reference, "*Volume 1: Systems and Facilities*," NASA, June 1988.
- Norton, Harry N. "*Biomedical Sensors: Fundamentals and Applications*." Noyes Publications Park Ridge, NJ , 1982.
- Ohanian, H.C., "*Physics*," W.W. Norton & Co., New York, 1985
- Orbital Sciences Corporation, "*Taurus*," Orbital Sciences Corporation, November 1990.
- Paragear Equipment Co., catalog #51, 1986.
- Project Mercury, A Chronology*, NASA SP-4001, 1963.
- Poynter, Dan , "Parachuting Equipment", *Parachuting, The Skydiver's Handbook*, 1989.
- Rausenbach H. S., "*Solar Cell Array Design Handbook*", New York: Van Nostram Peinhold Co. 1980.
- Raymer, Daniel P., "*Aircraft Design: A Conceptual Approach*," Washington, D.C.: AIAA, Inc., 1989.
- Rivello, "*Theory And Analysis Of Flight Structures*," 1969.
- Rusert, E.L., Hackett, T.L., and Drennen, D.N.: "*Development of an Improved Toughness Hyperpure Silica Reflective Heat Shield*," NASA CR-152297, 1979
- Shigley, Joseph E. and Charles R. Mischke "*Mechanical Engineering Design*," New York: MacGraw-Hill, Inc., 1989.
- Sinclair, Ian R. "*Sensors and Transducers*." BSP Professional Books Oxford : 1988
- Singh, Jasbir, "*Heat Transfer Fluids and Systems for Porcess and Energy Applications*," Marcel Dekker, Inc., New York, 1985.
- "*Smart Sensors*." Technical Insights ,New York, NY,1988.
- "*Space Materials Handbook*," NASA SP-3051, 1969.
- "*Space Tech: Conference Proceedings*." Anaheim, CA., September 23-25, 1985.
- Spitzer, C. R., "*Digital Avionics Systems*," New Jersey: Prentice Hall Inc., 1987.
- Stapp, Colonel John Paul. "Human Tolerance to Accelerations of Space Flight." *Physics and Medicine of the Atmosphere and Space*. Wily, NY, 1960.

- "Structural Design Concepts,"* NASA SP-5039, 1967.**
- Sutton G. P., *"Rocket Propulsion Elements,"* John Wiley & Sons, Inc., New York. 1986.**
- Thompson, T. William, *"Introduction to Space Dynamics,"* Dover Publishing, New York, 1985**
- Walker P.M.B., *"Cambridge Air and Space Dictionary,"* Cambridge University Press, 1990.**
- Wertz, J. R., *"Spacecraft Attitude Determination and Control,"* Boston, D. Reidel Publishing Co., 1986**
- Winters, C.W., and Barcalente, E.M., *"A Sensor for Obtaining Ablation Rates,"* NASA TN D-800, 1961**
- Varisco, A., Wolter, W., and Bell, P., *"Design and Fabrication of a Super Alloy Thermal Protection System,"* NASA CP-2065, September, 1978**
- Vizzini, A., *Composite Materials,* Unpublished.**
- Vizzini, A., Personal Interview, University of Maryland at College Park, 1991.**
- Young, W., *"Roark's Formulas for Stress and Strain,"* McGraw-Hill, Inc., 1989**
- Younger, *"Mechanics Of Aircraft Structures,"* 1942.**

	A	B	C	D	E	F	G
	System	Component	Mass Kg	Radias meters	length (Y) meters	height (Z) meters	width (x) meters
1	Main Life Support						
2		LiOH Canister	1.21		0.13	0.13	0.25
3		Spare LiOH Canister	1.21		0.13	0.13	0.25
4		Curculation Fan	1.00		0.10	0.10	0.10
5		Ethylene Glycol pump	1.00		0.10	0.10	0.10
6		Spare Pump	1.00		0.10	0.10	0.10
7		Heat Exchanger (w/ coolant	46.12		1.00	0.40	0.40
8	Secondary Life Supp.	Radiator	10.00		2.50	1.50	0.03
9		Reheater	0.50		0.10	0.10	0.10
10		Oxygen and tank	5.00	0.10			
11		Nitrogen and tank	2.20	0.10			
12		Helium and tank	2.00	0.10			
13		Survival Pack	22.30		0.15	0.45	0.45
14		Fan	0.50		0.10	0.10	0.10
15	Crew Cabin	Water Separator	5.00		0.25	0.10	0.10
16		LiOH Canister	2.42		0.50	0.10	0.10
17		Boiler Water Pump	0.50		0.10	0.10	0.12
18		Coolant Water Pump	0.50		0.10	0.10	0.10
19		Boiler Water and Tank	8.00	0.10			
20		Radiator and water	10.00		0.25	0.25	0.25
21		Oxygen and tank	1.00	0.10			
22	Avionics	Nitrogen and tank	1.00	0.10			
23		Helium and tank	1.00	0.10			
24		Fire extinguisher	4.50		0.13	0.13	0.43
25	Avionics	Astronaut/seat/suit	119.50	Provided	by	Human	factors
26		Control panel	15.00		0.25	0.50	0.50
27		CPU #1	8.00		0.10	0.10	0.20
28							

Appendix A.1: Capsule Mass Moment Of Inertia

	A	B	C	D	E	F	G
29		CPU #2	8.00		0.10	0.10	0.20
30		Main Memory	8.00		0.10	0.40	0.60
31		Transiever #1	5.00		0.12	0.18	0.20
32		Transiever #2	5.00		0.12	0.18	0.20
33		Transiever #3	5.00		0.12	0.18	0.20
34	Propulsion	Fuel and tank	0.54	0.05			
35		Oxidizer and Tank	0.86	0.05			
36		Helium and tank	1.29	0.12			
37		Thruster #1	1.13		0.11	0.06	0.06
38		Thruster #2	1.13		0.11	0.06	0.06
39		Thruster #3	1.13		0.06	0.06	0.11
40		Thruster #4	1.13		0.06	0.06	0.11
41		Thruster #5	1.13		0.11	0.06	0.06
42		Thruster #6	1.13		0.11	0.06	0.06
43		Thruster #7	1.13		0.06	0.06	0.11
44		Thruster #8	1.13		0.07	0.06	0.11
45	Power	Batteries	21.05		0.34	0.34	0.34
46	Structure	Capsule Structure	200.00				
47		Thermal Control	40.00	1.05		0.10	
48	Parachute	Main Parachute	30.00		0.60	0.55	0.50
49		Reserve Parachute	30.00		0.60	0.55	0.50
50	TOTALS		634.24				

Appendix A.1: Capsule Mass Moment Of Inertia

	H	I	J	K	L	M	N	O
1	Ixx	Iyy	Izz	Xbar	Ybar	Zbar	MXbar	MYbar
2	kg-m^2	kg-m^2	kg-m^2	meters	meters	meters	Kg-m	Kg-m
3	0.08	0.08	0.27	0.00	0.30	0.10	0.00	0.36
4	0.08	0.08	0.27	0.00	0.66	0.10	0.00	0.79
5	0.04	0.04	0.04	-0.25	0.30	0.10	-0.25	0.30
6	0.04	0.04	0.04	0.75	0.25	0.10	0.75	0.25
7	0.04	0.04	0.04	0.76	0.25	0.10	0.76	0.25
8	159.24	159.24	62.78	0.25	0.00	0.35	11.53	0.00
9	226.18	226.18	51.90	1.05	0.00	0.25	10.50	0.00
10	0.02	0.02	0.02	-0.14	-0.45	0.10	-0.07	-0.23
11	0.02	0.02	0.02	0.13	-0.70	0.10	0.63	-3.50
12	0.01	0.01	0.01	0.10	-0.70	0.10	0.22	-1.54
13	0.01	0.01	0.01	1.09	-0.70	0.10	2.18	-1.40
14	5.41	5.41	15.41	-0.50	6.25	0.52	-11.15	139.38
15	0.02	0.02	0.02	-0.55	-0.49	0.10	-0.28	-0.25
16	1.08	1.08	0.43	-0.55	0.30	0.10	-2.75	1.50
17	2.03	2.03	0.58	-0.55	-0.13	0.10	-1.33	-0.30
18	0.02	0.02	0.03	-0.75	0.13	0.10	-0.38	0.06
19	0.02	0.02	0.02	-0.80	-0.13	0.10	-0.40	-0.07
20	0.03	0.03	0.03	-0.75	0.35	0.10	-6.00	2.80
21	0.13	2.59	2.59	-1.05	0.00	0.20	-10.50	0.00
22	0.00	0.00	0.00	-0.63	-0.25	0.10	-0.63	-0.25
23	0.00	0.00	0.00	-0.63	-0.25	0.10	-0.63	-0.25
24	0.00	0.00	0.00	-0.63	-0.25	0.10	-0.63	-0.25
25	0.00	0.32	2.83	0.50	-0.63	0.52	2.25	-2.81
26	6.48	10.37	8.47	0.20	0.00	0.55	23.90	0.00
27	6.23	6.23	13.23	0.30	0.00	0.90	4.50	0.00
28	0.33	0.33	1.13	-0.30	-0.13	0.10	-2.40	-1.00

Appendix A.1: Capsule Mass Moment Of Inertia

	H	I	J	K	L	M	N	O
29	0.33	0.33	1.13	-0.30	0.06	0.10	-2.40	0.48
30	1.33	1.33	9.63	-0.30	-0.06	0.10	-2.40	-0.48
31	0.37	0.37	0.72	0.00	0.25	0.10	0.00	1.25
32	0.37	0.37	0.72	0.00	0.00	0.10	0.00	0.00
33	0.37	0.37	0.72	0.00	-0.25	0.10	0.00	-1.25
34	0.00	0.00	0.00	0.00	0.06	2.00	0.00	0.03
35	0.00	0.00	0.00	0.00	-0.06	2.00	0.00	-0.05
36	0.01	0.01	0.01	0.00	0.00	2.00	0.00	0.00
37	0.05	0.05	0.02	0.37	0.05	2.00	0.42	0.06
38	0.05	0.05	0.02	0.37	-0.05	2.00	0.42	-0.06
39	0.02	0.02	0.05	0.05	-0.37	2.00	0.06	-0.42
40	0.02	0.02	0.05	-0.05	-0.37	2.00	-0.06	-0.42
41	0.05	0.05	0.02	-0.37	-0.05	2.00	-0.42	-0.06
42	0.05	0.05	0.02	-0.37	0.05	2.00	-0.42	0.06
43	0.02	0.02	0.05	-0.05	0.37	2.00	-0.06	0.42
44	0.02	0.02	0.05	0.05	0.37	2.00	0.06	0.42
45	10.10	10.10	10.10	0.34	0.34	1.00	7.16	7.16
46	5.13	5.13	10.25	0.00	0.00	0.70	0.00	0.00
47	14.73	14.73	21.00	0.00	0.00	0.00	0.00	0.00
48	43.39	43.39	33.86	0.05	0.05	1.60	1.50	1.50
49	43.39	43.39	33.86	0.05	0.05	1.60	1.50	1.50
50							25.20	143.99

Appendix A.1: Capsule Mass Moment Of Inertia

	P	Q	R	S	T	U	V	W
1	MZbar	Dx	Dy	Dz	MDx^2	MDy^2	MDz^2	xx transposed
2	Kg-m	meters	meters	meters	kg-m^2	kg-m^2	kg-m^2	kg-m^2
3	0.12	0.04	0.75	0.53	0.00	0.68	0.34	1.10
4	0.12	0.04	0.75	0.53	0.00	0.68	0.34	1.10
5	0.10	0.29	0.75	0.53	0.08	0.56	0.28	0.88
6	0.10	-0.71	0.75	0.53	0.50	0.56	0.28	0.88
7	0.10	-0.72	0.75	0.53	0.52	0.56	0.28	0.88
8	16.14	-0.21	0.50	0.28	2.03	11.53	3.62	174.39
9	2.50	-1.01	0.60	0.38	10.20	3.60	1.44	231.22
10	0.05	0.18	0.75	0.53	0.02	0.28	0.14	0.44
11	0.50	-0.09	0.75	0.53	0.04	2.81	1.40	4.24
12	0.22	-0.06	0.75	0.53	0.01	1.24	0.62	1.86
13	0.20	-1.05	0.75	0.53	2.21	1.13	0.56	1.69
14	11.60	0.54	0.33	0.11	6.50	2.43	0.27	8.11
15	0.05	0.59	0.75	0.53	0.17	0.28	0.14	0.44
16	0.50	0.59	0.75	0.53	1.74	2.81	1.40	5.30
17	0.24	0.59	0.75	0.53	0.84	1.36	0.68	4.07
18	0.05	0.79	0.75	0.53	0.31	0.28	0.14	0.44
19	0.05	0.84	0.75	0.53	0.35	0.28	0.14	0.44
20	0.80	0.79	0.75	0.53	4.99	4.50	2.25	6.78
21	2.00	1.09	0.65	0.43	11.88	4.23	1.85	6.20
22	0.10	0.67	0.75	0.53	0.44	0.56	0.28	0.85
23	0.10	0.67	0.75	0.53	0.44	0.56	0.28	0.85
24	0.10	0.67	0.75	0.53	0.44	0.56	0.28	0.85
25	2.34	-0.46	0.33	0.11	0.95	0.49	0.05	0.55
26	65.73	-0.16	0.30	0.08	3.06	10.75	0.76	18.00
27	13.50	-0.26	-0.05	-0.27	1.01	0.04	1.09	7.36
28	0.80	0.34	0.75	0.53	0.92	4.50	2.25	7.08

Appendix A.1: Capsule Mass Moment Of Inertia

	P	Q	R	S	T	U	V	W
29	0.80	0.34	0.75	0.53	0.92	4.50	2.25	7.08
30	0.80	0.34	0.75	0.53	0.92	4.50	2.25	8.08
31	0.50	0.04	0.75	0.53	0.01	2.81	1.40	4.59
32	0.50	0.04	0.75	0.53	0.01	2.81	1.40	4.59
33	0.50	0.04	0.75	0.53	0.01	2.81	1.40	4.59
34	1.08	0.04	-1.15	-1.37	0.00	0.71	1.01	1.73
35	1.72	0.04	-1.15	-1.37	0.00	1.14	1.61	2.75
36	2.58	0.04	-1.15	-1.37	0.00	1.71	2.42	4.13
37	2.26	-0.33	-1.15	-1.37	0.12	1.49	2.12	3.66
38	2.26	-0.33	-1.15	-1.37	0.12	1.49	2.12	3.66
39	2.26	-0.01	-1.15	-1.37	0.00	1.49	2.12	3.63
40	2.26	0.09	-1.15	-1.37	0.01	1.49	2.12	3.63
41	2.26	0.41	-1.15	-1.37	0.19	1.49	2.12	3.66
42	2.26	0.41	-1.15	-1.37	0.19	1.49	2.12	3.66
43	2.26	0.09	-1.15	-1.37	0.01	1.49	2.12	3.63
44	2.26	-0.01	-1.15	-1.37	0.00	1.49	2.12	3.64
45	21.05	-0.30	-0.15	-0.37	1.89	0.47	2.88	13.45
46	140.00	0.04	0.15	-0.07	0.32	4.50	0.98	10.61
47	0.00	0.04	0.85	0.63	0.06	28.90	15.88	59.51
48	48.00	-0.01	-0.75	-0.97	0.00	16.88	28.23	88.49
49	48.00	-0.01	-0.75	-0.97	0.00	16.88	28.23	88.49
50	401.72							813.29

Appendix A.1: Capsule Mass Moment Of Inertia

	X	Y
1	yy transposedzz transposed	
2	kg-m^2	kg-m^2
3	0.42	0.95
4	0.42	0.95
5	0.41	0.69
6	0.83	1.11
7	0.84	1.12
8	164.89	76.34
9	237.82	65.70
10	0.18	0.32
11	1.46	2.87
12	0.63	1.25
13	2.77	3.34
14	12.19	24.34
15	0.34	0.48
16	4.22	4.98
17	3.55	2.79
18	0.47	0.62
19	0.51	0.65
20	7.27	9.52
21	16.32	18.70
22	0.73	1.01
23	0.73	1.01
24	0.73	1.01
25	1.32	4.27
26	14.19	22.28
27	8.33	14.28
28	3.50	6.55

	X	Y
29	3.50	6.55
30	4.50	15.05
31	1.79	3.54
32	1.79	3.54
33	1.79	3.54
34	1.01	0.72
35	1.62	1.14
36	2.43	1.71
37	2.29	1.64
38	2.29	1.64
39	2.14	1.54
40	2.15	1.55
41	2.36	1.71
42	2.36	1.71
43	2.15	1.55
44	2.14	1.54
45	14.87	12.47
46	6.42	15.07
47	30.67	49.96
48	71.62	50.74
49	71.62	50.74
50	716.60	494.81

	A	B	C	D	E	F	G
1	System	Component	Mass Kg	Radias meters	length (Y) meters	height (Z) meters	width (x) meters
2							
3	Structure	structure	150.00				
4		Capsule interface	20.00	1.05			
5	OMS System	O.M.S. Engine	20.00		0.16	0.36	0.16
6		Fuel and tank	85.60	0.27			
7		Oxidizer and Tank	106.50	0.26			
8		Helium and tank	4.70	0.18			
9	Power generation	Generator	25.20		0.50	0.50	0.50
10	RCS System	Thruster #1	5.00		0.34	0.34	0.34
11		Thruster #2	5.00		0.34	0.34	0.34
12		Thruster #3	5.00		0.34	0.34	0.34
13		Thruster #4	5.00		0.34	0.34	0.34
14	TOTALS		432.00				

	H	I	J	K	L	M	N	O
1	lxx	lyy	lzz	Xbar	Ybar	Zbar	MXbar	MYbar
2	kg-m^2	kg-m^2	kg-m^2	meters	meters	meters	Kg-m	Kg-m
3	3.80	3.80	7.69	0.00	0.00	0.38	0.00	0.00
4	11.03	11.03	22.05	0.00	0.00	0.75	0.00	0.00
5	3.85	9.03	2.12	0.00	0.00	0.18	0.00	0.00
6	2.41	2.41	2.41	0.50	-0.50	0.34	42.80	-42.80
7	2.70	2.70	2.70	-0.50	0.50	0.34	-53.25	53.25
8	0.06	0.06	0.06	-0.50	-0.50	0.34	-2.35	-2.35
9	5.23	5.23	5.23	0.50	0.50	0.34	12.60	12.60
10	2.40	2.40	2.40	1.22	0.00	0.58	6.09	0.00
11	2.40	2.40	2.40	0.00	-1.22	0.58	0.00	-6.09
12	2.40	2.40	2.40	-1.22	0.00	0.58	-6.09	0.00
13	2.40	2.40	2.40	0.00	1.22	0.58	0.00	6.09
14							-0.20	20.70

	P	Q	R	S	T	U	V	W
1	MZbar	Dx	Dy	Dz	MDx^2	MDy^2	MDz^2	Ixx transposed
2	Kg-m	meters	meters	meters	kg-m^2	kg-m^2	kg-m^2	kg-m^2
3	56.25	0.00	-0.05	0.00	0.00	0.38	0.00	4.18
4	15.00	0.00	-0.05	-0.38	0.00	0.05	2.84	13.92
5	3.60	0.00	-0.05	0.19	0.00	0.05	0.74	4.65
6	29.10	-0.50	0.45	0.03	21.36	17.33	0.09	19.84
7	36.21	0.50	-0.55	0.03	26.68	32.22	0.12	35.03
8	1.60	0.50	0.45	0.03	1.18	0.95	0.01	1.01
9	8.57	-0.50	-0.55	0.03	6.29	7.62	0.03	12.88
10	2.90	-1.22	-0.05	-0.21	7.41	0.01	0.21	2.63
11	2.90	0.00	1.17	-0.21	0.00	6.82	0.21	9.43
12	2.90	1.22	-0.05	-0.21	7.42	0.01	0.21	2.63
13	2.90	0.00	-1.27	-0.21	0.00	8.03	0.21	10.65
14	161.93							116.83

	X	Y
1	Iyy transposed	Izz transposed
2	kg-m^2	kg-m^2
3	3.80	8.06
4	13.87	22.10
5	9.78	2.17
6	23.86	41.10
7	29.49	61.59
8	1.24	2.19
9	11.54	19.14
10	10.02	9.82
11	2.61	9.21
12	10.03	9.83
13	2.61	10.43
14	118.86	195.65

Appendix B

B.1 Integration Results

The equations obtained by integration as described in Chapter 1.4.2 were used with a spreadsheet program to obtain L/D for a number of radii of curvature. The results of these calculations are plotted in Figure B.1.

The radius of curvature was selected as 5 meters in consultation with the aerodynamic heating group. As can be seen from the figure, there was relatively little variation in aerodynamic factors with radius of curvature. Table B.1 presents the numerical results of this calculation for the radius of curvature. Alpha is given in degrees.

The next task involved in determining the actual capsule aerodynamics during reentry was a determination of the effect of CG offset on the L/D for a stable capsule. The free body diagram for a reentering capsule is shown in figure B.2.

The moments were summed about the geometrical center of the heat shield. The resulting equation was solved for the CG offset delta required for a given L/D at the point of maximum acceleration during reentry. These results are presented in Table B.2 and Figure B.3. From this data it was determined that a reasonable L/D value to attempt would be .25. A more detailed examination of the region approximating this value is presented in Table B.3 and Figure B.4

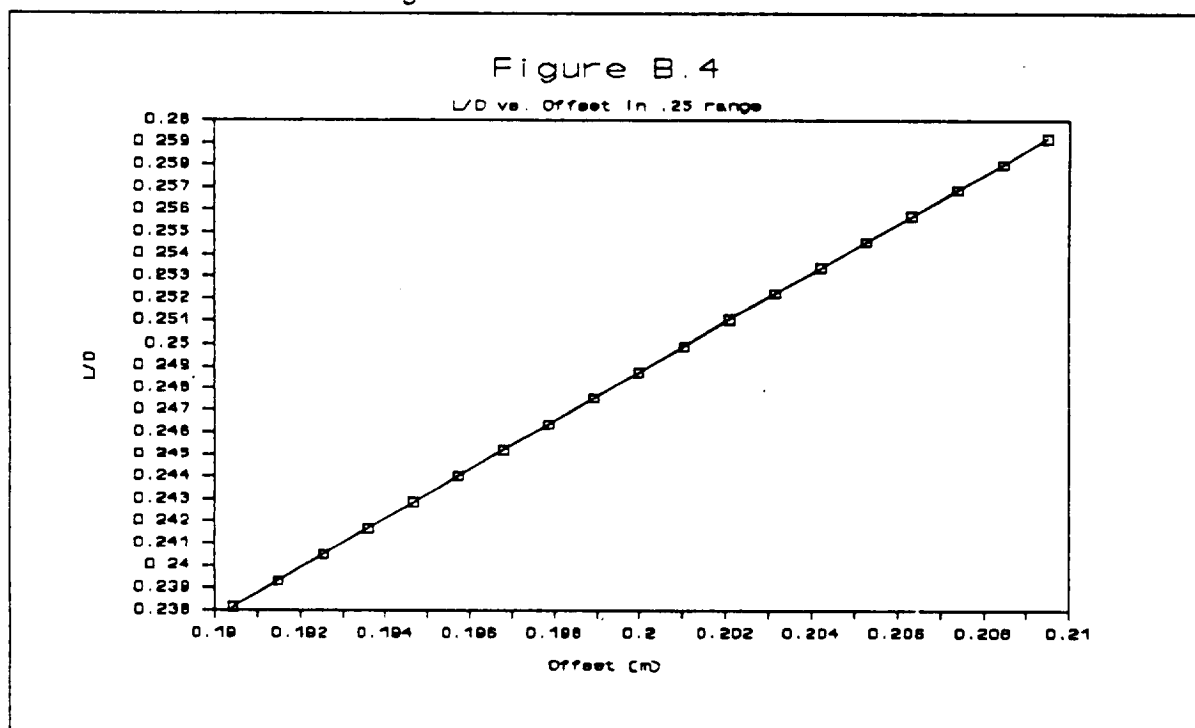


Figure B.1

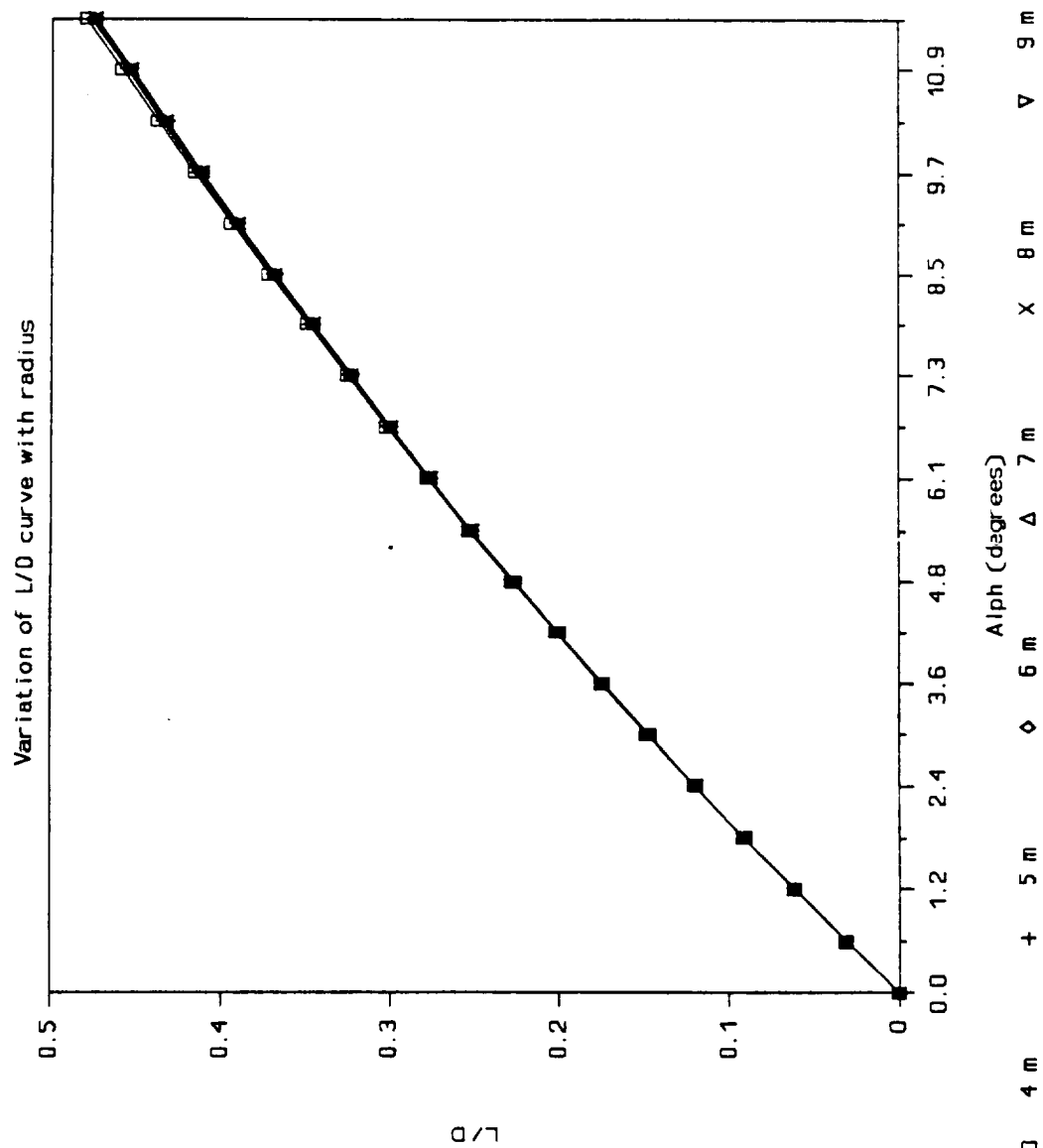


TABLE B.1: Variation of L/D for Alpha

ALPHA	Cp	Cd	Cl	L/D
0.0	-0.465	0.3104	2e-08	7e-08
0.6	-0.465	0.3152	0.0099	0.0313
1.2	-0.464	0.32	0.0197	0.0616
1.8	-0.464	0.3248	0.0295	0.0911
2.4	-0.464	0.3295	0.0394	0.1198
3.0	-0.463	0.3342	0.0492	0.1476
3.6	-0.463	0.3388	0.0591	0.1748
4.2	-0.462	0.3434	0.0689	0.2013
4.8	-0.461	0.3478	0.0787	0.2271
5.5	-0.46	0.3523	0.0885	0.2522
6.1	-0.459	0.3566	0.0983	0.2768
6.7	-0.458	0.3609	0.1081	0.3009
7.3	-0.457	0.3651	0.1179	0.3244
7.9	-0.456	0.3693	0.1277	0.3475
8.5	-0.454	0.3733	0.1374	0.3701
9.1	-0.453	0.3773	0.1471	0.3922
9.7	-0.451	0.3812	0.1569	0.414
10.3	-0.45	0.3849	0.1666	0.4354
10.9	-0.448	0.3886	0.1762	0.4565
11.5	-0.446	0.3922	0.1859	0.4772

TABLE B.2: Variation of CG ofset for L/D					
ALPHA	Cp	Cd	Cl	L/D	Offset (m)
0.0	-0.465	0.3104	2e-08	7e-08	5e-08
0.6	-0.465	0.3152	0.0099	0.0313	0.0225
1.2	-0.464	0.32	0.0197	0.0616	0.045
1.8	-0.464	0.3248	0.0295	0.0911	0.0675
2.4	-0.464	0.3295	0.0394	0.1198	0.09
3.0	-0.463	0.3342	0.0492	0.1476	0.1125
3.6	-0.463	0.3388	0.0591	0.1748	0.135
4.2	-0.462	0.3434	0.0689	0.2013	0.1575
4.8	-0.461	0.3478	0.0787	0.2271	0.1799
5.5	-0.46	0.3523	0.0885	0.2522	0.2023
6.1	-0.459	0.3566	0.0983	0.2768	0.2247
6.7	-0.458	0.3609	0.1081	0.3009	0.2471
7.3	-0.457	0.3651	0.1179	0.3244	0.2694
7.9	-0.456	0.3693	0.1277	0.3475	0.2918
8.5	-0.454	0.3733	0.1374	0.3701	0.314
9.1	-0.453	0.3773	0.1471	0.3922	0.3363
9.7	-0.451	0.3812	0.1569	0.414	0.3585
10.3	-0.45	0.3849	0.1666	0.4354	0.3807
10.9	-0.448	0.3886	0.1762	0.4565	0.4028
11.5	-0.446	0.3922	0.1859	0.4772	0.4249

Figure B.3

L/D vs. Offset

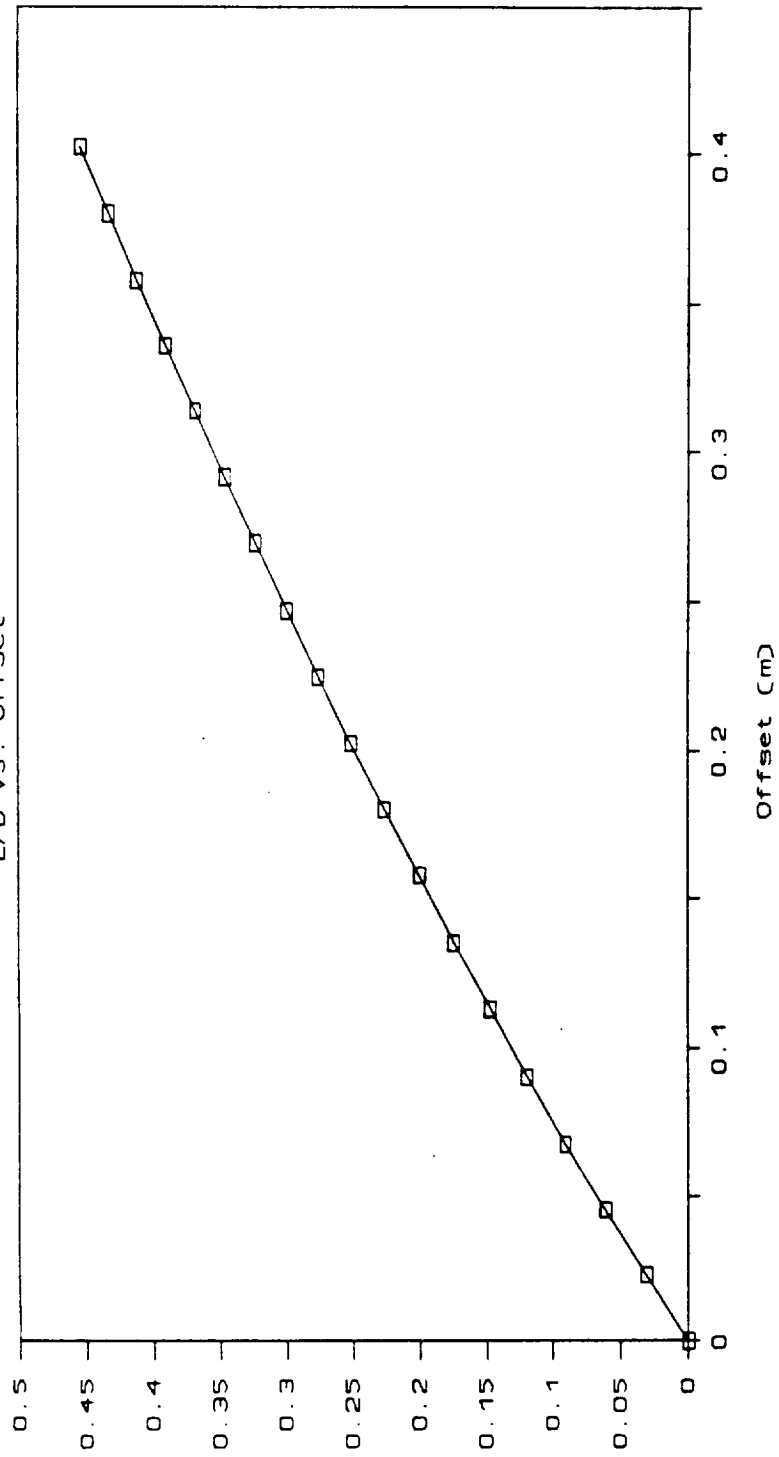


TABLE B.3: Variation of offset in range

ALPHA	Cp	Cd	Cl	L/D	Offset (m)
5.1	-0.461	0.3499	0.0833	0.2381	0.190
5.2	-0.461	0.3501	0.0838	0.2393	0.191
5.2	-0.461	0.3503	0.0843	0.2405	0.193
5.2	-0.461	0.3506	0.0847	0.2417	0.194
5.2	-0.461	0.3508	0.0852	0.2428	0.195
5.3	-0.461	0.351	0.0856	0.244	0.196
5.3	-0.461	0.3512	0.0861	0.2452	0.197
5.3	-0.461	0.3514	0.0866	0.2464	0.198
5.4	-0.461	0.3516	0.087	0.2475	0.199
5.4	-0.46	0.3518	0.0875	0.2487	0.200
5.4	-0.46	0.352	0.088	0.2499	0.201
5.4	-0.46	0.3522	0.0884	0.251	0.202
5.5	-0.46	0.3524	0.0889	0.2522	0.203
5.5	-0.46	0.3526	0.0894	0.2534	0.204
5.5	-0.46	0.3528	0.0898	0.2545	0.205
5.6	-0.46	0.3531	0.0903	0.2557	0.206
5.6	-0.46	0.3533	0.0907	0.2569	0.207
5.6	-0.46	0.3535	0.0912	0.258	0.208
5.6	-0.46	0.3537	0.0917	0.2592	0.210
5.7	-0.46	0.3541	0.0926	0.2616	0.212

Appendix C reliability breakdowns

RELIABILITY AREA	RELIABILITY		
abort system	0.98		
4 bolted lines	0.9999998		
2 explosive bolts		0.99999996	
each bolt			0.9998
1 ignition (for all 3 rockets)	0.983		
parachute	0.999916		
main		0.991	
back-up		0.991	
abort switches	0.999916		
computers	0.999916		
computer1		0.991	
computer2		0.991	
life support	0.999916		
power	0.999916		
structure	0.999916		

fig. C.1 :reliability breakdown for abort system

RELIABILITY AREA	RELIABILITY	
OM Rocket	0.999916	
helium tank	0.999988	
helium safety valve	0.999988	0.9965
redundant		0.9965
valve, pressure regulator,	0.999988	
isolation valve		0.9965
redundant		0.9965
fuel tank	0.999988	
oxidizer tank	0.999988	
fuel valve system	0.999988	0.9965
redundant		0.9965
oxidizer valve system	0.999988	0.9965
redundant		0.9965

fig. C.2 : breakdown for orbital maneuvering thruster

RELIABILITY AREA	RELIABILITY
survivability	0.999
power	0.999916
life support	0.999916
computers	0.999916
console	0.999916
OM Rocket	0.999916
heat shielding	0.999916
radiation shielding	0.999916
parachute system	0.999916
floatation	0.999916
search and retrieval	0.999916
structure	0.999916

fig. C.3 :reliability breakdown with successful taurus booste

RELIABILITY AREA	RELIABILITY
MISSION RELIABILITY	0.9
Taurus booster	0.95
life support	0.999916
power	0.999916
structure	0.999916
computers	0.999916
communications	0.9999
console	0.999916
OM Rocket	0.999916
payload(experiment)	0.956
ground control	0.9999
heat shielding	0.999916
radiation shielding	0.999916
floatation	0.999916
search and retrieval	0.999916
guidance control system	0.9999

fig. C.4 :breakdown for a mission reliability of .9

RELIABILITY AREA	RELIABILITY		
life support	0.999916		
system 1	0.991		
fan		0.999	
water separator		0.999	
electric heater		0.999	
LiOH cannister		0.999	
coolant pump		0.999	
radiator		0.999	
oxygen system		0.999	
tank			0.9997
pump			0.9997
regulator			0.9997
nitrogen system		0.999	
tank			0.9997
pump			0.9997
regulator			0.9997
system2	0.991		
fan		0.999	
LiOH cartridge		0.999	
sublimator/heat ex.		0.999	
water pump		0.999	
water pump2		0.999	
centrifical water sep.		0.999	
pressure suit		0.999	
oxygen system		0.999	
tank			0.9997
pump			0.9997
regulator			0.9997
nitrogen system		0.999	
tank			0.9997
pump			0.9997
regulator			0.9997

fig.C.5 :breakdown for life support system

Appendix D: Reentry Heating Analysis

The reentry analysis, as explained in section 1.5, is based on the assumption of thermodynamic equilibrium. The four terms of the equilibrium equation are the heating rates for convection, radiation, dissociation, and ablation. They yield the equation:

$$Q_{\text{convective}} = Q_{\text{radiative}} + Q_{\text{dissociative}} + Q_{\text{ablative}}$$

This is a quartic equation of wall temperature which can best be solved for by computer. The program developed inputs the velocity - altitude profile supplied by mission analysis. It then calculates the density and temperature at each altitude, using the standard atmosphere model (Anderson, 1985). From these temperatures and the velocity, the mach number at each point is determined. we now have all the variables in the equation. Each term is computed as follows:

$$Q_{\text{convective}} = \rho_{\infty}^{1/2} V_{\infty}^3 [1.83 \times 10^{-8} R^{-1/2} (1 - \frac{T_w}{T_{\text{atm}}(1 + 0.2M^2)})]$$

$$Q_{\text{radiative}} = \epsilon \sigma T^4 = (0.8)(5.67 \times 10^{-8}) T^4 = 4.53 \times 10^{-8} T^4$$

$$Q_{\text{dissociative}} = \rho V (0.8438 T - 67.92)$$

$$Q_{\text{ablative}} = 101.28 T$$

Once each of these terms is determined, the program iterates the equation in order to calculate the correct value of equilibrium temperature. After the temperature has been found, it plugs it back into the ablative term to determine the heat absorbed by the ablator. The results for the Taurus LMS and the final ablative heat shield are given in table D.1. It may be noted that the program gives inaccurate results at very high altitudes and at low speeds. In both of these cases, however, there is relatively little aerodynamic heating. The heating rates were then summed over the surface area of the capsule and over the time of reentry. The total heat absorbed by the capsule was 148.6 MJ. In order to make an analysis of a radiative heat shield the program was modified to neglect the ablative term and give only surface temperature. These results are given in table D.2.

The heating rates for the lifting body concept were also required. A simple modification to the program yielded these rates. Due to the extreme number of data points and the general nature of the lifting body concept, the time interval was increased to 200 seconds. The radius of curvature and planform area were also adjusted. The heat shield was assumed to be an ablative type, due to the lower mass results for a capsule. Three different biconical lifting bodies, each with a different L/D, were analyzed. The results, as expected, were much different than those of the capsule. The total heat loads of

the biconics varied from 4 to nearly 8 times the load for the capsule. Clearly, the increased mass of the required heat shield is a major disadvantage to the lifting body concept. This is one of the primary reasons this concept was rejected. See appendix Q for a complete discussion of the lifting body concept. The heating results for the lifting bodies are given in tables D.3,4, and 5.

The heating rate for the wall of the capsule was determined as in section 6.6.2. The rate is assumed proportional to the inverse of the root of the distance from the leading edge. I assumed that the heating rate would be the same at 0.025 meters from the main heat shield as at the stagnation point. Assuming a

mass distribution proportional to $\frac{1}{\sqrt{x}}$, the proportionality constant becomes:

$$c = (148.6/3.46)(.025)^{1/2} = 0.936$$

Integrating over the surface of the capsule gives a secondary heat shield mass of 9.064 kg.

References:

Anderson, John D: *Introduction to Flight*, McGraw-Hill, Inc., New York, 1985

[illegible]

ORIGINAL PAGE IS
OF POOR QUALITY

Figure D.1 -cont.

```

10000 REM CALCULATION OF TEMP AND DENSITY
10010 IF H(11)<1050000 THEN 10050
10020 TATN(11)=225.66
10030 DEN(11)=1.2079E-07*EXP(-S.8100001*(287+225.66)*(H(11)-1050000))
10040 RETURN
10050 IF H(11)<800000 THEN 10100
10060 TATN(11)=165.66-.004*(H(11)-800000)
10070 DEN(11)=2.3087E-06*(TATN(11)+165.66)*(-S.8100001*(-.004+287)+1)
10080 RETURN
10100 IF H(11)<790000 THEN 10150
10110 TATN(11)=165.66
10120 DEN(11)=2.23399E-05*EXP(-S.8100001*(287+165.66)*(H(11)-790000))
10130 RETURN
10150 IF H(11)<530000 THEN 10200
10160 TATN(11)=282.66-.0045*(H(11)-530000)
10170 DEN(11)=1.5781E-04*(TATN(11)+282.66)*(-S.8100001*(-.0045+287)+1)
10180 RETURN
10200 IF H(11)<470000 THEN 10250
10210 TATN(11)=282.66
10220 DEN(11)=.001588E+EXP(-S.8100001*(287+282.66)*(H(11)-470000))
10230 RETURN
10250 IF H(11)<250000 THEN 10300
10260 TATN(11)=216.66-.002*(H(11)-250000)
10270 DEN(11)=.04063E+*(TATN(11)+216.66)*(-S.8100001*(-.002+287)+1)
10280 RETURN
10300 IF H(11)<110000 THEN 10350
10310 TATN(11)=216.66
10320 DEN(11)=.3648*EXP(-S.8100001*(287+216.66)*(H(11)-110000))
10330 RETURN
10350 TATN(11)=288.66-.0085*H(11)
10360 DEN(11)=1.225*(TATN(11)+288.66)*(-S.8100001*(-.0085+287)+1)
10370 RETURN
50000 REM VELOCITY DATA (6 OF ITEMS) (END OF CURVED VELOCITY)
50010 DATA 48.8,0.7804,7807,7810,7814,7817,7820,7822,7825,7828,7829
50020 DATA 7828,7827,7822,7811,7780,7764,7717,7647,7636,7607
50030 DATA 7228,7020,6781,6560,6351,6158,5970,5819,5687,5571
50040 DATA 5466,5367,5272,5178,5080,4975,4856,4722,4586,4382
50050 DATA 4171,3990,3837,3690,3509
50100 REM 1111025 DATA
50110 DATA 111288,111586,111688,108835,106018,103152,100288,97342,94418
50120 DATA 91513,88618,85667,82688,79653,76557,73351,71142,68543,66166,64106
50130 DATA 62440,61227,60822,60387,60361,60782,61244,61861,62618,62875
50140 DATA 63262,63240,63181,63188,63086,63117,63027,62962,63162,63222
50150 DATA 64052,62228,61123,59226,58804

```

Table D.1: Ablative TPS Heating Data

Velocity (m/s)	Altitude (m)	Time (sec)	T(wall) (K)	Surface Heating (kW/m ²)	Total Heating Rate (kW)	Total Heat (MJ)
7804	117256	10	52.6	5.334	18.474	0.09
7807	114485	20	65.0	6.584	22.804	0.21
7810	111688	30	80.3	8.142	28.199	0.26
7814	108865	40	99.6	10.089	34.946	0.32
7817	106019	50	123.6	12.516	43.350	0.39
7820	103149	60	205.2	20.792	72.016	0.58
7823	100258	70	251.2	25.442	88.119	0.80
7826	97347	80	310.3	31.436	108.881	0.99
7828	94418	90	386.7	39.165	135.650	1.22
7829	91473	100	483.7	48.988	169.675	1.53
7829	88518	110	610.5	61.833	214.166	1.92
7827	85557	120	759.1	76.879	266.278	2.40
7822	82599	130	912.4	92.407	320.061	2.93
7811	79655	140	1064.8	107.846	373.535	3.47
7793	76745	150	1195.5	121.078	419.365	3.96
7764	73894	160	1308.3	132.501	458.930	4.39
7717	71142	170	1406.4	142.444	493.370	4.76
7647	68543	180	1488.5	150.757	522.163	5.08
7545	66168	190	1551.2	157.107	544.156	5.33
7407	64106	200	1591.4	161.182	558.269	5.51
7229	62440	210	1606.2	162.680	563.457	5.61
7020	61237	220	1596.0	161.651	559.894	5.62
6791	60523	230	1563.4	158.338	548.421	5.54
6560	60267	240	1514.1	153.346	531.129	5.40
6341	60361	250	1454.6	147.326	510.278	5.21
6143	60789	260	1391.0	140.881	487.954	4.99
5970	61344	270	1328.1	134.509	465.885	4.77
5819	61951	280	1268.5	128.478	444.995	4.55
5687	62519	290	1214.5	123.008	426.051	4.36
5571	62975	300	1167.7	118.267	409.628	4.18
5466	63263	310	1128.6	114.308	395.919	4.03
5367	63340	320	1097.3	111.139	384.940	3.90
5273	63181	330	1074.4	108.812	376.882	3.81
5178	62768	340	1058.4	107.195	371.280	3.74
5080	62098	350	1048.6	106.206	367.856	3.70
4974	61177	360	1042.9	105.626	365.845	3.67
4856	60027	370	1038.6	105.194	364.350	3.65
4722	58682	380	1032.8	104.598	362.287	3.63
4566	57193	390	1020.8	103.392	358.107	3.60
4383	55622	400	998.3	101.104	350.183	3.54
4171	54042	410	960.9	97.316	337.063	3.44
3930	52528	420	905.0	91.653	317.449	3.27
3667	51136	430	836.0	84.667	293.251	3.05
3390	49896	440	749.5	75.091	260.084	2.77
3109	48804	450	650.2	65.851	228.082	2.44

Total Heat (MJ) Absorbed by Capsule =

148.60

Table D.2: Radiative TPS Heating data

Velocity (m/s)	Altitude (m)	Time (sec)	T(wall) (K)
7804	117256	10	583
7807	114485	20	614.45
7810	111688	30	647.87
7814	108865	40	683.51
7817	106019	50	721.33
7820	103149	60	819.42
7823	100258	70	862.53
7826	97347	80	910.866
7828	94418	90	965.44
7829	91473	100	1027.393
7829	88518	110	1102.47
7827	85557	120	1188.8
7822	82599	130	1281.34
7811	79655	140	1379.65
7793	76745	150	1469.73
7764	73894	160	1551.82
7717	71142	170	1626.33
7647	68543	180	1690.62
7545	66168	190	1740.84
7407	64106	200	1773.48
7229	62440	210	1785.42
7020	61237	220	1776.82
6791	60523	230	1749.6
6560	60267	240	1709.65
6341	60361	250	1662.07
6143	60789	260	1612.16
5970	61344	270	1563.91
5819	61951	280	1519.29
5687	62519	290	1479.72
5571	62975	300	1446.12
5466	63263	310	1418.55
5367	63340	320	1396.75
5273	63181	330	1380.8
5178	62768	340	1369.74
5080	62098	350	1362.8
4974	61177	360	1358.48
4856	60027	370	1355.04
4722	58682	380	1350.38
4566	57193	390	1341.52
4383	55622	400	1325.388
4171	54042	410	1299.39
3930	52528	420	1261.47
3667	51136	430	1215.38
3390	49896	440	1158.64
3109	48804	450	1093.83

Table D.3: Biconical Heating Rates; L/D = 2.5

Time (sec)	T(wall) (K)	Wall Heating (kW/m ²)	Total Heating Rate (kW)	Total Heat (MJ)
200	199.4	20.198	69.959	6.996
400	1679.7	170.117	589.217	65.918
600	39.1	3.964	13.729	60.295
800	816.7	82.712	286.482	30.021
1000	1538.4	155.805	539.647	82.613
1200	859.6	87.064	301.554	84.120
1400	1634.1	165.499	573.222	87.478
1600	906.1	91.773	317.865	89.109
1800	933.8	94.571	327.556	64.542
2000	664.7	67.323	233.180	56.074
2200	273.5	27.697	95.933	32.911
2400	87.7	8.879	30.753	12.669
2600	44.5	4.506	15.607	4.636

Total Heat (MJ) Absorbed by Capsule = 677.380

Table D.4: Biconical Heating Rates; L/D = 3.0

Time (sec)	T(wall) (K)	Wall Heating (kW/m ²)	Total Heating Rate (kW)	Total Heat (MJ)
200	145.6	14.746	51.073	5.107
400	1608.0	162.862	564.087	61.516
600	576.8	58.422	202.352	76.644
800	20.9	2.119	7.340	20.969
1000	628.0	63.605	220.301	22.764
1200	1613.0	163.361	565.818	78.612
1400	110.4	11.183	38.734	60.455
1600	1598.2	161.863	560.627	59.936
1800	457.3	46.312	160.407	72.103
2000	1565.7	158.573	549.234	70.964
2200	1031.4	104.460	361.808	91.104
2400	1509.5	152.882	529.520	89.133
2600	1339.6	135.675	469.923	99.944
2800	1003.3	101.618	351.964	82.189
3000	699.4	70.832	245.334	59.730
3200	93.9	9.510	32.938	27.827

Total Heat (MJ) Absorbed by Capsule = 978.998

Table D.4: Biconical Heating Rates; L/D = 3.5

Time (sec)	T(wall) (K)	Wall Heating (kW/m ²)	Total Heating Rate (kW)	Total Heat (MJ)
200	145.6	14.746	51.073	5.107
400	1567.7	158.890	550.331	60.140
600	27.0	2.736	9.475	55.981
800	1571.6	159.177	551.324	56.080
1000	882.2	89.350	309.471	86.079
1200	1563.4	158.341	548.430	85.790
1400	805.4	81.568	282.520	83.095
1600	1544.0	156.379	541.634	82.415
1800	570.5	58.793	203.634	74.527
2000	1523.7	154.318	534.495	73.813
2200	1508.0	152.739	529.025	106.352
2400	1480.3	149.926	519.283	104.831
2600	1411.7	142.974	495.206	101.449
2800	1194.4	120.974	419.005	91.421
3000	386.1	39.107	135.453	55.446
3200	17.3	1.748	6.055	14.151

Total Heat (MJ) Absorbed by Capsule = 1136.678

Appendix E : Orbital Rendezvous

E.1 : Space Station Rendezvous

This is used as an example of rendezvous requirements and should not be interpreted as the only rendezvous scheme. Everything mentioned in this section is applicable to all rendezvous situations but since the Space Station as a very important part of America's and the World's space programs it is chosen as an example.

E.2 : Launch Window

In order to successfully rendezvous with anything in orbit without too many high power maneuvers a very tight launch window must be considered. Since one of the objectives is to be able to launch as quickly as possible it was decided that for maximum chance at success and conserving fuel at the same time the launch window should be about eight minutes. This would yield ideal launch conditions at the center of the launch window and hopefully give enough flexibility that the capsule will be able to launch easily at any time after pre-launch is done.

The Space Station's orbit has an inclination of 28.5° and a varying circular altitude between 450 and 500 kilometers. Since these calculations deal with the maximum capabilities of the spacecraft, it will always assumed it is in a 500 kilometer circular orbit. The nodal regression of this orbit is -7.5° degrees per solar day, this will allow approximately two launches per day or a launch opportunity every 11 hours and 45 minutes.

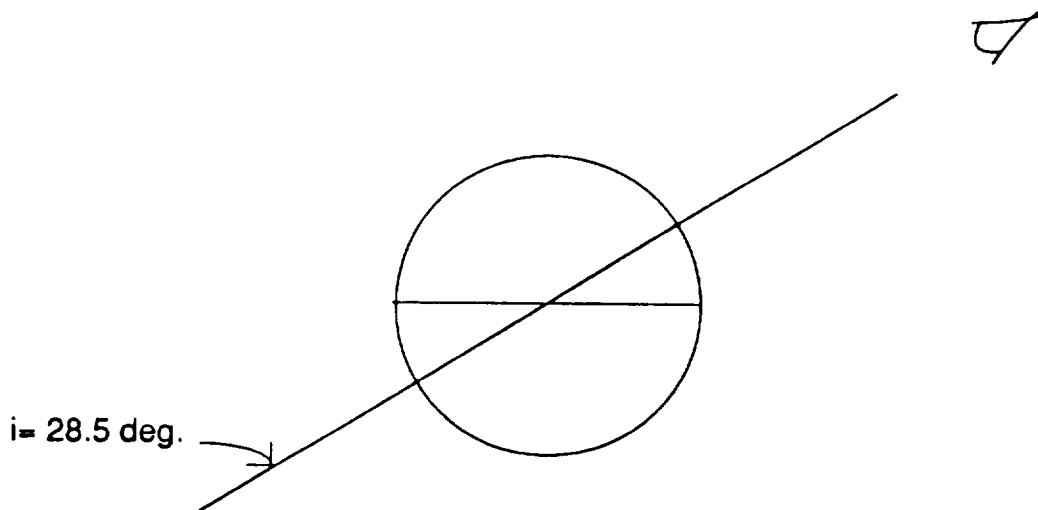


Fig. 1 : View of the Space Station orbit in it's plane

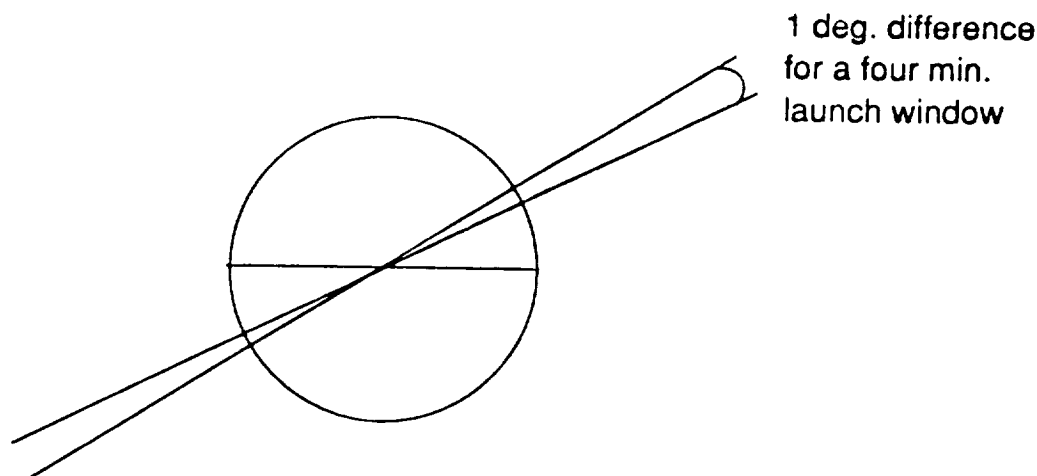


Fig. 2 : Two 28.5° orbits viewed in plane

This view is of where two orbits at 28.5° achieved at different times would intersect. The correction for this situation is what limits the launch window since as stated before plane changes are expensive. The allowance of four minutes to either side of the launch window would make a difference of $.9792^\circ$ at the extreme ends of the launch window. The ΔV for this correction would be about 130 meters/second.

E.3 : Where to launch to

There are many parameters involved in the decision on where to make initial orbital insertion. Since the capability of a quick rendezvous is desirable, the capsule may end up launching into a situation where it is extremely out of phase with the Space Station. Therefore there are two launch and rendezvous schemes : 1. launching into a lower chase orbit with more fuel and going through the chase routine and 2. launching directly to the Space Station orbit and performing an epoch maneuver. These are explained in a later section.

E.3.1 : About the Space Stations Orbital Characteristics

From the Space Stations period of 94.61 min. and its nodal regression rate of -7.5° per day it can be determined that its orbit passes around the Earth every 23.5 hours. The Space Station itself progresses in its orbit by 10% or 36° every 23.5 hours. This is useful since the epoch maneuver requires nearly twice the ΔV of the chase maneuver and this orbital progression will allow rather improved conditions after a short time.

E.4 : Orbital Insertion Errors

The insertion errors for the Taurus booster are as follows :

$\pm .2$ deg. in plane
 ± 5 km. in apogee height

The corrective ΔV for the plane error would be a maximum of 27.2 m/s for insertion at a 200 km. altitude. A total ΔV of 3.0 m/s is required to correct the apogee error at this same altitude.

E.5 : After burnout and coast

After burnout and coast phases are completed the booster's payload stage will circularize the orbit. The L.M.S. will make then up to three orbits to allow for accurate orbit determination. Once the correct orbit is determined corrective maneuvers will be performed if beneficial. After this, rendezvous procedures will begin. Rendezvous procedures involve a number of maneuvers which will have to be performed during the first day and a half or approximately 20 - 25 orbits to stay within the limited mission duration of three days and still allow time for proximity maneuvers and re-entry.

E.5.1 : The Chase Maneuver

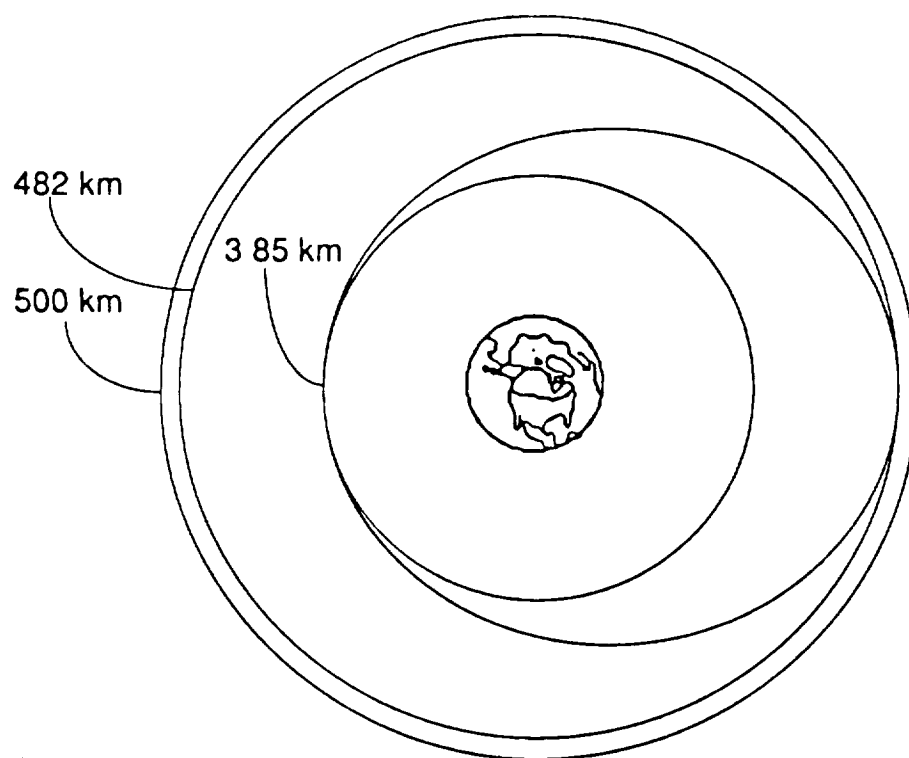


Fig. 3 : Chase Maneuver for Space Station Rendezvous

For the chase maneuver, the capsule will launch into a lower, faster period orbit and proceed to catch-up to the target until conditions are ideal to transfer to the target orbit and rendezvous. Once again working in the context of maximum maneuvers, it is assumed that the capsule will be launching into a situation where it is 180° or less out of phase behind the Space Station. For this situation the calculations show that a 20 orbit catch would require launching into a circular orbit at an altitude of 385 km. Since the error in apogee is at most 5 km., it would not be corrected unless the new catch-up rate would extend the mission beyond the 1.5 day limit for rendezvous.

The catch-up rate for the 385 km. orbit is 9.03° per Space Station orbit and in the final phase would include a Hohmann transfer to within 18 km. of the Space Stations orbit requiring a ΔV of approximately 63.69 m/sec. For phase differences of more than 180° more velocity change would be needed but this may be easier since the L.M.S. can carry a greater payload to the lower orbit.

E.5.2 : The Epoch Maneuver

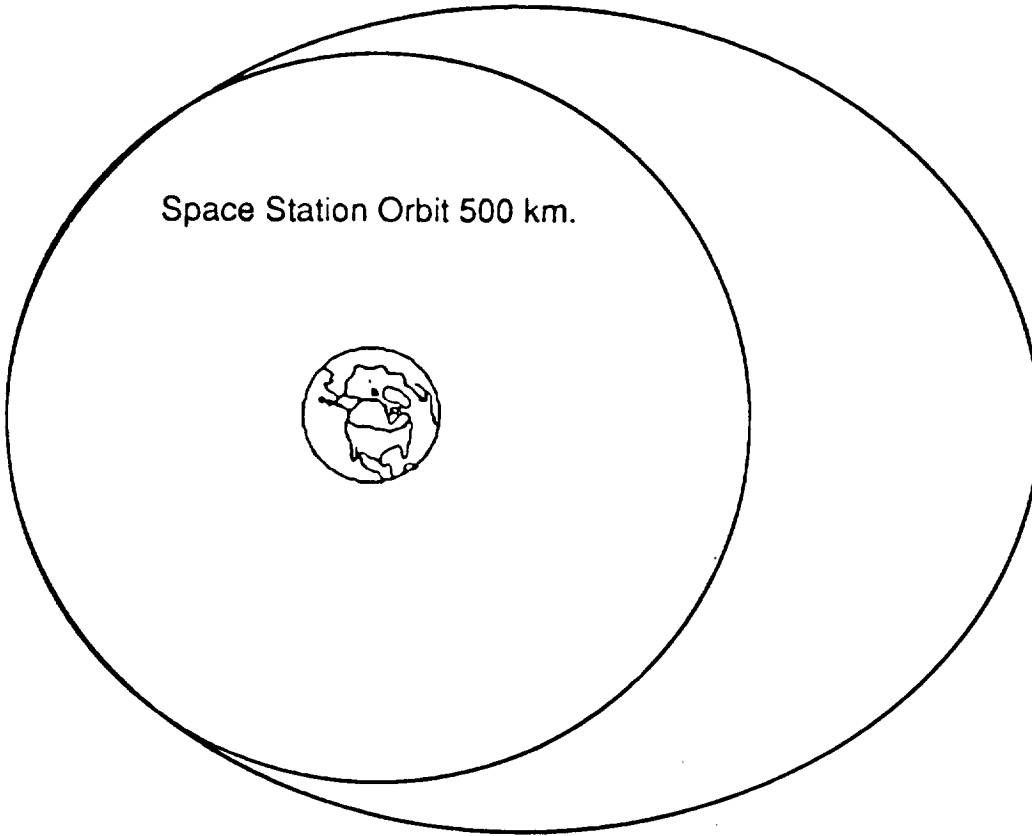


Fig. 4 : Epoch Maneuver

This will be the rendezvous scheme if the capsule is going to end up 90° or less out of phase in front of the Space Station. It requires nearly twice the power of the chase maneuver but is more efficient for this maneuver since it is designed to

slow down and let the Space Station catch-up with it. For this scenario, the capsule is launched directly into the Space Stations orbit and spends the same three orbits to allow for accurate orbit determination. After corrections are made to make sure that the capsule is in the Space Stations orbit, a burn is calculated that would place the spacecraft in an elliptic orbit that intersects the Space Station's orbit at it's perigee. This orbit has a slightly longer period than the Station's and is designed to allow the capsule to be in close proximity of the Station after 20 orbits of the Space Station. For the case of being 90° out of phase initially a 20 orbit catch up would be at a rate of 4.5° per Space Station orbit and require a total ΔV of about 60 m/sec. It can be seen from this that the Epoch maneuver uses nearly the same amount of fuel as the Chase maneuver but only does half as much, but it is still the most efficient for this situation.

E.5.3 : Situations In-between The Ideal Maneuvers

As stated before the Space Stations position in it's orbit will change by 36° per day and therefore a one day wait may yield better rendezvous conditions. In the case of emergency launch, it is hoped that by launching to a lower altitude, the fuel gain will be enough to allow Chase rendezvous maneuvers for up to 270° phase differences. There can be no fuel adjustment for the Epoch maneuver since it is performed by a direct launch to the Space Station orbit and is utilizing it's maximum mass to orbit already.

E.6 : Before Proximity Maneuvers

When the capsule achieves orbit within the specified 18 km. range of the Space Stations orbit either ground control or a type of onboard tracking system, like rendezvous radar, will be used to assess the final approach and determine if any adjustments are needed to give the capsule it's best approach possible. These adjustments will likely be done with the attitude control system since they tend to be more effective for small adjustments than the orbital maneuvering system.

E.7 : Terminal Phase Initiation

This maneuver will follow the procedure used for rendezvous on Space Shuttle missions. An altitude of 482 km. will be achieved with a slight catch-up rate with respect to the Space Station. When the angle between the local horizontal of the capsule and the Space Station is 27° , with the capsule behind the Space Station, a burn will be made so that the capsule obtains proximity relations within 130° of the capsules new orbit. The ΔV for this maneuver would be approximately 12 m/s and would vary with the Space Stations altitude (Rendezvous, 1983). This maneuver allows for the capsule Space Station system to be treated as an inertial system for the proximity maneuvers. During the coast phase of this burn sequence corrective maneuvers will be made to assure the proximity relation.

E.8 : Total ΔV Required for Space Station Docking

The current total ΔV for a Space Station rendezvous is currently 442 m/sec. This breaks down as follows:

Insertion corrections	
Plane change	= 67 m/sec
Apogee height	= 3 m/sec
Launch window correction	= 130 m/sec
Rendezvous	= 70 m/sec
Re-entry (currently)	= 160 m/sec
Terminal phase initiation	= 12 m/sec

The total ΔV of 442 m/s is currently well beyond the capabilities of the Taurus LMS. Even if the launch window were cut to zero time the capsule would only be capable of Space Station rendezvous if there were no insertion plane error.

E.9 : Explanation of Included Plots

Included are five plots to help clarify the requirements and trade-offs involved in coming to the final rendezvous conclusions.

Plot 1 is catch-up rate vs. Altitude, this was used to evaluate a chase altitude with respect to how quickly it would allow rendezvous with the target (Space Station). A catch-up rate was chosen based on it's capacity to achieve proximity relations within the specified day and a half time frame. This plot can be approximated as a linear relationship.

$$\text{Catch-up Rate} = 39.2457 - .0784774 * \text{Altitude in kilometers}$$

Plot 2 is ΔV vs. chase altitude, this was used to make sure that the rendezvous mission could be performed within the fuel constraints. The object was to find the best or most effective catch-up rate with the least ΔV required. This plot can also be approximated as linear.

Plot 3 shows the relation between catch-up rate and ΔV for various altitudes. This relationship is linear in the same respect as the previous plot relating ΔV and chase altitude.

$$\Delta V = 285.9494 - .574312 * \text{altitude in kilometers}$$

Plot 4 shows the relation between ΔV and time to rendezvous. The relationship expressed in the plot is based on the number of time required to rendezvous for two phase differences; 180° and 90°. The relationship used to make this plot allows for the determination of time to rendezvous in terms of the ΔV required. This relationship is not linear.

Plot 5 extends the relationship in plot 4 to an altitude based analysis. once again this relationship is not linear. This allows for the determination of initial orbital altitude based on the time to rendezvous.

Plot 6 shows the relation between catch-up rate and the total ΔV . This relationship is almost linear but it has a slight curve to which can be seen by looking at the plot from an oblique angle. The altitude of the spacecraft will always initially be that of the Space Station. It is clear here that the epoch maneuvers do require nearly twice the amount of total ΔV for a similar Chase maneuver scenario.

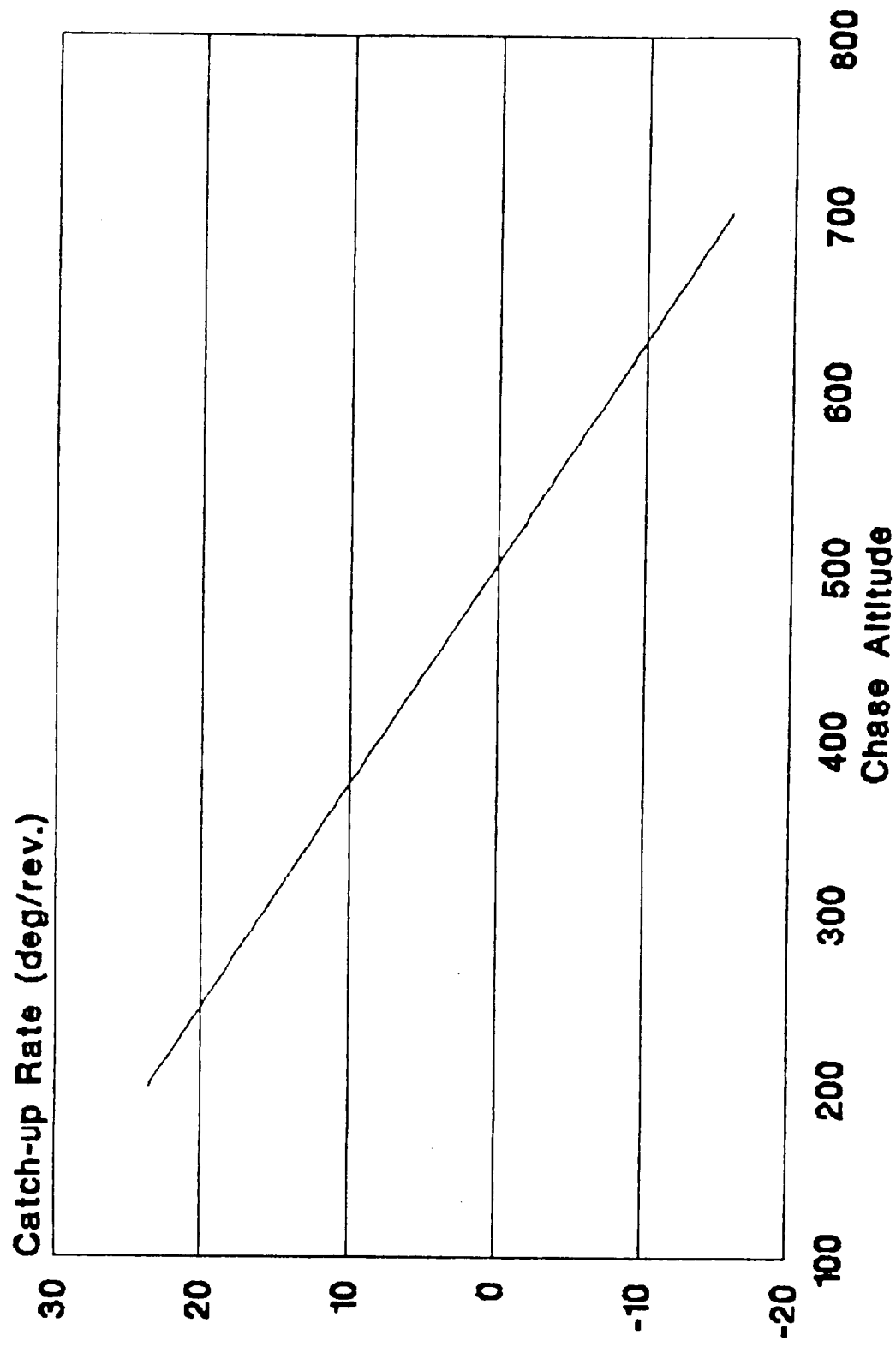
Chase Alt.	d	Chase Vel.	Hohmann V1	V2	Delta V		Catch Rate	Period	Catch Period
					km/s	m/s			
200.00	300.00	7.78	7.87	7.53	.17	170.64	23.62	845.03	88.49
205.00	295.00	7.78	7.86	7.53	.17	167.68	23.22	845.99	88.59
210.00	290.00	7.78	7.86	7.54	.16	164.73	22.83	846.95	88.69
215.00	285.00	7.78	7.85	7.54	.16	161.78	22.43	847.92	88.79
220.00	280.00	7.77	7.85	7.54	.16	158.83	22.04	848.88	88.89
225.00	275.00	7.77	7.84	7.54	.16	155.89	21.65	849.85	89.00
230.00	270.00	7.77	7.84	7.54	.15	152.94	21.25	850.81	89.10
235.00	265.00	7.76	7.83	7.54	.15	150.01	20.86	851.78	89.20
240.00	260.00	7.76	7.83	7.54	.15	147.07	20.47	852.75	89.30
245.00	255.00	7.76	7.83	7.55	.14	144.14	20.07	853.71	89.40
250.00	250.00	7.75	7.82	7.55	.14	141.21	19.68	854.68	89.50
255.00	245.00	7.75	7.82	7.55	.14	138.29	19.29	855.65	89.60
260.00	240.00	7.75	7.81	7.55	.14	135.37	18.89	856.61	89.70
265.00	235.00	7.75	7.81	7.55	.13	132.45	18.50	857.58	89.81
270.00	230.00	7.74	7.80	7.55	.13	129.53	18.10	858.55	89.91
275.00	225.00	7.74	7.80	7.56	.13	126.62	17.71	859.52	90.01
280.00	220.00	7.74	7.80	7.56	.12	123.72	17.32	860.49	90.11
285.00	215.00	7.73	7.79	7.56	.12	120.81	16.92	861.46	90.21
290.00	210.00	7.73	7.79	7.56	.12	117.91	16.53	862.43	90.31
295.00	205.00	7.73	7.78	7.56	.12	115.01	16.14	863.40	90.41
300.00	200.00	7.73	7.78	7.56	.11	112.12	15.74	864.37	90.52
305.00	195.00	7.72	7.77	7.56	.11	109.22	15.35	865.34	90.62
310.00	190.00	7.72	7.77	7.57	.11	106.33	14.96	866.31	90.72
315.00	185.00	7.72	7.76	7.57	.10	103.45	14.56	867.28	90.82
320.00	180.00	7.71	7.76	7.57	.10	100.57	14.17	868.25	90.92
325.00	175.00	7.71	7.76	7.57	.10	97.69	13.78	869.23	91.03
330.00	170.00	7.71	7.75	7.57	.09	94.81	13.38	870.20	91.13
335.00	165.00	7.71	7.75	7.57	.09	91.94	12.99	871.17	91.23
340.00	160.00	7.70	7.74	7.57	.09	89.07	12.59	872.15	91.33
345.00	155.00	7.70	7.74	7.58	.09	86.20	12.20	873.12	91.43
350.00	150.00	7.70	7.73	7.58	.08	83.34	11.81	874.09	91.53
355.00	145.00	7.69	7.73	7.58	.08	80.48	11.41	875.07	91.64
360.00	140.00	7.69	7.73	7.58	.08	77.62	11.02	876.04	91.74
365.00	135.00	7.69	7.72	7.58	.07	74.77	10.63	877.02	91.84
370.00	130.00	7.69	7.72	7.58	.07	71.92	10.23	877.99	91.94
375.00	125.00	7.68	7.71	7.58	.07	69.07	9.84	878.97	92.05
380.00	120.00	7.68	7.71	7.59	.07	66.23	9.45	879.95	92.15
385.00	115.00	7.68	7.70	7.59	.06	63.39	9.05	880.92	92.25
390.00	110.00	7.67	7.70	7.59	.06	60.55	8.66	881.90	92.35
395.00	105.00	7.67	7.70	7.59	.06	57.71	8.27	882.88	92.45
400.00	100.00	7.67	7.69	7.59	.05	54.88	7.87	883.86	92.56
405.00	95.00	7.67	7.69	7.59	.05	52.05	7.48	884.83	92.66
410.00	90.00	7.66	7.68	7.59	.05	49.23	7.08	885.81	92.76
415.00	85.00	7.66	7.68	7.60	.05	46.41	6.69	886.79	92.86
420.00	80.00	7.66	7.67	7.60	.04	43.59	6.30	887.77	92.97
425.00	75.00	7.65	7.67	7.60	.04	40.77	5.90	888.75	93.07
430.00	70.00	7.65	7.67	7.60	.04	37.96	5.51	889.73	93.17
435.00	65.00	7.65	7.66	7.60	.04	35.15	5.12	890.71	93.28
440.00	60.00	7.65	7.66	7.60	.03	32.34	4.72	891.69	93.38
445.00	55.00	7.64	7.65	7.60	.03	29.54	4.33	892.67	93.48
450.00	50.00	7.64	7.65	7.60	.03	26.74	3.94	893.65	93.58
455.00	45.00	7.64	7.65	7.61	.02	23.94	3.54	894.64	93.69
460.00	40.00	7.63	7.64	7.61	.02	21.14	3.15	895.62	93.79
465.00	35.00	7.63	7.64	7.61	.02	18.35	2.76	896.60	93.89
470.00	30.00	7.63	7.63	7.61	.02	15.56	2.36	897.58	93.99
475.00	25.00	7.63	7.63	7.61	.01	12.78	1.97	898.57	94.10
480.00	20.00	7.62	7.62	7.61	.01	10.00	1.57	899.55	94.20
485.00	15.00	7.62	7.62	7.61	.01	7.22	1.18	900.53	94.30
490.00	10.00	7.62	7.62	7.62	.00944	4.44	.79	901.52	94.41
495.00	5.00	7.62	7.61	7.62	.00666	1.67	.39	902.50	94.51

TABLE 1: FOR 4S
WITH PLOTS 1-5

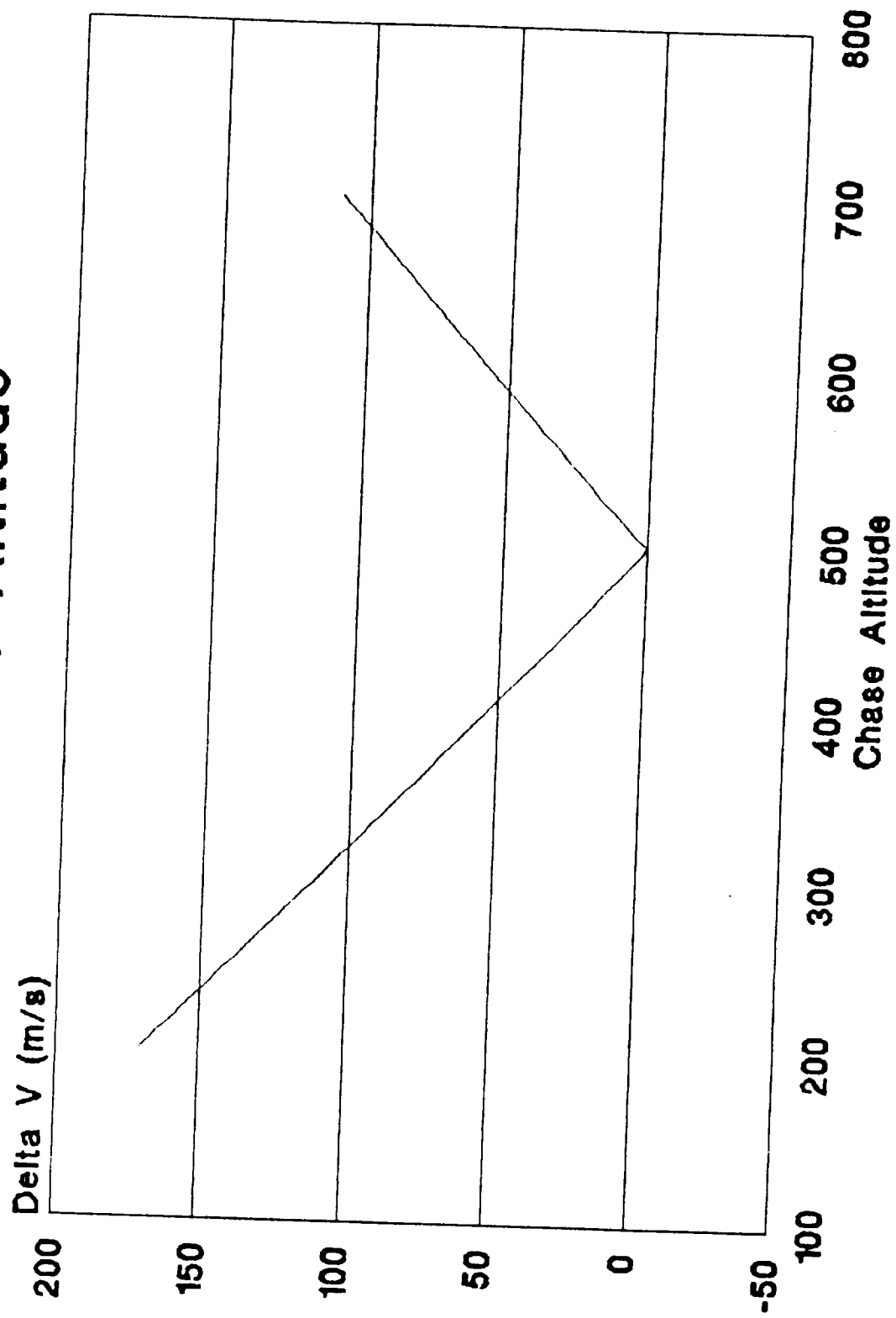
TABLE 1.

Chase Alt.	d	Chase Vel.	Hohmann V1	Hohmann V2	Delta V km/s	Delta V m/s	Catch Rate	Period Period	Catch Period
500.00	.00	7.61	7.61	7.62	-.0061	-1.10	.00	903.49	94.61
505.00	-5.00	7.61	7.60	7.62	-.0088	-3.87	-.39	904.47	94.72
510.00	-10.00	7.61	7.60	7.62	-.01	-6.63	-.79	905.46	94.82
515.00	-15.00	7.60	7.60	7.62	-.01	-9.39	-1.18	906.45	94.92
520.00	-20.00	7.60	7.59	7.62	-.01	-12.15	-1.57	907.43	95.03
525.00	-25.00	7.60	7.59	7.63	-.01	-14.91	-1.97	908.42	95.13
530.00	-30.00	7.60	7.58	7.63	-.02	-17.66	-2.36	909.41	95.23
535.00	-35.00	7.59	7.58	7.63	-.02	-20.41	-2.76	910.39	95.34
540.00	-40.00	7.59	7.57	7.63	-.02	-23.16	-3.15	911.38	95.44
545.00	-45.00	7.59	7.57	7.63	-.03	-25.90	-3.54	912.37	95.54
550.00	-50.00	7.59	7.57	7.63	-.03	-28.64	-3.94	913.36	95.65
555.00	-55.00	7.58	7.56	7.63	-.03	-31.38	-4.33	914.35	95.75
560.00	-60.00	7.58	7.56	7.64	-.03	-34.11	-4.72	915.34	95.85
565.00	-65.00	7.58	7.55	7.64	-.04	-36.84	-5.12	916.33	95.96
570.00	-70.00	7.57	7.55	7.64	-.04	-39.57	-5.51	917.32	96.06
575.00	-75.00	7.57	7.55	7.64	-.04	-42.30	-5.90	918.31	96.16
580.00	-80.00	7.57	7.54	7.64	-.05	-45.02	-6.30	919.30	96.27
585.00	-85.00	7.57	7.54	7.64	-.05	-47.74	-6.69	920.29	96.37
590.00	-90.00	7.56	7.53	7.64	-.05	-50.45	-7.08	921.28	96.48
595.00	-95.00	7.56	7.53	7.64	-.05	-53.17	-7.48	922.27	96.58
600.00	-100.00	7.56	7.53	7.65	-.06	-55.88	-7.87	923.26	96.68
605.00	-105.00	7.56	7.52	7.65	-.06	-58.59	-8.27	924.26	96.79
610.00	-110.00	7.55	7.52	7.65	-.06	-61.29	-8.66	925.25	96.89
615.00	-115.00	7.55	7.51	7.65	-.06	-63.99	-9.05	926.24	97.00
620.00	-120.00	7.55	7.51	7.65	-.07	-66.69	-9.45	927.24	97.10
625.00	-125.00	7.54	7.51	7.65	-.07	-69.39	-9.84	928.23	97.20
630.00	-130.00	7.54	7.50	7.65	-.07	-72.08	-10.23	929.22	97.31
635.00	-135.00	7.54	7.50	7.66	-.07	-74.77	-10.63	930.22	97.41
640.00	-140.00	7.54	7.49	7.66	-.08	-77.46	-11.02	931.21	97.52
645.00	-145.00	7.53	7.49	7.66	-.08	-80.14	-11.41	932.21	97.62
650.00	-150.00	7.53	7.49	7.66	-.08	-82.82	-11.81	933.20	97.72
655.00	-155.00	7.53	7.48	7.66	-.09	-85.50	-12.20	934.20	97.83
660.00	-160.00	7.53	7.48	7.66	-.09	-88.18	-12.59	935.20	97.93
665.00	-165.00	7.52	7.47	7.66	-.09	-90.85	-12.99	936.19	98.04
670.00	-170.00	7.52	7.47	7.67	-.09	-93.52	-13.38	937.19	98.14
675.00	-175.00	7.52	7.47	7.67	-.10	-96.19	-13.78	938.19	98.25
680.00	-180.00	7.52	7.46	7.67	-.10	-98.85	-14.17	939.19	98.35
685.00	-185.00	7.51	7.46	7.67	-.10	-101.52	-14.56	940.18	98.46
690.00	-190.00	7.51	7.45	7.67	-.10	-104.17	-14.96	941.18	98.56
695.00	-195.00	7.51	7.45	7.67	-.11	-106.83	-15.35	942.18	98.67
700.00	-200.00	7.50	7.45	7.67	-.11	-109.48	-15.74	943.18	98.77

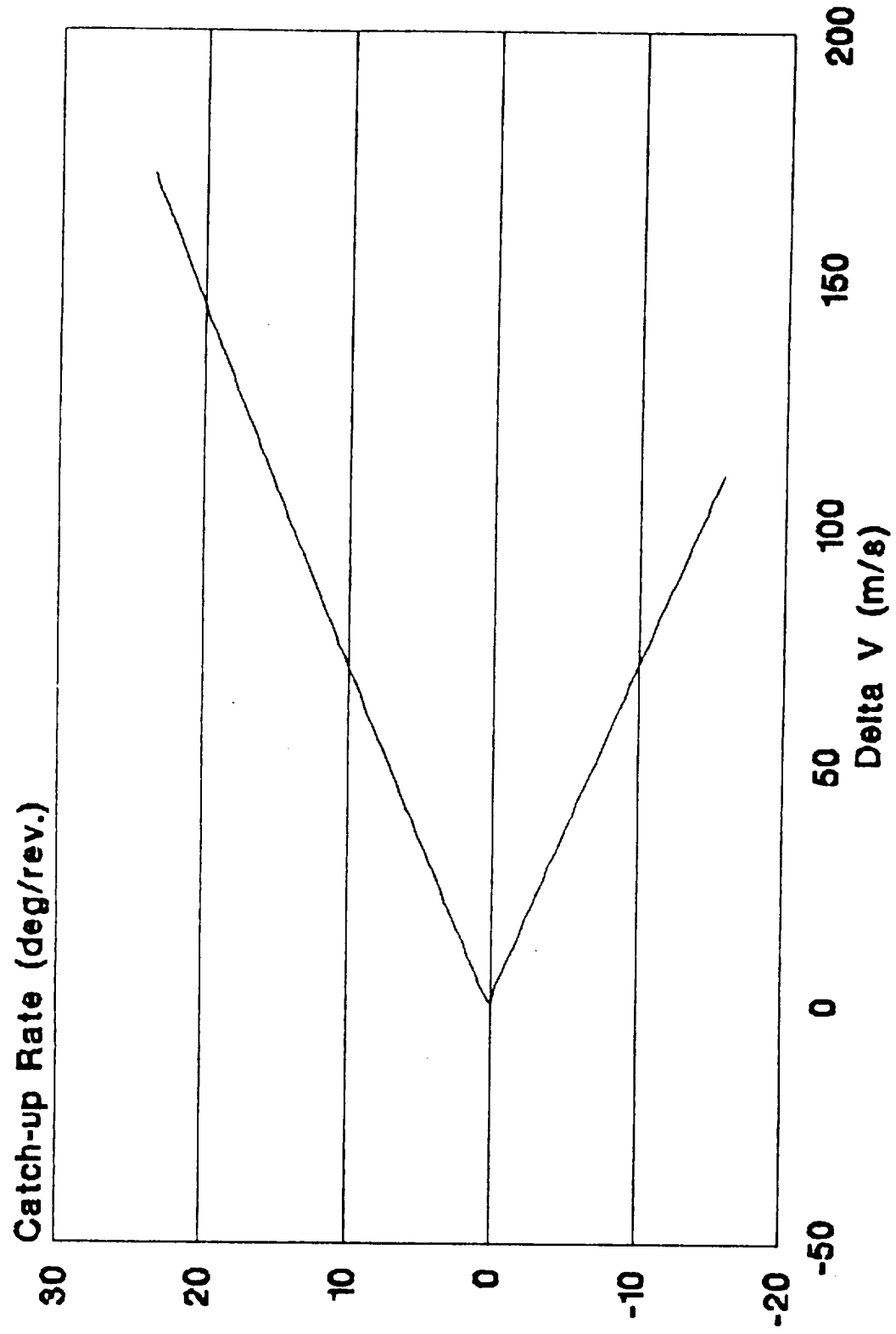
Catch-up Rate vs. Chase Altitude



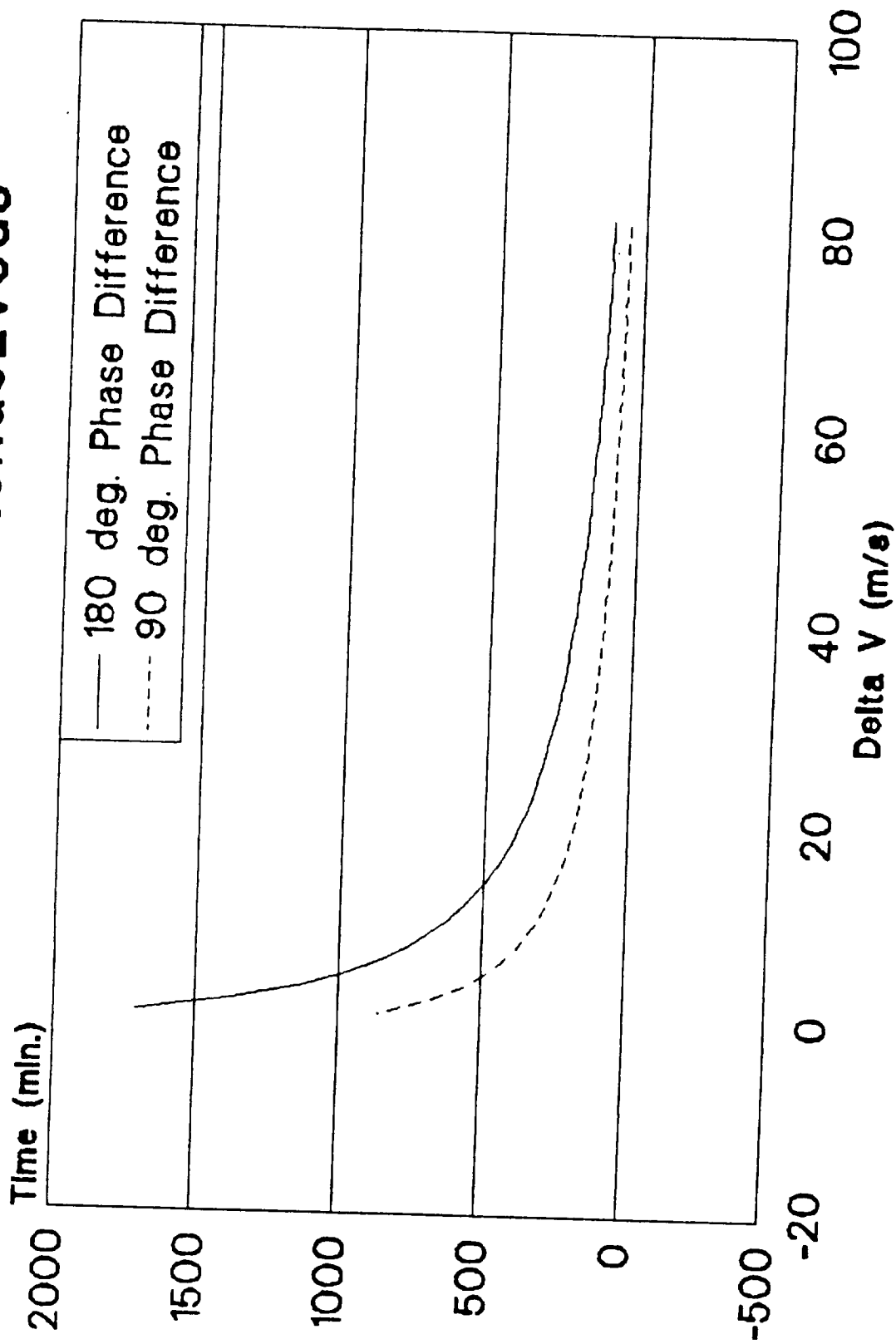
Delta V vs. Chase Altitude



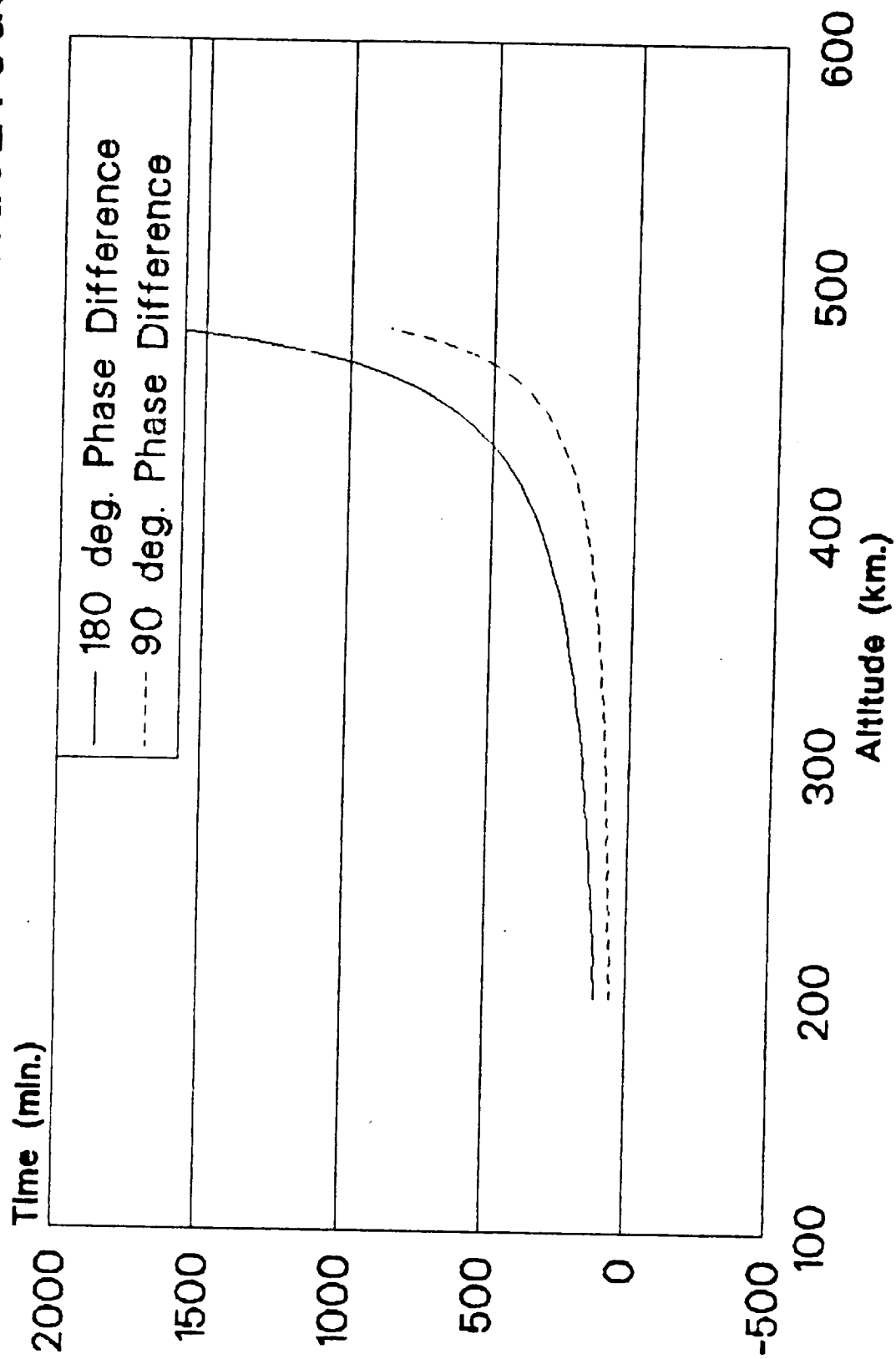
Catch-up Rate vs. Delta V



Delta V vs. Time to Rendezvous



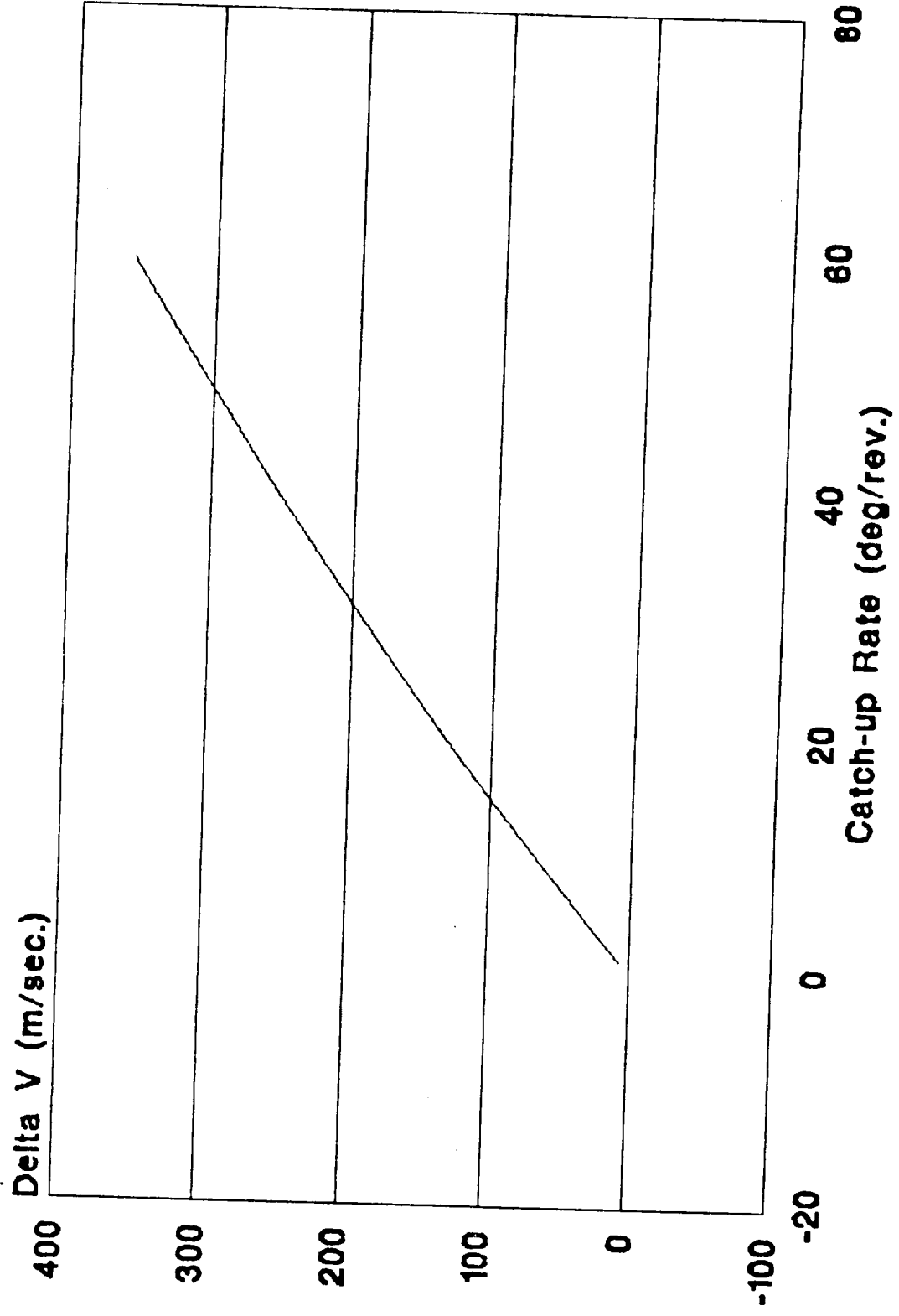
Chase Altitude vs. Time to Rendezvous



Leg. ahead	D Per.	A	Vel.1	delta V	dv m/s
1.00	15.75	6850.75	7.62	.01	7.04
2.00	31.58	6903.48	7.63	.01	14.04
3.00	47.37	6916.21	7.63	.02	21.00
4.00	63.16	6928.92	7.64	.03	27.92
5.00	78.95	6941.62	7.65	.03	34.81
6.00	94.74	6954.31	7.65	.04	41.65
7.00	110.53	6966.99	7.66	.05	48.46
8.00	126.32	6979.65	7.67	.06	55.24
9.00	142.11	6992.31	7.67	.06	61.97
10.00	157.89	7004.95	7.68	.07	68.67
11.00	173.68	7017.58	7.69	.08	75.34
12.00	189.47	7030.20	7.69	.08	81.97
13.00	205.26	7042.81	7.70	.09	88.56
14.00	221.05	7055.41	7.71	.10	95.12
15.00	236.84	7068.00	7.71	.10	101.64
16.00	252.63	7080.57	7.72	.11	108.13
17.00	268.42	7093.14	7.73	.11	114.59
18.00	284.21	7105.69	7.73	.12	121.01
19.00	300.00	7118.23	7.74	.13	127.39
20.00	315.79	7130.76	7.75	.13	133.75
21.00	331.58	7143.29	7.75	.14	140.07
22.00	347.37	7155.79	7.76	.15	146.36
23.00	363.16	7168.29	7.77	.15	152.61
24.00	378.95	7180.76	7.77	.16	158.84
25.00	394.74	7193.26	7.78	.17	165.03
26.00	410.53	7205.72	7.78	.17	171.19
27.00	426.32	7218.18	7.79	.18	177.32
28.00	442.11	7230.62	7.80	.18	183.42
29.00	457.89	7243.05	7.80	.19	189.48
30.00	473.68	7255.48	7.81	.20	195.52
31.00	489.47	7267.89	7.81	.20	201.53
32.00	505.26	7280.29	7.82	.21	207.50
33.00	521.05	7292.68	7.83	.21	213.45
34.00	536.84	7305.06	7.83	.22	219.36
35.00	552.63	7317.43	7.84	.23	225.25
36.00	568.42	7329.79	7.84	.23	231.11
37.00	584.21	7342.14	7.85	.24	236.93
38.00	600.00	7354.48	7.86	.24	242.73
39.00	615.79	7366.81	7.86	.25	248.51
40.00	631.58	7379.13	7.87	.25	254.25
41.00	647.37	7391.43	7.87	.26	259.96
42.00	663.16	7403.73	7.88	.27	265.65
43.00	678.95	7416.02	7.88	.27	271.31
44.00	694.74	7428.30	7.89	.28	276.94
45.00	710.53	7440.56	7.90	.28	282.55
46.00	726.32	7452.82	7.90	.29	288.12
47.00	742.11	7465.07	7.91	.29	293.67
48.00	757.89	7477.30	7.91	.30	299.20
49.00	773.68	7489.53	7.92	.30	304.70
50.00	789.47	7501.75	7.92	.31	310.17
51.00	805.26	7513.95	7.93	.32	315.61
52.00	821.05	7526.15	7.93	.32	321.03
53.00	836.84	7538.34	7.94	.33	326.43
54.00	852.63	7550.52	7.94	.33	331.80
55.00	868.42	7562.68	7.95	.34	337.14
56.00	884.21	7574.84	7.96	.34	342.46
57.00	900.00	7586.99	7.96	.35	347.75
58.00	915.79	7599.13	7.97	.35	353.02
59.00	931.58	7611.26	7.97	.36	358.27

TABLE 2: FOR USE WITH PLOT

Epoch Maneuver for Rendezvous



References :

Rendezvous and Proximity Operations Handbook RNDZ 2102
1983 NASA Houston Texas

Appendix F - Re-entry Model

The computer code listed on Figure F.1 was created to perform all the calculations necessary to compute the re-entry trajectory. The code computed the entire trajectory based on the conditions of the de-orbit burn (ΔV of the burn and altitude were the main parameters). First, the burn conditions were used to calculate the conditions at atmospheric interface, which were then used to integrate the equations of motion to find atmospheric trajectory.

The assumptions used to model re-entry are:

- 1) L/D is constant throughout the flight.
- 2) The atmosphere decays exponentially with altitude.
- 3) The acceleration of gravity is constant at the sea level value.
- 4) The coefficient of drag is constant at 1.

On the accompanying program:

Lines 10 through 210 initialized the variables needed.

Line 80 defined the function $\text{Arccos}(x)$ which is needed and basic lacks.

Line 90 set the re-entry mass at 675 kg.

Line 100 set the reference area as the projected frontal area of the craft based on a diameter of 2.1 meters.

Line 120 set the exponential atmosphere decay factor as $1/6700$ km. This value was chosen as being recommended as better for high atmosphere flight. (Ref. Space Vehicle Design)

Line 140 set the value of the coefficient of lift at 0.25.

Lines 160 through 190 sets the physical constants, the radius of the Earth, sea level air density, gravitational parameter of earth, and the acceleration of gravity at the Earth's surface.

Line 210 set the time step of integration as 1 second. It should be noted that this value was chosen because it gave a reasonable run time for the program and was accurate to less than 1% of what the solutions converged to for much smaller time steps.

Lines 280 through 360 vary the de-orbit burn conditions and compute the conditions at atmospheric interface (at 120 km.)

Line 300 sets the velocity after the burn as the difference between circular velocity and the ΔV produced by the burn. This is assuming that the burn is performed directly opposed to the motion of the craft.

Line 310 computer the velocity at 120 km using the conservation of energy equation.

Lines 350 and 360 reject any orbit which does not reach 120 km and uses the conservation of angular momentum to compute the flight path angle at the beginning of atmospheric flight.

Lines 401 through 409 perform the eccentric anomaly calculations to find the time of flight and angular distance traveled during the free flight phase.

Lines 450 through 520 sets the variables for the beginning of the atmospheric flight phase.

Lines 600 through 830 performs the integration of the equations of motion through the atmosphere.

Lines 600, 610 and 620 contain the differential equations for altitude, flight path angle and altitude, respectively.

Lines 640 through 670 update these three values as well as time.

Line 690 jumps to the trajectory printout after every 15 seconds of flight.

Lines 730 through 770 calculate both the deceleration and angular distance traveled. Any trajectories which produce over 12 gee's are rejected in line 770 (this was primarily a de-bugging tool).

Lines 745 and 746 calculate angular distance traveled, by dividing the horizontal distance traveled by the radius of curvature of the flight path.

After Earth impact is reached at 0 km, Line 870 jumps to the loop to printout the final information on the trajectory, and line 890 repeats the entire process for another trajectory.

Lastly, Lines 960 through 1050 are merely output loops.

Table F.1 contains the data output used to create Figures 2.4.D, 2.4.E, and 2.4.F in the main report.

Figure F.1

```
10 REM Program to vary de-orbit burn conditions, compute re-entry
20 REM conditions (at 120 km) and determine trajectory to 0 km
30 REM Program discards conditions which have perigee above 120 km or
40 REM produces gee forces greater than 12 gee
50 REM
60 REM ** Set initial conditions **
70 REM
75 PI = 3.141592654
80 DEF FNARCCOS(X) = -ATN(X/SQR(1-X*X)) + PI/2
90 M = 675:rem Re-entry mass (kg)
100 A = PI * (2.1 / 2)^2:rem Reference area (2.1 m diameter)
110 CD = 1:rem Hypersonic coefficient of drag
120 B = 1 / 6700:rem Exponential atmosphere parameter
130 Q = CD * A / M
140 CL = 0.25:rem Coefficient of lift
150 LD = CL / CD
160 R = 6378 * 1000:rem Radius of Earth
170 PO = 1.225:rem Sea level air density
180 U = 398601.28 * 1000^3:rem Gravitational parameter
190 G = 9.81:rem Acceleration of gravity
200 X = SQR( G/R )
210 DT = 1
220 REM
230 REM
240 REM ** Start loop to vary apogee conditions and relate to re-entry **
250 REM A (apogee) F (beginning of re-entry)
260 REM
270 REM
280 RA = (6378 + 300) * 1000
290 FOR DELTAV = 100 TO 220 STEP 10
300 VA = SQR( U/RA ) - DELTAV
310 VF = SQR( 2 * (0.5 * VA^2 - U/RA + U/6498000) )
320 REM
330 REM Next line checks to see if perigee occurs above 120 km
340 REM
350 IF ABS(RA*VA / (6498000 * VF) ) > 1 THEN PRINT "Not possible": GOTO
890
360 THETA = FNARCCOS(RA*VA / (6498000 * VF) )
370 REM
380 REM THETA = Initial Flight Path Angle
390 REM VF = Initial re-entry velocity
400 REM
401 REM ** Eccentric Anomaly Calculations
402 REM
403 ECC = SQR(1 + VA^2 * RA * (RA*VA^2/ U^2 - 2/U) )
404 EO = PI
405 NUF = FNARCCOS( RA^2 * VA^2 / (U*6498000) - 1) / ECC)
```

```

406 EF = 2 * PI - FNARCCOS( (ECC + COS(NUF) ) / (1 + ECC * COS(NUF) ) )
407 AA = -0.5 * U / (VA^2 / 2 - U / RA)
408 TIMEFREE = SQR( AA^3 / U ) * ( (EF - ECC * SIN(EF) ) - (EO - ECC *
SIN(EO) ) )
409 DE = EF - EO
410 REM
420 REM ** Set conditions at beginning of atmospheric re-entry (120 km) **
430 REM
440 REM
450 V = VF::rem Initial Velocity
460 H = 120 * 1000:rem Initial Altitude
470 THETA1 = THETA
480 TIME = 0
490 GMAX = 0
500 VV = 0
505 PHI = 0
510 Z = V / SQR( G * R ):rem Set velocity variable
520 BY = B * H:rem Set altitude variable
530 REM
540 REM
550 REM ** Integrate differential equations of motion to find trajectory **
560 REM
570 REM
580 REM Next 3 lines contain equations of motion
590 REM
600 DZ = (-0.5 * Q * R * PO * Z^2 * EXP(-1*BY) + SIN(THETA1)) * X * DT
610 DTHETA = ( (1/Z - Z) * COS(THETA1) - 0.5 * R * LD * Q * Z * PO * EXP(-
1*BY)) * X * DT
620 DBY = -B * R * Z * SIN(THETA1) * X * DT
630 REM
640 Z = Z + DZ
650 THETA1 = THETA1 + DTHETA
660 BY = BY + DBY
670 TIME = TIME + DT
680 REM
690 IF TIME / 15 = INT (TIME / 15) THEN GOSUB 940:rem Output Loop
700 REM
710 REM Calculate Deceleration
720 REM
730 VV = (Z - DZ) * SQR ( G * R )
740 V = Z * SQR ( G * R )
745 DPHI = V * COS(THETA1) * DT / (R + H)
746 PHI = PHI + DPHI
750 GEE = ( (V - VV) / DT ) / 9.81
760 IF ABS(GEE)>GMAX THEN GMAX = ABS(GEE)
770 IF GMAX > 12 THEN PRINT "Gmax too high":STOP
780 REM
790 REM Next 2 lines find altitude and check to see if still in flight regime
800 REM

```

```

810 H = BY / B
830 IF H>0 THEN GOTO 550
840 REM
850 REM * Reached 0 km, print results and restart *
860 REM
870 GOSUB 1010
880 REM
890 NEXT DELTAV
900 END
910 REM
920 REM * Print Trajectory
930 REM
940 H = BY / B
950 V = Z * SQR (G * R )
960 PRINT H,V,THETA1 * 180 / PI, TIME, GEE, PHI*180 / PI
970 RETURN
980 REM
990 REM ** Print Overall information
1000 REM
1010 PRINT "L/D = ";LD,"M = ";M;"kg",RA/1000 - 6378;"km, DV =" DELTAV;"m/s"
1020 PRINT V 120 km = ";VF;" m/s  Entry Angle = ";THETA*180/PI;" deg  Free
Flight ";TIMEFREE;" s"
1030 PRINT "Gmax = ";GMAX, "TOF (to 0 km) ";TIME;" s   dE = ";DE*180 / PI;"
deg  PHI = ";PHI * 180 / PI
1040 PRINT
1050 RETURN

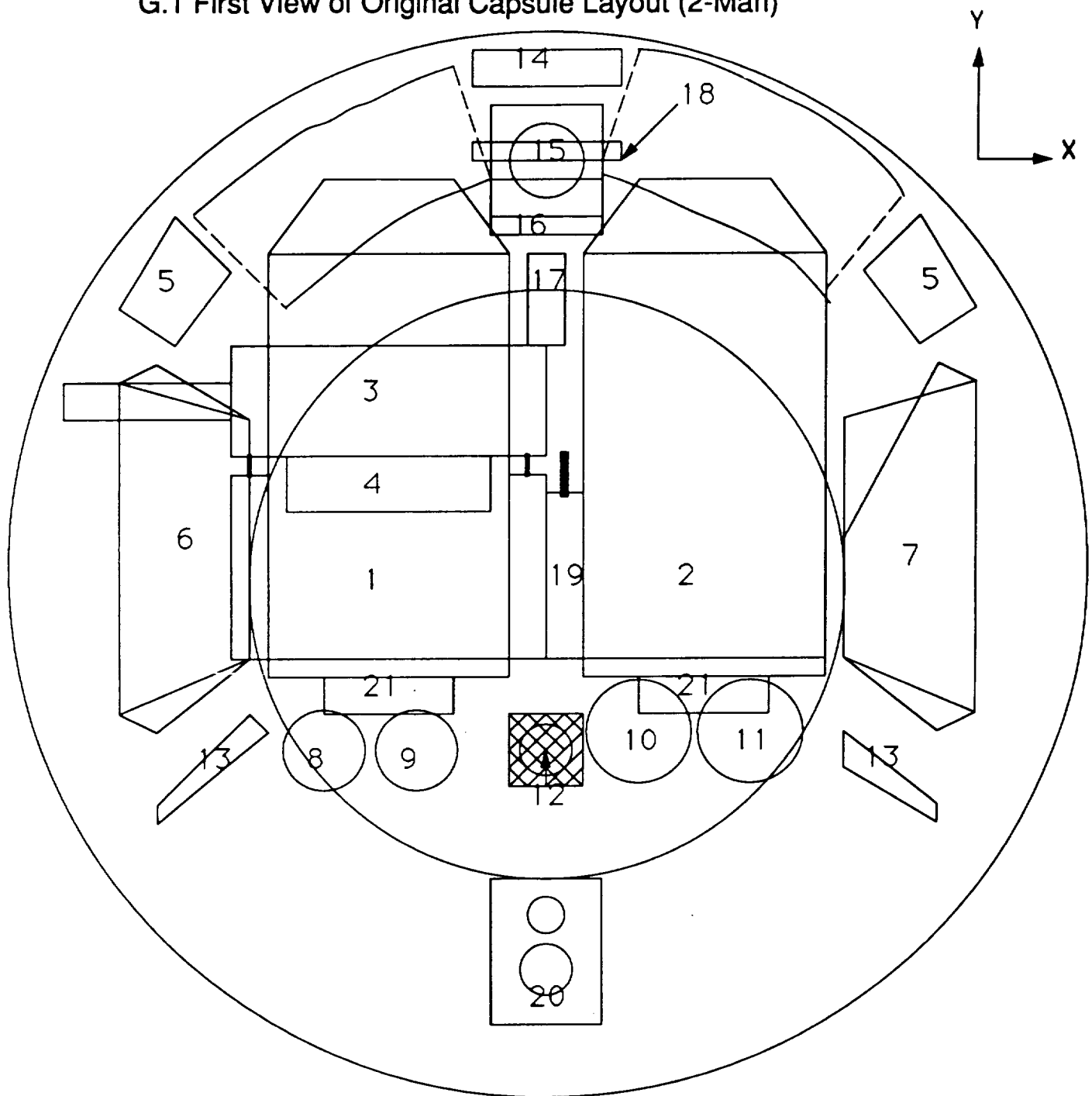
```

Table F.1 - Re-entry Trajectory from 300 km

Altitude (m)	Velocity (m/s)	Deceleration (Gee)	Flight Path Angle	Time (seconds)
120000	7800	0.00	2.00	0
115874	7805	0.00	2.03	15
111687	7810	0.00	2.06	30
107444	7816	0.00	2.08	45
103147	7820	0.00	2.11	60
98801	7825	0.00	2.13	75
94411	7829	0.00	2.15	90
89983	7830	0.00	2.16	105
85530	7829	0.03	2.17	120
81072	7821	0.09	2.17	135
76643	7800	0.20	2.15	150
72308	7754	0.41	2.09	165
68182	7666	0.77	1.97	180
64449	7506	1.33	1.74	195
61366	7252	2.02	1.38	210
59189	6901	2.60	0.90	225
58022	6495	2.81	0.38	240
57728	6094	2.63	-0.04	255
57981	5738	2.27	-0.28	270
58412	5438	1.91	-0.29	285
58710	5182	1.65	-0.11	300
58654	4954	1.50	0.23	315
58105	4739	1.47	0.67	330
57004	4518	1.55	1.18	345
55366	4274	1.75	1.69	360
53281	3991	2.07	2.17	375
50911	3652	2.47	2.56	390
48459	3254	2.85	2.84	405
46098	2813	3.07	3.09	420
43894	2363	3.03	3.45	435
41781	1936	2.80	4.17	450
39617	1554	2.47	5.52	465
37267	1222	2.12	7.78	480
34653	941	1.79	11.29	495
31764	708	1.45	16.50	510
28654	525	1.12	23.89	525
25426	389	0.80	33.66	540
22219	295	0.55	44.96	555
19190	232	0.38	55.75	570
16472	187	0.27	64.07	585
14112	154	0.20	69.38	600
12083	131	0.15	72.32	615
10324	113	0.11	73.79	630
8778	100	0.09	74.53	645
7400	89	0.07	74.92	660
6157	81	0.06	75.15	675
5023	74	0.05	75.30	690
3981	68	0.04	75.41	705
3017	63	0.04	75.50	720
2119	59	0.03	75.56	735
1279	55	0.03	75.61	750
489	52	0.03	75.66	765

Appendix G. Original TLMS Capsule Layout

G.1 First View of Original Capsule Layout (2-Man)

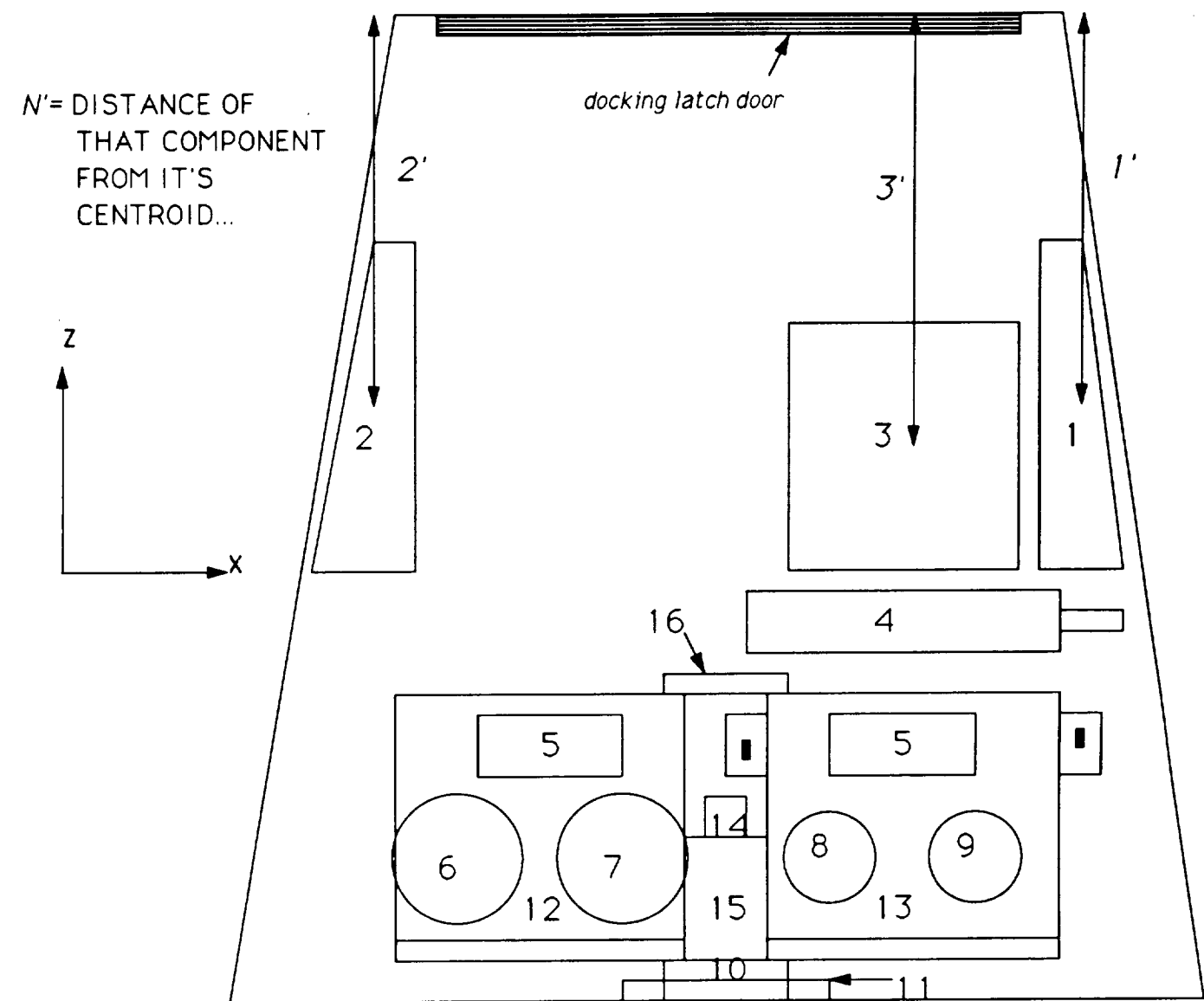


- 1 - Pilot seat w/ attitude and thrust controls
- 2 - EVA man seat
- 3 - main control board
- 4 - backup controls w/ sepearte power supply
- 5 - batteries
- 6 - backup computer
- 7 - main computer
- 8 - backup oxygen tank

- 9 - backup nitrogen tank
- 10-main oxygen tank
- 11-main nitrogen tank
- 12-air intake for water seperator
- 13-flourescent lights
- 14-reels for parachute lines w/motors
- 15-CRT for camera
- 16-LiOH canister

- 17-LiOH filter holder
- 18-flourescent light
- 19-console housing the camera joystick
- 20-camera w/spotlight built in

G.2 Second View of Original Capsule Layout (2-Man)



1 - backup computer

1' =

2 - main computer

2' =

3 - exp. storage box

3' =

4 - main control board

4' =

5 - survival kits

5' =

6 - main oxygen gas
without the tank
6.755 kg
5.92E-3 cu.m

6' =

7 - main nitrogen gas
without the tank
4.59 kg
5.67E-3 cu.m

7' =

8 - backup oxygen
without tank
1.36 kg
1.19E-3 cu.m

8' =

9 - backup nitrogen
without tank

9' =

10 - LiOH canister

10' =

11 - floures. light

11' =

12 - EVA man's seat

15 kg *

1 cu.m *

12' =

13 - Pilot's seat

15 kg *

1 cu.m *

13' =

14 - camera joystick
14' =

15 - water seperator
under console

15 kg *

.16 cu.m *

15' =

16 - air intake fan

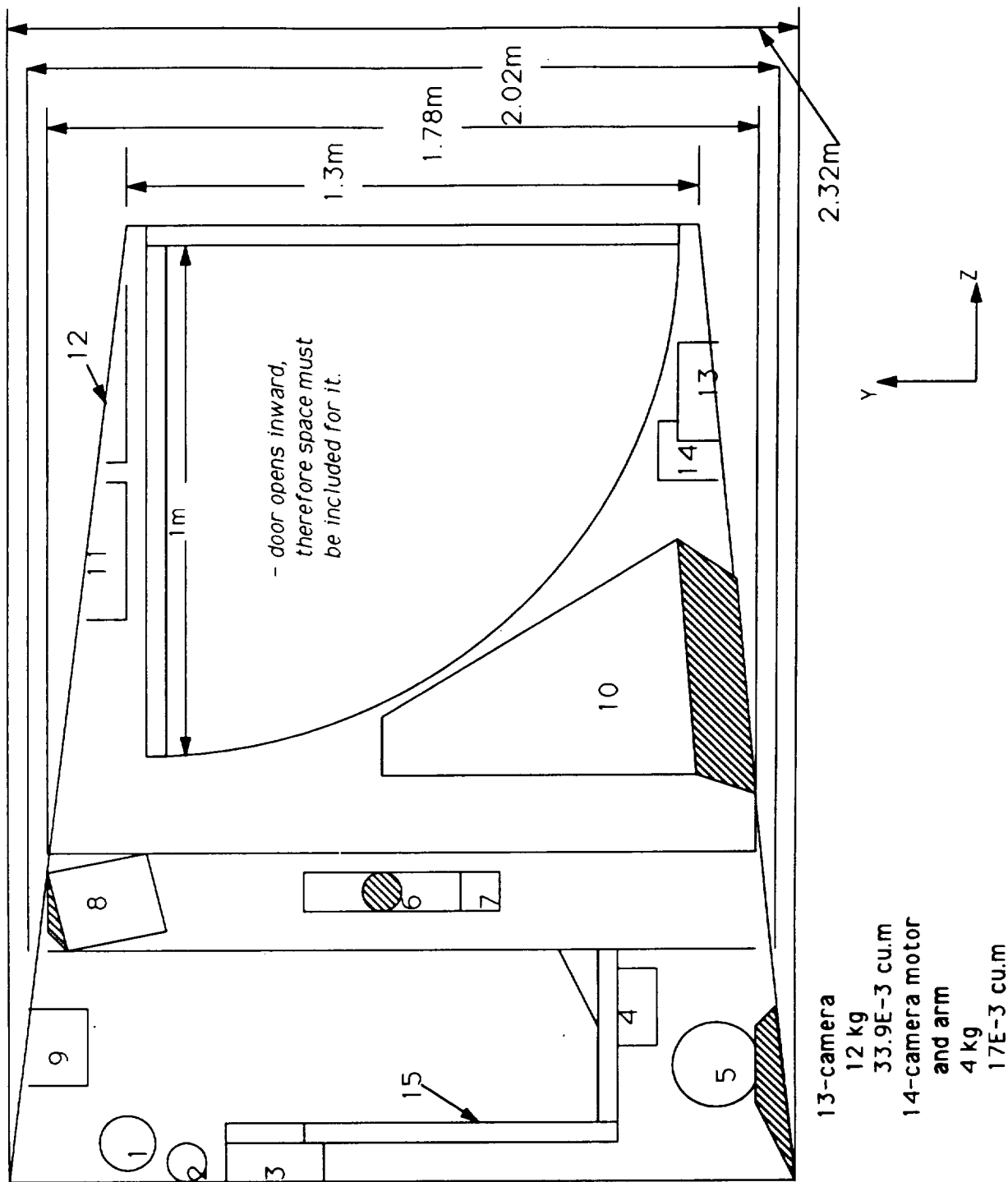
1 kg

3E-3 cu.m

16' =

G.3 Third View of Original Capsule Layout (2-Man)

(* = APPROXIMATE)



- 1 - LiOH canister
1.21 kg
- 2 - fluorescent light
2.96E-3 cu.m
- 3 - LiOH filter holder
1 kg *
- 4 - survival kit (2)
3 kg
- 5 - backup nitrogen gas without the tank
0.3186 cu.m each
0.50 kg
- 6 - main control board
6.17E-4 cu.m
- 7 - backup control box
2.5 kg *
- 8 - CRT for camera
16.39E-3 *
- 9 - parachute reels w/motors
2.0 kg *
- 10 - experiments storage box
8.19E-3 cu.m *
- 11 - main parachute(Ram-Air)
2.2 kg *
- 12 - reserve parachute(round)
15.7E-3 cu.m *
- 13 - camera
12 kg
- 14 - camera motor and arm
33.9E-3 cu.m
- 15 - bracing to withstand g-forces
4 kg



■ bracing to withstand
g-forces

- 13-camera
12 kg
- 14-camera motor
33.9E-3 cu.m
- 15 - bracing to withstand
4 kg

Appendix H.1 CARBON DIOXIDE REMOVAL :

The removal of carbon dioxide from the internal atmosphere of the vehicle is essential for manned space flight. If the percentage of carbon dioxide reaches a high enough amount, the astronauts will be unable to complete their mission and could suffocate to death. Many methods of carbon dioxide removal were examined for use in the vehicle. Figure H.1.a shows a number of methods. Because the planned flight will be of short duration, the most efficient method would be one of absorption. Although many of the others would not require as large of an oxygen supply, they required either large amounts of power and/or volumes which would not be feasible on a vehicle with the weight restrictions this one has. Both the alkali metal hydroxides and the alkali metal superoxides are good techniques for absorption. The superoxides have the advantage of producing oxygen from the carbon dioxide, which would require a smaller oxygen supply. The main problem with the superoxides is in controlling the amount of carbon dioxide removal and the amount of oxygen evolved from the process. This would require an auxiliary scrubber system, such as a lithium hydroxide scrubber system (Mausteller, 1982). Having two systems for such a short mission as that which the vehicle will be capable of, would be less efficient than having a single scrubber system. The decision was for alkali metal hydroxides.

There are four main hydroxides which could be used; soda lime, sodium hydroxide, baralyme, and lithium hydroxide. By far the best hydroxide to use for space flight is lithium hydroxide. Its carbon dioxide consumption is almost twice that of the others. For one gram of lithium hydroxide, .919 grams of carbon dioxide are consumed (Wang, 1982). The only disadvantage is its cost (Buban, 1982), but the cost is insignificant compared to the weight saved. Lithium hydroxide will be used for carbon dioxide removal in this vehicle.

FIGURE H.1.a
METHODS OF CARBON DIOXIDE REMOVAL

method	material	advantages	disadvantages	overall
Absorbtion	Alkali Metal hydroxides	light weight	need complete oxygen supply non-regenerative	best method for short durations of time (Wang,1982)
	Alkali Metal superoxides	produce O2 inexpensive (Mausteller,1982)	control of CO2 uptake/O2 evolution is not satisfactory w/o auxillary scrubber system (Mausteller,1982)	necessity of auxillary scrubber system is in-efficient for mission
Regenerable Absorbents	Metal Oxides	low energy requirements (Wang,1982)	slow reactions (Wang,1982) need high temperatures some are toxic (Langton,1982)	not good for short mission
Membrane Separation	Polymer films	filters other unwanted gases (Saurich,1982)	large power and area requirements (Wang,1982)	too much power required
Photo-synthesis	Algae	self-regulating food source (Langton,1969)	huge volume (Langton,1969) requirements	bad for short mission
Physical Removal	Freeze-out	liquifies CO2 eases removal (Langton,1969)	high power requirement low reliability (Wang,1982)	unreliable- no good
	H2O absorption	non-toxic solute (Langton,1969)	high energy requirement large quantities of H2O	too heavy too much energy

FIGURE H.1.b
ALKALI METAL HYDROXIDES

hydroxide	CO Consumption (gCO / g)	Advantages	Disadvantages	Exit temp. (1.5 lit. CO/ min.)
Soda lime 5% NaOH 95% Ca(OH) ₂	.488 (Wang,1982)	low cost lower exit gas temperature (buban,1982)	High weight Needs special bed loses efficiency at zero deg. C (buban,1982)	47 deg. C (buban,1982)
Sodium hydroxide 85% NaOH 15% diatomaceous earth	.550 (Wang,1982)	Effective to -7 degrees C 2/3 weight of soda lime (buban,1982)	Soluble in water Tends to dissolve and cake (buban,1982) High exit temp.	70 deg. C (buban,1982)
Baralyme 20% barium hydroxide octohydrate 80% calcium hydroxide	.503 (Wang,1982)	More effective at low temps. than soda lime (buban,1982)	weight (buban,1982)	-----
Lithium hydroxide LiOH	.919 (Wang,1982)	Very efficient lower weight and volume required Eff. to -32 deg. C (buban,1982)	cost (buban,1982)	52 deg. C (buban,1982)

REFERENCES:

Buban, E.E. and Haughey, J.R. "Lithium Hydroxides as a Carbon Dioxide Scrubber in Closed Circuit Breathing Apparatus." *The Characterization of Carbon Dioxide Absorbing Agents for Life Support Equipment*. ASME, New York, NY, 1982.

Langton, N.H. *Space Research Technology: The Space Environment*. Univ. of London Press Ltd.: London, 1969.

Mausteller, J.W. "Review of Potassium Superoxide Characteristics and Applications." *The Characterization of Carbon Dioxide Absorbing Agents for Life Support Equipment*. ASME, New York, NY, 1982.

Sarich, A.J. "Applications of Permeable Membranes as Carbon Dioxide Scrubbers." *The Characterization of Carbon Dioxide Absorbing Agents for Life Support Equipment*. ASME, New York, NY, 1982.

Wang, T. C. "Carbon Dioxide Scrubbing Materials in Life Support Equipment." *The Characterization of Carbon Dioxide Absorbing Agents for Life Support Equipment*. ASME, New York, NY, 1982.

Buban, E.E. and Haughey, J.R. "Lithium Hydroxide as a Carbon Dioxide Scrubber in Closed Circuit Breathing Apparatus".

Bibliography

Buban, E.E. and Haughey, J.R. "Lithium Hydroxides as a Carbon Dioxide Scrubber in Closed Circuit Breathing Apparatus." *The Characterization of Carbon Dioxide Absorbing Agents for Life Support Equipment*. ASME, New York, NY, 1982.

Langton, N.H. *Space Research Technology: The Space Environment*. Univ. of London Press Ltd.: London, 1969.

Mausteller, J.W. "Review of Potassium Superoxide Characteristics and Applications." *The Characterization of Carbon Dioxide Absorbing Agents for Life Support Equipment*. ASME, New York, NY, 1982.

Sarich, A.J. "Applications of Permeable Membranes as Carbon Dioxide Scrubbers." *The Characterization of Carbon Dioxide Absorbing Agents for Life Support Equipment*. ASME, New York, NY, 1982.

Wang, T. C. "Carbon Dioxide Scrubbing Materials in Life Support Equipment." *The Characterization of Carbon Dioxide Absorbing Agents for Life Support Equipment*. ASME, New York, NY, 1982.

Appendix H.2 Docking Ring

H.2.1 Background

Work was briefly done on developing a docking ring. A docking ring would have been needed in a previous mission choice for the vehicle. Although this mission was scrubbed before rigorous work could be done on the ring, what work had been done will be presented now. A specialized docking ring would have been needed for the taurus flown vehicle in order to save on weight. There were four major steps which the docking ring would need to perform. They are as follows:

1. The vehicle first has to be caught by the receiving space station.
2. The gap between the space station's receiving end and the vehicles docking ring must be closed.

3. The two must be locked together in a way that they can not come apart at an unexpected time .

4. An airlock between the two must be formed.

The key is to perform all of these steps with as little weight and energy required by all of the systems. One technique is to perform as many steps as possible with each system. The weight and energy requirements on the vehicle are such that which ever systems need not be in the docking ring should not be present.

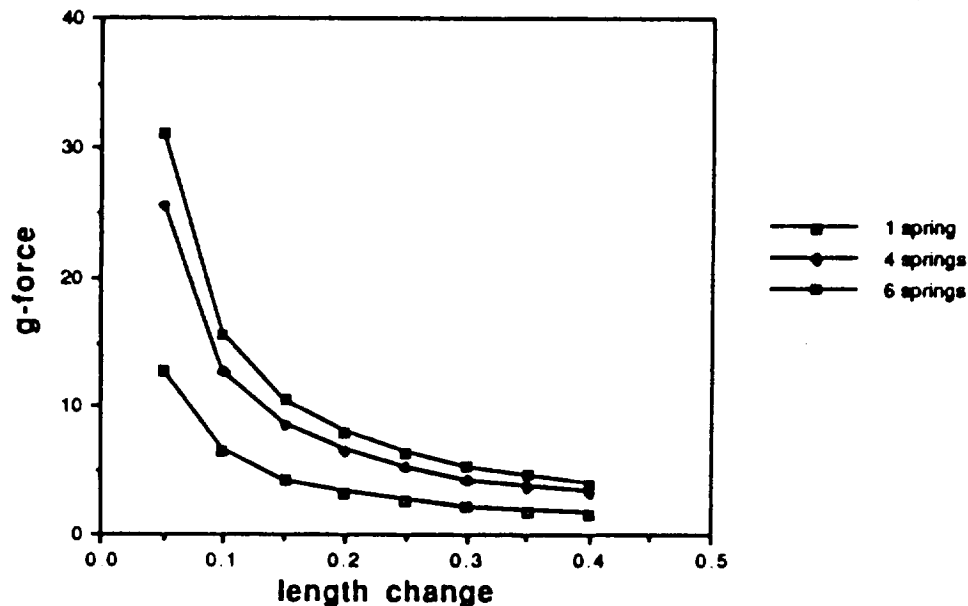
H.2.2 Catching the vehicle

The system used for catching the vehicle was going to be one which involved interlocking pedals on both the docking ring and also the receiving station. In order to reduce the chance of damage occurring to either the space station or the docking ring, a shock absorber will be placed at each of the pedals on the station receiving ring. These shock absorbers will consist of a spring and a dashpot. The dashpot will be such that it only affects movement in one direction. The spring will stop the momentum of the vehicle, and then the dashpot will come into effect while the spring is rebounding. This is done to reduce the chance of the vehicle being pushed away from the station during spring rebound. In determining the length of the shocks, the momentum of the vehicle, relative to the station, had to be determined. In doing so, a maximum value of velocity, relative to the station, was set on the vehicle. This was set at 2.5 km/hr (approximately 5 mi./hr). Using this velocity and an estimated mass of 1400 kg for the vehicle, the momentum was determined to be 3500 kg-m/sec.

The maximum momentum was then used to determine the g-force associated with various spring length changes under three different scenarios. The spring length change is the amount the spring compresses. The first scenario is that only one spring takes all of the momentum. This would be a worst case scenario where the pilot was well off target with the receiving ring. This case was used in determining the spring constant for the springs on the docking ring. The next two cases were to determine the affects of having either 4 pedals or 6 pedals on the ring. The force on the vehicle was determined if all springs acted equally in stopping the momentum, a perfect docking. In this case,

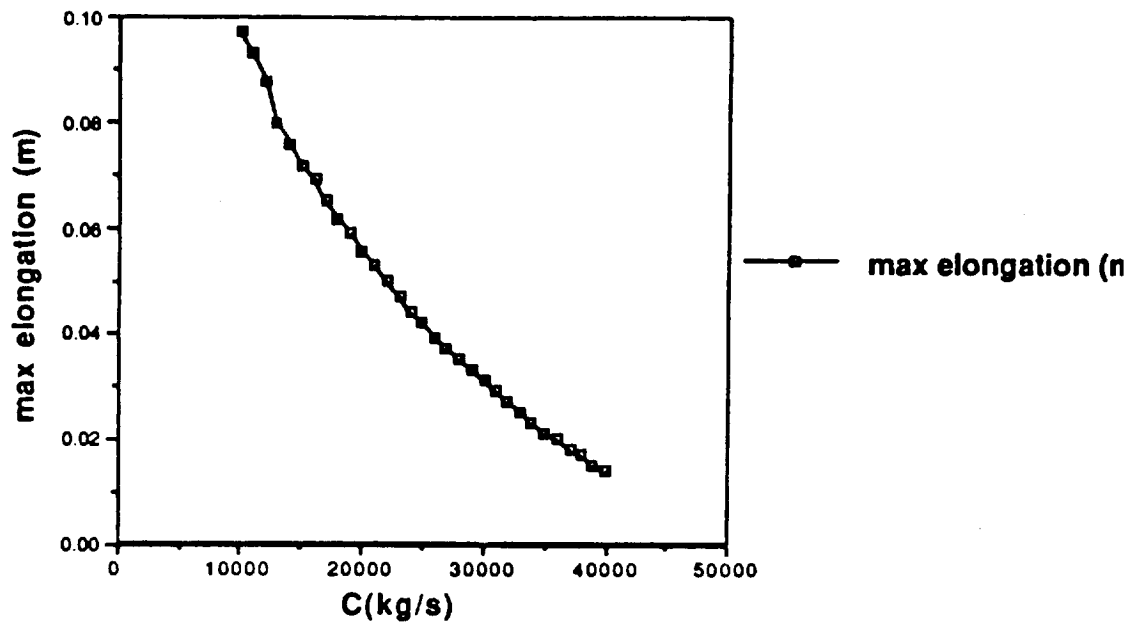
the springs would act with an equivalent spring constant equal to the number of spring multiplied by the spring constant of each. With this equivalent spring constant, the amount of compression could be determined using conservation of energy, $\frac{1}{2} m \cdot v^2 = \frac{1}{2} k_{eq} \cdot x^2$, where x is the compressive distance. With this value, x , the force on the vehicle was found using the formula: $F = k \cdot x$. Then, the g-force associated with this force was found by dividing the force of gravity on earth from the force. The g-force was plotted against the initial compression distance of a single spring, with the same value of k as each spring in the different combinations. Figure H.2.a shows this plot. The structure has been built for a maximum of 10 g's. For this reason, it was determined that with six springs, the initial length change would need to be at least .15 meters.

fig. H.2.a: g-force associated with spring length change



Now that the springs had been chosen, it was necessary to determine the value of c to use with the dashpot. The worst case scenario was used. If all the momentum was transferred to a single spring, the dashpot would be working against the velocity induced by the force of the compressed spring. Using the formula: $m \cdot a - C \cdot v - K \cdot x = 0$, conservation of forces acting on a body. By taking incremental values of x and a small initial velocity, the acceleration of the vehicle could be determined at each incremental time. The new velocity and compressive distance could be found using this acceleration, the previous velocity, and the previous distance. This process was continued until the velocity was zero. At this point, the value of x was equal to the maximum extensive distance of the spring. The maximum extensive distance was then plotted against the value of C associated with it. This plot is shown in figure H.2.b. The value for C depends on the properties of the fluids used. The docking ring was killed before more research could be done on the fluids associated with the dashpot, but the desired fluids would be able to survive the extreme temperature and also lead to a high value of C .

fig. H.2.b: C value affect on rebounding spring length



The entire length of the shock can be determined as follows. First, the initial spring length must be determined. In this report, the spring length will be modeled as twice the maximum compression distance. This leads to a spring length of .30 meters. This is the length of the shock. The length of the dashpot will have to be at least the maximum compressive distance plus the maximum extensive distance, which is determined by C.

The pedals not only have the affect of stopping the vehicle, but they also help to guide the docking ring to the receiving ring.

At this point, work on the docking ring was terminated well before completion due to the realization that the vehicle being designed was over the mass requirements of the taurus booster.

velocity of ship= 2.5 m/s		
mass of ship= 1400 kg		
momentum= 3500 kg-m/s		
delta x .05 m		
spring constant= 350000 kg/(s*s)		
spring number:1	4	6
x-delta= .05 m	.025 m	2.00412E-02 m
force= 175000 newtons	350000 newtons	428660.7 newtons
accel.= 125 m/s^2	250 m/s^2	306.1842 m/s^2
veloc= 12.7481	25.4962	31.21744
delta x .1 m		
spring constant= 375000 kg/(s*s)		
spring number:1	5	6
x-delta= .1 m	5.000001E-02 m	4.082466E-02 m
force= 37500 newtons	175000 newtons	214280.4 newtons
accel.= 62.5 m/s^2	125 m/s^2	153.0731 m/s^2
veloc= 6.371049	12.7421	15.23532
delta x .15 m		
spring constant= 342500.7 kg/(s*s)		
spring number:1	4	6
x-delta= .15 m	.075 m	6.123744E-02 m
force= 31335.93 newtons	110625.7 newtons	142886.9 newtons
accel.= 41.06667 m/s^2	33.22222 m/s^2	102.0621 m/s^2
veloc= 4.2-7366	8.474732	10.40233
delta x .2 m		
spring constant= 213750 kg/(s*s)		
spring number:1	4	6
x-delta= .2 m	.1 m	8.164564E-02 m
force= 42750 newtons	37500.01 newtons	107133.2 newtons
accel.= 31.25 m/s^2	62.50001 m/s^2	76.54675 m/s^2
veloc= 3.185523	6.37105	7.802711
delta x .25 m		
spring constant= 140000 kg/(s*s)		
spring number:1	4	6
x-delta= .25 m	.125 m	.1020621 m
force= 35000 newtons	70000 newtons	85732.14 newtons
accel.= 25 m/s^2	50 m/s^2	61.23725 m/s^2
veloc= 1.34642	5.05664	6.242328
delta x .3 m		
spring constant= 97222.22 kg/(s*s)		
spring number:1	4	6
x-delta= .3 m	.15 m	.11224745 m
force= 29166.67 newtons	53333.33 newtons	71619.54 newtons
accel.= 30.33333 m/s^2	31.66667 m/s^2	51.66164 m/s^2
veloc= 2.123623	4.247366	5.20194
delta x .35 m		
spring constant= 71422.55 kg/(s*s)		
spring number:1	4	6
x-delta= .35 m	.175 m	.11420549 m
force= 25000 newtons	35000 newtons	61227.125 newtons
accel.= 17.14286 m/s^2	35.71429 m/s^2	46.54082 m/s^2
veloc= 1.1303	5.5006	4.55406
delta x .4 m		
spring constant= 54000.4 kg/(s*s)		
spring number:1	4	6
x-delta= .4 m	.2 m	.11522943 m
force= 21600 newtons	40000 newtons	50555.56 newtons
accel.= 10.825 m/s^2	31.25 m/s^2	38.27327 m/s^2
veloc= 1.512762	5.135223	5.701455

```

1 1/AT=1000
2 1/DTOR=1
3 FOR I=1 TO 1000000 STEP 10000
4   VEL=0
5   X=
6   Y=.15
7   DX=.0000001
8   X=X-DX
9   DT=DX/VEL
10  ACC=(K*X-C*VEL)/MAB
11  X=X+DX
12  N=N+1
13 IF N>10 THEN DX=.0005
14 VEL=VEL+ACC*DT
15 IF VEL<0 THEN GOTO 85
16 PRINT "C=";C, "displacement=";X
17 NEXT C

```

ORIGINAL PAGE IS
OF POOR QUALITY

= 10000	displacement=-9.702190E-02
= 11000	displacement=-9.302197E-02
= 12000	displacement=-8.902194E-02
= 13000	displacement=-8.402195E-02
= 14000	displacement=-8.002194E-02
= 15000	displacement=-7.602193E-02
= 16000	displacement=-7.202191E-02
= 17000	displacement=-6.902192E-02
= 18000	displacement=-6.502191E-02
= 19000	displacement=-6.202191E-02
= 20000	displacement=-5.850000E-02
= 21000	displacement=-5.602189E-02
= 22000	displacement=-5.302187E-02
= 23000	displacement=-5.002188E-02
= 24000	displacement=-4.702188E-02
= 25000	displacement=-4.402187E-02
= 26000	displacement=-4.202187E-02
= 27000	displacement=-3.902186E-02
= 28000	displacement=-3.702185E-02
= 29000	displacement=-3.502185E-02
= 30000	displacement=-3.302185E-02
= 31000	displacement=-3.102184E-02
= 32000	displacement=-2.902185E-02
= 33000	displacement=-2.702185E-02
= 34000	displacement=-2.502185E-02
= 35000	displacement=-2.302186E-02
= 36000	displacement=-2.102186E-02
= 37000	displacement=-2.002186E-02
= 38000	displacement=-1.802187E-02
= 39000	displacement=-1.702187E-02
= 40000	displacement=-1.502187E-02
= 41000	displacement=-1.402187E-02
= 42000	displacement=-1.302187E-02
= 43000	displacement=-1.202187E-02
= 44000	displacement=-1.002187E-02
= 45000	displacement=-9.021868E-03
= 46000	displacement=-8.021848E-03
= 47000	displacement=-7.102186E-03
= 48000	displacement=-6.102186E-03
= 49000	displacement=-5.102186E-03
= 50000	displacement=-4.021848E-03

ORIGINAL PAGE IS
OF POOR QUALITY

APPENDIX I : Abort Motor Chamber Pressure Study

ABORT DATA VARIABLES	ABORT VARIABLES	ABORT DATA VARIABLES
	[DB/AP-HMX/AL]	
Abort Radial distance (m)	Specific Impulse (sec)	Liner Thickness (m)
805.0000	270.0000	0.0025
Abort time, Max (sec)	Specific density (kg/m^3)	Liner Density (kg/m^3)
5.0000	1799.0000	1107.0000
Abort accel. (m/sec^2)	Specific Heat ratio	Engine Propellant Mass (kg)
74.2100	1.2400	43.1949
Abort acceleration, (g)	Flame Temperature (°C)	Engine Prop. Vol (m^3)
7.5647	3707.0000	0.0240
Mass of Capsule (kg)	Number of engines used	Engine Diameter (m)
900.0000	3.0000	0.3000
Av. Thrust Required, (n)	Thrust per Engine (n)	Nozzle cone angle °
67300.2036	22433.4012	0.1745
Total Impulse, It (n-sec)	Casing Material Density (kg/m^3)	Nozzle correction factor
336501.0178	1384.0000	0.9924
Ambient pressure (n/m^2)	Factor of Safety	Tower attachment angle
101325.0000	3.5000	0.0000
	Casing Tensile strength (n/m^2)	
	1723700000.0000	

APPENDIX I : Abort Motor Chamber Pressure Study

Chamber Pressures (n/m ²)	Burn Rates (m/sec)	Web Thickness (m)
4000000.0000	0.0111	0.0556
4900000.0000	0.0119	0.0597
5000000.0000	0.0120	0.0601
6200000.0000	0.0132	0.0661
6894800.0000	0.0140	0.0698
7000000.0000	0.0141	0.0704
8400000.0000	0.0157	0.0786
9000000.0000	0.0165	0.0824
10600000.0000	0.0187	0.0935
11000000.0000	0.0193	0.0965
11500000.0000	0.0201	0.1004
11700000.0000	0.0204	0.1020
12800000.0000	0.0223	0.1113
13500000.0000	0.0235	0.1176
15000000.0000	0.0265	0.1324
Engine Wall Thickness (m)	Outside Grain Diam.(m)	Inside Grain Diam.(m)
0.0012	0.2925	0.1813
0.0015	0.2919	0.1726
0.0015	0.2919	0.1716
0.0019	0.2911	0.1589
0.0021	0.2907	0.1511
0.0021	0.2907	0.1498
0.0026	0.2898	0.1325
0.0027	0.2894	0.1245
0.0032	0.2885	0.1014
0.0034	0.2882	0.0951
0.0035	0.2879	0.0871
0.0036	0.2878	0.0838
0.0039	0.2871	0.0646
0.0041	0.2867	0.0515
0.0046	0.2858	0.0211

APPENDIX I : Abort Motor Chamber Pressure Study

Effective Length (m)	Case free Vol (m ³)	Web Fraction
0.5805	0.0056	0.3800
0.5515	0.0062	0.4087
0.5485	0.0062	0.4120
0.5138	0.0071	0.4541
0.4955	0.0076	0.4804
0.4929	0.0077	0.4845
0.4603	0.0089	0.5427
0.4479	0.0096	0.5697
0.4192	0.0115	0.6485
0.4130	0.0121	0.6699
0.4059	0.0129	0.6976
0.4033	0.0132	0.7090
0.3906	0.0152	0.7751
0.3843	0.0167	0.8203
0.3764	0.0207	0.9263
Pressure Ratio Pc/Pa	Thrust Coef. Cf	Throat Area, At (m ²)
39.4769	1.5100	0.0037
48.3592	1.5200	0.0030
49.3462	1.5400	0.0029
61.1892	1.5600	0.0023
68.0464	1.5700	0.0021
69.0846	1.5700	0.0020
82.9016	1.5900	0.0017
88.8231	1.6000	0.0016
104.6139	1.6200	0.0013
108.5616	1.6250	0.0013
113.4962	1.6300	0.0012
115.4700	1.6350	0.0012
126.3262	1.6370	0.0011
133.2346	1.6400	0.0010
148.0385	1.6500	0.0009

APPENDIX I : Abort Motor Chamber Pressure Study

L/D ratio	Opt. Exp. Ratio A_e/A_t	Exit Area, A_e (m ²)
1.9849	5.5000	0.0204
1.8893	5.7000	0.0172
1.8791	6.0000	0.0175
1.7647	7.0000	0.0162
1.7044	7.5000	0.0155
1.6957	9.0000	0.0184
1.5882	9.5000	0.0160
1.5473	10.5000	0.0164
1.4531	10.7500	0.0140
1.4330	11.0000	0.0138
1.4099	11.5000	0.0138
1.4012	12.0000	0.0141
1.3604	12.5000	0.0134
1.3406	13.0000	0.0132
1.3169	13.5000	0.0122
Throat Diamter (m)	Case mass (kg)	Liner mass (kg)
0.0344	1.0418	1.7372
0.0310	1.2197	1.6604
0.0305	1.2385	1.6522
0.0272	1.4503	1.5603
0.0257	1.5627	1.5119
0.0255	1.5792	1.5048
0.0231	1.7863	1.4185
0.0223	1.8695	1.3856
0.0204	2.0811	1.3096
0.0200	2.1327	1.2933
0.0195	2.1972	1.2745
0.0193	2.2231	1.2674
0.0185	2.3677	1.2338
0.0180	2.4637	1.2173
0.0170	2.6898	1.1961

APPENDIX I : Abort Motor Chamber Pressure Study

Exit Diam. (m)	Nozzle length (m)	Total Individual Motor Mass (kg)
0.0806	0.1312	47.1798
0.0739	0.1218	47.1153
0.0746	0.1252	47.1839
0.0719	0.1268	47.3326
0.0703	0.1266	47.3935
0.0765	0.1446	47.7439
0.0713	0.1365	47.7063
0.0722	0.1415	47.8529
0.0669	0.1318	47.8027
0.0663	0.1313	47.8294
0.0662	0.1323	47.8943
0.0669	0.1350	47.9629
0.0653	0.1327	48.0313
0.0648	0.1327	48.1100
0.0624	0.1288	48.2438
Nozzle Mass (kg)	Igniter mass (kg)	Total Abort System Mass (kg)
1.2059	0.0298	141.5691
1.0403	0.0318	141.3776
1.0982	0.0320	141.5835
1.1271	0.0349	142.0327
1.1239	0.0367	142.2171
1.4650	0.0370	143.2687
1.3066	0.0412	143.1601
1.4029	0.0432	143.6020
1.2171	0.0492	143.4572
1.2084	0.0509	143.5390
1.2277	0.0531	143.7360
1.2775	0.0541	143.9429
1.2349	0.0597	144.1537
1.2342	0.0638	144.3939
1.1630	0.0742	144.8057

APPENDIX I : Abort Motor Diameter Study

ABORT DATA VARIABLES	ABORT VARIABLES	ABORT DATA VARIABLES
	[DB/AP-HMX/AL]	
Abort Radial distance (m)	Specific Impulse (sec)	Opt Exp Ratio Ae/At
805	270	5.9
Abort time, Max (sec)	Specific density (kg/m ³)	Throat area (m ²)
5	1799	0.002992317
Abort accel. (m/sec ²)	Specific Heat ratio	Throat Diameter (m)
74.21	1.24	0.030862341
Abort acceleration, (g)	Burn Rate (m/sec)	Exit area (m ²)
7.564729867	0.011931475	0.017654671
Mass of Capsule (kg)	Chamber Pressure (n/m ²)	Exit Diameter (m)
900	4900000	0.074964366
Av. Thrust Required, (n)	Flame Temperature (°C)	Nozzle length (m)
67300.20356	3707	0.125059645
Total Impulse, It (n-sec)	Pressure Ratio Pc/Pa	Casing Density (kg/m ³)
336501.0178	48.35924007	1384.93
Ambient pressure (n/m ²)	Av. motor Burn Area (m ²)	Factor of Safety
101325	3.870847429	3.5
Number of engines used	Liner Thickness (m)	Casing Tensile strength (n/m ²)
3	0.00254	1723700000
Thrust per Engine (n)	Liner Density (kg/m ³)	Nozzle cone angle (10°)
22433.40119	1107	0.17453
Engine Propellant Mass (kg)	Web Thickness (m)	Nozzle correction factor
43.19490545	0.059657376	0.9924
Engine Prop. Vol (m ³)	Thrust Coeff. Cf	Tower attachment angle
0.024010509	1.53	0

APPENDIX I : Abort Motor Diameter Study

Engine Diameter (m)	Engine Wall Thickness (m)	Outside Grain Diam.(m)
0.14	0.000696467	0.133527066
0.16	0.000795962	0.153328076
0.18	0.000895457	0.173129085
0.2	0.000994953	0.192930095
0.22	0.001094448	0.212731104
0.24	0.001193943	0.232532113
0.26	0.001293439	0.252333123
0.28	0.001392934	0.272134132
0.3	0.001492429	0.291935142
0.32	0.001591924	0.311736151
0.34	0.00169142	0.331537161
0.36	0.001790915	0.35133817
0.38	0.00189041	0.37113918
0.4	0.001989905	0.390940189
Inside Grain Diam.(m)	Effective Length (m)	Case free Vol (m^3)
0.014212314	1.734287367	0.019390957
0.034013324	1.367677097	0.01529191
0.053814333	1.129015079	0.012623446
0.073615343	0.961271534	0.010747916
0.093416352	0.836925267	0.009357608
0.113217362	0.741064151	0.008285791
0.133018371	0.664906054	0.007434272
0.152819381	0.602942519	0.006741462
0.17262039	0.551543408	0.006166772
0.1924214	0.508219189	0.005682366
0.212222409	0.471205576	0.00526852
0.232023418	0.439217368	0.004910861
0.251824428	0.411296163	0.004598676
0.271625437	0.386712699	0.00432381

APPENDIX I : Abort Motor Diameter Study

Web Fraction	Case mass (kg)	Liner mass (kg)
0.893562295	0.750593151	2.188051949
0.778166368	0.779997407	1.989547187
0.68916642	0.82332032	1.866712332
0.618435149	0.875543893	1.78660685
0.56087121	0.934380955	1.733334432
0.513110856	0.998711221	1.6982818
0.472846174	1.0679817	1.67637637
0.438440965	1.141942354	1.664436447
0.408702943	1.220516975	1.660365255
0.38274275	1.303734907	1.662724832
0.359883494	1.391692613	1.670496124
0.33960088	1.484530891	1.682936795
0.321482501	1.582420784	1.699493271
0.305199504	1.685554538	1.719744327
L/D ratio	Nozzle mass (kg)	Igniter mass (kg)
12.98828332	1.096718469	0.0708
8.919939098	1.096718469	0.0600
6.521232859	1.096718469	0.0524
4.982486201	1.096718469	0.0469
3.934193217	1.096718469	0.0425
3.186932508	1.096718469	0.0391
2.635032795	1.096718469	0.0362
2.215607845	1.096718469	0.0338
1.889266927	1.096718469	0.0318
1.630286339	1.096718469	0.0300
1.421275296	1.096718469	0.0284
1.2501271	1.096718469	0.0271
1.108199257	1.096718469	0.0259
0.98918635	1.096718469	0.0248

APPENDIX I : Abort Motor Diameter Study

Total Individual Motor Mass (kg)
47.23026902
47.06116851
46.98165657
46.95377466
46.9593393
46.98861694
47.03598199
47.09800272
47.17250615
47.25808366
47.35381265
47.4590916
47.57353797
47.69692278
Total Abort System Mass (kg)
141.7616244
141.2434769
140.9974076
140.9081781
140.9205421
141.0049038
141.1441442
141.3278106
141.549277
141.804242
142.0898827
142.4043537
142.746476
143.1155384

APPENDIX I : Abort Motor Nozzle Angle Study

ABORT DATA VARIABLES	ABORT VARIABLES	ABORT DATA VARIABLES
	[DB/AP-HMX/AL]	
Abort Radial distance (m)	Specific Impulse (sec)	Casing Density (kg/m ³)
805	270	1384.93
Abort time, Max (sec)	Specific density (kg/m ³)	Factor of Safety
5	1799	3.5
Abort accel. (m/sec ²)	Specific Heat ratio	Casing Tensile strength (n/m ²)
74.21	1.24	1723700000
Abort acceleration, (g)	Burn Rate (m/sec)	Engine Diameter (m)
7.564729867	0.011931475	0.2
Mass of Capsule (kg)	Chamber Pressure (n/m ²)	Engine Wall thickness (m)
900	4900000	0.000995
Av. Thrust Required, (n)	Flame Temperature (°C)	Outside Grain Diam.(m)
66789	3707	0.19293
Total Impulse, It (n-sec)	Pressure Ratio Pc/Pa	Inside Grain Diam.(m)
333945	48.35924007	0.073615248
Ambient pressure (n/m ²)	Liner Thickness (m)	Web Thickness (m)
101325	0.00254	0.059657376
Number of engines used	Liner Density (kg/m ³)	Web Fraction
3	1107	0.618435452
	Thrust Coeff. Cf	Opt Exp Ratio Ae/At
	1.53	5.9

APPENDIX I : Abort Motor Nozzle Angle Study

Nozzle angle, °	Nozzle angle, rad	Nozzle angle correction factor
5	0.087266127	0.9981
6	0.104719352	0.9973
7	0.122172577	0.9963
8	0.139625803	0.9951
9	0.157079028	0.9938
10	0.174532254	0.9924
11	0.191985479	0.9908
12	0.209438704	0.9891
13	0.22689193	0.9872
14	0.244345155	0.9851
15	0.26179838	0.9830
16	0.279251606	0.9806
17	0.296704831	0.9782
18	0.314158056	0.9755
Engine Prop. Mass (kg)	Engine Prop. Vol (m ³)	Effective Length (m)
42.94851799	0.023873551	0.955789037
42.98453858	0.023893573	0.956590649
43.02716031	0.023917265	0.957539166
43.0764093	0.023944641	0.958635168
43.13231573	0.023975717	0.959879326
43.19491396	0.024010514	0.961272406
43.26424253	0.024049051	0.962815264
43.3403442	0.024091353	0.964508853
43.42326607	0.024137446	0.966354221
43.51305955	0.024187359	0.968352512
43.60978052	0.024241123	0.970504969
43.71348933	0.024298771	0.972812935
43.82425094	0.02436034	0.975277857
43.94213496	0.024425867	0.977901283

APPENDIX I : Abort Motor Nozzle Angle Study

Thrust per Engine	Engine total Impulse, It (n-sec)	Throat area (m ²)
22305.43914	111527.1957	0.002975249
22324.14654	111620.7327	0.002977744
22346.28226	111731.4113	0.002980697
22371.85986	111859.2993	0.002984108
22400.89504	112004.4752	0.002987981
22433.40561	112167.0281	0.002992318
22469.4116	112347.058	0.00299712
22508.93523	112544.6762	0.003002392
22552.00095	112760.0047	0.003008137
22598.63546	112993.1773	0.003014357
22648.86777	113244.3389	0.003021057
22702.72925	113513.6463	0.003028242
22760.25362	113801.2681	0.003035915
22821.47703	114107.3852	0.003044081
Av. motor Burn Area (m ²)	Case free Vol (m ³)	Exit area (m ²)
3.848767782	0.010686616	0.017553967
3.851995713	0.010695579	0.017568689
3.855815197	0.010706184	0.01758611
3.860228572	0.010718439	0.017606239
3.865238544	0.01073235	0.017629089
3.870848192	0.010747925	0.017654674
3.877060968	0.010765176	0.01768301
3.883880707	0.010784112	0.017714115
3.891311627	0.010804745	0.017748007
3.899358337	0.010827088	0.017784707
3.908025843	0.010851154	0.017824239
3.917319555	0.010876959	0.017866627
3.927245292	0.01090452	0.017911898
3.937809294	0.010933852	0.017960079

APPENDIX I : Abort Motor Nozzle Angle Study

Throat Diameter (m)	L/D ratio	Case mass (kg)
0.030774194	4.954071615	0.87083861
0.030787097	4.958226556	0.871532667
0.030802357	4.963142934	0.872353918
0.03081998	4.968823758	0.873302865
0.030839973	4.975272513	0.87438009
0.030862344	4.982493161	0.875586255
0.030887101	4.990490147	0.876922102
0.030914255	4.999268404	0.878388456
0.030943814	5.008833364	0.879986224
0.030975792	5.019190959	0.881716397
0.031010199	5.030347632	0.883580051
0.03104705	5.042310347	0.885578349
0.031086359	5.055086596	0.887712543
0.031128141	5.068684408	0.889983974
Exit Diameter (m)	Nozzle Length (m)	Nozzle mass (kg)
0.074750259	0.251325329	2.197718437
0.074781598	0.209290672	1.830912998
0.074818664	0.179242726	1.568825295
0.074861471	0.156686357	1.372184885
0.074910034	0.139124252	1.219174673
0.074964373	0.12505801	1.096704233
0.075024509	0.113534086	0.996443138
0.075090464	0.103916773	0.912837626
0.075162264	0.095765955	0.842042646
0.075239936	0.088767249	0.781311604
0.075323512	0.0826901	0.728630204
0.075413022	0.07736158	0.682487607
0.075508503	0.07264944	0.641728345
0.075609991	0.068450811	0.60545361

APPENDIX I : Abort Motor Nozzle Angle Study

Liner mass (kg)	Total Individual Motor Mass (kg)
1.776920958	47.793996
1.778337162	47.4653214
1.7800129	47.24835243
1.781949199	47.10384625
1.784147246	47.01001774
1.78660839	46.95381284
1.789334148	46.92694192
1.792326201	46.92389649
1.7955864	46.94088134
1.799116767	46.97520432
1.802919499	47.02491027
1.806996969	47.08855225
1.81135173	47.16504356
1.81598652	47.25355906
Igniter mass (kg)	Total Abort System Mass (kg)
0.0467	143.4286548
0.0467	142.4426585
0.0467	141.7917839
0.0468	141.3583028
0.0468	141.0768598
0.0469	140.9082926
0.0469	140.8277325
0.0470	140.8186539
0.0470	140.8696714
0.0471	140.9727084
0.0472	141.1218995
0.0472	141.3129039
0.0473	141.5424616
0.0474	141.8080972

APPENDIX I : Abort Tower Attachment Study

[illegible]

APPENDIX I : Abort Tower Attachment Study

Motor Attach. angle, °	Motor angle, rad	Motor angle correction factor
5	0.087266127	0.9981
6	0.104719352	0.9973
7	0.122172577	0.9963
8	0.139625803	0.9951
9	0.157079028	0.9938
10	0.174532254	0.9924
11	0.191985479	0.9908
12	0.209438704	0.9891
13	0.22689193	0.9872
14	0.244345155	0.9851
15	0.26179838	0.9830
16	0.279251606	0.9806
17	0.296704831	0.9782
18	0.314158056	0.9755
19	0.331611282	0.9728
20	0.349064507	0.9698
21	0.366517732	0.9668
22	0.383970958	0.9636
23	0.401424183	0.9603
24	0.418877409	0.9568
25	0.436330634	0.9532
Engine Prop. Mass (kg)	Engine Prop. Vol (m ³)	Effective Length (m)
43.46576054	0.024161068	0.967299906
43.50221493	0.024181331	0.968111172
43.54534998	0.024205308	0.969071112
43.59519208	0.024233014	0.970180313
43.65177182	0.024264465	0.971439456
43.71512394	0.02429968	0.972849312
43.78528745	0.024338681	0.974410752
43.86230564	0.024381493	0.976124738
43.94622616	0.024428141	0.97799233
44.03710105	0.024478655	0.980014686
44.13498686	0.024533067	0.982193066
44.23994467	0.024591409	0.984528828
44.35204022	0.024653719	0.987023436
44.47134395	0.024720036	0.989678456
44.59793115	0.024790401	0.992495566
44.73188202	0.024864859	0.995476548
44.87328179	0.024943458	0.9986233
45.02222084	0.025026248	1.001937834
45.17879483	0.025113282	1.005422278
45.34310483	0.025204616	1.009078881
45.51525746	0.02530031	1.012910017

APPENDIX I : Abort Tower Attachment Study

Thrust per Engine	Engine total Impulse, It (n-sec)	Throat area (m ²)
22574.07058	112870.3529	0.003011081
22593.00327	112965.0164	0.003013606
22615.40559	113077.0279	0.003016594
22641.29123	113206.4562	0.003020047
22670.67608	113353.3804	0.003023966
22703.57819	113517.891	0.003028355
22740.01782	113700.0891	0.003033216
22780.01744	113900.0872	0.003038551
22823.60181	114118.009	0.003044365
22870.79795	114353.9898	0.00305066
22921.63523	114608.1762	0.003057441
22976.14538	114880.7269	0.003064712
23034.36253	115171.8127	0.003072477
23096.32328	115481.6164	0.003080742
23162.06671	115810.3336	0.003089511
23231.63449	116158.1725	0.003098791
23305.07088	116525.3544	0.003108586
23382.42281	116912.1141	0.003118904
23463.73997	117318.6999	0.003129751
23549.07486	117745.3743	0.003141133
23638.48283	118192.4141	0.003153059
Av. motor Burn Area (m ²)	Case free Vol (m ³)	Exit area (m ²)
3.895119707	0.010815319	0.017765375
3.898386513	0.010824389	0.017780275
3.902251996	0.010835122	0.017797905
3.906718522	0.010847524	0.017818276
3.911788831	0.010861603	0.017841402
3.917466038	0.010877366	0.017867295
3.923753637	0.010894825	0.017895972
3.930655508	0.010913988	0.017927451
3.938175921	0.01093487	0.017961751
3.946319539	0.010957482	0.017998894
3.955091431	0.010981838	0.018038902
3.96449707	0.011007954	0.0180818
3.974542346	0.011035846	0.018127616
3.985233573	0.011065532	0.018176378
3.996577498	0.01109703	0.018228117
4.008581306	0.01113036	0.018282866
4.021252637	0.011165543	0.018340659
4.034599589	0.011202603	0.018401533
4.048630735	0.011241562	0.018465528
4.063355133	0.011282447	0.018532685
4.078782335	0.011325282	0.018603048

APPENDIX I : Abort Tower Attachment Study

Throat Diameter (m)	L/D ratio	Tower Height, (m)
0.030958952	5.013735062	8.357974911
0.030971931	5.017940042	6.770396868
0.030987283	5.02291563	5.63618242
0.031005012	5.02866487	4.785494651
0.031025125	5.03519129	4.123982735
0.03104763	5.042498898	3.595039362
0.031072536	5.050592194	3.162645034
0.031099853	5.059476171	2.80279024
0.03112959	5.069156324	2.49885664
0.031161759	5.079638659	2.238977766
0.031196373	5.090929695	2.014455465
0.031233445	5.103036481	1.818770197
0.03127299	5.115966598	1.64694067
0.031315023	5.129728173	1.495096946
0.03135956	5.144329889	1.360188396
0.031406619	5.159780997	1.239779286
0.031456219	5.176091329	1.131902808
0.031508379	5.19327131	1.034954947
0.03156312	5.211331975	0.947616071
0.031620463	5.23028498	0.868792168
0.031680433	5.250142625	0.797570218
Exit Diameter (m)	Nozzle Length (m)	Tower Mass (kg)
0.075199032	0.104066357	45.96886201
0.07523056	0.104109987	37.23718277
0.075267848	0.10416159	30.99900331
0.075310912	0.104221185	26.32022058
0.075359767	0.104288794	22.68190504
0.075414432	0.104364444	19.77271649
0.075474929	0.104448164	17.39454769
0.07554128	0.104539986	15.41534632
0.075613511	0.104639945	13.74371152
0.075691649	0.10474808	12.31437771
0.075775727	0.104864432	11.07950506
0.075865775	0.104989048	10.00323609
0.075961828	0.105121975	9.058173684
0.076063926	0.105263265	8.223033205
0.076172106	0.105412974	7.481036178
0.076286413	0.10557116	6.818786076
0.07640689	0.105737886	6.225465446
0.076533586	0.105913219	5.692252206
0.076666552	0.106097226	5.21188839
0.076805839	0.106289983	4.778356925
0.076951504	0.106491565	4.3866362

APPENDIX I : Abort Tower Attachment Study

Case mass (kg)	Liner mass (kg)	Total Individual Motor Mass (kg)
0.880805023	1.797257135	46.26573238
0.881507439	1.798690395	46.30439206
0.882338581	1.800386315	46.35013652
0.883298956	1.802345933	46.40299377
0.884389154	1.804570451	46.46299622
0.885609845	1.807061236	46.53018071
0.886961781	1.809819821	46.60458861
0.888445795	1.812847909	46.68626582
0.890062805	1.816147371	46.77526284
0.891813815	1.819720256	46.87163488
0.893699913	1.823568785	46.97544188
0.895722278	1.827695361	47.08674861
0.897882174	1.832102568	47.20562476
0.900180961	1.836793176	47.33214504
0.902620088	1.841770144	47.46638926
0.905201101	1.847036626	47.60844246
0.907925642	1.852595973	47.75839501
0.910795453	1.858451738	47.91634274
0.913812376	1.864607683	48.08238707
0.916978359	1.87106778	48.25663518
0.920295457	1.877836222	48.43920009
Nozzle mass (kg)	Igniter mass (kg)	Total Abort System Mass (kg)
0.121909675	0.0471	184.8131187
0.121979288	0.0471	176.1974461
0.122061647	0.0471	170.0965327
0.122156798	0.0472	165.5763595
0.122264793	0.0472	162.1180941
0.122385692	0.0472	159.410507
0.12251956	0.0473	157.255615
0.122666473	0.0474	155.5215035
0.122826511	0.0474	154.1169231
0.122999762	0.0475	152.9767741
0.123186324	0.0476	152.0533963
0.123386301	0.0476	151.3111267
0.123599804	0.0477	150.7227772
0.123826954	0.0478	150.2672874
0.124067878	0.0479	149.9281183
0.124322714	0.0480	149.6921284
0.124591607	0.0481	149.5487717
0.124874709	0.0482	149.4895134
0.125172185	0.0484	149.5073999
0.125484204	0.0485	149.5967358
0.12581095	0.0486	149.7528385

APPENDIX I : Thrust Loss with Altitude Study

Chamber Pressure, P_o (n/m ²)	Specific Impulse
4000000.0000	269.7351298
4900000.0000	269.8594691
5000000.0000	269.8704957
6200000.0000	269.9748616
6894800.0000	270.0185709
7000000.0000	270.0244276
8400000.0000	270.0883249
9000000.0000	270.1095927
10600000.0000	270.1544846
11000000.0000	270.1636584
11500000.0000	270.1742247
11700000.0000	270.1781974
12800000.0000	270.1978198
13500000.0000	270.2086362
15000000.0000	270.2284044
30000000	270.3171943
50000000	270.3526341
80000000	270.37255
100000000	270.3791856
200000000	270.3924522
500000000	270.4004093
Exit Pressure Ideally Expanded	Fuel Burn Temperature °C
To atmospheric, P_e (n/m ²)	3707
101325.0000	
	Specific Heat ratio (θ)
Universal Gas Constant "R"	1.2400
170.97	

APPENDIX I : Thrust Loss with Altitude Study

Altitude (m)	Atmospheric pressure (N/m ²)	Specific Impulse
0	101325	269.8594691
500	95461	269.8913647
1000	89874	269.9217209
1500	84556	269.950586
2000	79495	269.9780294
2500	74683	270.0040984
3000	70109	270.0288563
3500	65765	270.0523497
4000	61641	270.0746357
4500	57729	270.0957602
5000	54021	270.1157688
5500	50508	270.1347125
6000	47182	270.1526363
6500	44062	270.16944
7000	38252	270.2007054
7500	35601	270.21496
8000	33100	270.2284017
8500	30744	270.2410583
9000	28525	270.2529739
9500	26437	270.2641816
10000	26437	270.2641816
20000	5475	270.3764589
30000	1172	270.3994531
40000	278	270.4042281
50000	76	270.4053069
	Specific Impulse =	
	$1/g\sqrt{((2\partial R/(\partial-1))*To(1-Pe/Po)^{(\partial-1/\partial)})}$	

APPENDIX I : Thrust Loss with Altitude Study

Flame Temperature, To (°C)	Specific Impulse
2500	225.2550947
2600	229.2804851
2700	233.2364122
2800	237.1263526
2900	240.9535022
3000	244.7208069
3100	248.4309894
3200	252.0865717
3300	255.6898957
3400	259.2431404
3500	262.7483378
3600	266.2073856
3700	269.62206
3707	269.8594691
3800	272.9940263
3900	276.3248478
4000	279.615995
4100	282.8688526
4200	286.0847268
4300	289.264851
4400	292.4103917
4500	295.5224531
4600	298.6020821
4700	301.6502719
4800	304.6679663

APPENDIX I : Thrust Loss with Altitude Study

Altitude (m)	Atmospheric pressure (N/m ²)	Thrust at Altitude (N)	Thrust Loss, Pa vs Pe (N)	% Thrust Loss
0	101325	23382.423	0	0
500	95461	23274.5254	107.8976	0.461447473
1000	89874	23171.7246	210.6984	0.901097376
1500	84556	23073.8734	308.5496	1.319579241
2000	79495	22980.751	401.672	1.717837369
2500	74683	22892.2102	490.2128	2.096501291
3000	70109	22808.0486	574.3744	2.456436615
3500	65765	22728.119	654.304	2.798272874
4000	61641	22652.2374	730.1856	3.122796983
4500	57729	22580.2566	802.1664	3.430638476
5000	54021	22512.0294	870.3936	3.722426885
5500	50508	22447.3902	935.0328	3.998870434
6000	47182	22386.1918	996.2312	4.260598656
6500	44062	22328.7838	1053.6392	4.506116411
7000	38252	22221.8798	1160.5432	4.963314538
7500	35601	22173.1014	1209.3216	5.171925938
8000	33100	22127.083	1255.34	5.3687336
8500	30744	22083.7326	1298.6904	5.554130981
9000	28525	22042.903	1339.52	5.728747615
9500	26437	22004.4838	1377.9392	5.893055651
10000	26437	22004.4838	1377.9392	5.893055651
20000	5475	21618.783	1763.64	7.542588721
30000	1172	21539.6078	1842.8152	7.881198625
40000	278	21523.1582	1859.2648	7.951548905
50000	76	21519.4414	1862.9816	7.967444606
Exit Pressure (n/m ²)		Exit Area (m ²)	Engine Thrust (N)	
101325		0.0184	23382.423	

Appendix I : Equations required for Abort Motor design (Sutton,1986)

Specific Requirements and Preliminary Calculations:

- **Abort distance and Acceleration**

- $D = V_o \cdot t + (0.5) \cdot a \cdot t^2$

- $a = 2 \cdot (D - V_o \cdot t) / t^2$

D = abort distance
V_o = initial velocity
t = fuel burn time
a = acceleration

- **Average thrust required**

- $T = m \cdot a$

T = thrust (force)
m = mass

- **Total impulse**

- $I_t = T \cdot t$

I_t = total impulse

- **Mass of the solid fuel (initial)**

- $M_f = I_t / (I_{sp} \cdot G_o)$

M_f = solid propellant mass
I_{sp} = specific impulse
G_o = acceleration of gravity

- **Specific impulse calculation**

- $I_{sp} = 1 / G_o \cdot (((2 \cdot \bar{\partial} \cdot R) / (\bar{\partial} - 1) \cdot T_o \cdot (1 - P_e / P_o)^{((\bar{\partial} - 1) / \bar{\partial})})^{0.5}$

I_{sp} = specific impulse
 $\bar{\partial}$ = specific heat
R = gas constant
T_o = flame temperature
P_e = exit pressure
P_o = chamber pressure

Abort Motor Design Calculations :

- **Propellant burn rate**

- $r = 0.0081056 \cdot e^{(7.8903e10 - 8 \cdot P_o)}$

r = solid fuel burn rate

- **Propellant volume**

- $V_p = M_f / \rho_p$

V_p = propellant volume
 ρ_p = solid propellant density

- **Casing wall thickness**

- $d = (f_s \cdot p \cdot D) / (2 \cdot \beta)$

d = casing wall thickness
f_s = factor of safety
p = chamber pressure
D = engine diameter
 β = tensile strength of material

Appendix I : Equations required for Abort Motor design (Sutton,1986)

Abort Motor Design Calculations -continued- :

- **Web thickness**

- $b = r \cdot t$

b = web thickness

- **Effective motor length**

- $L = (V_f \cdot 4) / (\pi \cdot (D_o^2 - D_i^2))$

L = effective length

D_o = outer fuel diameter

D_i = inner fuel diameter

- **Web fraction**

- $2 \cdot b / D$

- **L/D ratio**

- L / D

- **Area of solid propellant burn**

- $A_b = T / (dp \cdot r \cdot I_{sp})$

A_b = area of burn

- **Case free volume**

- $V_{cf} = \pi/4 \cdot L \cdot D_o^2 - V_p$

V_{cf} = case free volume

- **Throat area**

- $A_t = T / (p \cdot C_f)$

A_t = throat area

C_f = thrust coefficient

- **Throat diameter**

- $D_t = 2 \cdot (A_t / \pi)^{0.5}$

D_t = throat diameter

- **Exit area**

- $A_e = A_t \cdot e$

A_e = nozzle exit area

e = optimum expansion ratio

- **Nozzle Length (cone)**

- $L_n = (D_e/2 - D_t/2) / \tan \emptyset$

L_n = nozzle length

D_e = exit diameter

\emptyset = nozzle half cone angle

- **Nozzle correction factor**

- $c = 0.5 \cdot (1 + \cos \emptyset)$

c = nozzle correction factor

- **Propellant mass fraction**

- $F_p = M_f / M_t$

F_p = propellant mass fraction

M_t = total mass of motor

- **Volumetric loading**

- $V_f = V_p / (V_{cf} + V_p)$

V_f = volumetric loading

Appendix I : Equations required for Abort Motor design (Sutton,1986)

Motor Mass Estimation :

• Casing mass

$$\bullet \bullet M_c = d \cdot \pi \cdot D \cdot L \cdot d_w + (\pi/4) \cdot d \cdot D^2 \cdot d_w$$

M_c = casing mass
 d_w = casing density

• Liner mass

$$\bullet \bullet M_l = l \cdot \pi \cdot D_o \cdot L \cdot d_l + (\pi/4) \cdot l \cdot D_o^2 \cdot d_l$$

M_l = liner mass
 d_l = liner density
 l = liner thickness

• Ignitor charge mass

$$\bullet \bullet M_i = 0.5 \cdot (V_{cf})^{0.7}$$

M_i = ignitor charge mass

• Nozzle mass

$$\bullet \bullet M_n = (2 \cdot \pi \cdot (D_e - D_t) \cdot L_n \cdot d \cdot (d_w + d_n) + d_n \cdot t_i^3 \cdot 2 \cdot \pi)^{0.7}$$

M_n = nozzle mass
 d_n = density of nozzle insert
 t_i = thickness of nozzle insert

Appendix J : ΔV vs Mass

$$R = (1250 / (1250 - \text{fuel mass}))$$

$$\Delta V = g \cdot I_{sp} \cdot \ln(R)$$

$$I_{sp} = 291.3 \text{ sec}$$

<u>Fuel Mass (kg)</u>	<u>R</u>	<u>ΔV (m/sec)</u>
50	1.042	117
55	1.046	129
60	1.050	141
65	1.055	153
70	1.059	165
75	1.064	177
80	1.068	189
85	1.073	201
90	1.078	214
95	1.082	226
100	1.087	238
105	1.092	251
110	1.096	263
115	1.101	276
120	1.106	288
125	1.111	301
130	1.116	314
135	1.121	327
140	1.126	339
145	1.131	352
150	1.136	365
155	1.142	378
160	1.147	391
165	1.152	405
170	1.157	418
175	1.163	431
180	1.168	444
185	1.174	458
190	1.179	471
195	1.185	485
200	1.190	498
205	1.196	512
210	1.202	526
215	1.208	539
220	1.214	553
225	1.220	567
230	1.225	581
235	1.232	595
240	1.238	609
245	1.244	623

250	1.250	638
255	1.256	652
260	1.263	666
265	1.269	681
270	1.276	695
275	1.282	710
280	1.289	725
285	1.295	740
290	1.302	754
295	1.309	769
300	1.316	784
305	1.323	799
310	1.330	815
315	1.337	830
320	1.344	845
325	1.351	861
330	1.359	876
335	1.366	892
340	1.374	907
345	1.381	923
350	1.389	939
355	1.397	955
360	1.404	971
365	1.412	987
370	1.420	1003
375	1.429	1019
380	1.437	1036
385	1.445	1052
390	1.453	1069
395	1.462	1085
400	1.471	1102
405	1.479	1119
410	1.488	1136
415	1.497	1153
420	1.506	1170
425	1.515	1188
430	1.524	1205
435	1.534	1222
440	1.543	1240
445	1.553	1258
450	1.563	1275
455	1.572	1293
460	1.582	1311
465	1.592	1330
470	1.603	1348
475	1.613	1366
480	1.623	1385
485	1.634	1403

490	1.645	1422
495	1.656	1441
500	1.667	1460
505	1.678	1479
510	1.689	1498
515	1.701	1518
520	1.712	1537
525	1.724	1557
530	1.736	1577
535	1.748	1596
540	1.761	1617
545	1.773	1637
550	1.786	1657
555	1.799	1678
560	1.812	1698
565	1.825	1719
570	1.838	1740
575	1.852	1761
580	1.866	1782
585	1.880	1804
590	1.894	1825
595	1.908	1847
600	1.923	1869

Appendix J : Thrust Chamber Design, Equatlons and Results

$$\frac{A_t}{A_e} = \left(\frac{k+1}{2} \right)^{\frac{1}{k-1}} \left(\frac{P_e}{P_c} \right)^{\frac{1}{k}} \sqrt{\left[\frac{k+1}{k-1} \left(1 - \left(\frac{P_e}{P_c} \right)^{\frac{k-1}{k}} \right) \right]}$$

$$E = \frac{A_e}{A_t}$$

$$I_{sp} = \frac{1}{g} \sqrt{\frac{2kRT_c}{k-1}} \sqrt{\left(1 - \left(\frac{P_e}{P_c} \right)^{\frac{k-1}{k}} \right)}$$

$$V_e = g I_{sp}$$

$$C_t = \sqrt{\frac{2k^2}{k-1} \left(\frac{2}{k+1} \right)^{\frac{k+1}{k-1}} \left(1 - \left(\frac{P_e}{P_c} \right)^{\frac{k-1}{k}} \right)} + \frac{(P_e - P_a) A_e}{P_c A_t}$$

$$A_t = \frac{F}{(c_f C_t P_c)}$$

$$D_t = \sqrt{\frac{4 A_t}{\pi}}$$

$$A_e = \frac{A_e}{A_t} A_t$$

$$D_e = \sqrt{\frac{4 A_e}{\pi}}$$

Where :

A_t/A_e = Area Ratio

A_t = Area of the throat

E = Expansion Ratio

Specific Heat Ratio

P_c = Chamber Pressure

P_e = Exit Pressure

P_a = Atmospheric Pressure

I_{sp} = Specific Impulse

R = Universal Gas Constant

g = Gravitaional constant

V_e = Exhaust Velocity

C_t = Coefficient of Thrust

c_f = Correction Factor for Thrust

F = Thrust

D_t = Throat Diameter

D_e = Exit Diameter

Chamber Pressure (psia)	Exit Pressure (psia)	At/Ac	Expansion Area Ratio	Isp (sec)
100	1	9.556E-02	10.46	274.32
200	1	5.740E-02	17.42	285.61
300	1	4.244E-02	23.56	291.33
400	1	3.420E-02	29.24	295.04
500	1	2.892E-02	34.58	297.75
600	1	2.520E-02	39.69	299.85
700	1	2.242E-02	44.60	301.56
800	1	2.026E-02	49.35	302.99
900	1	1.853E-02	53.97	304.21
1000	1	1.710E-02	58.47	305.27

Exhaust Velocity (m/sec)	Cf	Thrust (lbs)	At at P1=100psi (m^2)	At at P1=200psi (m^2)
2691.06	1.71	100	3.92E-04	1.91E-04
2801.82	1.76	200	7.84E-04	3.81E-04
2857.93	1.79	300	1.18E-03	5.72E-04
2894.39	1.80	355	1.39E-03	6.77E-04
2920.92	1.82	400	1.57E-03	7.63E-04
2941.55	1.82	500	1.96E-03	9.53E-04
2958.29	1.83	600	2.35E-03	1.14E-03
2972.29	1.84	700	2.75E-03	1.33E-03
2984.27	1.84	710	2.78E-03	1.35E-03
2994.70	1.85	800	3.14E-03	1.53E-03
		900	3.53E-03	1.72E-03
		1000	3.92E-03	1.91E-03

At at P1=300psi (m^2)	Dt at P1=300psi (m)	Ae at P1=300psi (m^2)	Dc at P1=300psi (m)	At at P1=400psi (m^2)
1.25E-04	0.013	2.95E-03	0.061	9.31E-05
2.51E-04	0.018	5.91E-03	0.087	1.86E-04
3.76E-04	0.022	8.86E-03	0.106	2.79E-04
4.45E-04	0.024	1.05E-02	0.116	3.31E-04
5.01E-04	0.025	1.18E-02	0.123	3.73E-04
6.27E-04	0.028	1.48E-02	0.137	4.66E-04
7.52E-04	0.031	1.77E-02	0.150	5.59E-04
8.77E-04	0.033	2.07E-02	0.162	6.52E-04
8.90E-04	0.034	2.10E-02	0.163	6.61E-04
1.00E-03	0.036	2.36E-02	0.173	7.45E-04
1.13E-03	0.038	2.66E-02	0.184	8.38E-04
1.25E-03	0.040	2.95E-02	0.194	9.31E-04

At at P1=700psi (m^2)	At at P1=800psi (m^2)	At at P1=900psi (m^2)	At at P1=1000psi (m^2)	Ae at P1=400psi (m^2)
5.24E-05	4.57E-05	4.05E-05	3.63E-05	2.72E-03
1.05E-04	9.14E-05	8.10E-05	7.27E-05	5.45E-03
1.57E-04	1.37E-04	1.21E-04	1.09E-04	8.17E-03
1.86E-04	1.62E-04	1.44E-04	1.29E-04	9.67E-03
2.10E-04	1.83E-04	1.62E-04	1.45E-04	1.09E-02
2.62E-04	2.28E-04	2.02E-04	1.82E-04	1.36E-02
3.14E-04	2.74E-04	2.43E-04	2.18E-04	1.63E-02
3.67E-04	3.20E-04	2.83E-04	2.54E-04	1.91E-02
3.72E-04	3.24E-04	2.87E-04	2.58E-04	1.93E-02
4.19E-04	3.65E-04	3.24E-04	2.91E-04	2.18E-02
4.72E-04	4.11E-04	3.64E-04	3.27E-04	2.45E-02

<u>Ae at P1=100psi(m^2)</u>	<u>Ae at P1=200psi(m^2)</u>
4.10E-03	3.32E-03
8.21E-03	6.64E-03
1.23E-02	9.97E-03
1.46E-02	1.18E-02
1.64E-02	1.33E-02
2.05E-02	1.66E-02
2.46E-02	1.99E-02
2.87E-02	2.33E-02
2.91E-02	2.36E-02
3.28E-02	2.66E-02
3.69E-02	2.99E-02
4.10E-02	3.32E-02

<u>At at P1=500psi(m^2)</u>	<u>At at P1=600psi(m^2)</u>
7.40E-05	6.14E-05
1.48E-04	1.23E-04
2.22E-04	1.84E-04
2.63E-04	2.18E-04
2.96E-04	2.45E-04
3.70E-04	3.07E-04
4.44E-04	3.68E-04
5.18E-04	4.30E-04
5.26E-04	4.36E-04
5.92E-04	4.91E-04
6.66E-04	5.52E-04
7.40E-04	6.14E-04

<u>Ae at P1=500psi(m^2)</u>	<u>Ae at P1=600psi(m^2)</u>
2.56E-03	2.44E-03
5.12E-03	4.87E-03
7.68E-03	7.31E-03
9.09E-03	8.65E-03
1.02E-02	9.74E-03
1.28E-02	1.22E-02
1.54E-02	1.46E-02
1.79E-02	1.71E-02
1.82E-02	1.73E-02
2.05E-02	1.95E-02
2.30E-02	2.19E-02

5.24E-04

4.57E-04

4.05E-04

3.63E-04

2.72E-02

Ac at P1=700psi (m^2) Ac at P1=800psi (m^2) Ac at P1=900psi (m^2) At at P1=1000psi (m^2)

2.34E-03

2.25E-03

2.185E-03

2.13E-03

4.67E-03

4.51E-03

4.370E-03

4.25E-03

7.01E-03

6.76E-03

6.555E-03

6.38E-03

8.29E-03

8.00E-03

7.757E-03

7.54E-03

9.35E-03

9.02E-03

8.740E-03

8.50E-03

1.17E-02

1.13E-02

1.093E-02

1.06E-02

1.40E-02

1.35E-02

1.311E-02

1.28E-02

1.64E-02

1.58E-02

1.530E-02

1.49E-02

1.66E-02

1.60E-02

1.551E-02

1.51E-02

1.87E-02

1.80E-02

1.748E-02

1.70E-02

2.10E-02

2.03E-02

1.967E-02

1.91E-02

2.34E-02

2.25E-02

2.185E-02

2.13E-02

Appendix J : Heat Transfer Analysis

$$a = c \sqrt{\frac{2kt}{R_r R_c C_p \rho} \ln \left(1 + \frac{R_r R_v C_p (T_{aw} - T_d)}{L_p} \right)} \frac{P_c^{0.4}}{100}$$

This equation predicts the necessary thickness for the combustion chamber and throat.

where

a = char depth

c = correction factor based on experimental data

R_r = weight fraction of resin content in the ablative material

R_v = weight fraction of pyrolyzed resin versus total resin content R_r

C_p = heat capacity at constant pressure

k = heat conductivity of char

t = thrust chamber firing duration

L_p = latent heat of pyrolysis

T_{aw} = adiabatic wall temperature of the gas

T_d = decomposition temperature of resin

P_c = chamber pressure

$$a = b t^{0.5} e^{-0.0247 \epsilon}$$

This equation predicts the necessary thickness for the nozzle.

where

b = constant depending on the nature of the ablative material

e = nozzle expansion area ratio at the investigated section

The following values were used to determine the thicknesses:

C = 1.05

R_r = 0.3

R_v = 0.41

C_p = 0.38 Btu/lb degree F

density = 0.061 lb/in³

L_p = 686 Btu/lb

T_{aw} = 5142 R

T_d = 1460 R

b = 0.0335

t = 90 sec

The thickness for the throat turned out to be 1.54 cm (once all the units were converted).

The thickness for the nozzle was 0.71 cm (once again, units were converted)

Appendix J : Injector Design Equations

$$w = \frac{F}{c}$$

$$w_o = \frac{wr}{(r+1)}$$

$$w_f = \frac{w}{(r+1)}$$

$$Q_o = \frac{w_o}{\rho_o}$$

$$Q_f = \frac{w_f}{\rho_f}$$

$$\Sigma A_o = \frac{w_o}{(C_d \sqrt{2 \Delta p \rho_o})}$$

$$\Sigma A_f = \frac{w_f}{(C_d \sqrt{2 \Delta p \rho_f})}$$

$$v = C_d \sqrt{\frac{2 \Delta p}{\rho}}$$

$$\sin \gamma_f = r \left(\frac{v_o}{v_f} \right) \sin \gamma_o$$

where

w_o=oxidizer flow rate

w_f=fuel flow rate

r=mixture ratio

Q's=propellant injection volume flow rate

A= areas of orifices

v=injection velocities

Δp=pressure drop

gamma=fuel injection angle

Appendix J : Isothermal vs Adiabatic Expansion Analysis

Isothermal Analysis

Equation of State : $PV = \text{constant}$

Initial Conditions: $P_{He} = P_{He}$

$$V_{He} = V_{He}$$

Final Conditions: $P_{He} = P_{\text{propellant}}$

$$V_{He} = V_{\text{propellant}} + V_{He \text{ initial}}$$

$$(PV)_{\text{initial}} = (PV)_{\text{final}}$$

$$P_{He} V_{He} = P_{\text{Prop}} (V_{He} + V_{\text{prop}})$$

Solving this equation for the volume of helium we get the following:

$$V_{He} = (P_{\text{prop}} V_{\text{prop}}) / (P_{He} - P_{\text{prop}})$$

The mass of helium can be determined by multiplying its density by the volume obtained.

Let density = 51 kg/m³ , pressure of the propellants = 3.447MPa, volume of the propellants = 0.159 m³ and the pressure of helium= 27.579 MPa. The result obtained is a mass of 1.16 kg of helium.

Adiabatic Expansion Analysis

Conservation of Energy: $m_{He} c_v T_{He} + m_p c_p T_p + P_p V_p = m_{He0} c_v T_{He0}$

Solving for the mass of helium the following equation is obtained:

$$m_{He \text{ initial}} = (P_{\text{prop}} V_{\text{prop}} k) / (R T_{He \text{ initial}} (1 - (P_g / P_{He \text{ initial}})))$$

The mass of helium obtained for the same aforementioned conditions is 1.33kg. There is only a difference of 0.17

Appendix J : Pressure Drop Analysis

$$\Delta p = k \frac{\rho v^2}{288}$$

This equation was presented in the Nasa Report "Design of Liquid Propellant Rocket Engines". It is an equation which estimates the pressure drops in various components of a feed system. The value "k" is a constant obtained from experiments performed numerous times. The authors present a table with values for this constant according to the component under study.

In this analysis three components were studied namely, tee connections, fuel and oxidizer valves, and pipes. An explicit calculation will be presented for the fuel and oxidizer valves.

An assumed value of 100 ft/sec was taken for the characteristic velocity of the valve. The value for the constant k given in the table is 0.31. Finally, the densities of the fuel and oxidizer are 63.05 lb/ft³ and 89.90 lb/ft³, respectively. Substituting these values into the above equation gives the following results :

$$\Delta p \text{ for fuel} = 21.21 \text{ psi}$$

$$\Delta p \text{ for oxidizer} = 30.24 \text{ psi}$$

Appendix K: Orbital Maneuverability

K.1 Epoch Maneuvers

For the epoch maneuver sequence a total of five burns are made. These are broken down in figure K.A.

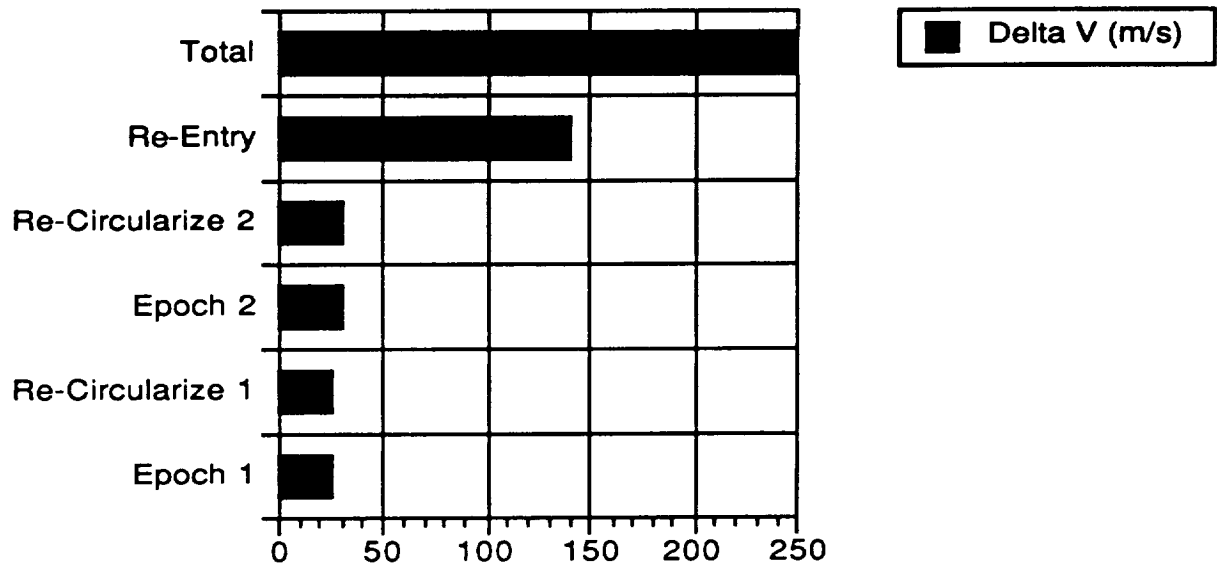


Fig. K.A Breakdown of Epoch Maneuver Burns

The sequence for these burns is from bottom to top, i.e. the epoch 1 burn is first. This sequence is portrayed in Fig. K.B. The capsule's orbit is circularized before re-entry for simplicity in re-entry calculations and trajectories.

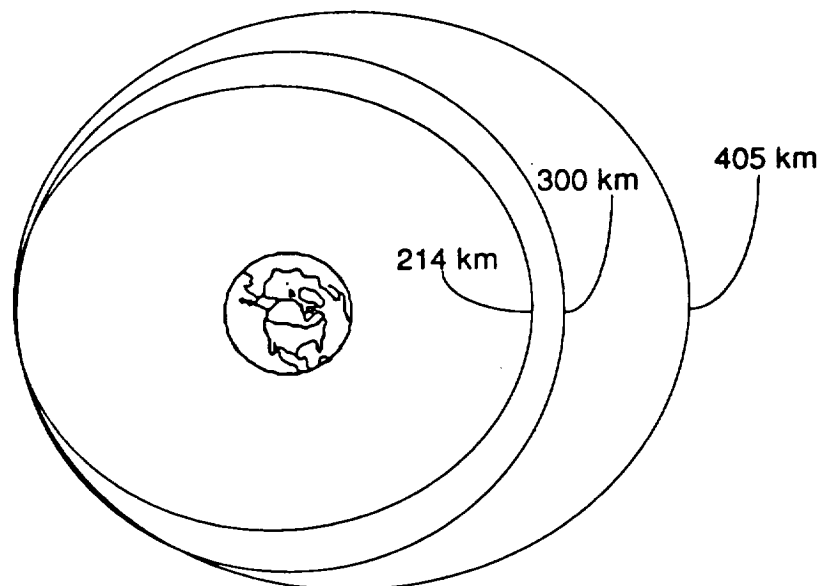


Fig. K.B Epoch Maneuvers

K.2 Hohmann Transfer

The third mission involves a Hohmann or minimum energy transfer. The maximum altitude achievable for a single transfer is 500 km. This maneuver breaks down as follows :

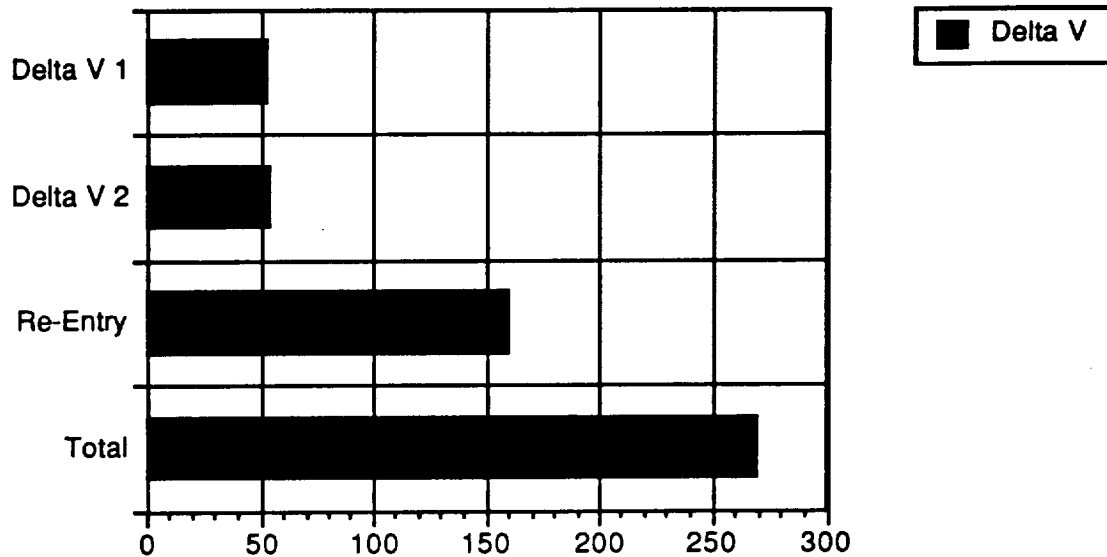


Fig. K.C Breakdown of Burns for Hohmann Transfer

The total ΔV for this mission is 269 m/s which is very close to the total available. This is not critical though since the Reaction Control System uses the same fuel and runs off of the same tanks. A diagram of this maneuver is given below.

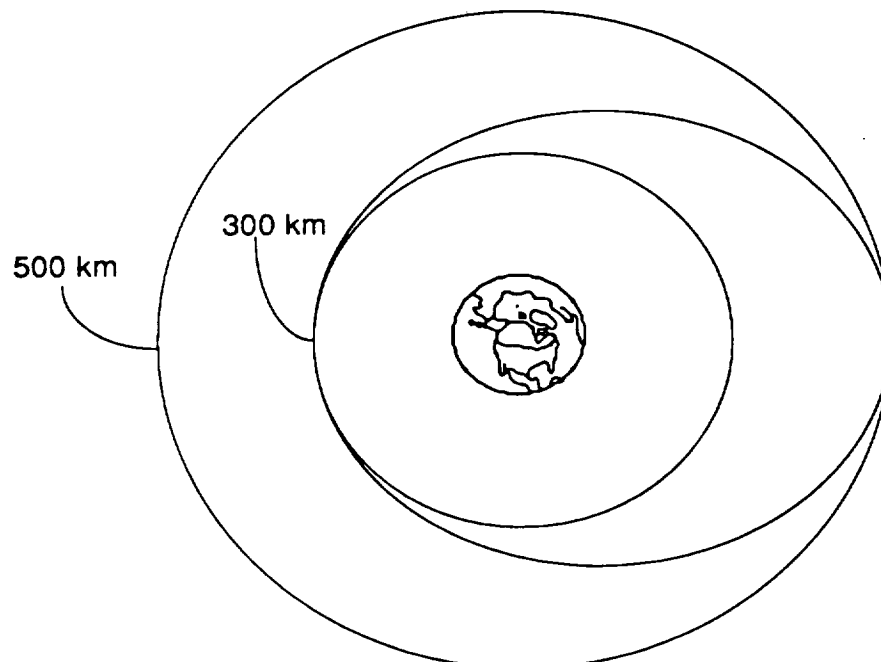


Figure K.D Hohmann Transfer

K.3 Plane Change

A plane change maneuver is essential for any rendezvous mission and is therefore a desired capability. The maximum plane change capability of the LMS is 1.5 degrees. The ΔV would be 100 m/s. A diagram of this maneuver is given below.

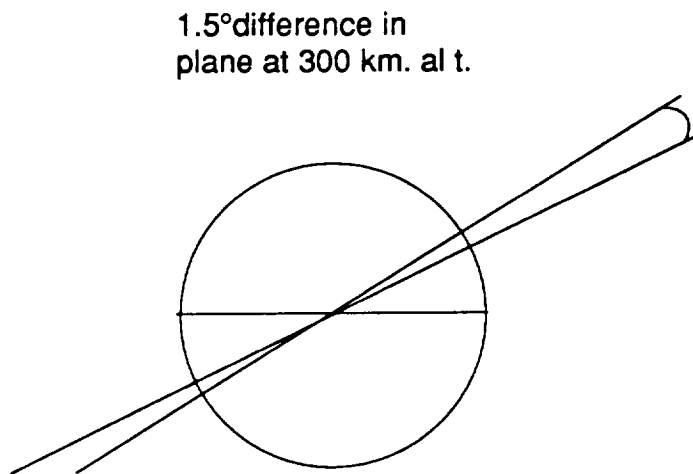


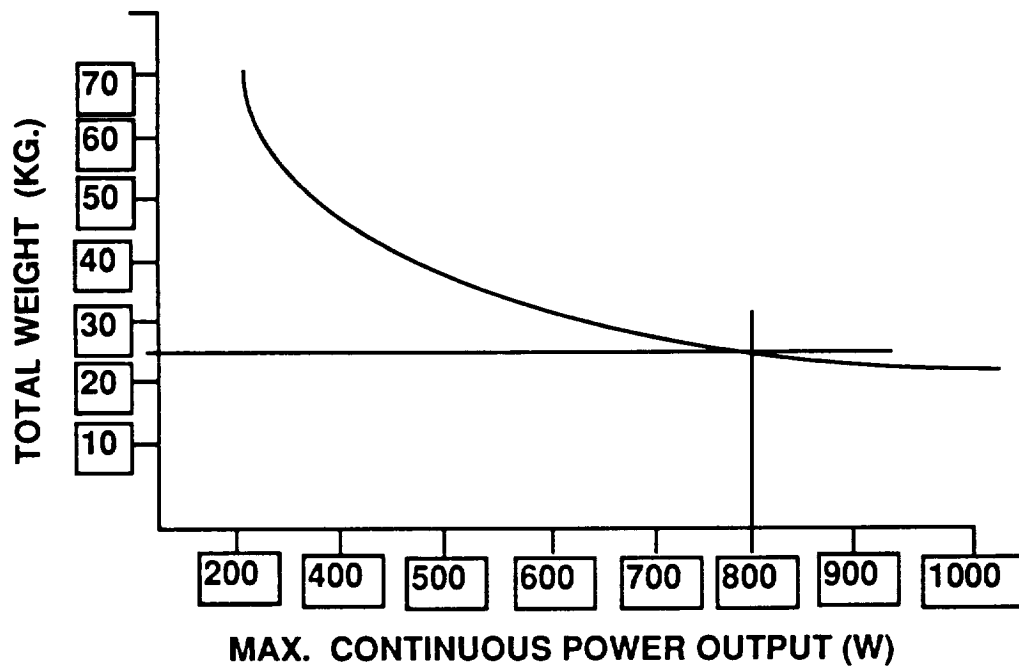
Figure KE Plane Change Maneuver

The plane change maneuver in this case does not include an altitude change and therefore the altitude of the new orbit will be the same. The ΔV required for re-entry for this maneuver is 140 m/s.

APPENDIX L: Power Systems

1. Calculation of Engine's weight:

The following graph shows the relation between the weight of the engine and the power output it delivers. This graph was made for an H₂-O₂ engine, but it works with the new adapted engine for the Taurus since the only thing that changes is the fuel. All the mechanisms inside the engine remain the same.



So, it can be seen that for an engine that produces 800 W, the weight will be 25.2 Kg. This total weight consists the compressor, alternator, cooling system, and plumbing. This engine was developed to work better at power outputs of about 1 KW to 6 KW. This engine is not a good choice for power outputs lower than 600 Watts.

2. Calculation of the Engine's Size:

The volume was obtained from a table similar to the weight-power graph. The following table shows the relation between the size and the energy needed during the mission.

Mission (KW-hr)	Volume (m ³)
10	0.0513
15	0.0767
20	0.1032
40	0.2132

By interpolating the data, a volume was obtained for the 19.2 KW-hr needed. This came out to be:

$$19.2 \text{ KW-hr} = 0.00973 \text{ m}^3$$

It can be seen that as the mission gets longer, the size of the engine increases. This engine works best in shorth missions where low power outputs are needed.

3. Calculation of the Weight of Fuel:

The fuel used will be Hydrazine (N₂H₄), and Nitrogen-tetraoxyde (N₂O₄)
Their respective energies are:

$$\text{N}_2\text{H}_4 = 1.327 \times 10^3 \text{ BTU/Kg} = 0.3888 \text{ KW-hr/Kg.}$$

$$\text{N}_2\text{O}_4 = 392.42 \text{ BTU/Kg.} = 0.11498 \text{ KW-hr/Kg.}$$

The energy given off when the chemicals are combined is:

$$0.503815 \text{ KW-hr/Kg}$$

Since the mixing ratio was set at $\frac{\text{N}_2\text{H}_4}{\text{N}_2\text{O}_4} = 1.34$

To produce the required energy for the mission, 19.2 KW-hr, the weight of

$$\text{N}_2\text{H}_4 = 16.3 \text{ Kg.}$$

The weight of

$$\text{N}_2\text{O}_4 = 21.8 \text{ Kg.}$$

The density of N₂H₄ is 1010 Kg/m³, the N₂H₄ will have a volume of

$$0.01614 \text{ m}^3.$$

The density of N₂O₄ is 1450 Kg/m³, the N₂O₄ will have a volume of

$$0.01503 \text{ m}^3.$$

Appendix M - Re-entry Accuracy Evaluation

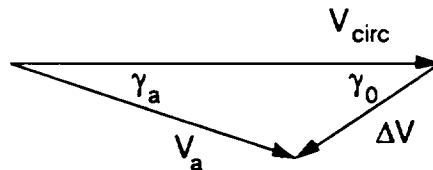
The accuracy required for LMS re-entry had to be determined to evaluate the effect of inaccuracies in pointing and altitude of the guidance computers. Errors in pointing and altitude would affect the entire re-entry trajectory. Either or both of these errors will cause the actual re-entry conditions to vary from what will be expected. This in turn will cause an inaccuracy in landing site.

The analysis to determine the effect of these errors was based on a computer model (see Table M.1) in which the error in altitude and angular pointing could be inputted. The code returns the values of flight path angle and velocity at re-entry interface (120 km altitude). These values were passed to the re-entry model described in Appendix F, and the angular distances traveled were outputted. The difference in angular distance between the "errored" values and the exact values allowed the landing site error to be computed. This was done by the equation $s = R \Delta\theta$, where,

s = distance along the surface of Earth

R = radius of Earth

$\Delta\theta$ = difference in angular distance traveled



The code is based on the conservation of angular momentum and energy equations. The accompanying code basis the calculations on re-entry from 300 km altitude with a ΔV of 140 m/s. γ_0 is the error in pointing as measured from directly opposed to the direction of motion, V_{circ} . This is the direction that the de-orbit burn is expected to be performed in. From γ_0 the flight path angle (γ_a) and Velocity (V_a) at the burn location can be calculated by the law of cosines (see above vector diagram.) Then knowing V_a , γ_a , and the altitude (plus or minus uncertainty, h), the conditions at re-entry interface are calculated (as described in Section 2.4.2). These values are passed to the re-entry program (Appendix F) and the error in landing site due to inaccuracies in pointing and altitude determination.

Altitude errors ranging from 1 meter to 100 meters were evaluated and it was found that slight altitude variations cause insignificant changes in angular distance traveled and hence landing site.

Point errors ranging from 0.1° to 10° (see table M.1) were evaluated. It was found that 0.2° gives a landing site error of 7.715 km. This is within the accuracy of the sun and horizon attitude sensors used on the LMS.

Table M.1

Point Error	Landing Site Error
0.2°	7.715 km
1.0°	12.203 km
2.0°	28.042 km
5.0°	229.871 km
10.0°	1233.506 km

Figure M.1

```

10 REM * Program to determine the accuracy needed for re-entry
20 PI = 3.141592654
30 DEF FNARCCOS(x) = -ATN( X / SQR( 1 - X*X)) + PI / 2
40 U = 398601.28 * 1000 ^ 3
50 PRINT " Enter altitude error (m)"; INPUT H
60 PRINT " Enter angular error (deg)"; INPUT GO
70 DV = 140
80 GO = GO * PI / 180
90 RA = 6678*1000 + H
100 RF = 6498*1000
110 VC = SQR( U / RA )
120 VA = SQR( ( VC - DV * COS( GO ) )^2 + (DV * SIN( GO ) )^2 )
130 PRINT "Va = ";VA
140 VF = SQR( 2 * (VA^2 / 2 + U / RF - U / RA ))
150 PRINT "Vf = ";VF
160 GA = FNARCCOS ( (DV^2 - VA^2 - VC^2 ) / ( -2 * VC * VA ) )
170 GA = GA * 180 / PI
180 PRINT " Ga = "; GA
190 GF = FNARCCOS( RA * VA * COS( GA * PI / 180) / (RF * VF ) )
200 GF = GF * 180 / PI
210 PRINT "Gf = ";GF

```


APPENDIX N

Design Calculations for Capsule Structure:

As mentioned earlier in section 6.7.3 the structural analysis was estimated often from similar members from Project Mercury, and often available data on this NASA endeavor was limited. Therefore, some highly conservative mass estimates are given to help in this feasibility study.

$$m_{\text{stringers}} = 14(3 \times .002 \times .02)2.34 = 10.62 \text{ kg}$$

$$\begin{aligned} m_{\text{skin}} &= \pi \rho L \{ [(r_{\text{base}} + t)^2 - (r_{\text{top}})^2] - [(r_{\text{base}})^2 - (r_{\text{top}})^2] \} \\ &= \pi(2700)(2.34)(.002261) = 42.41 \text{ kg} \end{aligned}$$

The formentioned estimates may be seen in Table-6.3.A.

Appendix O : Tank Design for the OMS, Equations and Results

The first step in the design was to calculate the required masses for the fuel and oxidizer in the OMS. This was done by using the mixture ratio of the bipropellant combination and the mass allotment given by the Systems Integration Group.

The next step was to calculate the required volumes of fuel and oxidizer. Since mass at this point had been determined, the volumes were obtained by dividing the masses by their respective densities. An additional volume referred to as trapped volume was included in the calculations. The trapped volume takes into account propellants trapped in tanks, ducts and other components. Since this volume cannot be precisely measured an estimate of about 2% of the calculated volume was made.

The tanks were designed to be spherical. The radius of the tanks was determined using the first equation below. The thickness of the walls was determined using the second equation.

$$r = \left(\frac{3}{4} \frac{V}{\pi} \right)^{\frac{1}{3}}$$

$$t = \frac{4P_t r}{2S_w e_w}$$

where P_t is the pressure of the tanks, r is the radius of the tank obtained from the volume of a sphere, V is the volume, S_w is the maximum allowable stress of the tank construction material, e_w is the weld efficiency, and a safety factor of 4 is used.

For the fuel the calculations for the radius and thickness are given as follows:

$$r = \left(\frac{3}{4} \frac{0.08476}{\pi} \right)^{\frac{1}{3}} = 27.25 \text{ cm}$$

$$t = \left(\frac{(4)(3.447 \text{ MPa})(27.25 \text{ m})}{(2)(1698 \text{ MPa})(1)} \right) = 1.106 \text{ mm}$$

For the oxidizer the calculations for the radius and thickness are as follows:

$$r = \left(\frac{3}{4} \frac{0.07446}{\pi} \right)^{\frac{1}{3}} = 26.10 \text{ cm}$$

$$t = \left(\frac{(4)(3.447 \text{ MPa})(26.10 \text{ m})}{(2)(1698 \text{ MPa})(1)} \right) = 1.060 \text{ mm}$$

C-4

For the mass of the tanks the following equation was used.

$$m = 4\pi r^2 \rho$$

For the fuel the mass is:

$$m = 4\pi(0.2725)^2(1.106 \times 10^{-3})(1610) = 1.66 \text{ kg}$$

For the Oxidizer the mass is:

$$m = 4\pi(0.2610)^2(1.106 \times 10^{-3})(1610) = 1.46 \text{ kg}$$

Now to calculate the mass of the helium an isothermal expansion was assumed and the following equation was used:

$$m_{\text{He}} = \left(\frac{\rho_{\text{He}} P_{\text{prop}} V_{\text{prop}}}{P_{\text{He}} - P_{\text{prop}}} \right)$$

$$m_{\text{He}} = \left(\frac{\left(51 \frac{\text{kg}}{\text{m}^3} \right) (3.447 \times 10^6) (0.07446 \text{ m}^3 + 0.08476 \text{ m}^3)}{27.579 \times 10^6 - 3.447 \times 10^6} \right) = 1.160 \text{ kg}$$

Using the above equations for the radius, thickness and mass the following values were obtained for the Helium tank:

$$\text{Volume} = 0.0227 \text{ m}^3$$

$$r = 17.58 \text{ cm}$$

$$t = 5.71 \text{ mm}$$

$$\text{mass of tank} = 3.57 \text{ kg}$$

APPENDIX O

The formentioned equations used in calculating the sizes of the main propulsion tanks are the basis for the following calculations, so the formulas will not be included.

Definition of terms:

- m=mass
- v=volume
- r=radius
- t=thickness

Design of Reentry Control Thrusters:

• Fuel Tank:

$$m_{\text{fuel}} = .524 \text{ kg}$$

$$v_{\text{tank}} = \frac{.524}{1010} = 0.00052 \text{ m}^3$$

$$v_{\text{trapped}} = .02(.00052) = .000009 \text{ m}^3$$

$$v_{\text{total}} = .000529 \text{ m}^3$$

$$r = [.75/\pi(.000529)]^{1/3} = 5.0 \text{ cm}$$

$$t = \frac{4(3.447)(.05)}{2(1698)} = .21 \text{ mm}$$

$$m = 4\pi(.05)^2(.00021)(1610) + .524 = .535 \text{ kg}$$

• Oxidizer tank:

$$m_{\text{fuel}} = .848 \text{ kg}$$

$$v_{\text{tank}} = \frac{.848}{1440} = 0.00059 \text{ m}^3$$

$$v_{\text{trapped}} = .02(.00059) = .000012 \text{ m}^3$$

$$v_{\text{total}} = .0006 \text{ m}^3$$

$$r = [.75/\pi(.0006)]^{1/3} = 5.2 \text{ cm}$$

$$t = \frac{4(3.447)(.052)}{2(1698)} = .21 \text{ mm}$$

$$m = 4\pi(.052)^2(.00021)(1610) + .848 = .535 \text{ kg}$$

- Helium tank:

$$m_{\text{fuel}} = .3199 \text{ kg}$$

$$v_{\text{tank}} = \frac{.3199}{51.0} = 0.0063 \text{ m}^3$$

$$r = [.75/\pi(.0063)]^{1/3} = 11.45 \text{ cm}$$

$$t = \frac{4(27.579)(.1145)}{2(1698)} = 3.72 \text{ mm}$$

$$m = 4\pi(.1145)^2(.00372)(1610) + .3199 = .535 \text{ kg}$$

Design of Cryogenic Life Support Tanks:

Scaling of Project Mercury tanks was done to calculate the radius and wall thickness of the outer sphere (NASA SP-4001, 1963).

Primary Unit:

- Liquid Nitrogen Tank:

$$v_{\text{inner}} = \frac{4.055}{.809} \times \frac{1000}{100^3} = 0.00501 \text{ m}^3$$

$$r_{\text{inner}} = [.75/\pi(.00501)]^{1/3} = 10.62 \text{ cm}$$

$$t_{\text{inner}} = \frac{4(2.465)(.1062)}{2(480)} = 1.1 \text{ mm}$$

$$m_{\text{inner}} = 4\pi(.1062)^2(.0011)(2700) = .42 \text{ kg}$$

$$r_{\text{outer}} = 10.62 + 2.9 = 13.52 \text{ cm}$$

$$t_{\text{outer}} = 2(1.1) = 2.2 \text{ mm}$$

$$m_{\text{outer}} = 4\pi(.1352)^2(.0022)(2700) = 1.36 \text{ kg}$$

$$m_{\text{total}} = m_{\text{inner}} + m_{\text{outer}} + m_{\text{hardware}} = 2.48 \text{ kg}$$

- Liquid Oxygen Tank:

$$V_{inner} = \frac{2.066}{.865} \times \frac{1000}{100^3} = 0.0024 \text{ m}^3$$

$$r_{inner} = [.75/\pi(.0024)]^{1/3} = 8.29 \text{ cm}$$

$$t_{inner} = \frac{4(2.465)(.0829)}{2(480)} = .85 \text{ mm} \approx 1.0 \text{ mm}$$

$$m_{inner} = 4\pi(.0829)^2(.001)(2700) = .233 \text{ kg}$$

$$r_{outer} = 8.29 + 2.9 = 11.19 \text{ cm}$$

$$t_{outer} = 2(1.0) = 2.0 \text{ mm}$$

$$m_{outer} = 4\pi(.1119)^2(.002)(2700) = .85 \text{ kg}$$

$$m_{total} = m_{inner} + m_{outer} + m_{hardware} = 1.78 \text{ kg}$$

Secondary Unit:

• Liquid Nitrogen Tank:

$$V_{inner} = \frac{1.0}{.809} \times \frac{1000}{100^3} = 0.00124 \text{ m}^3$$

$$r_{inner} = [.75/\pi(.00124)]^{1/3} = 6.66 \text{ cm}$$

$$t_{inner} = \frac{4(2.465)(.0666)}{2(480)} = .7 \text{ mm} \approx 1.0 \text{ mm}$$

$$m_{inner} = 4\pi(.0666)^2(.001)(2700) = .15 \text{ kg}$$

$$r_{outer} = 6.66 + 2.9 = 11.19 \text{ cm}$$

$$t_{outer} = 2(1.0) = 2.0 \text{ mm}$$

$$m_{outer} = 4\pi(.0956)^2(.002)(2700) = .62 \text{ kg}$$

$$m_{total} = m_{inner} + m_{outer} + m_{hardware} = 1.27 \text{ kg}$$

• Liquid Oxygen Tank:

$$V_{\text{inner}} = \frac{9835}{.865} \times \frac{1000}{100^3} = 0.00114 \text{ m}^3$$

$$r_{\text{inner}} = [.75/\pi(.00114)]^{1/3} = 6.47 \text{ cm}$$

$$t_{\text{inner}} = \frac{4(2.465)(.0647)}{2(480)} = .67 \text{ mm} \approx 1.0 \text{ mm}$$

$$m_{\text{inner}} = 4\pi(.0647)^2(.001)(2700) = .14 \text{ kg}$$

$$r_{\text{outer}} = 6.47 + 2.9 = 9.37 \text{ cm}$$

$$t_{\text{outer}} = 2(1.0) = 2.0 \text{ mm}$$

$$m_{\text{outer}} = 4\pi(.0937)^2(.002)(2700) = .60 \text{ kg}$$

$$m_{\text{total}} = m_{\text{inner}} + m_{\text{outer}} + m_{\text{hardware}} = 1.24 \text{ kg}$$

Appendix P: The Taurus Camera System

P.1 Introduction

Realizing that visibility would be limited on the TLMS, the original plan was to use a real time, closed circuit camera mounted at the nose of the capsule to assist in missions. However, limitations on fuel and size of the spacecraft eliminated any need for the camera since it's original missions were cut. The following describes the original camera and requirements.

P.2 Analysis

When considering the requirements for the Taurus capsule's video camera system, some elementary assumptions were made (based on current projections), which are as follows; (1) The windows will be so small that navigation using them will be extremely inefficient. Their primary function will be orientation and a backup for the camera. (2) The camera will be needed to assist in docking with the space station. (3) The camera will be necessary for inspection of satellites if EVA is undesirable or impossible. (4) The capsule may not be able to get very close to the satellite due to it's limited maneuvering capability.

Considering these assumptions valid for now, the requirements for the camera are as follows; (1) That it be a continuously running, real time camera that shows live video to the crew (and possibly to ground control). (2) That it be mounted up close to the nose of the capsule so it can assist with docking. (3) That it have the ability to change focal length, or zoom, from wide angle (for simple navigation) to telephoto (for inspections). (4) That it have a servo system which allows it rotate about any of the three axes. (5) That it's aperture be wide enough so that it can be used in very low light, say when the sun is behind the Earth. (6) That it's resolution be high enough that it can inspect a satellite adequately without hitting it with thruster plume. (7) It's mounted so that it not interfere with the flow dynamics for the vehicle. The current idea is for it to be mounted under the skin and would pop in / out on command, such as during in-atmosphere flight and landing. (8) That it's reliability be high, since a second camera is not projected due to space and weight limitations.

Also, the camera itself must be a special type, able to withstand the conditions of high acceleration flight and space. It must be able to take high g forces, vibrations, extreme temperature gradients, radiation and micro-meteorite collisions (if possible). In short, it must be a space rated camera.

Appendix Q: Biconic Lifting Body Configuration

Q.1 Summary

A lifting body trade study was performed to determine the optimum shape for the manned spacecraft. The benefits of a lifting body included more control over landing site, and less deceleration on the crew. Various lifting body designs were examined. The biconic lifting body is one possible configuration that was studied. The results of this analysis are presented in this appendix.

Q.2 Biconic Model

The value of L/D was calculated to determine the re-entry parameters for two missions: launch and return, and rendezvous and docking. The lift and drag forces on the biconic lifting body were determined using the following equations:

- coefficient of lift, $c_L = \iint c_n \cos\Phi_1 dA + \iint c_n \cos\Phi_2 dA$
- coefficient of drag, $c_D = \iint c_n \sin\Phi_1 dA + \iint c_n \sin\Phi_2 dA$

where c_n is the normal force and Φ_1 and Φ_2 are the angles of each cone.

Initially, a rendezvous and docking mission was feasible; however, due to mass constraints, it was ruled out. Therefore, only launch and return data is presented in this appendix. The Taurus L.M.S. capsule has the following dimensions:

- upper radius, $r_2 = 0.37$ m
- lower radius, $r_3 = 1.05$ m
- middle radius = r_1
- height of the upper cone = h_1
- height of the lower cone = h_2
- height of the frustum of the upper cone = z_1
- height of the frustum of the lower cone = z_2

These dimensions are shown in Figure Q.1A.

The solutions for the integrals used to determine the lift and drag coefficients in terms of the above dimensions are:

$$\bullet c_L = c_n \{ [\pi r_3 - (\pi r_3/h_2) \times (h_2 - z_2)^2] \times (r_3^2 + h_2^2)^{1/2} [h_2/(0.25r_3^2 + h_2^2)^{1/2}] \\ + [\pi r_1 - (\pi r_1/h_1) \times (h_1 - z_1)^2] \times (r_1^2 + h_1^2)^{1/2} [h_1/(0.25r_1^2 + h_1^2)^{1/2}] \}$$

$$\bullet c_D = c_n \{ [\pi r_3 - (\pi r_3/h_2) \times (h_2 - z_2)^2] \times (r_3^2 + h_2^2)^{1/2} [0.5r_3/(0.25r_3^2 + h_2^2)^{1/2}] \\ + [\pi r_1 - (\pi r_1/h_1) \times (h_1 - z_1)^2] \times (r_1^2 + h_1^2)^{1/2} [0.5r_1/(0.25r_3^2 + h_2^2)^{1/2}] \}$$

where r_1, r_3, z_1 and z_2 are shown below.

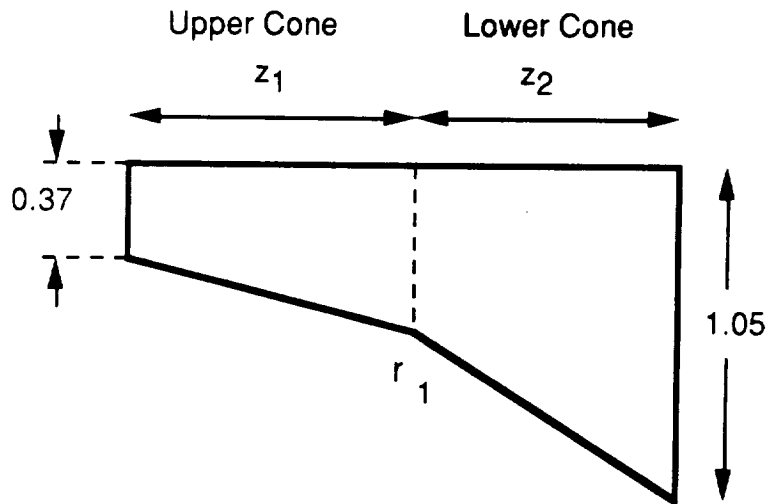


Figure Q.1A: Biconic Model

Q.3 L/D Determination

The dimensions of the model shown in Figure Q.1A were varied. For each combination, the lift coefficient and the drag coefficient were calculated using the above equations. Then, L/D was determined by dividing the lift coefficient by the drag coefficient. In order to find the optimum dimensions, the volume of each combination was also determined. The volume of the lifting body was constrained by two factors. First, it has a minimum volume that is necessary to carry the components needed for the mission, such as a pilot, fuel, avionics and oxygen. Second, it has a maximum mass constraint due to the mass limitations of the Taurus L.M.S.; thus, the lifting body has a maximum allowable volume. These two factors, equipment and mass, limited the L/D of the lifting body.

The program used to determine the L/D and the volume of the lifting body for various combinations of dimensions is shown on the following page. The height of the frustum of the lower cone, z_1 , must be at least 1 m for the pilot.

```

*****
*      Jennifer Plotkin      *
*      Biconical Lifting Body Configuration  *
*      ENAE 412: Design of the LMS Taurus    *
*****
*      This program calculates the lift/drag coefficient for a
*      biconical lifting body design as well as the volume of the
*      capsule given the dimensions r1,z1 and z2. The program
*      determines the optimum volume and L/D for a launch and return
*      mission.

      real r1, r2, r3, z1, z2, h1, h2, cphi, sphi
      real ctheta, stheta, l1, l2, a1, a2, c1, cd
      real ld, vol1, vol2, vol3, vol4, volume

*      For a launch and return mission the dimensions must be:
      r2=0.74
      r3=2.1

      print *, '      R1          Z1          z2          Volume          L/D'
      do 10 r1=0.8,2.0,0.1
        do 20 z1=1.0,2.5,0.25
          do 40 z2=1.0,2.0,0.25
            h1=(r1*z1)/(r1-r2)
            h2=(r3*z2)/(r3-r1)
            l1=(r1**2+h1**2)**0.5
            l2=(r3**2+h2**2)**0.5

            cphi=h2/((0.25*r3**2+h2**2)**0.5)
            ctheta=h1/((0.25*r1**2+h1**2)**0.5)
            sphi=(0.5*r3)/((0.25*r3**2+h2**2)**0.5)
            stheta=(0.5*r1)/((0.25*r1**2+h1**2)**0.5)

            a1=(1.57*r3)-(((1.57*r3)/h2)*(h2-z2)**2)
            a2=(1.57*r1)-(((1.57*r1)/h1)*(h1-z1)**2)

            c1=(a2*l2*cphi)+(a1*l1*ctheta)
            cd=(a2*l2*sphi)+(a1*l1*stheta)

            ld=c1/cd

            vol1=1.047*((0.5*r3)**2)*h2
            vol2=1.047*((0.5*r1)**2)*(h2-z2)
            vol3=1.047*((0.5*r1)**2)*h1
            vol4=1.047*((0.5*r2)**2)*(h1-z1)
            volume=vol1-vol2+vol3-vol4
            if (volume .lt. 5.0.and.ld .gt.1.0) then
              go to 50
            else
              go to 40
            endif
          print 30,r1,z1,z2,volume,ld
        continue
      continue
    continue
  format (1x, 5f10.3)
end

```

Q.4 Optimization Results

The lifting body configuration was optimized by plotting L/D versus volume.

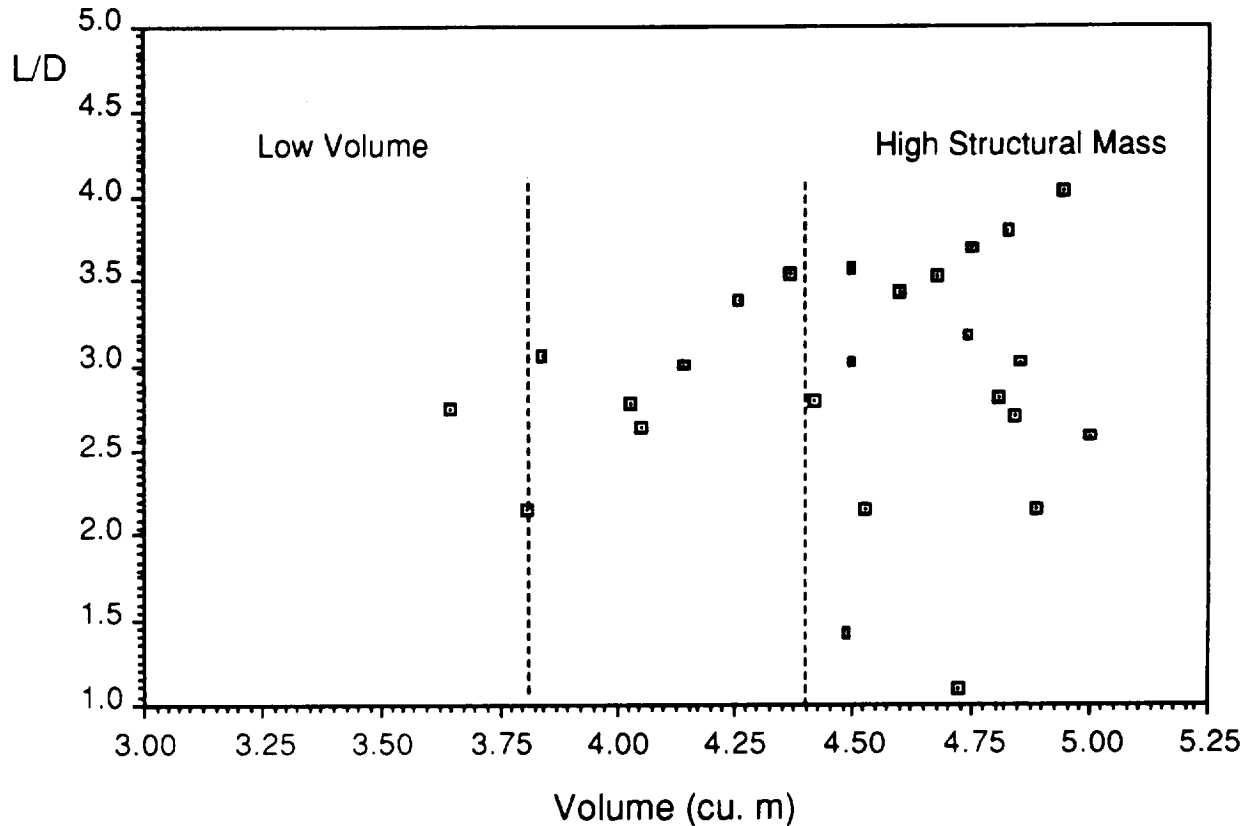


Figure Q.1B: Optimization of the Biconic Configuration

The L/D values in this volume range vary from 2.5 to 3.5. Therefore, L/D values of 2.5, 3.0 and 3.5 were analyzed.

Q.5 Analysis of Re-entry Parameters

The time of re-entry for values of L/D = 2.5, 3.0 and 3.5 were determined using a re-entry program developed by Bernie Kelm. Re-entry parameters for these L/D are:

- For L/D = 2.5:
 $\Delta V = 140$ m/sec
Time of Re-entry = 5700 sec
- For L/D = 3.0:
 $\Delta V = 140$ m/sec
Time of Re-entry = 6990 sec

- For $L/D = 3.5$:
 $\Delta V = 140 \text{ m/sec}$
Time of Re-entry = 8310 sec

These high re-entry times result in large aerodynamic heating on the body. Increasing the burn rate lowers the re-entry time only slightly.

- For $L/D = 3.0$:
 $\Delta V = 900 \text{ m/sec}$
Time of Re-entry = 4620 sec

Therefore, for $L/D = 3.0$, increasing the burn rate by four times only lowers the re-entry time by one third.

Q.6 Aerodynamic Heating

The total heat absorbed by the Taurus L.M.S. capsule was determined to be 148.596 MJ by Curt Neidhart. An ablative heat shield would be used on any lifting body design because the mass of ceramic tiles is too high. The total heat absorbed by the biconic lifting body, and the resulting heat shield mass for three values of L/D are:

- For $L/D = 2.5$:
Total Heat Absorbed = 684.95 MJ
Mass of Heat Shield = 72 kg
- For $L/D = 3.0$:
Total Heat Absorbed = 985.54 MJ
Mass of Heat Shield = 97 kg
- For $L/D = 3.5$:
Total Heat Absorbed = 1139.71 MJ
Mass of Heat Shield = 110 kg

Although the rate of aerodynamic heating for the capsule is close to that of the lifting body, the longer period of re-entry results in a higher amount of heat absorbed. The mass of the heat shield on the capsule is approximately 27 kg. The mass of the heat shield on a biconic lifting body with $L/D = 2.5$ is over twice that of the heat shield on the capsule.

Q.7 Conclusion

The primary drawback of a lifting body configuration over the L.M.S. capsule is the increase in mass. A lifting body of the optimum size and shape would be too heavy to fly on the Taurus booster. Given the volume constraints, the biconic lifting body configuration is no better than the L.M.S. capsule.

Lifting bodies are beneficial because they produce less re-entry deceleration force on the crew; however, the L.M.S. has a relatively low re-entry deceleration of three gees. One other benefit is that a lifting body provides more control over landing site location; however, the L.M.S. capsule is landing on water, and, with an $L/D \approx 0.24$, the capsule has some re-entry landing site control.

Other drawbacks of the lifting body include a greater amount of aerodynamic heating on the structure, resulting in both a higher structural mass and heat shield mass. One other possible problem that a biconic lifting body with these volume and mass constraints may encounter is stability. The optimum configuration with these limitations has an upper cone which is significantly shorter than the lower cone; these dimensions could result in possible stability problems. Due to all of the drawbacks encountered, a biconic lifting body configuration is not a viable option.

Appendix R

R.1 Introduction

During the initial preparation of the design for the Taurus Low Mass Spacecraft a brief survey of possible configurations was completed. Winged vehicles, lifting bodies, and capsules were examined. Historical data for vehicles in the various classes were compiled and a graph of overall weight versus volume was made. From this rough analysis the winged vehicle and the lifting body were eliminated from consideration. At a later stage, a more detailed analysis of these vehicles was made, as presented in Table R.1. This analysis included only the best available estimate for the actual structural weight of the vehicle. Where data on structural mass fraction was unavailable, an estimate was made.

From the Table R.1 and Figure R.1 it can be seen that the winged body was in most cases considerable heavier than the lifting body per unit of mass. A further reduction of this data to allow for the greater efficiency (volumetrically) of large structures would increase the differential. Based on these data, it was decided to eliminate winged vehicles but give further consideration to lifting bodies.

R.2 Design Configuration

The configuration of the vehicle was at this time constrained by the requirements to meet the mission objectives of the capsule vehicle. The vehicle was to be able to rendezvous with and dock with the space station carrying a crew of two. From work completed for the capsule configuration the maximum diameter was fixed at 2.35 meters, with a 1.5 meter docking ring accommodated on the vehicle.

The initial configuration study was completed by drawing components to scale and placing them within a generic lifting body shape. The position of the crew compartment was fixed at the point of maximum cross sectional area on the vehicle. From these studies, it became apparent that the variable with the greatest impact on the configuration of the design was the placement of the docking ring.

Three possible placements of the docking ring were explored. The docking ring was placed forward of the crew compartment behind a folding break in the vehicle forebody, aft of the crew compartment on the aft end of the service module, and over the crew compartment.

Placement of the docking ring forward has the benefit of requiring the shortest tunnel and of providing good access to components located in the forward avionics bay. This configuration also allows for visual docking of the vehicle with a direct view through the windows. Disadvantages include the added complexity of a folding mechanism and the requirement for a long forebody.

The placement of the docking ring at the aft end of the vehicle is a common solution to the problem of docking ring requirements. This position has been adopted by Hermes and by the NASA IHL-20 study for a manned vehicle carried by Titan. This configuration places the least constraint on fuselage shaping, as the docking ring is aft of the point of maximum cross sectional area. The docking ring can also be jettisoned before reentry in this configuration, allowing for a lighter vehicle. However, adoption of this configuration would require the adoption of a periscope or other auxiliary viewing system, and the adoption of a dual motor OMS. The tunnel for access to the ring is considerably longer in this configuration, and a

thermally protected airtight hatch is required behind the crew compartment.

The overhead placement of the docking ring requires no tunnel and no hatches for emergency egress; the docking ring can be the only hatch in the vehicle. This configuration, however, forces the body to be much thicker, with a minimum thickness of 2.6 meters. This configuration also makes docking approaches more difficult, and eliminates the possibility of providing the crew with a forward facing window. The overhead hatch also reduces the redundancy of the vehicle, as there is no escape system if the hatch latches fail. For these reasons, this configuration seemed least desirable.

The forward ring configuration was selected for further consideration. The weight model was not greatly affected by the additional length required, and the folding mechanism would be relatively simple. The degree of commonality in OMS and power systems and plumbing was the primary reason for the selection of this configuration. Figure R.1 shows the configurations considered, and Figures R.2 and R.3 show the baseline configuration.

R.3 Weights

The weight of this vehicle was originally intended to be calculated by historical modeling. However, the relatively small number of lifting body designs actually constructed prevented a mathematically valid multiple regression model from being constructed. For this reason I used the following equations for the weight of the fuselage and fins, respectively:

$$W_{\text{fuselage}} = .499 * .774 * W^{.35} * N^{.25} * L^{.5} * D^{.849} * S^{.685}$$

$$W_{\text{fin}} = .452 * (WN)^{.488} * S^{.118} * M^{.341} * L_{1-10} * 1.273 * A^{.233} * (1 + \lambda)^{.25} * \cos(\text{Sweep})^{.323}$$

These models are for tactical aircraft and are taken from Raymer, 1989. The size of the fins was fixed, and their weight was calculated as 83.53 kg. Dimensions of the fuselage were varied, and results are presented in Table R.1 and R.2.

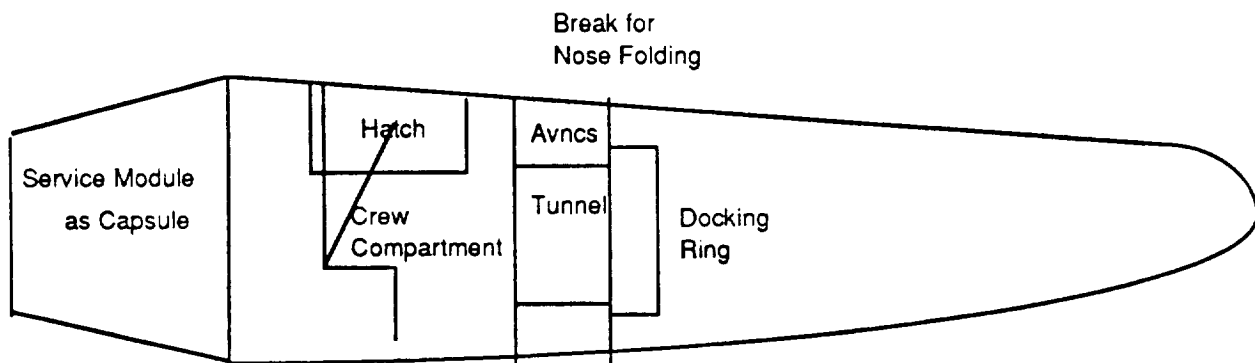
Table R.1 Span Varying Weight

Span	Depth	Length	Weight
2.5	2.35	4.7	228.8514
2.75	2.35	4.7	238.6421
3	2.35	4.7	248.156
3.25	2.35	4.7	257.4231
3.5	2.35	4.7	266.4681
3.75	2.35	4.7	275.3116
4	2.35	4.7	283.9712
4.25	2.35	4.7	292.4619
4.5	2.35	4.7	300.7966
4.75	2.35	4.7	308.9866
5	2.35	4.7	317.0419
5.25	2.35	4.7	324.9712
5.5	2.35	4.7	332.7825
5.75	2.35	4.7	340.4826
6	2.35	4.7	348.078
6.25	2.35	4.7	355.5743
6.5	2.35	4.7	362.9767
6.75	2.35	4.7	370.29
7	2.35	4.7	377.5184
7.25	2.35	4.7	384.6659

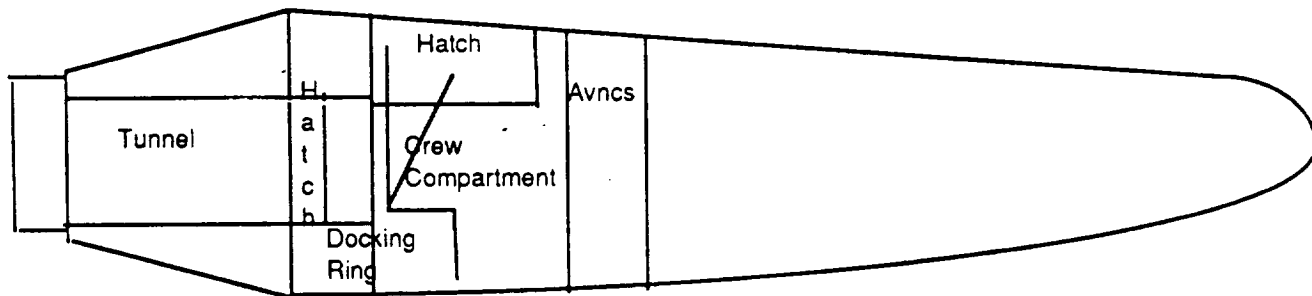
Table R.2 Length Varying Weight			
Span	Depth	Length	Weight
3.75	2.35	2.3	167.5653
3.75	2.35	2.5	167.9155
3.75	2.35	2.7	168.2401
3.75	2.35	2.9	168.5426
3.75	2.35	3.1	168.8259
3.75	2.35	3.3	169.0923
3.75	2.35	3.5	169.3438
3.75	2.35	3.7	169.582
3.75	2.35	3.9	169.8083
3.75	2.35	4.1	170.0238
3.75	2.35	4.3	170.2295
3.75	2.35	4.5	170.4264
3.75	2.35	4.7	170.6151
3.75	2.35	4.9	170.7963
3.75	2.35	5.1	170.9706
3.75	2.35	5.3	171.1386
3.75	2.35	5.5	171.3006
3.75	2.35	5.7	171.4572
3.75	2.35	5.9	171.6086
3.75	2.35	6.1	171.7552

Table R.3 Weight Breakdown				
	1u/1d	1u/2d	2u/2d	1u/2d
Life Support	180	180	350	180
Crew Cabin	15	30	30	30
Abort (effective)	40	40	40	40
RCS	40	40	40	40
Fuel and tanks				
OMS	20	20	20	20
Power Generation	200	200	200	200
Fuel and Tanks				
Battery Pack	23	23	23	23
Capsule Structure	250	250	250	270.4
SM Structure	150	150	150	150
Booster Interface	31.3	31.3	31.3	31.3
Thermal Control				
Communications	30.5	30.5	30.5	30.5
Sensors	25	25	25	25
Data Processing	25	25	25	25
Guidance and Control	29	29	29	29
Docking Ring	100	100	100	100
Parachute	100	100	100	100
	1258.8	1273.8	1443.8	1294.2

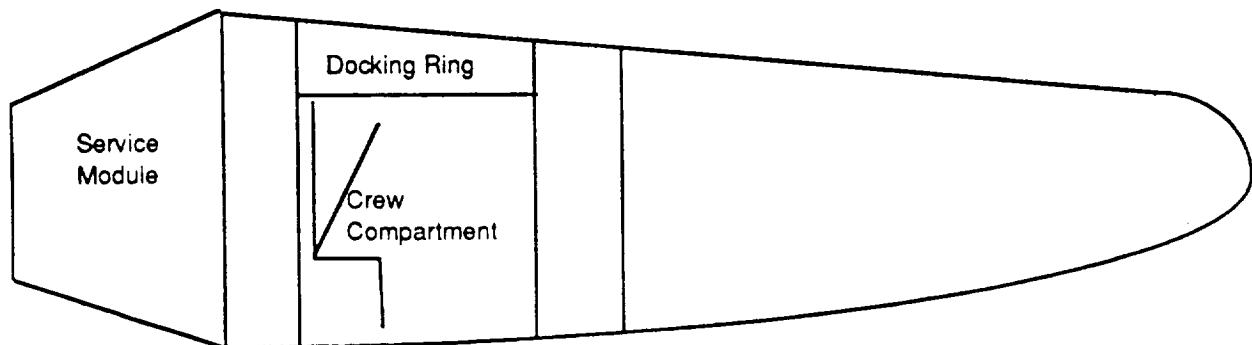
Figure R.1
Possible Internal Layouts For Lifting Bodies



CONFIGURATION 1
Forward ring-Folding Body



CONFIGURATION 2
Aft Ring

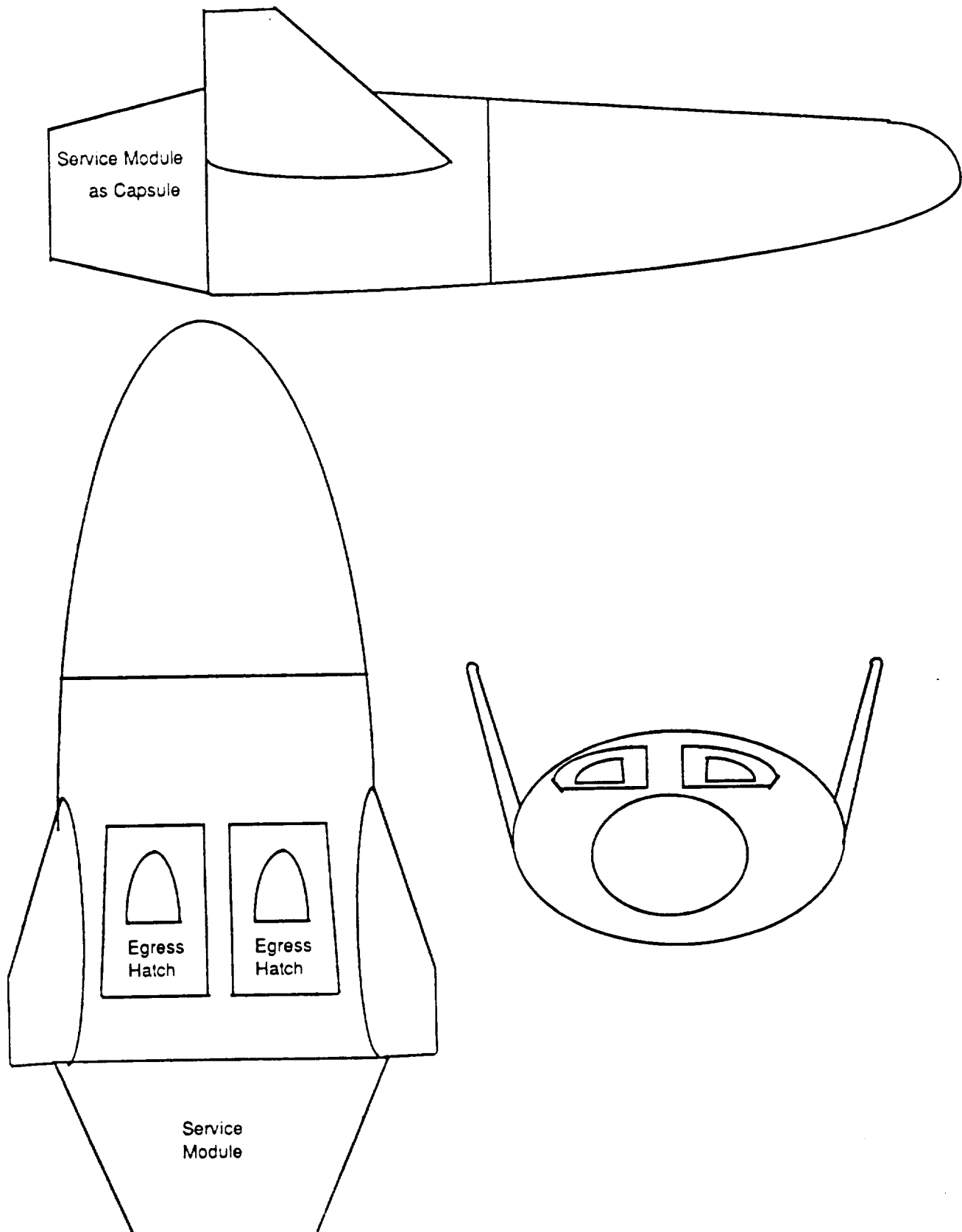


CONFIGURATION 3
Overhead Ring

Avnics=Avionics

Figure R.2

Generic Arbitrary Lifting Body



Three View

Scematic Internal Layout

General Lifting Body

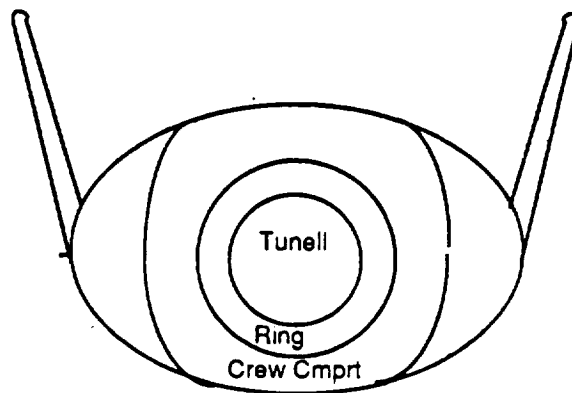
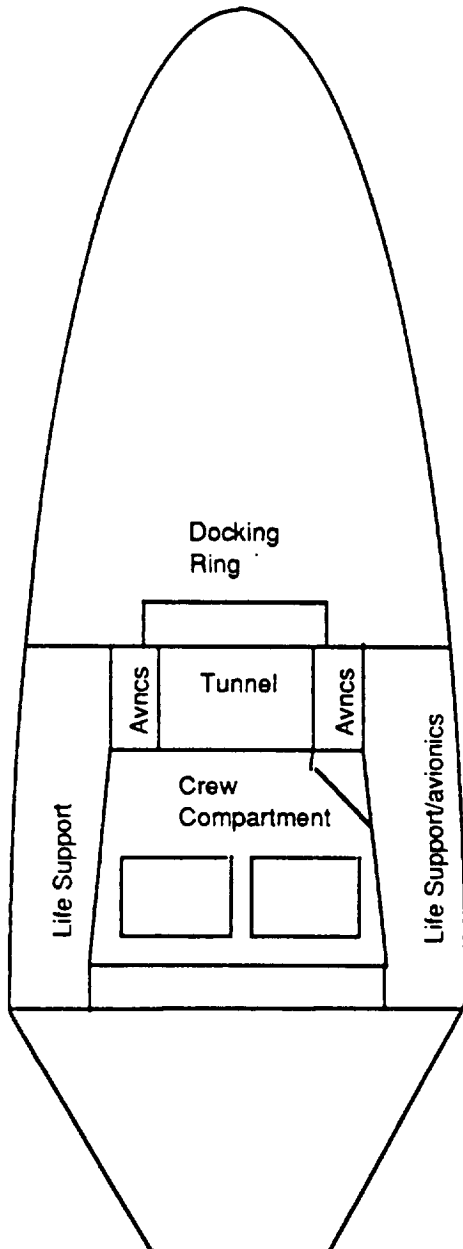
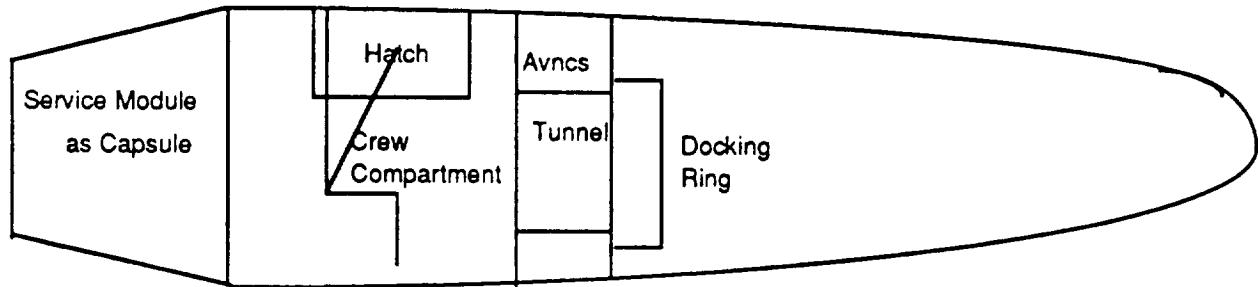


FIGURE R.4
LENGTH VARYING WEIGHT

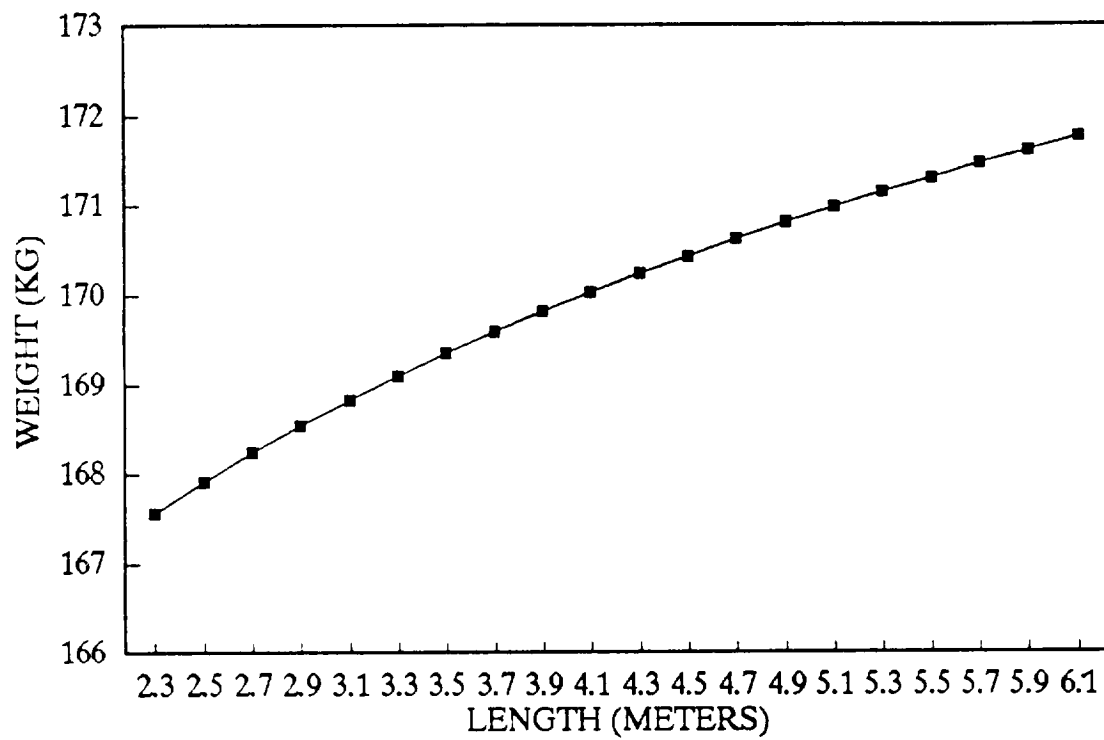
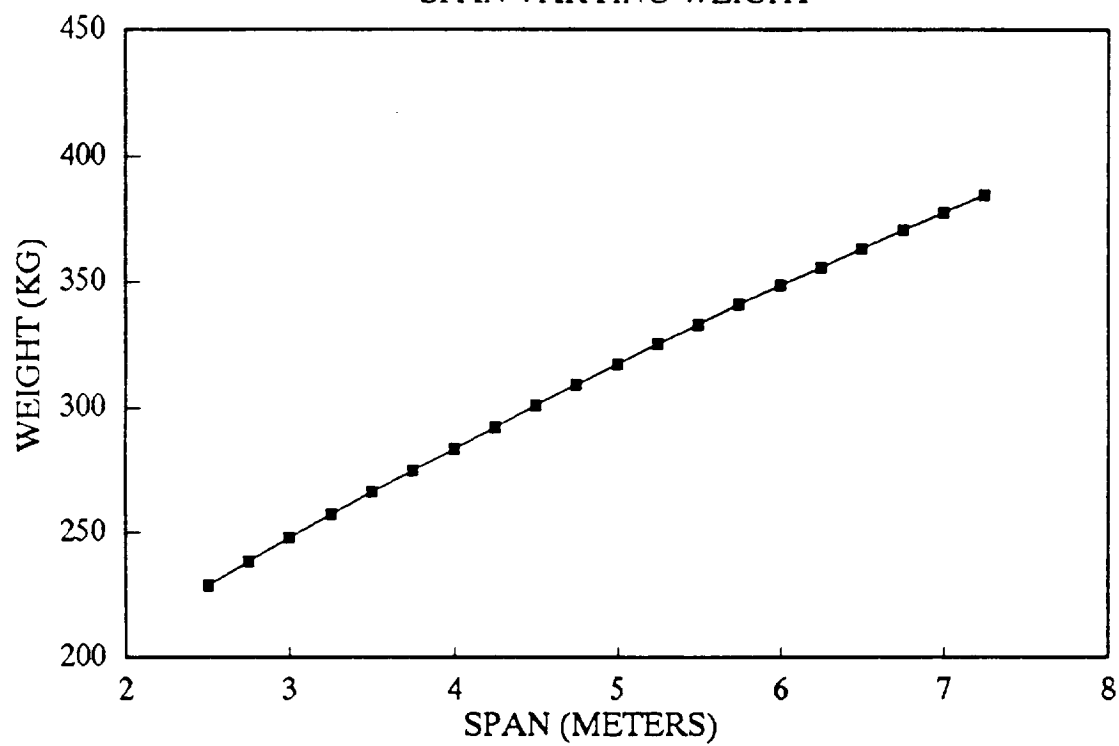


FIGURE R.5
SPAN VARYING WEIGHT



References

- Raymer, Daniel P., *Aircraft Design: A Conceptual Approach*, American Institute of Aeronautics and Astronautics, 1989
- Taylor, John W. R., *Jane's All The World's Aircraft, 1969-70*, McGraw Hill, New York, 1969
- Taylor, John W. R., *Jane's All The World's Aircraft, 1975-76*, McGraw Hill, New York, 1975
- Taylor, John W. R., *Jane's All The World's Aircraft, 1989-90*, McGraw Hill, New York, 1989

Bibliography

- Aiken, David, personal interview
- Anderson, J. D. Jr., *Introduction to Flight: Its Engineering and History*, McGraw Hill, New York, 1978
- Anderson, J. D. Jr., *Modern Compressible Flow*, McGraw Hill, New York, 1990
- Anderson, J. D. Jr., personal interview
- Aviation Week and Space Technology, McGraw Hill, 1980-1991
- Lewis, Mark, personal interview
- Raymer, Daniel P., *Aircraft Design: A Conceptual Approach*, American Institute of Aeronautics and Astronautics, 1989
- Sweetman, Bill, *High Speed Flight*, Janes Publishing Company, Ltd, London, 1983
- Taylor, John W. R., *Jane's All The World's Aircraft, 1969-70*, McGraw Hill, New York, 1969
- Taylor, John W. R., *Jane's All The World's Aircraft, 1975-76*, McGraw Hill, New York, 1975
- Taylor, John W. R., *Jane's All The World's Aircraft, 1989-90*, McGraw Hill, New York, 1989

Appendix S: Single Crew Lifting Body

S.1: Introduction

The single crew lifting body emerged as a result of the deletion of the docking and the multi crew member functions from the mission profile. The single crew lifting body accommodates only one crewmember and has no docking capability. The vehicle can be made significantly smaller as a result of the deletion of the docking ring and a slight reduction in maximum diameter.

S.2 Configuration

The single crew lifting body configuration chosen was similar to the configuration of the X-24A experimental vehicle. This configuration provided the largest internal volume for its dimensions of any of the successful lifting body designs. The configuration of the vehicle was modified by truncating the afterbody. The LMS vehicle would be considerably smaller than an X-24A.

The configuration houses a single pilot near the aft end of the vehicle, surrounded by life support and avionics bays. Access to the vehicle is provided by an overhead hatch. It was decided to recover the vehicle by parachute because of the anticipated water landing scenario and because of the added weight and complexity of a landing gear. The vehicle would be lowered by parachute in its flight attitude. A configuration for the single crew lifting body is provided in figure S.1.

S.3 Weights

The weights for this vehicle were modeled similarly to the weights of the two crew lifting body, using historical estimations for tactical aircraft from Raymer, 1989. The length and the span were both varied, with considerably more dependence being observed on span than on length. The height of the vehicle was set by minimum height of the crew compartment, and the length and the width were estimated by comparison with lifting body designs from historical sources. A mass budget is provided for the two crew member lifting body, and it can be seen from this budget that the vehicle was considerably overweight. At this point consideration of lifting bodies was terminated.

Table S.1 Length Varying Weight

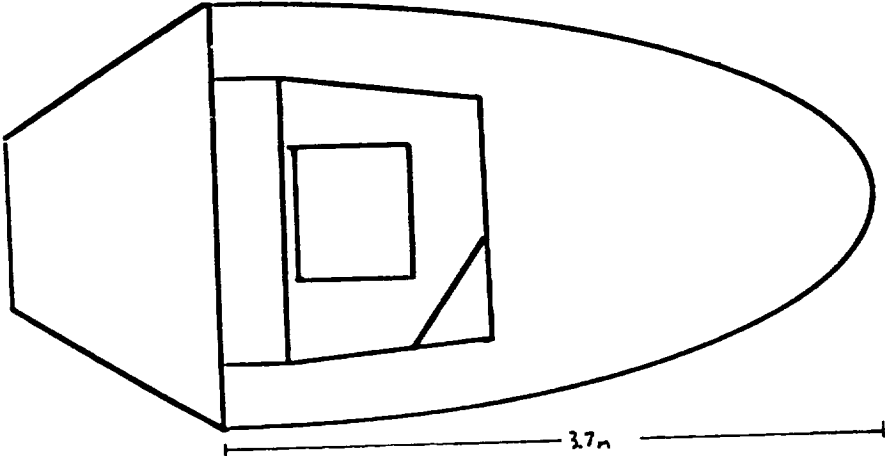
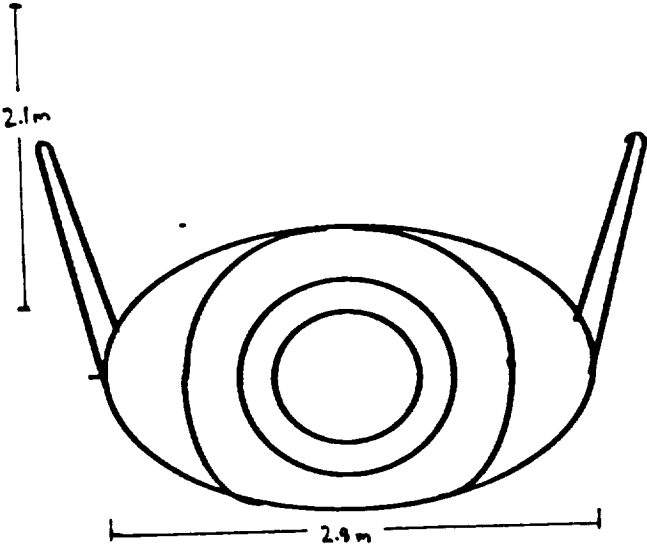
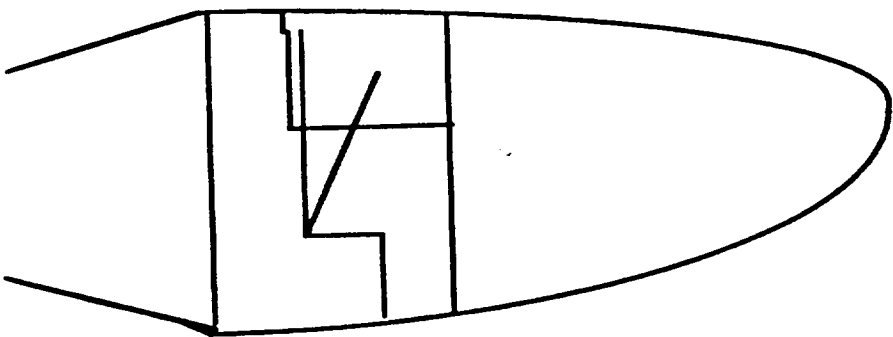
Span	Depth	Length	Weight
2.5	2.1	4.5	134.4406
2.58	2.1	4.5	135.7425
2.66	2.1	4.5	137.0318
2.74	2.1	4.5	138.3089
2.82	2.1	4.5	139.5743
2.9	2.1	4.5	140.8284
2.98	2.1	4.5	142.0717
3.06	2.1	4.5	143.3046
3.14	2.1	4.5	144.5273
3.22	2.1	4.5	145.7402
3.3	2.1	4.5	146.9437
3.38	2.1	4.5	148.138
3.46	2.1	4.5	149.3235
3.54	2.1	4.5	150.5003
3.62	2.1	4.5	151.6688
3.7	2.1	4.5	152.8292
3.78	2.1	4.5	153.9817
3.86	2.1	4.5	155.1266
3.94	2.1	4.5	156.264
4.02	2.1	4.5	157.3941

Table S.2 Length Varying Weight

Span	Depth	Length	Weight
3.55	2.1	2.3	141.6921
3.55	2.1	2.5	141.9987
3.55	2.1	2.7	142.2829
3.55	2.1	2.9	142.5477
3.55	2.1	3.1	142.7957
3.55	2.1	3.3	143.0289
3.55	2.1	3.5	143.2491
3.55	2.1	3.7	143.4576
3.55	2.1	3.9	143.6557
3.55	2.1	4.1	143.8444
3.55	2.1	4.3	144.0245
3.55	2.1	4.5	144.1968
3.55	2.1	4.7	144.362
3.55	2.1	4.9	144.5207
3.55	2.1	5.1	144.6733
3.55	2.1	5.3	144.8203
3.55	2.1	5.5	144.9622
3.55	2.1	5.7	145.0992
3.55	2.1	5.9	145.2317
3.55	2.1	6.1	145.3601

Figure S.1
Minimal Lifting Body Configuration

Crew Compartment



Crew Compartment

Figure S.2
Weight Variation with Length

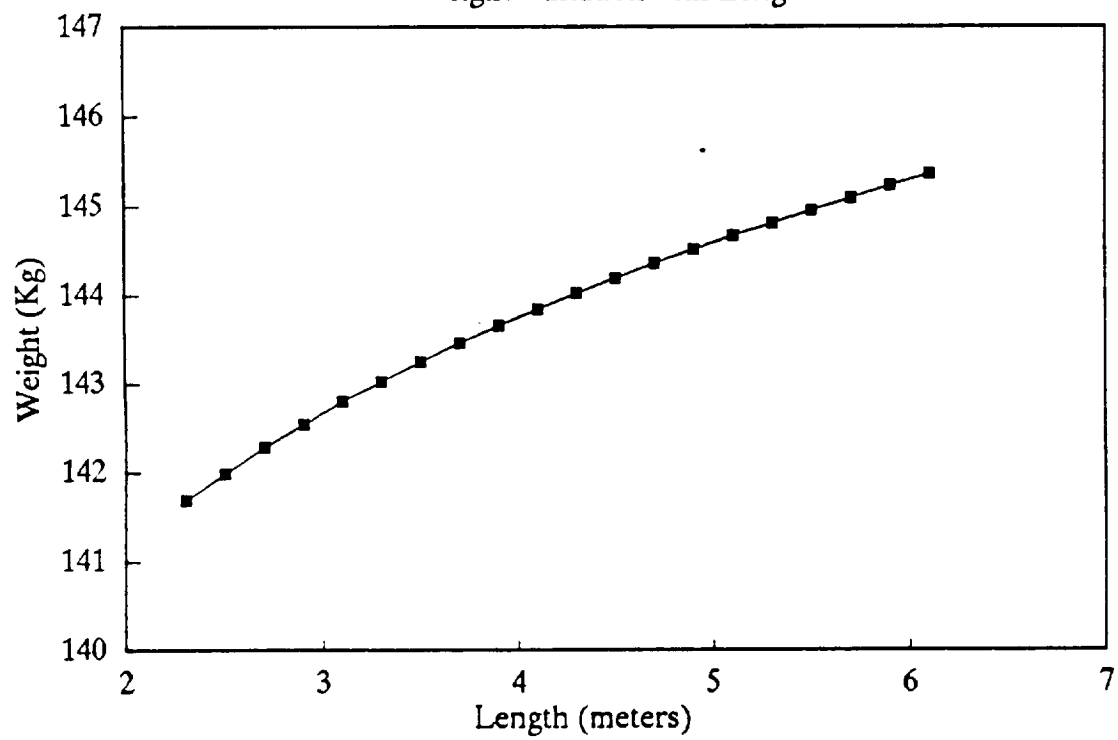
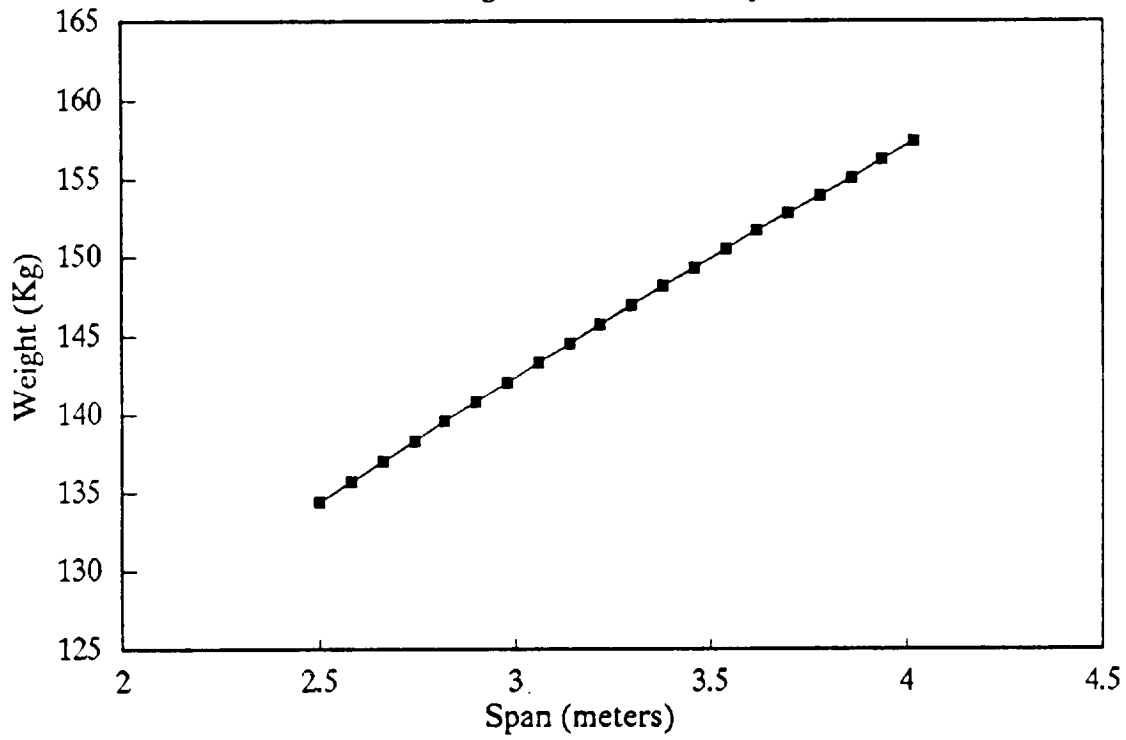


Figure S.3

Weight Variation with Span



References

- Raymer, Daniel P., *Aircraft Design: A Conceptual Approach*, American Institute of Aeronautics and Astronautics, 1989
- Taylor, John W. R., *Jane's All The World's Aircraft, 1969-70*, McGraw Hill, New York, 1969
- Taylor, John W. R., *Jane's All The World's Aircraft, 1975-76*, McGraw Hill, New York, 1975
- Taylor, John W. R., *Jane's All The World's Aircraft, 1989-90*, McGraw Hill, New York, 1989

Bibliography

- Aiken, David, personal interview
- Anderson, J. D. Jr., *Introduction to Flight: Its Engineering and History*, McGraw Hill, New York, 1978
- Anderson, J. D. Jr., *Modern Compressible Flow*, McGraw Hill, New York, 1990
- Anderson, J. D. Jr., personal interview
- Aviation Week and Space Technology, McGraw Hill, 1980-1991
- Lewis, Mark, personal interview
- Raymer, Daniel P., *Aircraft Design: A Conceptual Approach*, American Institute of Aeronautics and Astronautics, 1989
- Sweetman, Bill, *High Speed Flight*, Janes Publishing Company, Ltd, London, 1983
- Taylor, John W. R., *Jane's All The World's Aircraft, 1969-70*, McGraw Hill, New York, 1969
- Taylor, John W. R., *Jane's All The World's Aircraft, 1975-76*, McGraw Hill, New York, 1975
- Taylor, John W. R., *Jane's All The World's Aircraft, 1989-90*, McGraw Hill, New York, 1989

Appendix T: EVA

T.1 Introduction

The TLMS design team originally intended for the TLMS to have an EVA capability for such a mission as satellite repair. When Human Factors looked deeper into this option however, it was realized that EVA would be too expensive in terms of weight and fuel. The following are three different scenarios that were investigated.

T.2 Launching with Equipment

The first way to do EVA would be to launch with the EVA equipment. The EMU (weight: 116 kg with backpack), MMU (weight: 153 kg, and 1.2 m long) and tools (approximately 10 kg) would add 270 kg to launch mass, including the 20 lbs. subtracted for the now unnecessary pressure suit. This scenario was therefore out of the question from the start since the TLMS was already near maximum weight.

T.3 Use TLMS as MMU

The second way was to require the TLMS to come within 1 meter of a satellite and let the tethered astronaut (in an EMU with lifeline) to crawl outside the spacecraft and do repair work. Although the most interesting form of EVA, the TLMS not have a cold gas thruster bank would mean that the satellite and astronaut may be plumed unless it was done perfectly. This meant that the satellite could only be approached one way (see fig T.1), and that external controls may be needed outside the cabin. It would be a difficult, probably dangerous maneuver because of how close the TLMS needs to be to the satellite. If the vehicle struck the satellite, one or both could be damaged, possibly prohibiting the TLMS from reentering safely. This scenario would also add 23 kg to the capsule's mass. It was therefore discarded due to the skill required for a safe mission.

T.4 Space Station Supply

This scenario was the most realistic. The EMU, MMU, and tools could be picked up at the space station Freedom, therefore not requiring additional mass for them on launch. However, the TLMS currently has insufficient fuel to reach Freedom, and has no docking ring to dock if it did. The MMU would also have to be mounted somewhere on the exterior of the vehicle, and would have to be returned after the satellite repair.

T.5 Additional Requirements

NASA's policy is that no EVA be performed until the astronaut spends three days in space. Since the TLMS will only carry 1 day's worth of air, food and water, more mass for them would be needed to do EVA. Also, much more fuel would be needed to catch a satellite or the space station, adding mass. A camera system would

also have to be added for docking or inspections. Due to all these extra requirements and the mass of the EVA equipment, EVA was determined to be unfeasible for the TLMS.

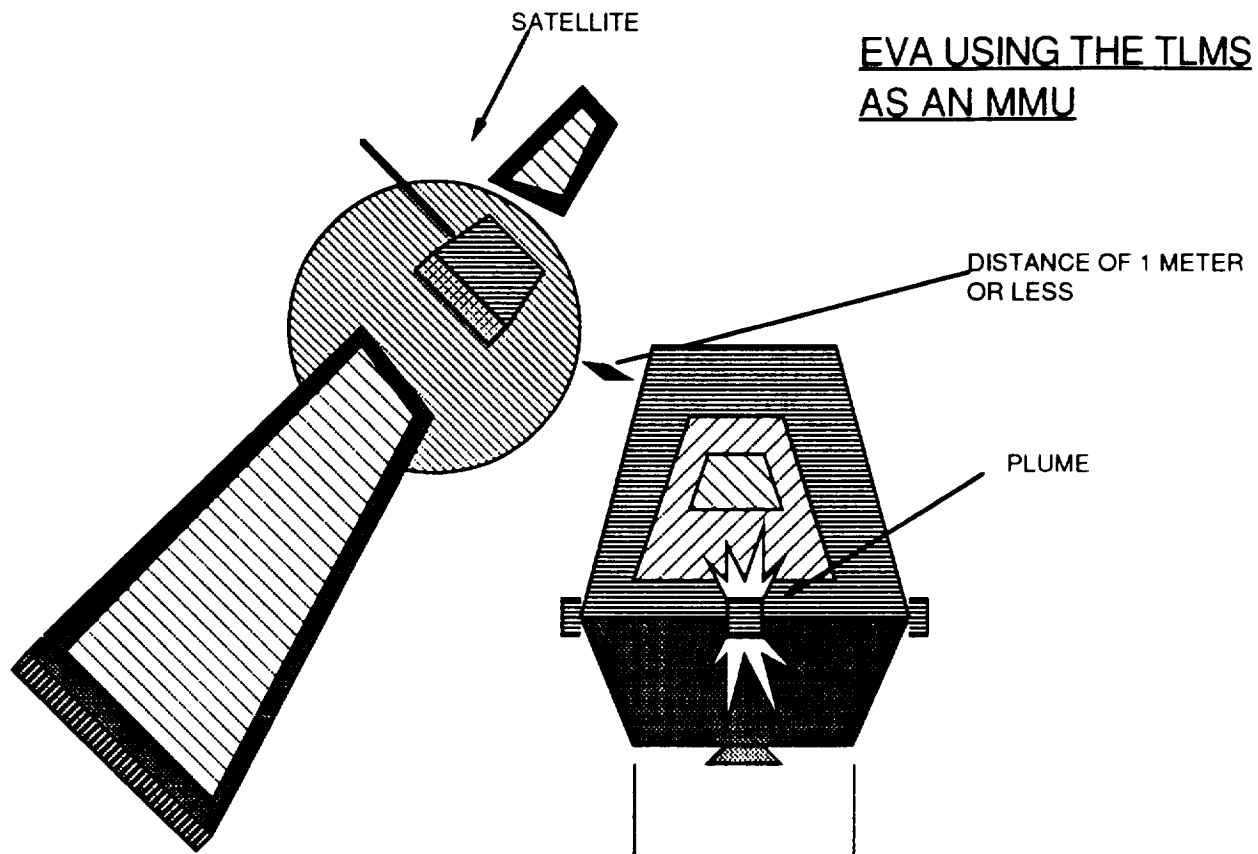


Figure T.1 EVA using the TLMS as an MMU.

Appendix U

U 1 Explosive Bolt

P = load in tension on the main plates

$$F_{\text{escape tower}} = 156\text{kg} \cdot 1g = 1528.8 \text{ N}$$

$$F_{\text{capsule}} = 675\text{kg} \cdot 1g = 6615\text{N}$$

to determine the load, P, sum moment at point A to get

$$2 \cdot P \cdot 1.05\text{m} = (6615\text{N} \cdot 0.77\text{m} + 1528.8\text{N} \cdot 2.52\text{m}) \cdot 1.2$$

$$P = 5112.1\text{N}$$

yield shearing strength of alluminum alloy 1100-H14 = 55MPa =
 $P/2A$

where A = cross-section area of the bolt = 46.47mm^2

d = diameter of the bolt = 7.70mm

the minimum allowable distance between two bolts, D =

$$\frac{(2 \cdot \text{yield strength in compression} + \text{yield strength in tension}) \cdot d}{\text{yield strength in tension}} = 75\text{mm}$$

U2 Heat Shield Support Truss Analysis

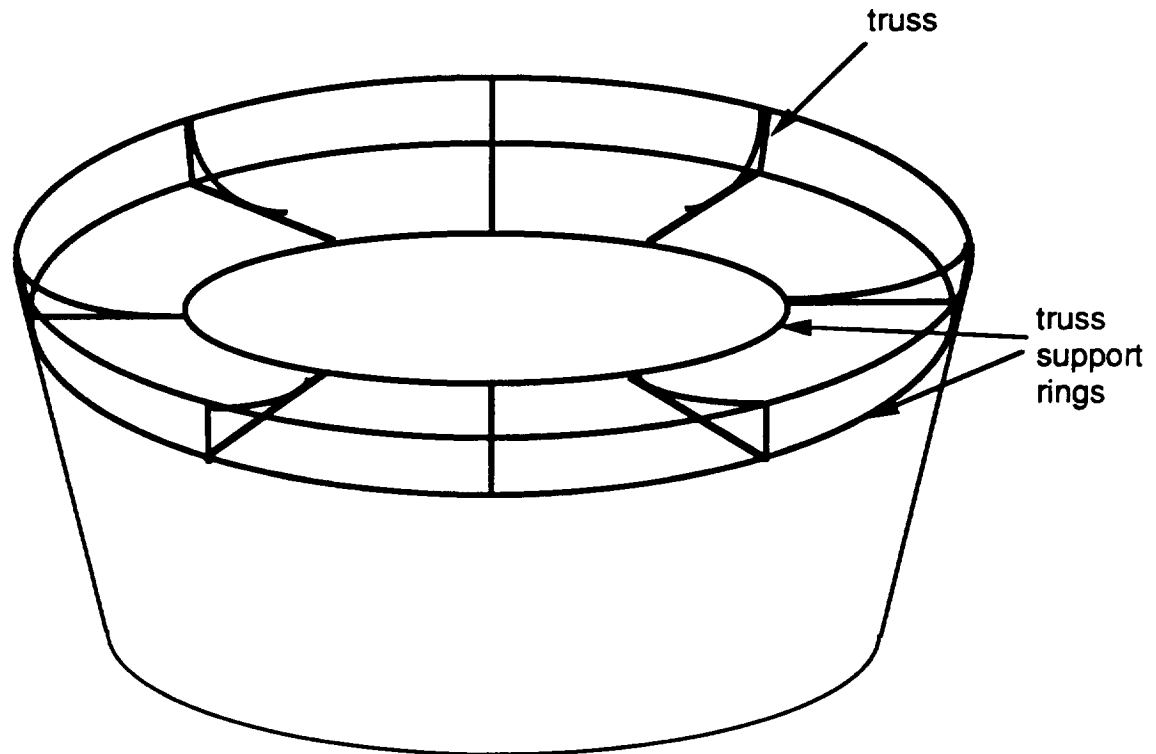


Fig 6.4.4.1 3-D View of the Capsule Supporting truss

Assumptions: neglect the shear and moment on $7/8$ part of the escape tower and capsule weight. On each truss element $1/8$ of the formentioned weight.

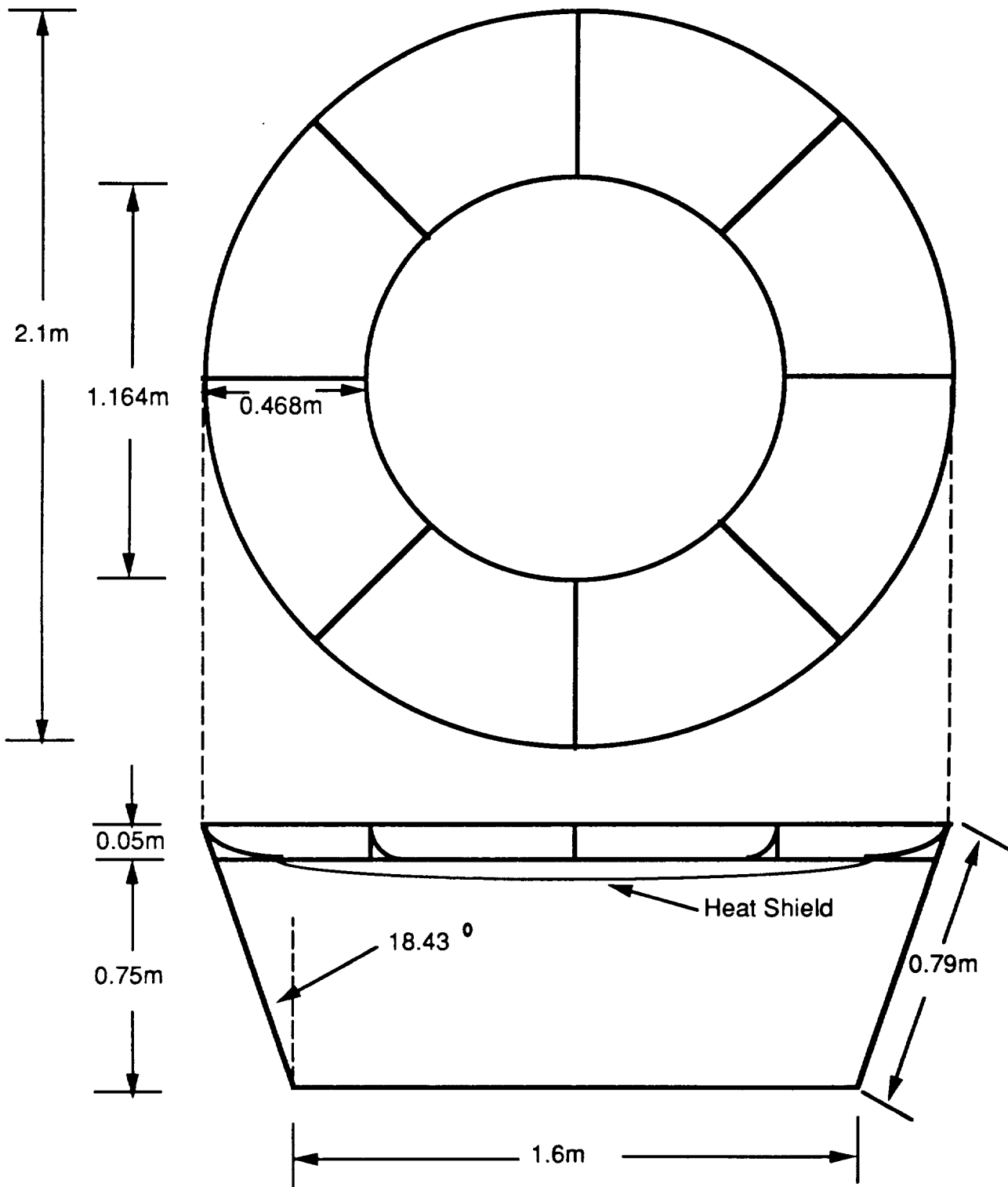
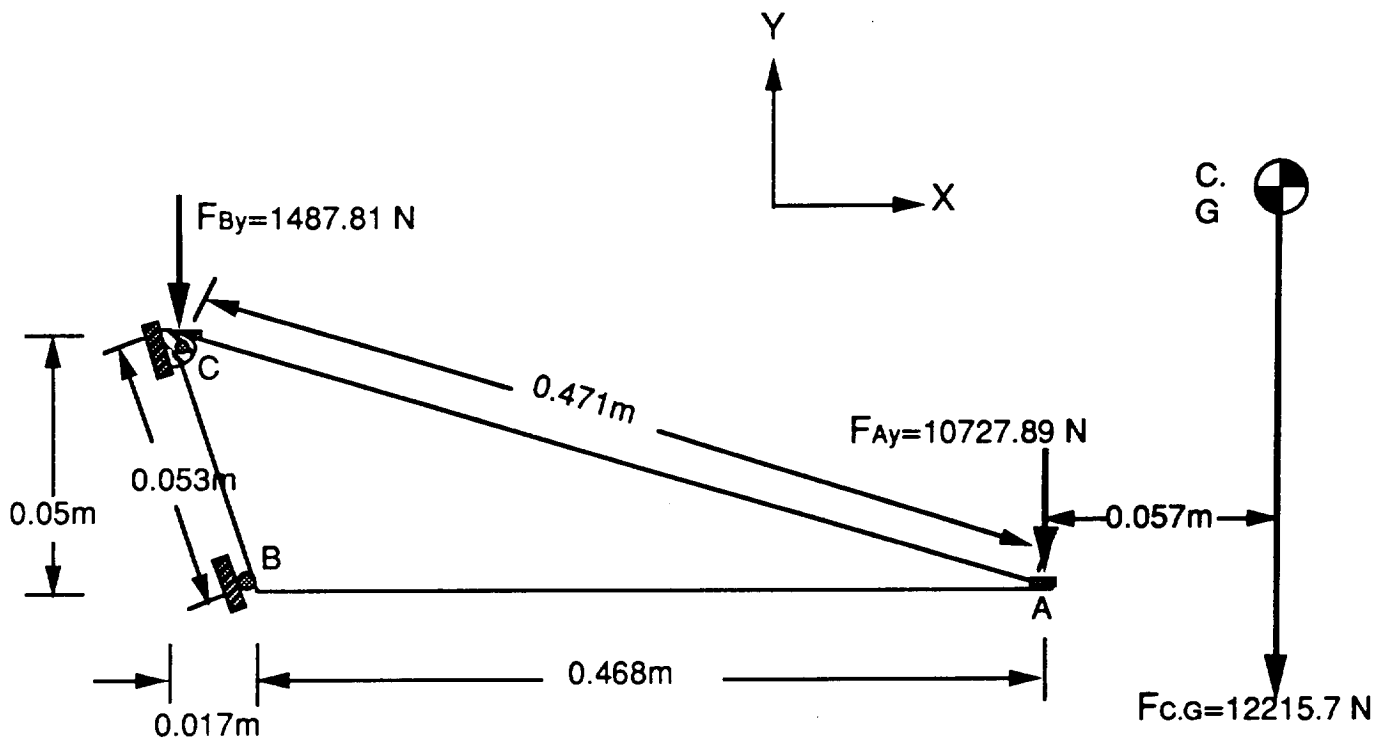


Fig 6.4.4.2 Top and Side View of the Heat Shield Support



Assumptions: Truss AC is analyzed as a straight beam. Yield stress equal to 255 MPa = 100955 N/A where A is the minimum design cross-sectional area of the truss, A = 395.9 sq. mm.

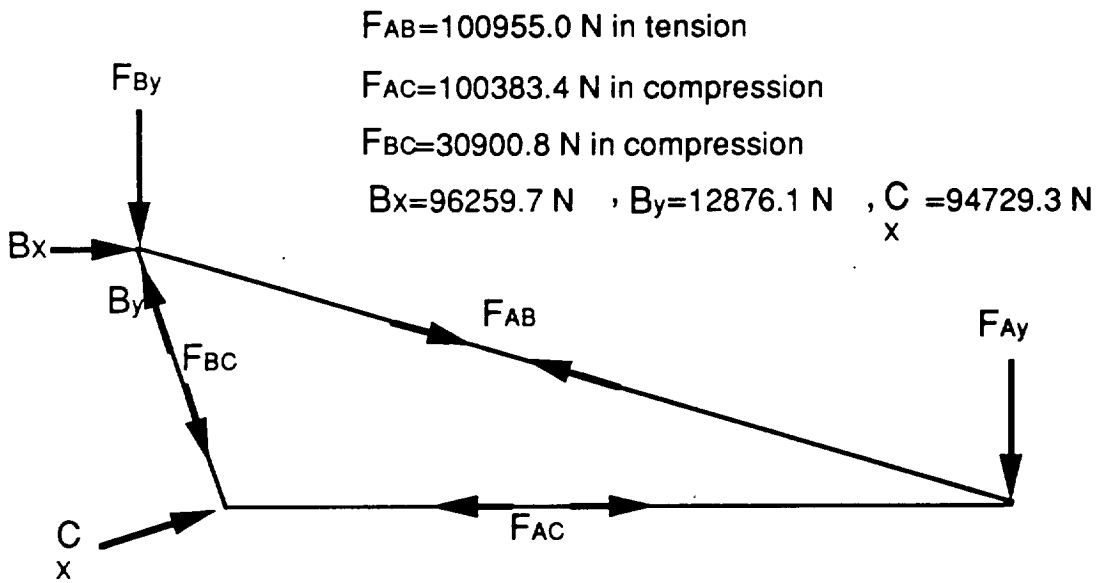


Fig 6.4.4.3 Free-Body Diagram of the Heat Shield Support(not drawn in scale)

U 3 Shear Flow Analysis

Determine the C.G location of the combine escape tower, capsule and service module:

$$\sum M_A = 0; 675\text{Kg} \times 9.8 \frac{\text{m}}{\text{s}^2} \times 1.75\text{m} + 450\text{Kg} \times 9.8 \frac{\text{m}}{\text{s}^2} \times (1.75\text{m} + 0.906\text{m}) = 1281\text{Kg} \times 9.8 \frac{\text{m}}{\text{s}^2} \times Y$$

$$Y = 1.855\text{m}, Y_1 = 0.42\text{m} + 1.33\text{m} + 0.77\text{m} + 0.136\text{m} + 0.614\text{m} - 1.855\text{m} = 1.415\text{m}$$

$$R = 1281\text{Kg} \times 9.8 \frac{\text{m}}{\text{s}^2} \times 1.2 = 15064.56\text{N}$$

Determine the forces and shear flow acting on the stringers and the skin

$$I_2 = \sum A \times y_3^2 = (3.3 \times 10^{-4} \text{m}^2) \times 2 \times 0.8\text{m}^2 + (3.3 \times 10^{-4} \text{m}^2) \times 4 \times (0.8\text{m} \times \cos 45) + (3.3 \times 10^{-4}) \times 2 \times 0\text{m}^2 = 8.448 \times 10^{-4} \text{m}^4$$

$$s_{11} = \frac{M_2 y_3}{I_2} = \frac{15064.56\text{N} \times 1.415\text{m} \times 0.8\text{m}}{8.448 \times 10^{-4} \text{m}^4} = 20.186 \times 10^6 \frac{\text{N}}{\text{m}^2}$$

= stress act perpendicular to the cross section area of the stringer

$$P(\text{perpendicular}) \text{ acting on stringers 1 (compression) and 5 (tension)} \\ = A \times s_{11} = (3.3 \times 10^{-4} \text{m}^2) (20.186 \times 10^6 \frac{\text{N}}{\text{m}^2}) = 6661.38\text{N}$$

$$P(\text{perpendicular}) \text{ acting on stringers 2, 8 (compression) and 4, 6 (tension)} = A \times s_{11} \times \cos 45 = 4710.31\text{N}$$

P(perpendicular) acting on stringers 3 and 7 are zero.

$$R = \sum P_{33} + R' = (2105.96\text{N} \times 2) + (1052.98\text{N} \times 4) + R' = 15064.56\text{N}$$

where R' = (shear) only part of R, carried by the skin = -23488.4N

To determine the shear flow, q:
at stringer 1:

$$q_{out} - q_{in} = \frac{R \cdot Q_2}{I_2} = \frac{R(A \times y_3)}{I_2} \rightarrow 0 - (q_1 + q_8) = \frac{-23488.4 \text{ N} (3.3 \times 10^{-4} \text{ m}^2) (0.8 \text{ m})}{8.448 \times 10^{-4} \text{ m}^4} = 7340.125 \frac{\text{N}}{\text{m}}$$

$$q_1 = q_8 = 3670.06 \text{ N/m} = q_4 = q_5$$

at stringer 2:

$$q_1 - q_2 = \frac{-23488.4 \text{ N} (3.3 \times 10^{-4} \text{ m}^2) (0.8 \text{ m} \times \cos 45)}{8.448 \times 10^{-4} \text{ m}^4} = -5190.25 \frac{\text{N}}{\text{m}}$$

$$q_2 = 8860.31 \text{ N/m} = q_7 = q_6 = q_3$$

To determine the thickness of the skin, t:

$$t = \frac{q_{\max}}{\sigma_{\text{shear}}} = \frac{8860.31 \frac{\text{N}}{\text{m}}}{1409 \times 10^6 \frac{\text{N}}{\text{m}^2}} = 63.3 \times 10^{-6} \text{ m}$$

$$P_{22,1} = P_{\text{perpendicular}} \times \cos 18.43 = 6319.72 \text{ N}$$

$$P_{22,2} = 4710.3 \text{ N} \times \cos 18.43 \times \sin 45 = 3159.8 \text{ N}$$

$$P_{33,1} = P_{\text{perpendicular}} \times \sin 18.43 = 2105.96 \text{ N}$$

$$P_{33,2} = 4710.31 \text{ N} \times \sin 18.43 \times \sin 45 = 1052.98 \text{ N}$$

The above numbers are shown in Fig 6.4.5.2